GEOCHEMICAL AND PETROGRAPHICAL STUDY OF THE SHARAWRA FORMATION, OLD QUSAIBA VILLAGE, CENTRAL SAUDI ARABIA

BY

MUHAMMAD ASIF ABBAS

A Thesis Presented to the

DEANSHIP OF GRADUATE STUDIES

KING FAHD UNIVERSITY OF PETROLEUM & MINERALS

DHAHRAN, SAUDI ARABIA

In Partial Fulfillment of the
Requirements for the Degree of

MASTER OF SCIENCE

In

GEOLOGY

NOVEMBER, 2015

KING FAHD UNIVERSITY OF PETROLEUM & MINERALS

DHAHRAN- 31261, SAUDI ARABIA

DEANSHIP OF GRADUATE STUDIES

This thesis, written by **MUHAMMAD ASIF ABBAS** under the direction of his thesis advisor and approved by his thesis committee, has been presented and accepted by the Dean of Graduate Studies, in partial fulfillment of the requirements for the degree of **MASTER OF SCIENCE IN GEOLOGY.**

Michael A Kaminski

Dr. Michael A. Kaminski
(Advisor)

Dr. Abdulaziz Al-Shaibani
Department Chairman

Prof. Gabor Korvin
(Member)

Dr. Salam A. Zummo
Dean of Graduate Studies

Dr. Sedat Inan
(Member)

13/12/15

Date

DEDICATION

I would like to dedicate this work to my mentor, His Excellency, Sahibzada Pir Shahzad Ahmed Mairvi, to my Father, Noor Ahmed, and my Mother, Kulsoom Akhtar

&

To my beloved country ‘Pakistan’

ACKNOWLEDGEMENTS

"In the name of ALLAH, The Most Gracious and The Most Merciful"

All acknowledgements belong to Almighty ALLAH (s.w.t.) for his mercy and graciousness. I am thankful to Almighty Allah for providing me with the research opportunities and I'm grateful to the Holy Prophet (P.B.U.H) for his blessings.

My parents have always been encouraging throughout my educational career. My brothers, Mr. Muhammad Babar Abbas, Mr. Muhammad Abid Abbas, and Mr. Asad Haroon were the happiest people, when I received the approval from KFUPM, I am thankful to them for their support. I am also thankful to my sister Nazia Ahmed for her prayers and wishes. Dr, Sadia Sadaf has been a special chapter in my life, being more than a sister she deserves bundles of thanks for all the encouragement and fun time.

Behind every success, there is always a thought and idea. I am grateful to my friends for igniting the idea to joining KFUPM, Mr. Imran Ali (My instructor at Pakistan Oil Fields Limited) initiated this thought and later on the encouragement was provided by Mr. Kamran Zia.

I would like to acknowledge my advisor Dr. Michael Kaminski for all the scientific help and support through thick and thin. Prof. Ahmed Umran Dogan introduced me to the world of geochemistry. I am also grateful to him for his immense efforts on my writing and presentation skills. Prof. Gabor Korvin and Dr. Sedat Inan have been more than helpful in detailed reviews of my thesis. Mr. Hammad Malik and Saad Ali Iqbal Khan helped me a lot during field works and I really acknowledge their efforts. For the analysis part, I am thankful to Mr. Mushabab, Mr. Omar Atef Radwan, Mr. Syed Haroon Ali, Mr. Muhammad Benaafi, Mr. Hameed and Mr. Ayyaz Mustafa.

Last but not the least, some people were special in bring life to life. Waleed Ejaz and Hafiz Abdur Rehman have added lots of color into the busy schedule at KFUPM. Their role deserves to be acknowledged. I am also thankful to Mr. Amjad Ali, and Naveed Butt for their time and support.

TABLE OF CONTENTS

LIST OF TABLES

LIST OF FIGURES

LIST OF ABBREVIATIONS

XRD	:	X-Ray Diffraction
SEM	:	Scanning Electron Microscopy
EDS	:	Energy Dispersive Spectroscopy
ICP-OES	:	Inductively Coupled Plasma Optical Emission Spectrometry
QFM	:	Quartz Feldspar Mica
LF	:	Lithofacies
DF	:	Discriminating Function

ABSTRACT

FULL NAME : MUHAMMAD ASIF ABBAS

THESIS TITLE : GEOCHEMICAL AND PETROGRAPHIC STUDY OF SHARAWRA FORMATION, OLD QUSAIBA VILLAGE, CENTRAL SAUDI ARABIA.

MAJOR FIELD : GEOLOGY

DATE OF DEGREE : NOVEMBER, 2015

The Silurian Sharawra Formation has great importance as it rests over the richest source rock of the Qusaiba Formation. The Sharawra Formation has four members including Jarish, Khanafriyah, Nayyal, and Zubliyat. The formation mainly consists of sandstone and siltstone with subordinate shale sequences. The lack of published research on this formation requires fundamental studies that can lay the foundation for future research. Three outcrops were selected from the Old Qusaiba Village in Central Saudi Arabia for petrographical, petrophysical, and geochemical study. Quantitative mineralogical characterization was performed using state-of-the-art of techniques including scanning electron microscopy – energy dispersive spectroscopy, powder x-ray diffraction (XRD) for both minerals, cements, and clay minerals (detrital and authigenic). The outcrops were logged precisely and nine different lithofacies have been identified in the field. The thin section study has revealed the Sharawra Formation is mainly subarkosic, while the mica content increases near to its contact with the Qusaiba Formation. The XRD data has also revealed a prominent change in mineralogy with inclusion of minerals like phlogopite and microcline with depths. The other minerals occurring constantly thoughout the formations are albite, orthoclase, and kaolinite. The porosity values do not

vary much, as the average porosity for the sandstone facies is 15 percent, for the siltstones it ranges around 7 percent. The permeability is variable throughout the formation, the values range from 50 md to 300 md. Although sandstone has a good porosity and permeability the siltstone facies exhibit poor petrophysical characteristics. Due to repetitive siltstone facies, the Sharawra Formation should be considered as a potential unconventional reservoir. This study has provided a base for future quantitative studies in siliciclastic formations in the area. Major and trace elements geochemistry of the Sharawra Formation indicate a passive continental margin as the tectonic setting of the sandstone. The source area discriminating plots show the probable source rock for the Sharawra Formation to be acid, felsic, and granitic. CIA and CIW indicated a moderate weathering in the source area of these Silurian clastic sediments.

ملخص الرسالة

الاسم الكامل:محمد آصف عباس

عنوان الرسالة: دراسة صخرية وجيوكيميائية لمتكون شرورا، قرية قصيبة القديمة، وسط المملكة العربية السعودية

التخصص: جيولوجيا

تاريخ الدرجة العلمية: نوفمبر 2015

تحتل دراسة متكون شرورا أهمية كبيرة لتموضعه فوق متكون قصيبة؛ أغنى صخور المصدرعلى الإطلاق. يتكون متكون شرورا ذو العمر السيليوري من عضو جريش، عضو الخنافرية، عضو نيال وعضو زبليات. يمثل الصخر الرملي والغرين و الطفلي المكون الرئيس لمتكون شرورا. تم اختيار ثلاثة مكاشف بقرية قصية القديمة لدراستهم دراسة بتروجرافية، جيو كيميائية، و بتروفيزيائية. تمت هذه الدراسة باستخدام التقنيات الآتية؛ المجهر المستقطب، المجهر الإليكتروني، وحيود الأشعة السينية. تم التعرف على تسع سحنات صخرية. من خلال الدراسة تحت المجهر المستقطب يظهر أن المكون الرئيس لمتكون شرورا هو تحت الأركوز مع ازدياد كم الميكا قرب الحد الفاصل بينه وبين متكون قصيبة. وتظهر نتائج تقنية حيود الأشعة السينية تغيرا ملحوظا في المحتوى المعدني مع العمق حيث يزداد كم الميكروكلين و الفلوقوبايت. تظهر تواجدات أخرى من المعادن على امتداد شرورا كالأرثوكليز، الألبيت والكاولينيت. يصل متوسك المسامية لسحنات الصخر الرملي ل 15% في حين تصل ل 7 % لسحنات الصخر الغرين. تتراوح قيم النفاذية بين 50 و 300 مللي دارسي. في حين تعد سحنات الصخر الرملي خزانا جيدا، تعد سحنات الصخر الغرين خزانا فقيرا. ونظرا لتعدد سحنات الصخر الغرين، يمكن اعتبار متكون شرورا خزانا غير تقليدي محتملا. تشير نتائج التحليل الكيميائي للعناصر الأساسية والنادرة للوضع حافة قارية ساكنة كوضع تكتوني للصخر الرملي. تقدم هذه الدراسة أساسا للدراسات الكمية المستقبلية للمتكونات في هذه المنطقة.

CHAPTER 1

INTRODUCTION

The Sharawra Formation has faced diverse nomenclature variations in the last six decades. Initially researchers considered it as a formation, whereas it has been mentioned as a member by many authors. There has been no conclusive word on the name of this unit. Helal (1964) named the entire Silurian sequence of Saudi Arabia as the Sharawra Formation. Janjou et al. (1996) included it as the Sharawra Formation of the Qalibah Group. Vaslet (1987) grouped the Silurian units into the Tayyarat Formation, and designated the Qusaiba and Sharawra as members. Mahmoud et al. (1992) used Qalibah Formation and named the lower shale-dominated part as the Qusaiba Member, and the sand-dominated part as the Sharawra Member. The Sharawra Member of the Qalibah Formation was also used by Al-Hajri (1998). Al- Laboun (1982, 1986) named it as the Sharawra Sandstone Member of the Tayyarat Formation. Later, it was considered as the Shararwra Formation of the Qalibah Group by Al-Laboun (2009, 2013) and Halawani (2003). The Saudi Stratigraphic Committee (SSC) used the work of Janjou et al. (1996) and concluded it as the Sharawra Formation of the Qalibah Group (SSC, 2013).

The Sharawra Formation is well exposed along northwestern Saudi Arabia. Outcrop exposures are present in the northern and central Arabia, and also in the subsurface. The Sharawra Formation consists of micaceous sandstone with thin siltstone layers, and subordinate shale interbeds (Al-Laboun, 2009). It is distinguished from the upper part of the Qusaiba Member on the basis of sandstone dominance. Outcrops in the Qasim region

have thin gypsum layers, present between the sand beds as recent deposits. Within the Sharawra Formation, the sequence is coarsening upward. The upper part is more sandy, while the lower part is more silty. High gamma radiation values from the Sharawra sandstones are due to its micaceous nature (Mahmoud et al., 1992).

The Sharawra Formation is underlain by the Qusaiba Formation. The contact between the Sharawra Formation and the Qusaiba Formation is gradational (Mahmoud et al., 1992). The Qusaiba Formation has clay dominance throughout; however, the lower part of it is mostly shale and upper part contains subordinate sandstone. The Silurian rocks were deposited just after the glaciation event of Ordovician. The Qusaiba shale unit was deposited in deep marine conditions. This unit is one of the most prolific source rocks in the world. It is also named the ‘‘Qusaiba hot shale’’ (McGillivary & Al-Husseini 1992; Mahmoud et al., 1992; Cole et al., 1994). The formation acts as a source rock for the Paleozoic reservoirs and also to some Mesozoic reservoirs. The formation underlies disconformably to the Devonian Tawil Formation and its correlative units. The Khussayan Formation overlies the Qalibah group in Wajid Plateau (Jones & Stump, 1999). Paleozoic units of Saudi Arabia are described in Figure 1.1.

Eurypterid remains and its polymorphs in the Sharawra formation are indicative of shallow marine environment (Al-Hajri, 1998). The lower parts of the Sharawra Formation have shallow to deep subtidal facies on storm-dominated shelf and middle to upper offshore to proximal offshore facies. The upper part of the Sharawra Formation is bioturbated and contains upper proximal upper offshore facies. The Qusaiba Formation was deposited during the transgression, while the Sharawra Formation deposited under a series of repetitive transgressions and regressions (Janjou et al., 1996).

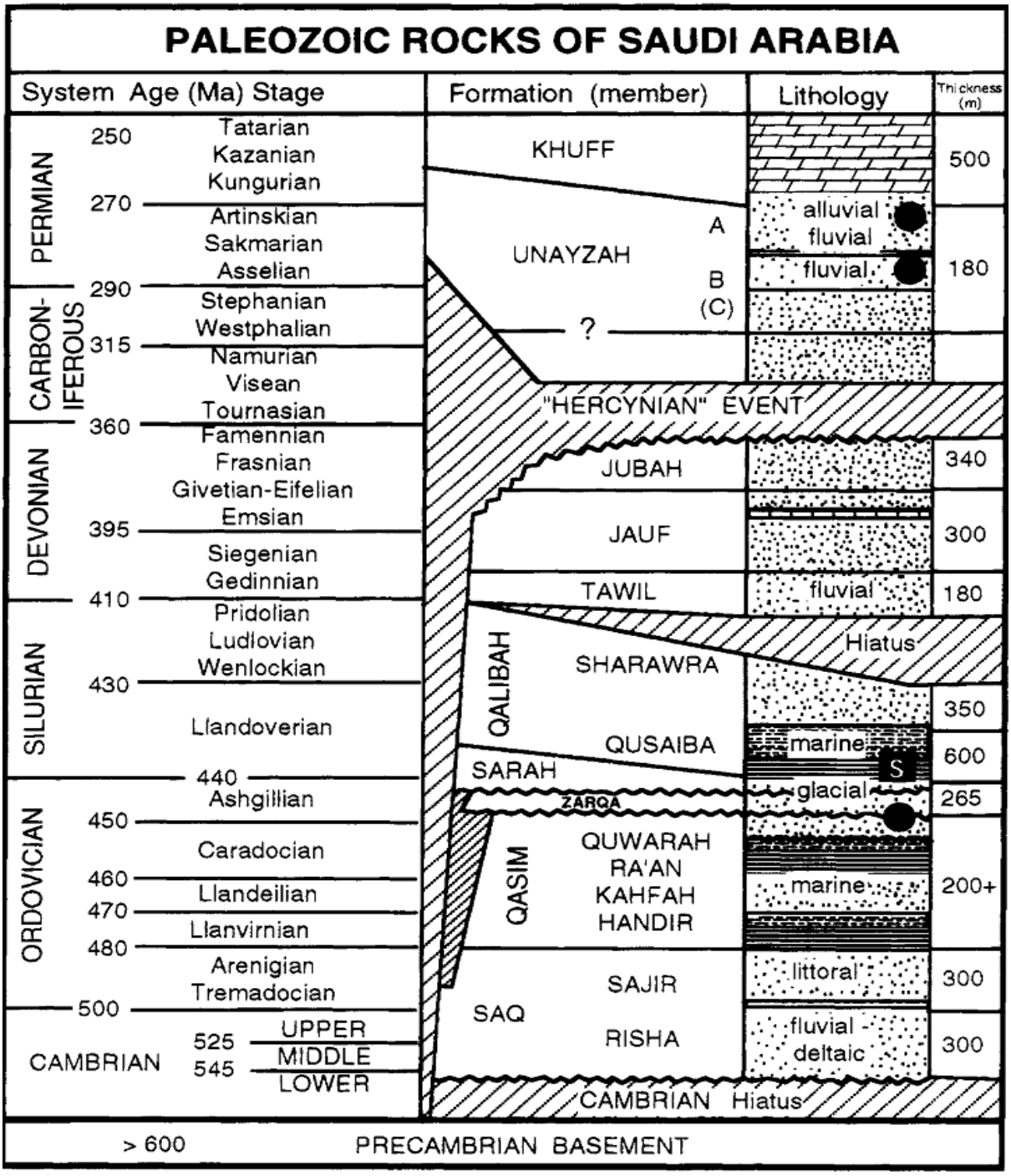

Figure 1.1 Paleozoic geology of Saudi Arabia (Cole et al., 1994).

Three chitinozoans facies and palynological evidences indicate a Wenlock (Early to Middle Silurian) age for the Sharawra Formation. The lower part of the Sharawra Formation contains *S. solivdina* and *Angochitina* Macclure and eight biozones have been

identified in the Early Silurian (Paris et al., 1995). On the basis of trilobites and tentacutiles, Janjou et al. (1996) gave a Late Wenlock to Early Ludlovian age to the Sharawra Formation. Although no graptolites have been identified in the Sharawra Formation, an Early to Middle Silurian age has been designated on the basis of the identified biozones.

Sharawra Formation has been divided into four members Jarish, Khanafriyah, Nayyal, and Zubliyat (Janjou et al., 1996, Halawani, 2003). The Jarish Member is the basal unit of the Sharawra Formation. It was named after Qian Jarish, located in the southeast of Al Qalibah quadrangle. In the type section its thickness is about 70 meters. This member contains greenish to yellowish, clayey, and micaceous siltstone. The sandstone is fine grained and is greenish to greyish in color. Hummocky cross beddings and mega ripples are present in the sandstone. The massive sandstone also has ball and pillow structures. The bioturbation is well developed. The Jarish Member rests over the Qusaiba Formation and is overlain by the upper Khanafriyah Member. On the basis of macrofauna, this member is dated as Early to Middle Silurian (Late Wenlockian). New species of tentaculitidae have been reported by Janjou et al., (1996). The second unit of the Sharawra Formation is the Khanafriyah Member. It was named after Jibal al Khanafriyah in the Al Qalibah Quadrangle. The thickness of the member is about 110 meters. The Khanafriyah Member has a variegated lithology. The lower part of this member is mainly yellowish siltstone and greenish sandstone, and has similar sedimentary structures to the Jarish Member. Grey to yellow siltstone overlies these units having linguoid ripples and fine-grained sandstone lenticular beds. Burrows and trails are also present. The overlying unit has more sandstone and siltstone (clayey). The sandstone is fine grained with beds

having wavy and subparallel laminae. The topmost part of this member is mainly siltstone of yellowish and greenish color. It has convoluted laminations and trails and burrows of Cruziana. This member has a conformable upper and lower contact with the Nayyal and Jarish members, respectively. On the basis of *Brongniartella janjoui* reported by Janjou et al., (1996), the member is dated as Middle to Late Silurian. The third unit of the Sharawra Member is the Nayyal Member, named after Wadi Nayyal in northwest Saudi Arabia. At the type section, the Nayyal Member is 125 meters thick. It also has alternating sandstone and siltstone beds. The lower sandstone is fine grained, massive bedded, and is of rusty brown color. This sandstone is highly bioturbated. The overlying unit is yellow to pink, friable siltstone. The siltstone has red-colored micro-conglomerates and phosphatic grains. The siltstone is overlain by brown to pink bioturbated sandstone. The sandstone is lenticular and has massive ball and pillow structures. Overlying the sandstone beds, is hummocky cross bedded silty sandstone. At the top of the Nayyal Member, the sandstone becomes coarser and thicker. It contains fossil debris and phosphatic grains. The Nayyal Member has a conformable contact with the overlying Zubliyat Member and with the underlying Khanafriyah Member. On the basis of *Brongniartella benderi* (trilobite) at the basal part of the Nayyal Member, it was dated as Middle to Late Silurian. The uppermost unit of the Sharawra Formation is the Zubliyat Member. It was named after the Az Zubliyat Plateau in the northeast of Al Qalibah town. The thickness of this member is 119 meters. It contains yellowish to brownish fine-grained sandstone at the base of the member. The sandstone has wavy bedding and parallel ripples. It also contains reworked claystone chips. Above the sandstone is the yellow to grey highly bioturbated siltstone. This horizon is coarsening

upward. Above the siltstone are grey to yellow sandstones having large-scale ball and pillow structures. At the top of the Zubliyat Member pale grey to violet siltstone is found with bioturbation. The upper contact of the formation is disconformable with the overlying Tawil formation. The lower contact of the formation is conformable with the Nayyal Member of the Sharawra formation. The age of the Zublyat formation is Middle to Late Silurian on the basis of its stratigraphic position.

My study is focused on petrographical, mineralogical, and geochemical characterization of the Sharawra Formation. An outcrop has been selected for this study. This work can be correlated to the other outcrops in the northwestern Saudi Arabia and to the subsurface. As the inorganic geochemical studies have been overlooked for the Silurian rocks in Saudi Arabia, this study can open a gateway for future research for other Paleozoic rocks.

1.1 Problem Statement

The sandstone succession of the Sharawra Formation has a very important stratigraphic position. As it overlies one of the most prolific source rocks in the world, it can have significant hydrocarbon reserves as a result of upward petroleum migration. Moreover, less consideration has been given to the geochemical characterization of the formation. It is possible that this formation can act as a reservoir. Moreover, very few studies have been performed and no published data are available on the inorganic geochemistry of this formation.

1.2 Study Area

The study area lies in central Saudi Arabia. This study was carried out on a well exposed section in Old Qusaiba Village in Qasim District, Central Saudi Arabia. In the outcrop section the thickness of the formation ranges to about 85 meters (Al-Laboun, 2013). Silurian deposits extend along an area of six kilometers in this area from northwest to southeast. The study area is shown in Figure 1.2.

1.3 Objectives

The aim of this study had been to investigate geochemical properties, understand the petrography, and conduct reservoir characterization of the Sharawra Formation. The study is based on field observations and laboratory work on the collected samples. The core objectives of my research had been stated as follows:

- Recognition and characterization of facies types
- Determination of the geochemical variation
- Porosity estimation of sandstones
- Assessments of mineralogical variations and relation to facies

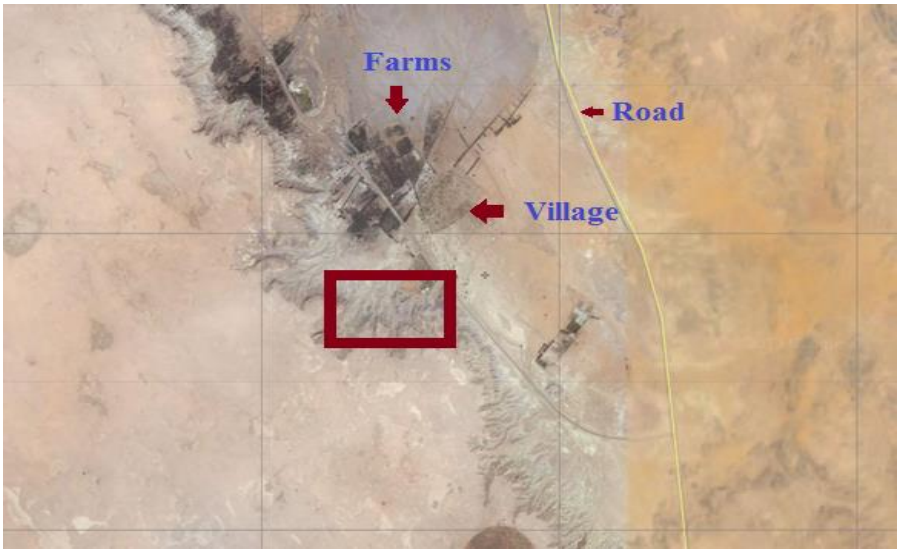

Figure 1.2 Location map of the study area

CHAPTER 2

LITERATURE REVIEW

Paleozoic rocks can be located with reference to the Arabian Shield. Arabian Shield rocks are mostly exposed towards the western part (Mahmoud et al., 1992). Arabia was attached to Africa during the Paleozoic. All Paleozoic formations are exposed around north, northeast, and south of the Arabian Shield. The outcrops are present in non-continuous and separated belts. Paleozoic sedimentary units are located in three major zones, namely Tabuk region (NW), Qasim region (Central), and SW Saudi Arabia (Al-Dabbagh, 2013; Jones & Stump, 1999). The Qalibah group is located in the north and northeastern part of the Arabian shield.

The central Arabian arch is a major surface and structural feature of the Arabian Peninsula and it is assumed that the arch has major control over the reservoir potential of central Arabia. The Idas orogeny and the Najd trend are the major events of the Precambrian that established the major structural tends. Orogeny was followed by hiatus in the central Arabia, while intracontinental rift with evaporites formed in the surrounding regions (McGillivray and Husseini, 1992). In the Cambrian and Ordovician, central Arabia was a subsiding shelf of the Gondwana continent, hence the siliciclastics of the Saq formation were deposited during the Cambrian. The late Ordovician was a glacial period. The Sarah and Zarqah formations were deposited during the glacial period. The glaciation events subdivided the Cambrian–Ordovician–Silurian succession into three depositional cycles: a preglacial cycle (Saq and Qasim formations), a synglacial

cycle (Zarqa/Sarah formations), and a postglacial cycle (Uqlah, Qusaiba, Sharawra formations) (Al-Laboun, 2013). The abrupt sea level rise during the Silurian deposited the coarsening upward sequence of the both the Qusaiba Member and the Sharawra Member of the Qalibah Formation (McGillivray and Husseini, 1992). Climatic and tectonic events are the reasons for the subdivisions of strata and facies variation on the Paleozoic stratigraphy of Saudi Arabia (Al-Laboun, 2009; 2010). These have subdivided the Paleozoic units into megadepostional cycles and smaller cycles. Three main events took place in the Paleozoic history. An uplift event due to Taconic tectonic events followed by the glaciation event affected the rocks of Precambrian to Early Ordovician. The Late Silurian tectonic event synchronous to the Acadian event affected the Ordovician and Silurian deposits. The Acadian cycle also subdivides the Silurian and Devonian successions into three: the pre-Acadian cycle represents the Qusaiba and Sharawra formations, the syn-Acadian is the Tawil Formation, and the post-Acadian is shown by the Jawf Formation. The thick Silurian sequences in the Tabuk area are truncated in the Qusaiba depression due to the sub-Tawil unconformity (Laboun, 2013). The third event is related to Hercynian activity, it affected the whole sequence from Carboniferous to Precambrian. Three unconformities: sub-Zarqa/Sara, sub-Tawil, and sub-Shajara are attributed to Taconic, Acadian, and Hercynian movements, respectively (Al-Laboun, 2010). The Hercynian produced the deepest erosion in the Arabian Peninsula, and changed the overall shape of Saudi Arabia (Jones & Stump, 1999).

The Paleozoic successions are important for water reserves, as well as the oil and gas potential in central Saudi Arabia (Al-Dabbagh, 2013). The Paleozoic petroleum system is charged by the widely spread and organic-rich lower Qusaiba shale of Silurian age (Cole

et al., 1994). The whole Silurian succession deposited in a time span of 120 million years and is grouped into supergroup IV. The supergroup IV formations are important source and reservoir rocks (Jones & Stump, 1999). Most of the reservoirs of Saudi Arabia are hosted by the Mesozoic deposits; however, significant reservoirs have been discovered in the Paleozoic deposits. Carbonate and clastic rocks have proved as Paleozoic reservoirs. The carbonate reservoir is predominantly the Khuff formation. The clastic reservoirs include the Quwarah Member of the Saq Formation, the Sarah Formation of the Ordovician, the Sharawra Member of the Middle to Late Silurian, the Tawil formation, and the Jauf Formation of Devonian age. The Silurian Qusaiba ‘‘hot shale’’ is the most important source rock with organic matter (2% to 11%) and type II organic matter preserved in the shale (Guoping, 2007). Total Organic Carbon (TOC) content of the Qusaiba shale Member indicates it as organic rich shale. The highly radioactive ‘‘hot shale’’ sequence is 20 to 70 m thick in subsurface having TOC content up to 6.15 percent (McGillivray and Husseini, 1992) and 15 to wt % (Cole et al., 1994). Hydrocarbon shows from the Sharawra Formation have also been reported by Abu-Ali et al., (1999).

The Sharawra Formation is well exposed along the northwestern Saudi Arabia. Outcrop exposures are present in the northern and central Arabia, and also in the subsurface (Al-Laboun, 2009). Type section of this formation is in the east of Wadi Al Qalibah in the Az Zubliyat area. The thickness of the Sharawra Formation is about 422 meters and 510 meters in the type locality and the Tabuk region, respectively. In the Baq’a area the thickness is about 90 meters (Halawani, 2003). In the reference section, the thickness of Sharawra Formation is about 234 meters and has been reported up to 35 meters from Udaynan-1 well (Mahmoud et al., 1992). The thickness of the formation is double in

subsurface than in the outcrop. This has been determined from the isopach maps from 14 wells with complete section and 29 wells with eroded tops (Mahmoud et al., 1992). In outcrops of southwestern Saudi Arabia, the formation is only exposed in a narrow strip. Here, the thickness is about 6 to 10 meters (Al-Ajmi, 2015). Jones and Stump (1999) reported that the Sharawra Member is rarely present in the Wajid Plateau; however, it is present in wells. The thickness of Silurian deposits decreases from the northwestern part in Tabuk to the Qusaiba depression in the east. The thickness of the Sharawra Formation in different regions of Saudi Arabia is shown in Figure 2.1. In terms of depositional thinning, paleo-highs are the major reason. The uppermost part of the Qalibah is locally eroded at places due to Hercynian and other younger structural activities (Mahmoud et al., 1992). The Qusaiba Member has been locally eroded and the moderately to well sorted sandstone of the Sharawra Member is deposited as fluvial channel fills (Jones & Stump, 1999).

The Sharawra Formation consists of moderately sorted sandstone, siltstone, and shale (Jones & Stump, 1999; Al-Laboun, 2009). The upper part of the formation is highly bioturbated and has ferruginous surfaces. The conglomeratic sandstone at the top is also phosphatic (Halawani, 2003). The formation is a coarsening upward sequence of sandstone, siltstone, with intercalated shale. The upper part of the formation is bioturbated and burrowed, while the lower part contains phosphatic bioclasts and conglomerates (Halawani, 2003). It is distinguished from the upper part of the Qusaiba Member on the basis of sandstone dominance. Outcops in the Qasim region have thin gypsum layers, probably are the recent deposits. Within the Sharawra Formation, the sequence is coarsening upward. The upper part is more sandy, while the lower part is

more silty. High gamma radiation values from the Sharawra sandstones are due to its micaceous nature (Mahmoud et al., 1992). The Qalibah formation of Halawani, (2003) in the southwestern part of Saudi Arabia also consists of two members: the lower member is shale-dominated Qusaiba Member and the overlying is the clastic Sharawra Member. The formation has been divided into four members the Jarish, Khanafriyah, Nayyal, and Zubliyat (Janjou et al., 1996; Halawani, 2013).

The Cambrian to Devonian units of Saudi Arabia unconformably overlie the basement and are overlain by an erosional surface of late Permian (Al-Dabbagh, 2013). The Silurian succession is missing in the Qusaiba depression. In central Saudi Arabia, the Sharjara Formation overlies the Devonian to Paleozoic rocks (Al-Laboun, 2013). The Silurian rocks are mainly divided into three units as the Uqlah Formation, Qusaiba Formation, and Sharawra Formation (Al-Laboun, 2009). Due to the presence of reworked layer containing orthoclone debris, the lower contact of the Sharawra Formation is disconformable with Qusaiba formation while, Sharawra Formation is overlain with an erosional disconformity by the Tawil Formation (Halawani, 2003; Jones & Stump, 1999). The Qalibah/Tawil unconformity exists between Wenlockian-early Ludlowvian part of the Sharawra Member and late Ludlowvian Tawil Formation. The contact of the Qusaiba Member and Sharawra Member in the subsurface is gradational over a long vertical distance ranging from 65 to 200 ft. The contact of Qusaiba and Sharawra is conformable regionally (Jones & Stump, 1999). The upper part of Qusaiba member cannot be easily distinguished from the Sharawra Member on the basis of their lithostratigraphic features; however, the upper contact of Sharawra Member with the Tawil Formation is sharp and prominent (Al-Hajri, 1998). In Wajid group outcrops, Sharawra Formation has a sharp

and unconformable upper contact with the Khusayyayn formation of Devonian age (Al-Ajmi, 2015).

In Saudi Arabia, the Silurian clastics represent a progradational sequence. These units deposited on a broad continental shelf after the deglaciation phase of Gondwana polar ice cap. The micaceous sandstone and siltstone of the Sharawra Member represent a prodeltaic facies (Al-Hajri). The formation was deposited on the stable continental shelf in eastern Arabia. The Qalibah Formation and its overlying units prograded towards the north and northeastward. The Sharawra Member deposited as shallow water prodeltaic clastics. The Sharawra member was deposited in shallower water depths than the Qusaiba member. The fact is supported by high flow regime structures, the grain size of sandstone, absence of middle and outer shelf taxa, and increase in terrigenous organic matter (Jones & Stump, 1999). The absence of carbonates in the Silurian is due to high paleo-latitude position of Gondwana (Mahmoud et al., 1992). The lower parts the Sharawra Formation have shallow to deep subtidal facies on storm-dominated shelf and middle to upper offshore to proximal offshore facies. The upper part of the Sharawra Formation is bioturbated and contains upper proximal upper offshore facies. The Qusaiba Formation was deposited during the transgression, while the Sharawra Formation was deposited under a series of repetitive transgressions and regressions (Janjou et al., 1996). A pterygotid eurypterid from the lower part of the Sharawra indicates hyposaline marginal marine conditions (Al-Hajri, 1998).

Three chitinozoan facies and palynological evidence indicate Wenlock (Early to Middle Silurian) age of the Sharawra Formation. The lower part of the Sharawra Formation contains *S. solivdina* and *Angochitina* Macclure and eight biozones have been identified

in the Early Silurian (Paris et al., 1995). On the basis of trilobites and tentaculites, Janjou et al. (1996) gave a Late Wenlock to Early Ludlovian age to the Sharawra Formation. Although no graptolites have been identified in the Sharawra formation, an Early to Middle Silurian age has been designated on the basis of identified biozones. In terms of biostratigraphy, the Sharawra Member has not yielded any graptolites. This character makes is highly different from the Qusaiba member, which is rich in graptolites. Pterygotid eurypterids from the lower part of Sharawra have also been reported (Al-Hajri, 1998). The biozone Angochitina hemeri has been identified from the lower part of the Sharawra member. Another species is also found in abundance is named as *Angochitina* Macclure (Paris et al., 1995). The age of the Sharawra Formation ranges from Middle to Late Llandovery in the central Arabia and Pridoli in northern Saudia Arabia (Jones & Stump, 1999).

The chitinozoan biozones and assemblages are correlative more with those of Libya and Algeria and less to those of Spain. Few of the species discovered are significant and can be correlated for inter-continentally between northern Gondwanaland and Baltica. The species show no affinities to the Afro-Brazilian species, but show some affinities with China (Paris et al., 1995).

The correlatives of the Qalibah Group are present from east to north in Saudi Arabia and extend to Jordan and to Oman and southern parts of Saudi Arabia. It also has equivalents from Egypt to Morocco and southward into Ghana. The individual beds of the Qalibah Formation also correlate along a large distance in the subsurface and have a sheet-like geometry (Jones & Stump, 1999).

Sandstones undergo variety of processes which are responsible for the alteration in its physical and chemical properties. These processes include weathering, erosion, transport, and deposition (Johnsson, 1993). Moreover, the variation could have occurred before the transport due to lithification and diagenesis. The composition of the rocks from which the clastic rocks form has a great influence on them. The framework of the grains and geochemistry of the bulk rock can provide information about the provenance of rocks. Petrographic and geochemical studies can therefore, prove prolific to acquire information regarding the provenance (Dickinson and Suczek, 1979; Dickinson et al., 1983) and the geochemistry of bulk rock (Bhatia, 1983; Bhatia and Crook, 1986; Roser and Korsch, 1986).

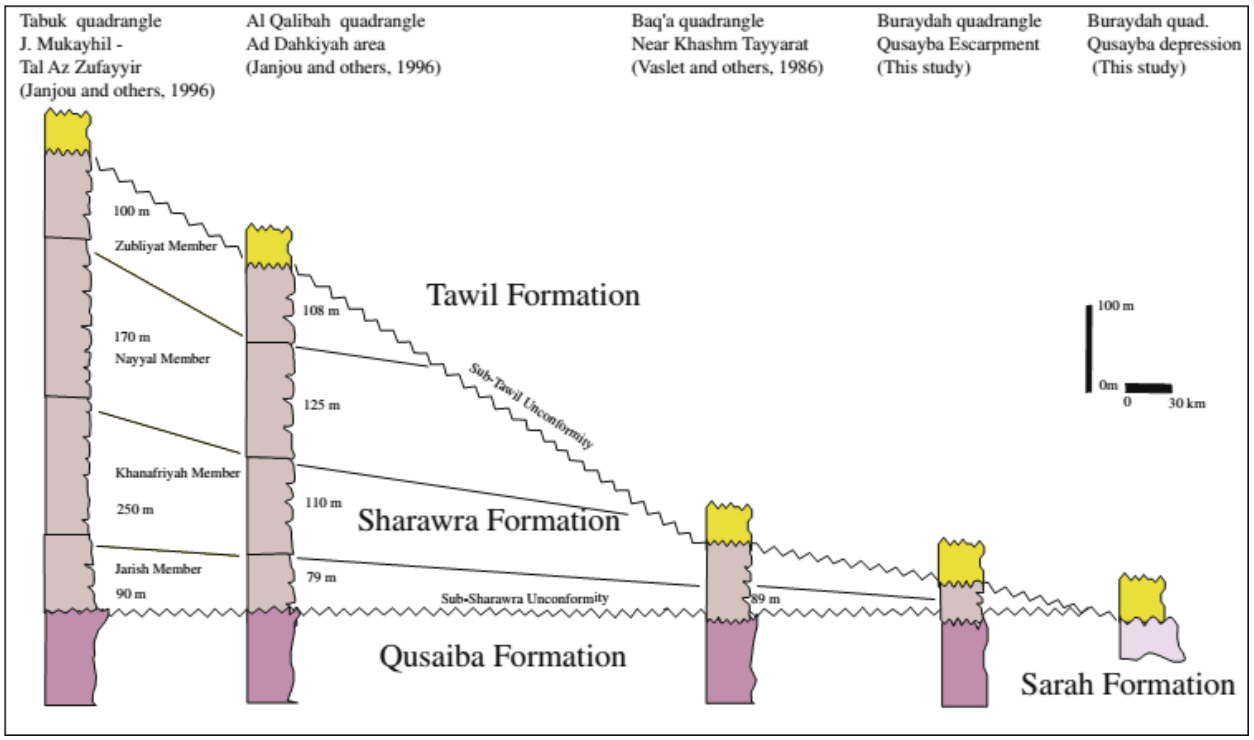

Figure 2.1 Thickness variations of Sharawra formation from Tabuk quadrangle to Buraydah quadrangle (Al-Laboun, 2009).

CHAPTER 3

METHODOLOGY

To carry out this research, methodology has been divided into four main parts. The first segment is the geological field and data obtained from the field. The field work is followed by sample preparation. The third major portion deals with different analyses carried out in the laboratories. The final segment is related to interpretation of the results obtained from the field work and laboratory analysis.

3.1 Field Work

Three outcrops of the Sharawra Formation were selected from the old Qusaiba village through a reconnaissance field trip. Panoramic photos were also taken during the reconnaissance to have a better view of the outcrop, with visible differences in the units (Figure 3.1). For the field observations all the three outcrops were studied, while two of them were used for the geochemical analysis. These two outcrops are the complete section of the Sharawra Formation, exposed in the study area. However, two more outcrops were studied only for the field observations and correlations. Field work started with taking panoramic photographs of the Qusaiba Formation. The panoramic photos were taken again to have better view of the outcrop, with visible differences in the units. Zoomed in photos were taken for each unit. Global Positioning System (GPS) readings were also taken for each location. The emphasis of the field work was on measuring the stratigraphic section for the two outcrops and to collect representative samples from each interval of sandstone, siltstone and shale. Samples were taken vertically in most cases,

however; lateral equivalents of every possible bed were also taken. The systematic sampling strategy is illustrated in Fig. 3.2. Vertical thickness of each bed was measured very precisely. A total of one hundred and twenty eight (128) samples were collected from the two major outcrops. Detailed sample description was done by using hand lens. Each sample was photographed with proper scale. Examples of sample photographs are shown in Figs. 3.3 and Fig. 3.4. These samples are the representatives of each bed and serve for further use for detailed petrographic, geochemical, and petrophysical analysis. Samples were properly numbered and packed well in the plastic bags and photos for each sample location were also taken.

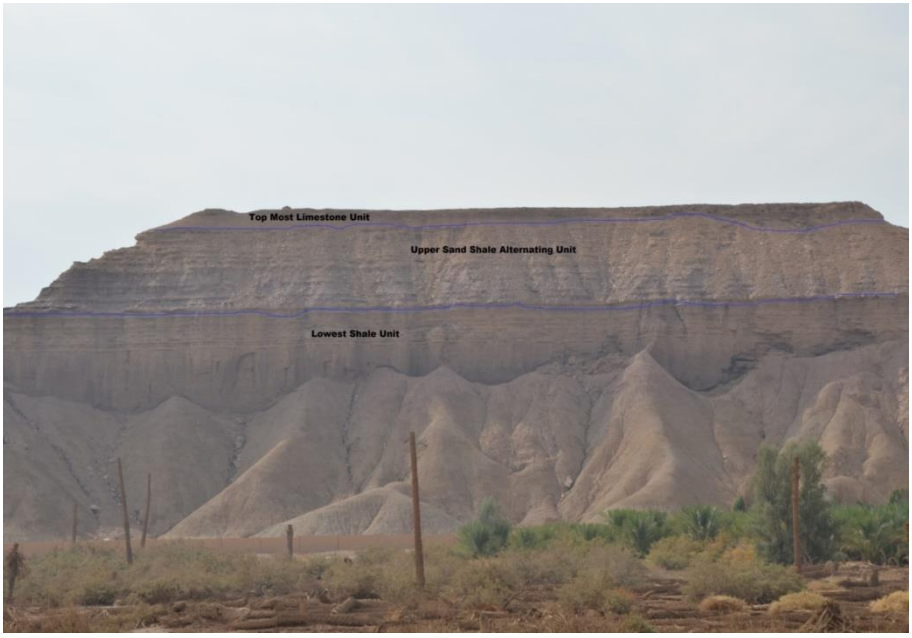

Figure 3.1 Panoramic view of the Silurian units in Old Qusaiba Village.

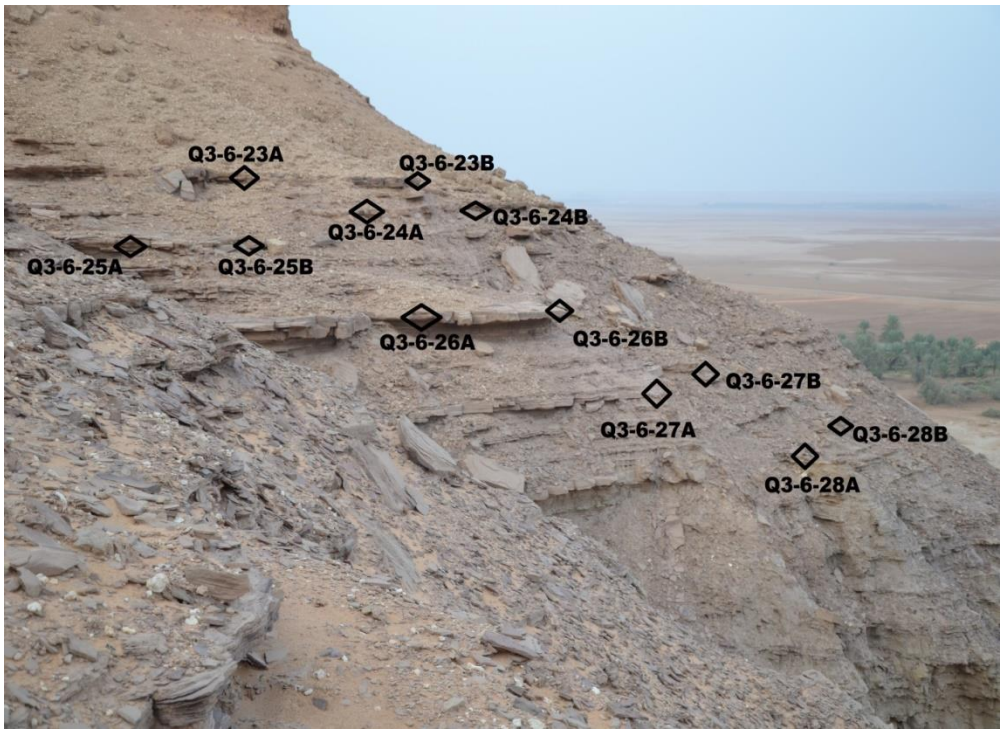

Figure 3.2 Sample locations at the upper part of the outcrop 2.

Figure 3.3 Sample photograph for sample UD-14-Q49.

Figure 3.4 Sample photograph for sample UD-14-Q28.

3.2 Sample Preparation

Sample preparation is an important step in this type of research. The quality and reliability of the results is directly upon sample preparation. The correct procedure and handling the equipment lead to quality results that can produce quality research. In this thesis study, I used different techniques to characterize the sandstone and shale units of Sharawra Formation.

- The petrographic consisted of making the thin sections from all the sandstone samples collected from the two outcrops.
- The petrophysical section dealt with making core plugs and then analyzing them under helium porosimeter and permeameter.
- SEM involves an easy sample preparation before acquiring high resolution microscopy of the sandstone samples.

- Powdered XRD analysis also has a quick sample preparation to get the mineral analysis. However, XRD for clay minerals is not simple, and requires four different steps to get satisfactory results.
- Geochemical investigation is concerned with the sample preparation for XRF and ICPMS. TOC measurement was also performed, after a simple sample preparation.

Sample preparation for each analysis will be discussed in detail under the laboratory work section. Sample preparation for all the analysis has been carried out in different labs of the Earth Sciences Department and Research Institute of King Fahd University of Petroleum and Minerals. I have conducted the sample preparation myself for all the analysis techniques used in this research.

3.3 Laboratory Work

3.3.1 Optical Microscopy

Thin section study shows the micro-scale features of the rock samples. In optical microscope, light is used as a source and optical lenses under the phenomenon of reflection provide a magnified image. Petrographic study reveals important features of mineral composition, estimation of the percentage of each mineral, visual porosity estimation, determination of grain size, grain contact, grain sorting, and grain shape. Thin section petrographic analyses were done for fifty four samples. In order to prepare the thin sections, sample chips were cut using the diamond bit cutter. Blue epoxy was used to impregnate the sample chips in the pressurized incubator. The chips were left overnight after impregnation. The impregnated rock chips are showed in Fig 3.5. By using Canada balsam, the samples were glued to glass slides and kept under pressure to stick to the

glass appropriately. The excess rock piece was cut down from glass slides leaving the thin layer of sample on the glass. To get a polished and smooth surface, silicon carbide is used for grinding the glass-mounted slab. The top surface of the thin section was not covered with glass. All the thin sections were prepared in the Earth Sciences Department (ESD) thin section preparation lab. Thin sections images were examined under plane and polarized light. Polarizing microscope is used for analysis of thin sections. The optical microscope used for the thin section study is a student microscope having different resolving powers and magnifications (max. up to 400X). I used the optical microscope at ESD and RI for the description and photographs, respectively. Photographs of the thin sections were taken at different magnification (40X and 200X).

Figure 3.5 Impregnated sample chips.

3.3.2 Petrophysical Measurements

Once the representative samples were selected for porosity measurements, core plugs were cut using the core plug drill machine. Twenty samples were cored vertically to get 24 core plugs. The core plugs were prepared in RI workshop. The core plug machine is shown in Figure 3.6. The shape of the core plugs is cylindrical. Porosity and permeability

measurements were done for all cores. The porosity calculation procedure used in this study was gas expansion and saturation method. To calculate the permeability gas permeability method was used. Helium is used for both porosity and permeability measurements. Helium porosimeter and permeameter require a definite core plug diameter but different core lengths can be used. One inch diameter cores were made. The lengths of all the core plugs were measured using Vernier caliper. The weight of each core plug was measured. All the core size parameters were uploaded to the system to calculate the grain volume, pore volume and bulk volume. In this way, grain density is obtained, which finally leads to get percentage porosity.

Figure 3.6 Core plugs cutting machine at RI.

3.3.3 Scanning Electron Microscopy-Energy Dispersive Spectroscopy

The SEM gives a detailed qualitative analysis and helps in better understanding of the microstructure. SEM provides a high resolution three dimensional image with higher magnification. Grains of each mineral can been easily observed under SEM. Grain size, grain shape, and grain contacts are relatively much clear under SEM. Overgrowths

around a mineral grain can also be observed. Moreover, the cement can also be distinguished by determining its elemental composition from the EDS attachment. Pore geometry, pore sizes, and pore system can also be studied in detail. If there is any diagenetic clay in the sample, the EDS can also confirm it. Paragenetic sequence of the minerals can also be observed. The SEM is usually performed on the fresh surface of the sample. Maximum magnification of an optical microscope is 2000 times, in case of oil immersion. SEM provides a much higher magnification. The necessary sample preparation for SEM requires the samples to be coated with gold or carbon. This coating is done under vacuum, thus not allowing the electron build up on surfaces, to avoid charging. SEM can achieve resolution better than 1 nanometer and magnification reaches up to 500,000 times. 21 representative samples were selected for the SEM-EDS analysis on the basis of thin section results. Small chips were cut from the sample using a geological hammer. The samples were coated with gold (Figure 3.7). Cressington sputter coater was used for this purpose. The coating normally takes 25 minutes for the geological samples. Samples were coated with gold (Figure 3.8). To insert the sample in SEM needs precision as it is important to maintain vacuum. 11 samples were analysed at ESD, while 10 were analysed at RI (Figure 3.10).

Figure 3.7 Cressington Sputter Coater (RI).

Figure 3.8 Samples coated with gold.

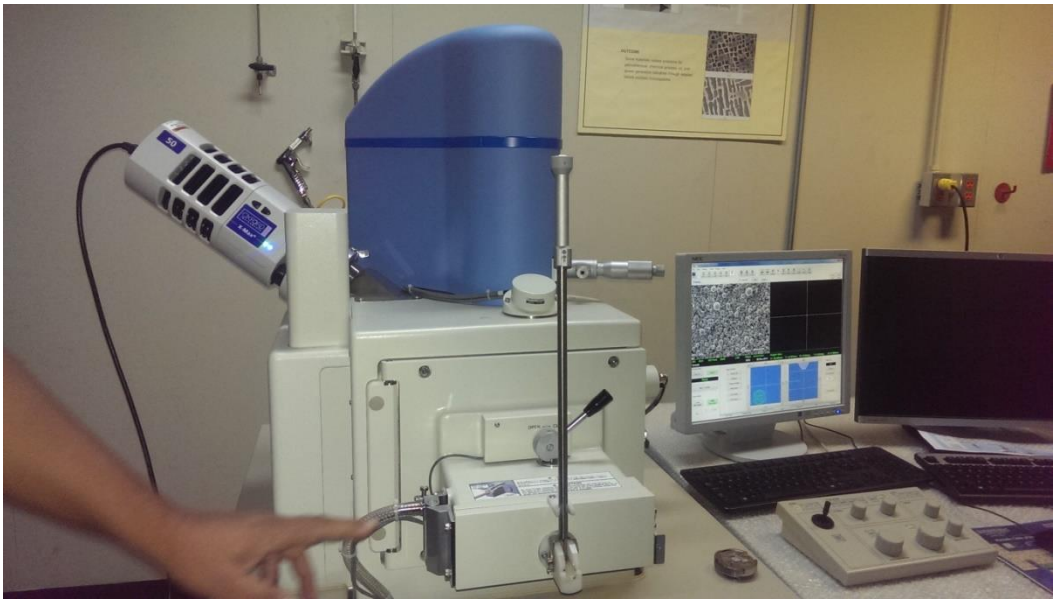

Figure 3.9 SEM-EDS (JSM 6610LV) at RI.

3.3.4 X-Ray Diffraction (XRD)

XRD is the best mineral identification technique. Although, other techniques like Scanning Electron Microscopy-Energy Dispersive Spectroscopy (SEM-EDS) can give some information about the minerals, but XRD is far better than many other techniques. The XRD has two types:

a) Single crystal X-Ray Diffraction
b) Powder X-Ray Diffraction

In single crystal X-Ray Diffraction only one crystal is analysed. It is non-destructive. Powder X-Ray Diffraction is done for the geological samples mainly. Firstly, the sample is powdered and the bulk sample is analysed under the XRD.

The principle behind the XRD is the generation of X-Rays from the cathode ray tube. The generated X-Rays strike the sample under analysis. These X-Rays undergo a constructive interference after striking the crystals of the sample. Due to this diffraction takes place obeying the Bragg's law $n\lambda = 2d\sin\theta$. The diffracted X-rays are detected by scintillation counters and results are obtained in the form of XRD pattern. The important parameters are 2θ, d, intensity, relative intensity (RI), and background. 2θ depends upon the angle at which the diffraction is taking place. d is the d-spacing and it depends upon interlayer spacing within a mineral structure. 2θ and d are inversely related to each other. Intensity is obtained from the counts per seconds and is dependent upon the chemical composition, position of atoms in the structure and sample preparation. For an acceptable XRD pattern, the intensity should be high. Relative intensity is expressed in percentages and gives the percentage difference between the different reflections of the same mineral. This helps in

the identification of a mineral. The background is very important as higher background is problematic. Smaller peaks can be missed due to high background. Net peak intensity is required to know the exact intensity. Background also depends upon sample preparation. Threshold value or modeling is used to get the net peak intensity. Background can be minimized by better sample preparation and increasing the analysis time.

The XRD equipment used is shown in Figure (3.11) below. It is a Japanese brand named Rigaku. It has the option of multi sample holder. There is a slot to prepare and grind the sample. The sample preparation should be done with care to get satisfactory results. This XRD has a thin film attachment for filter samples and powdered diffraction attachment for geological samples. The X-ray diffraction technique provides the analysis of the structure of a material from the scattering pattern produced when a beam of radiation or particles (as X rays or neutrons) interacts with it.

Selected (15) samples of shale and sandstone were analysed under XRD. The XRD facility at RI was used for analyzing the samples. The shale samples were analysed to know the variation in the clay minerals. Clay mineral analysis is not as simple as the typical mineral analysis of sandstones. It actually involves four different steps.

Complexity in clay mineral analysis is also due to their small size and different type of clays e.g. smectite, chlorite, illite, and kaolinite. It is usual to run XRD at least four times for the clay analysis. The first XRD spectrum is carried out to know about the presence of clays in the powdered sample. If the clays are present, the analysis will head to the next steps. The powdered sample is then treated with distilled water, stirring is done. Following from the Stoke's law few of the particles (having size larger than 2 μm) will

deposit at the bottom of the container while some will be left suspended in water. As the size of clays is less than 2 μm, so the suspended particles are the desired ones. These suspended particles are filtered out by the help of filter paper. After filtering the remaining particles are the clays. Second XRD is carried out for clay size fraction. To distinguish between different kinds of clays glycerin or glycol is added to these clays and the sample is left for approximately 12 hours. Doing this will separate the swelling and non-swelling clays. The clays swell because the glycerin evaporates in few hours and as it passes, it makes its way through the layers of clay mineral and hence the clay gets swollen. The third XRD spectrum is obtained at this time to know further about the clays. After the third X-Ray the sample is heated to 550 ºC. Some of the clays will be able to bear this heat while others will collapse. This collapse will generate a certain spectrum that makes them distinguishable from the other clays.

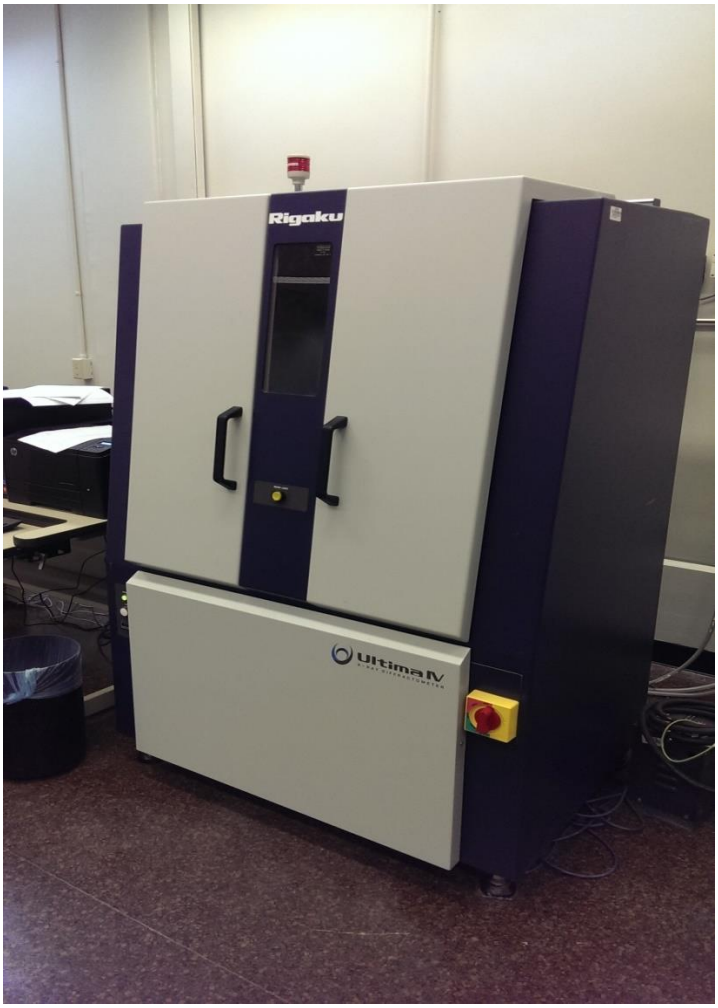

Figure 3.10 XRD at RI

3.3.5 X-Ray Fluorescence (XRF)

XRF is an analytical technique that allows the elemental analysis of bulk samples. This technique can analyze solid and liquid samples. It determines the chemical composition of each element present in a given sample and also provides the concentration of elements present in a bulk sample. The analysis time depends upon the number of elements present in the sample. Samples having high number of elements will take more

time to get analyzed. The results of XRF are accurate and reliable if the samples are prepared at ideal standards.

The working principal of XRF is simple. When an intense beam of X-rays strikes the atoms of element under analysis, an inner shell electron is knocked out. Hence, a vacancy is created. This vacancy is filled by an outer shell electron, the outer shell electron jumps to the vacancy with the release of certain amount of energy according to Bohr's law. Every element in the periodic table has a difference in this energy. This energy is released in the form of characteristic X-rays. These characteristic X-rays are the fluorescent X-rays. After this release of energies, an energy spectrum is generated having different peaks.

These fluorescent X-rays are captured by detectors, after processing the spectrum is generated from which numerical results are computed. The spectral peaks provide the qualitative as well as quantitative analysis of the elements in a bulk sample. Qualitative analysis is the identification of elements in a given sample, while the intensity of X-rays provides the quantitative analysis by giving the concentration of each element (Grieken and Markowicz, 2002).

The sample preparation for the XRF is relatively more simple and quicker than other elemental analysis techniques. The sample preparation has slight differences for solid, liquid, and filters samples. For a quality study the sample preparation is a key. As the sample preparation is easy in XRF, it is preferred in industry for elemental analysis of bulk samples. Here the rock samples were ground by the grinding machine and then placed in the small plastic holders of the XRF. A good quality study requires the sample

to be homogenous, with smooth surfaces and that it should be representative of the whole bulk material.

The basic idea for all spectrometers is similar. There is a source, sample, and a detection system, but there are few variations according to the demands of the analysis. A typical XFR has the following components:

i. X-ray tube (source)
ii. Filters
iii. Collimators
iv. Discriminators
v. Counters
vi. Dead time correction

Altogether 47 samples from shale and sandstones have been analysed under XRF to acquire the detailed elemental composition of the Sharawra Formation and to have the lateral and vertical variation in the chemical composition of different units in two outcrops. The XRF facilities of RI and ESD were used for this purpose (Figures 3.19 and 3.20).

3.3.6 Inductively Coupled Plasma-Optical Emission Spectroscopy

Besides XRF, the other chemical analysis technique used in this research was ICP-OES. It is related to inorganic chemical determination of major and minor trace elements. ICP-OES provides both qualitative and quantitative analyses. Compared to atomic absorption spectrophotometers, in which the excitation temperature of air-acetylene flame measures

2000 to 3000 K, the excitation temperature of argon ICP is 5000 to 7000 K, which efficiently excites many elements. Hence, it provides more precision and trace elements can be determined at ppm level.

ICP underlies the concept of optical emission spectrometry. The atoms within an element get excited, as the sample gains plasma energy. Emission rays get released as the exited atoms gain a low energy position. The released emission rays are characteristic and correspond to the photon wavelength and are measured. On the basis of these photon rays and their intensity the type of element is determined. In order to generate plasma argon gas is supplied to torch coil, followed by high frequency current applied to the coil and the tip of the torch. In this way argon gas gets ionized and plasma is produced. For the excitation-emission of the sample, the high temperate and higher electron density of the plasma is used. The temperature of plasma reaches up to (10000K). A narrow tube in the middle of torch is used to introduce the Solution samples. Equipment for ICP optical emission spectrometry consists of a light source unit, a spectrophotometer, a detector and a data processing unit. The elements that are not easily analysed under atomic absorption spectrometry such as Zr, Ta, rare earth, P and B can be analysed easily under ICP-OES. It also enables to analyse multiple elements simultaneously, has high sensitivity, and ~~is~~ gives a much more stable analysis, as plasma is the excitation source.

In geology, performing ICP has many applications, including the determination of U in ores, analysis of continental and marine sediments for several metals and geological history of rocks, and determination of rare earth, major and minor trace elements in carbonate cores.

15 sandstone samples were analysed for ICP-OES. The analysis was carried out in Center of Water and Environment (CEW), RI. CEW is equipped with an ICP of Agilent brand of 7500 series (Figure 3.12). Here, there was no facility to treat the samples with HF, so, silica was not identified during the analysis. However, silica concentrations were already determined by XFR This vacancy is filled by an outer shell electron, the outer shell electron jumps to the vacancy with the release of certain amount of energy according to Bohr's law. Every element in the periodic table has this energy different. This energy is released in the form of characteristic X-rays. These characteristic X-rays are the fluorescent X-rays. After this release of energies, an energy spectrum is generated having different peaks.

Figure 3.11 ICP at CEW, RI.

3.3.7 Total Organic Carbon (TOC)

TOC analysis can be performed on solid and liquid samples for a variety of purposes. In this study the TOC was determined to acquire a generalized trend for the source rock

potential of the shale interbeds. In this research TOC analysis is the only technique that belongs to organic geochemistry. The TOC analysis was carried out in CEW, RI. CEW is equipped with a Total Organic Carbon Analyzer of Shimadzu. It is a Japanese brand and the model is TOC-V $_{CPN}$ (Figure 3.13).

The sample preparation starts with powdering the sample. It is required that the sample should be ground very finely. The next step is to weigh the sample using a weighing balance. Only 200 mg of the sample is required. Purified air is passed through the Total Carbon (TC) combustion tube at the flow rate of 150 mL/min and then heated to 680 °C. The prepared sample is injected into the combustion tube through the sample injection system. This oxidizes the TC in the sample which is decomposed in the form of CO_2.The combustion products in the carrier tubes are dehumidified and cooled in the dehumidifier, after this they pass through the halogen scrubber into the sample cell, and the CO_2 is detected in the non-dispersive infrared detector (NDIR). The NDIR signal is analogue and it forms a peak. The peak area is calculated by the data processor. The TC standard solution predetermines the relationship between TC concentration and peak area; this helps to measure TC concentration. TC consists of both organic carbon and inorganic carbon. To separate them the acidified sample is inserted into the system as it only contains the inorganic carbon. This will only provide the concentration of inorganic carbon. Subtracting this value from the TC will give the TOC. All in all 15 shale samples were analysed to acquire the TOC results.

Figure 3.12 TOC analyzer at CEW, RI.

CHAPTER 4

RESULTS AND DISCUSSIONS-FIELD WORK

The section covers the lithofacies distribution of the Sharawra Formation in Qusaiba village. Three outcrops were studied for this purpose. The Silurian rocks extend from northwest to southeast in this area. The outcrops have been named as outcrop 1, outcrop 2, and outcrop 3 for the northwestern, central, and southeastern outcrop (Table 4.1).

Outcrop 2 is the most representative one, as it is a complete section and the thickness of the Sharawra Formation is maximum at this point. The facies are described vertically. The outcrop 2 was selected on the basis of field observation and literature review. Other outcrops of the Qusaiba Village were also carefully studied for lithofacies distribution and correlations. The facies description of each outcrop includes grain size classification, color identification, sorting, thickness of each unit, and sedimentary structures. All the sections were precisely measured for thickness, and photographs were taken for all the outcrops and units. As the major aim of this research is to geochemically characterize the Sharawra Formation, samples were taken from every possible location, to document geochemical variations. Samples were also taken from every possible change in lithology. Locations of the three outcrops are shown on the in map (Figure 4.1).

Table 4.1 Coordinates of the Sharawra Formation outcrops at Qusaiba Village.

Sr. No.	GPS Location	
Outcrop 1(Northwestern)	N 26°51’35,	E 43°34’19’’
Outcrop 2 (Central)	N 26º 50.207'	E 043º 35.22'
Outcrop 3 (Southeastern)	N 26°50’2.8’’	E 43°36’00’’

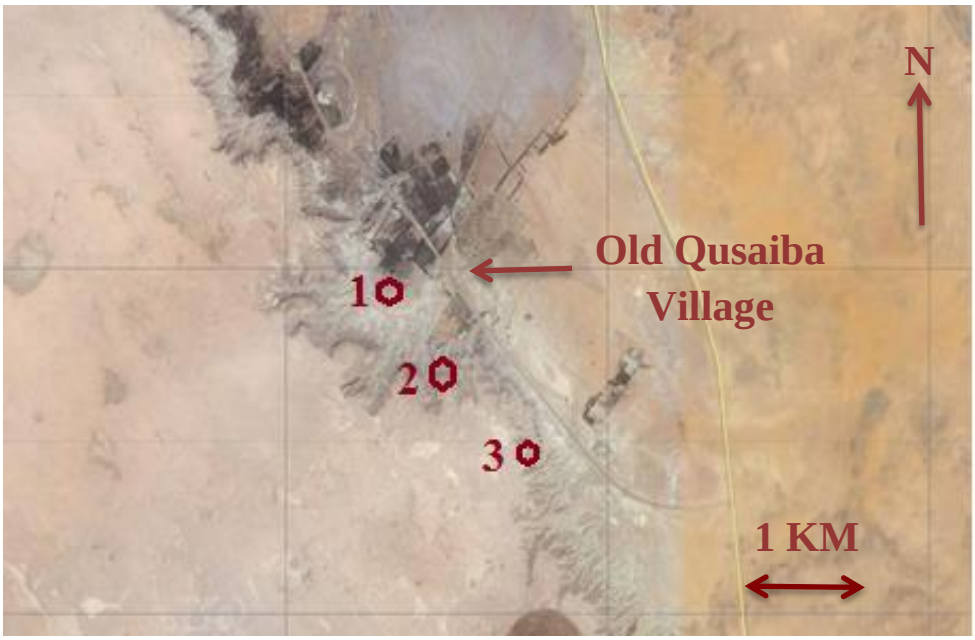

Figure 4.1 Outcrops location for Sharawra Formation in Qusaiba Village.

4.1 Lithofacies Description

The purpose of acquiring the lithofacies data in this research had been to detect the facies variation and document the geochemical variation in Sharawra Formation with respect to

facies change. The depositional environment study of this formation has already been done by Janjou et al, (1996) and has been documented as pro deltaic in a SGS special report in 2013. The lithofacies distribution I found will describe the formation being deposited as a fluvial part of the delta or as shallow marine deposit. A lateral and vertical profile of each outcrop were carefully prepared in the field and this will allow to understand the lithofacies association that leads towards the interpretation of depositional environment and ultimately helps in understanding architectural elements of the Sharawra Formation. The lithofacies description is based on primary depositional attributes, mainly grain size, color, texture, sedimentary structure and bedding plane. The major lithofacies were identified in outcrop 2, which is the most representative of all the Formation.

4.1.1 Outcrop 1 (Northwestern)

The total thickness of outcrop 1 is about 72 feet. Each bed was measured precisely to produce the logs. The log data were measured in the field, followed by describing all the samples collected from outcrop 1. The lithological log with description of samples is shown in Figure 4.2. Six different lithofacies were observed in this outcrop. Lowermost packages of units are the purple-colored siltstone facies (LF 7). Three beds having composite thickness of 10 feet represent this facies. The second facies is very fine grained horizontally stratified sandstone (LF 6). The thickness is about 6 feet. The third facies is the variegated colored siltstone (LF 5). The two beds comprising this facies are about 4.5 feet in thickness. The fourth of the lithofacies is the medium to fine-grained hummocky cross bedded sandstone (LF 3). Its two beds are about 3.5 feet thick. The topmost are the calcareous sandstone facies, about 11 feet in thickness. Fine to medium

grained calcareous sandstone facies (LF 2) is overlain by medium to coarse grained bioturbated calcareous sandstone (LF 1). The stratigraphic log from this outcrop presenting the lithofacies is shown in Fig. 4.2. The lowermost purple-colored siltstone facies lie directly over the topmost part of the Qusaiba Formation. The thickness of the individual beds is greater than in other outcrops. The lithofacies log is shown in Figure 4.3.

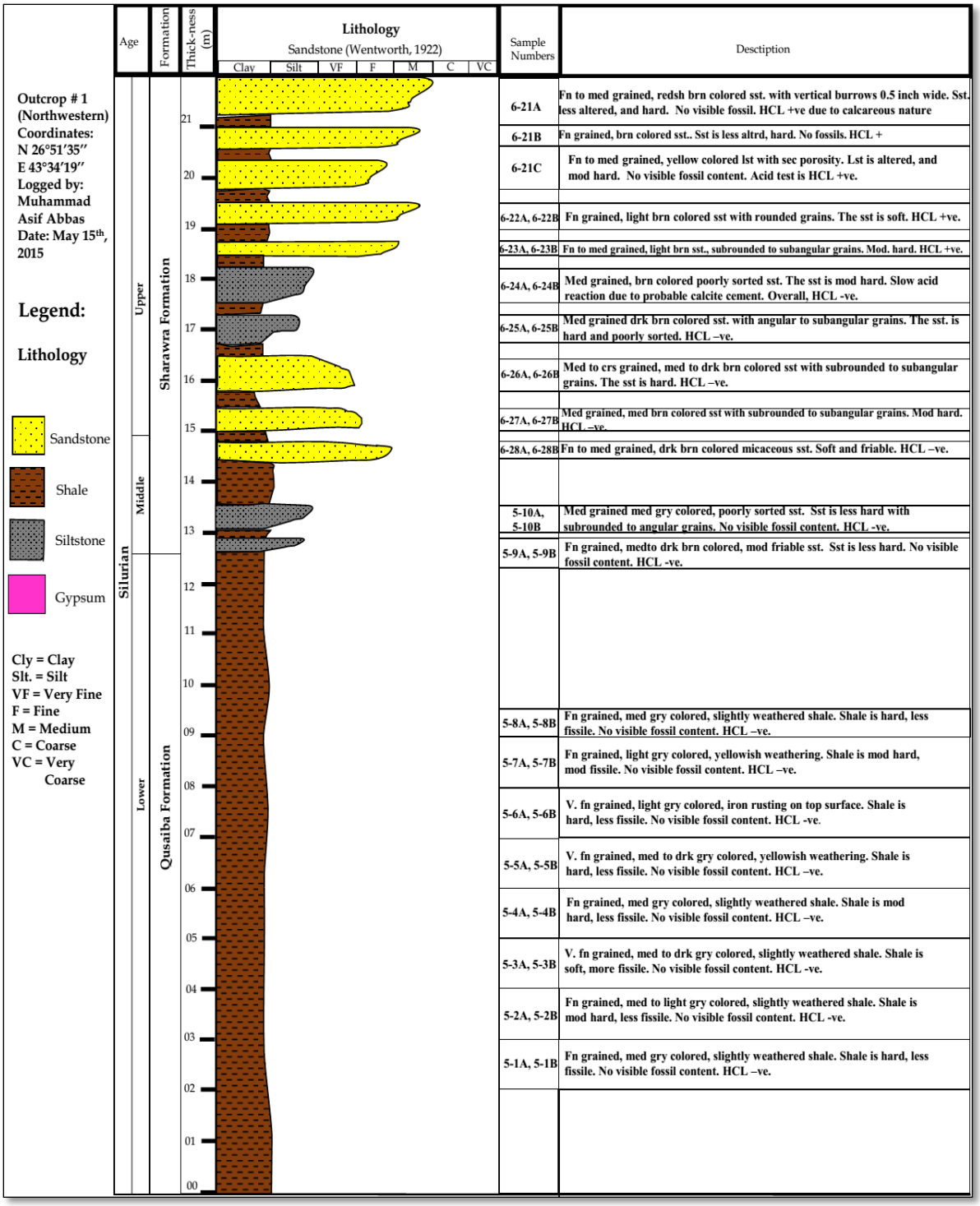

Figure 4.2 Lithological log of outcrop 1 with sample description.

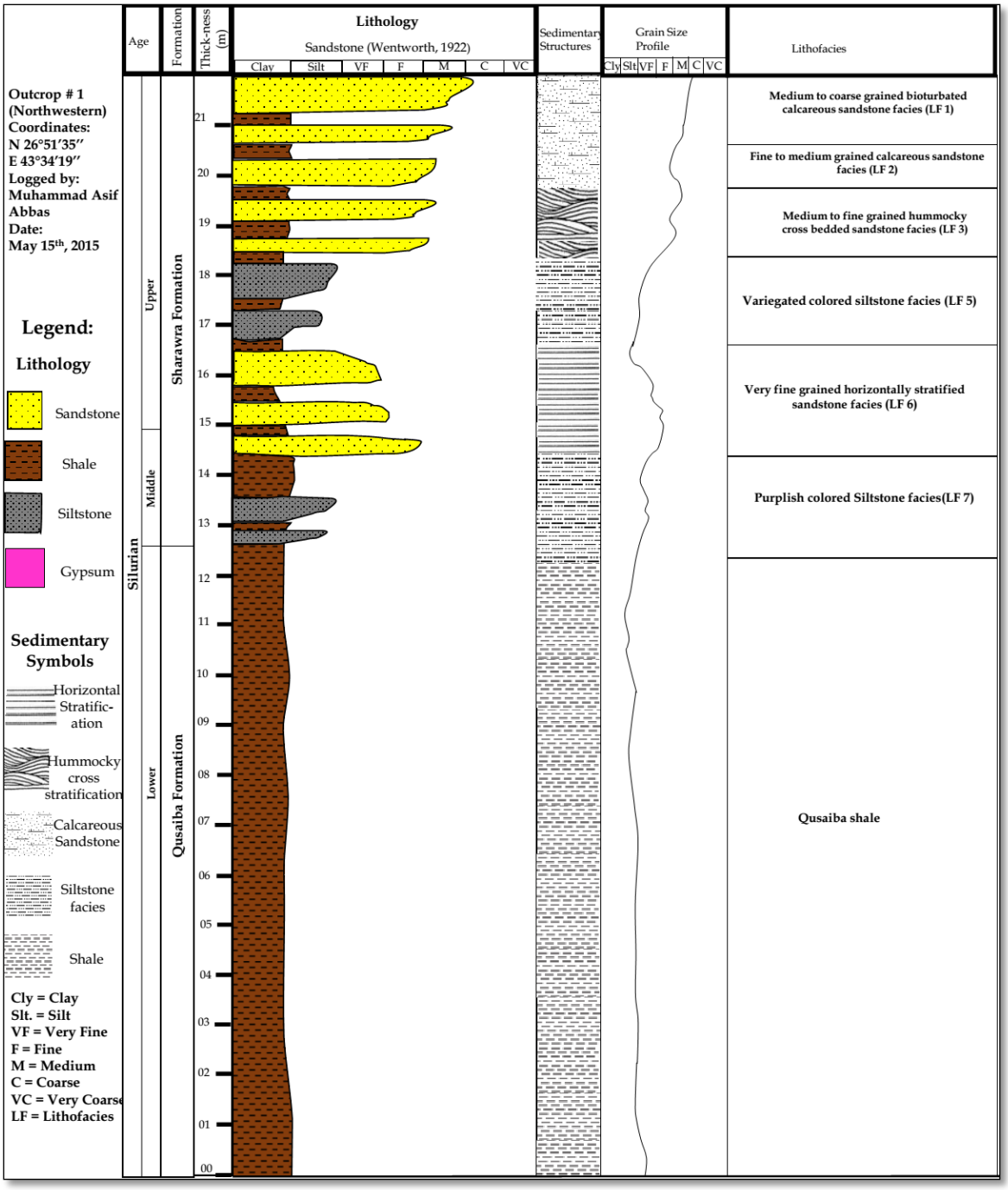

Figure 4.3 Lithofacies log of outcrop 1.

4.1.2 Outcrop 2 (Central)

The total thickness of outcrop 2 is about 88 feet. Its lithostratigraphic column is shown in Figure 4.4. Nine different lithofacies have been identified from this outcrop. The

lowermost sandstone facies is directly residing over the uppermost part of Qusaiba Formation. The lowermost units represent the very fine-grained massive bedded sandstone facies (LF 9). The overall thickness of these units is 10 feet. The second package of units has an individual thickness of 2 feet, and is separated by shale interbeds. The facies is recognized as very fine-grained trough cross bedded sandstone (LF 8). The third unit is a purple-colored siltstone facies (LF 7), the individual beds representing this facies have a thickness of 1 foot. The fourth facies is the very fine grained horizontally stratified sandstone facies (LF 6). The beds of this facies range from 1 foot to 1.5 feet in thickness. This fifth facies is a multi-colored siltstone (LF 5). The beds of this facies have a thickness of more than 2 feet. After the siltstone very fine-grained massive bedded sandstone facies are present (LF 4). The seventh facies is a fine-grained hummocky cross-bedded sandstone (LF 3). The thickness of beds representing these facies is about 1 foot. The topmost units are calcareous sandstones divided into two different facies. The lower one is Fine to medium grained calcareous sandstone (LF 2), the topmost is medium to coarse grained bioturbated calcareous sandstone (LF 1). All the sandstone or siltstone beds are separated by shale interbeds of different thickness throughout the outcrop. The stratigraphic column showing lithofacies for outcrop 2 is shown in Fig 4.5.

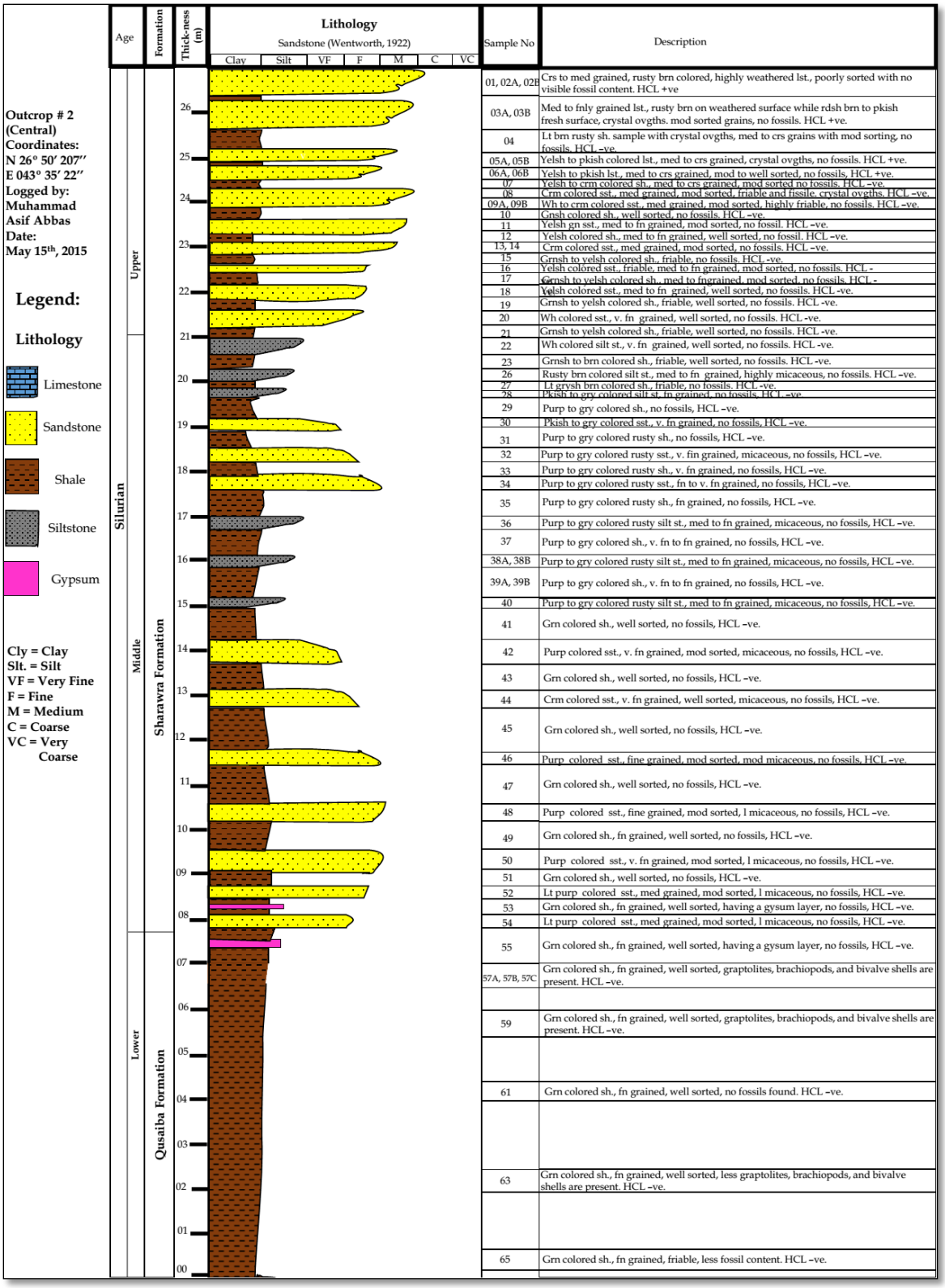

Figure 4.4 Lithological log of outcrop 2 with sample description.

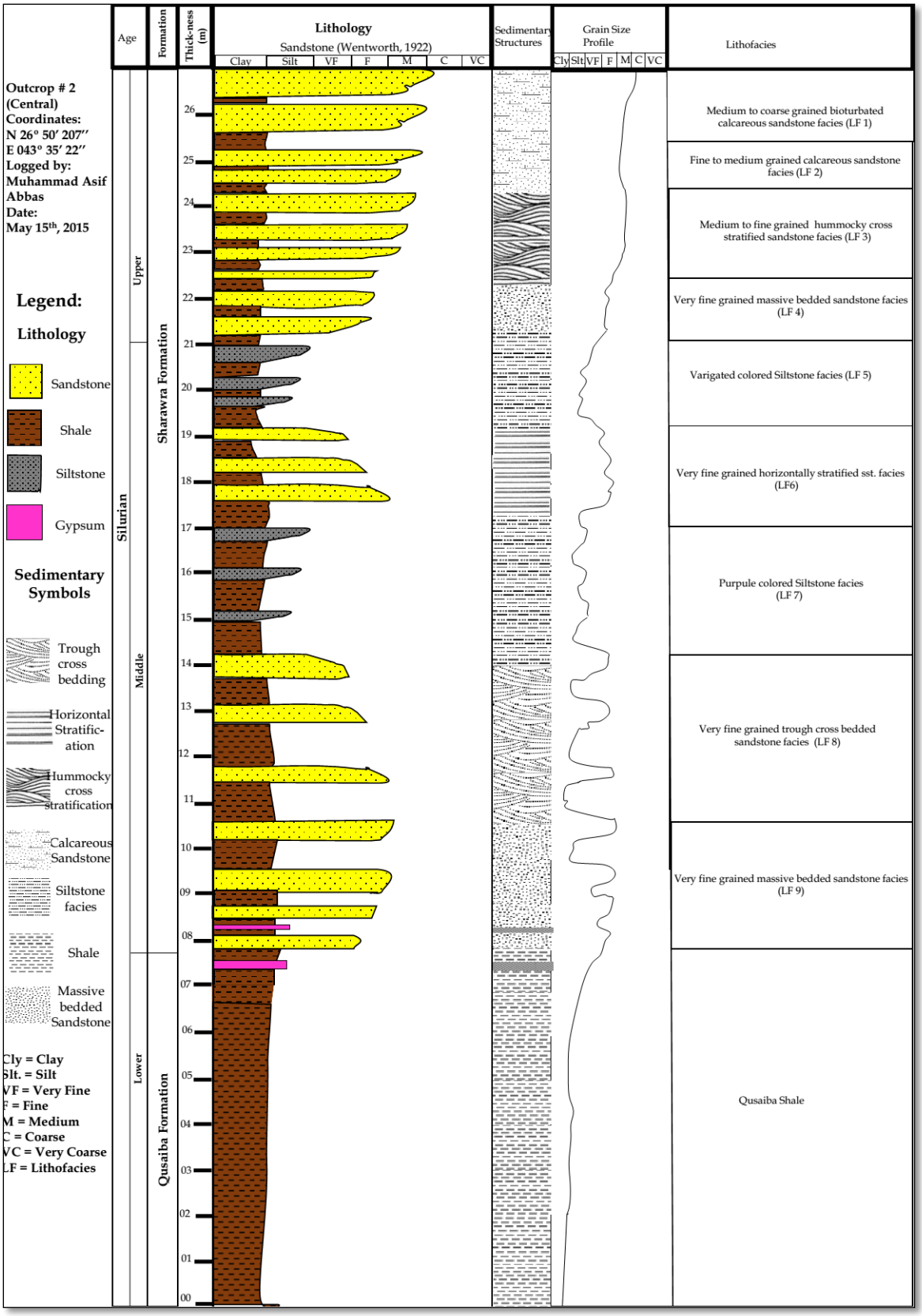
Outcrop # 2 (Central)
Coordinates:
N 26° 50′ 207″
E 043° 35′ 22″
Logged by:
Muhammad Asif Abbas
Date:
May 15th, 2015
Legend:
Lithology
Sandstone
Shale
Siltstone
Gypsum
Sedimentary Symbols
Trough cross bedding
Horizontal Stratific-ation
Hummocky cross stratification
Calcareous Sandstone
Siltstone facies
Shale
Massive bedded Sandstone
Cly = Clay
Slt. = Silt
VF = Very Fine
F = Fine
M = Medium
C = Coarse
VC = Very Coarse
LF = Lithofacies
Age
Formation
Thick-ness (m)
Lithology
Sandstone (Wentworth, 1922)
Clay
Silt
VF
F
M
C
VC
Sedimentary Structures
Grain Size Profile
Cly
Slt
VF
F
M
C
VC
Lithofacies
Silurian
Upper
Middle
Lower
Sharawra Formation
Qusaiba Formation
26
25
24
23
22
21
20
19
18
17
16
15
14
13
12
11
10
09
08
07
06
05
04
03
02
01
00
Medium to coarse grained bioturbated calcareous sandstone facies (LF 1)
Fine to medium grained calcareous sandstone facies (LF 2)
Medium to fine grained hummocky cross stratified sandstone facies (LF 3)
Very fine grained massive bedded sandstone facies (LF 4)
Varigated colored Siltstone facies (LF 5)
Very fine grained horizontally stratified sst. facies (LF6)
Purpule colored Siltstone facies (LF 7)
Very fine grained trough cross bedded sandstone facies (LF 8)
Very fine grained massive bedded sandstone facies (LF 9)
Qusaiba Shale

Figure 4.5 Lithofacies log of outcrop 2

4.1.3 Outcrop 3 (Southeastern)

The outcrop is 55 feet high. Nearly half of the thickness from the base is occupied by the upper part of Qusaiba Formation. Five different lithofacies are resting over the Qusaiba shale. The sequence is complete from LF 9 to LF 5. The whole upper part of the formation is missing here. The lithofacies log for outcrop 3 is shown in Figure 4.6.

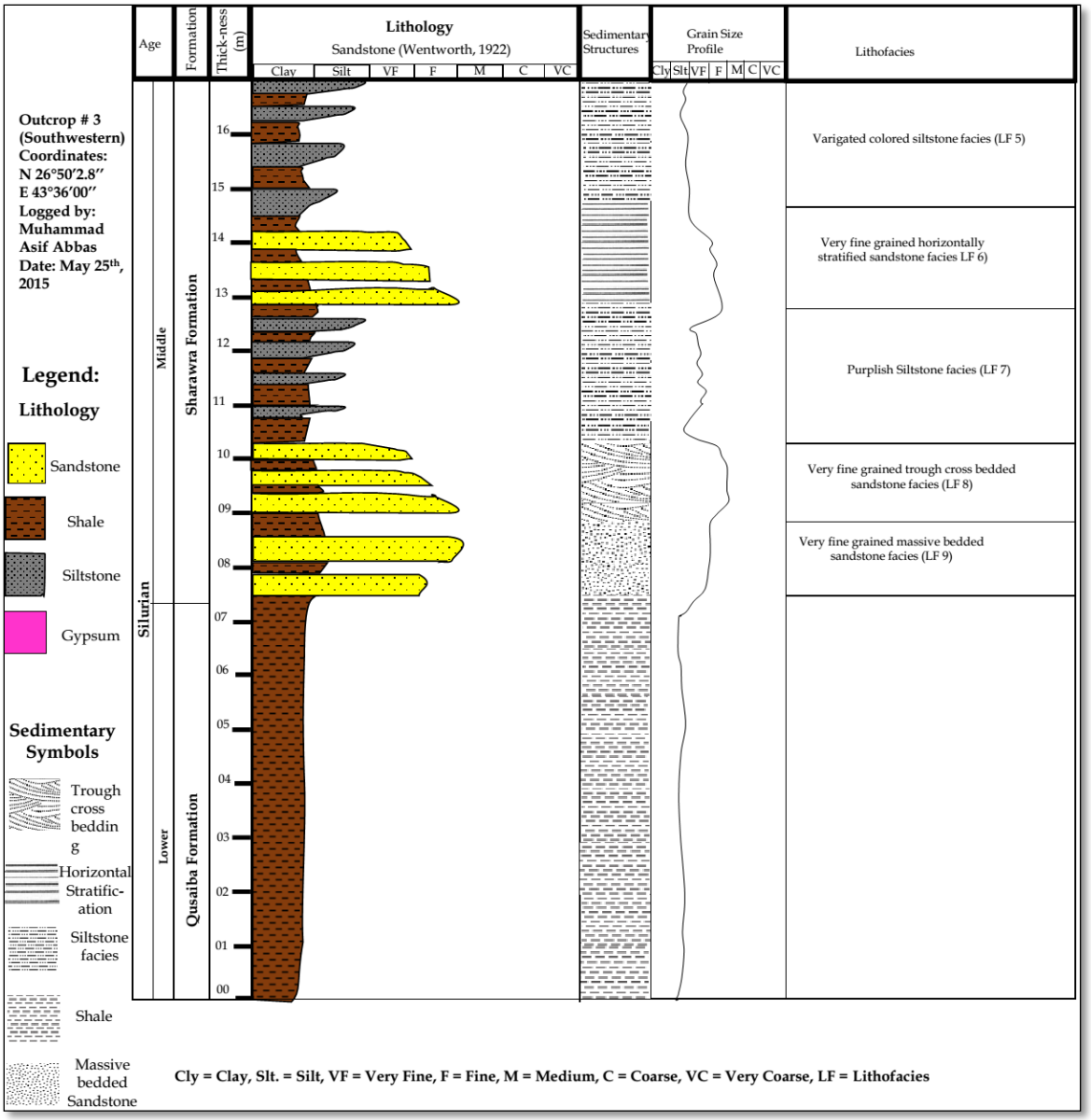

Figure 4.6 Lithofacies log of outcrop 3.

4.2 Facies Correlation

Correlation of the lithofacies is important as it describes the lateral continuity of strata within a region. In Qusaiba village, the maximum thickness of Sharawra Formation has been observed in outcrop 2. Outcrop 2 shows the maximum number of lithofacies observed as compared to all other studied outcrops. Six lithofacies have been identified in

outcrop 1 and five of them were observed in outcrop 3. Correlation chart shows that similar lithofacies have been linked to each other (Figure 4.7). The correlations were performed after acquiring precise information from the optical microscopy. This has been done to accurately determine the grain size, as it is one of the criteria for facies subdivision. The units representing similar lithofacies have more thickness in the northwestern part (outcrop 1) as compared to the units in the central part (outcrop 2) and southwestern part (outcrop 3). The trend is similar as central and southwestern parts are compared. The units in the southwestern part are thinner than the central part. Thus, it is obvious that the thinning of strata is happening from northwestern to the southeastern part of the study area. Most of the upper part of the formation is also missing in the southeastern part. Probably, the upper part of the formation is eroded here. The upper part of the formation has not been observed in the whole southeastern part.

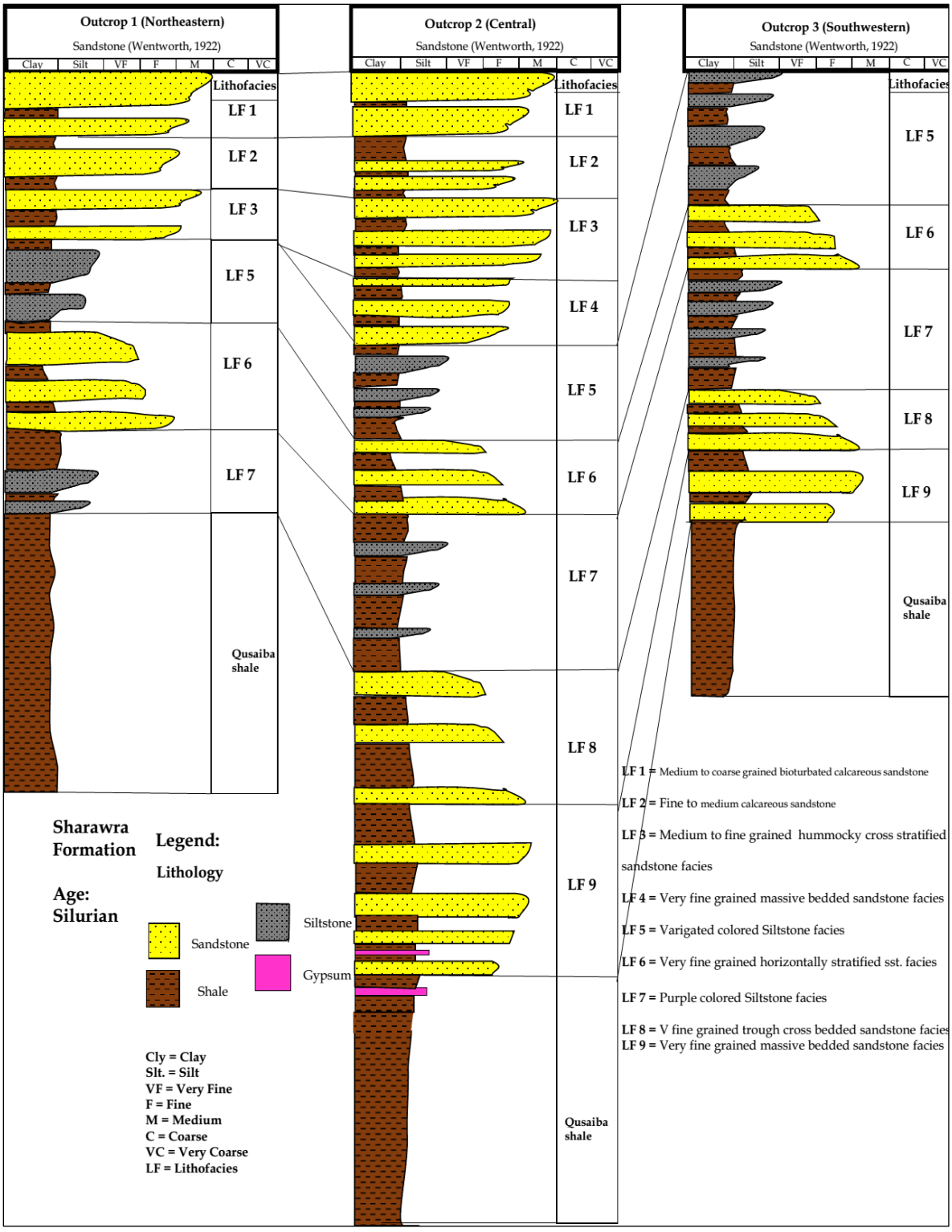

Figure 4.7 Correlation of the lithofacies.

4.3 Field Photographs

Qusaiba village was visited on three occasions for the current research. Logging the Sharawra Formation had been the primary objective. Field photographs were taken throughout the field trips. A reconnaissance trip was carried out to locate possible outcrops for a thorough study. The Silurian succession of Old Qusaiba Village consists of the Sharawra Formation and Qusaiba Formation. Figure 4.8 shows a distant view of the strata in the village. Sampling has been done for the two outcrops, the northwestern and central ones. The southeastern outcrop was studied for the lithofacies and correlation purposes. All necessary samples were taken from the outcrop and their position photographed (Figure 4.9).

The central outcrop was sampled first, as it represented the maximum thickness of the Sharawra Formation in the region. Samples were taken from top to bottom, depending upon their accessibility. The topmost units are the highly calcareous sandstones, overlying the sandstone and shale alternating sequences (Figure 4.10). Figure 4.11 shows a wide view of the central outcrop. Nine lithofacies have been identified from this outcrop. Seven of them have been marked and shown in Figure 4.12. The outcrop has a moderate thickness of beds as compared to other studied outcrops. Shale interbeds are continuously present throughout the outcrop. A gypsum layer has been observed at the bottom of the Sharawra Formation (Figure 4.13). The contact of the Sharawra Formation with the Qusaiba Formation is shown in Figure 4.14. Different sedimentary structures have also been observed in these outrcops. These sedimentary structures are a major parameter in subdividing the lithofacies. Calcareous sandstone facies are shown in

Figures 4.15 and 4.16. Other sandstone lithofacies are shown from Figure 4.17 to Figure 4.21.

Outcrop 2 (northwestern) was explored after the central outcrop. Samples were also taken from this outcrop (Figure 4.22). Six lithofacies were identified from this outcrop. The highly calcareous sandstone facies overlie the sandstone facies. The thickness of individual beds is maximum at this outcrop. The sampling strategy is shown in Figure 4.23. Figure 4.24 shows a distant view of outcrop 3 (southeastern). The beds are thinner here as compared to the other outcrops. The shaly part is more dominant, and almost half of the outcrop is shale (Figure 4.25 and 4.26).

Figure 4.8 Three prominent subdivisions of strata at Old Qusaiba Village.

Figure 4.9 Position of the sample Q3-5-8A.

Figure 4.10 Topmost part of outcrop 2.

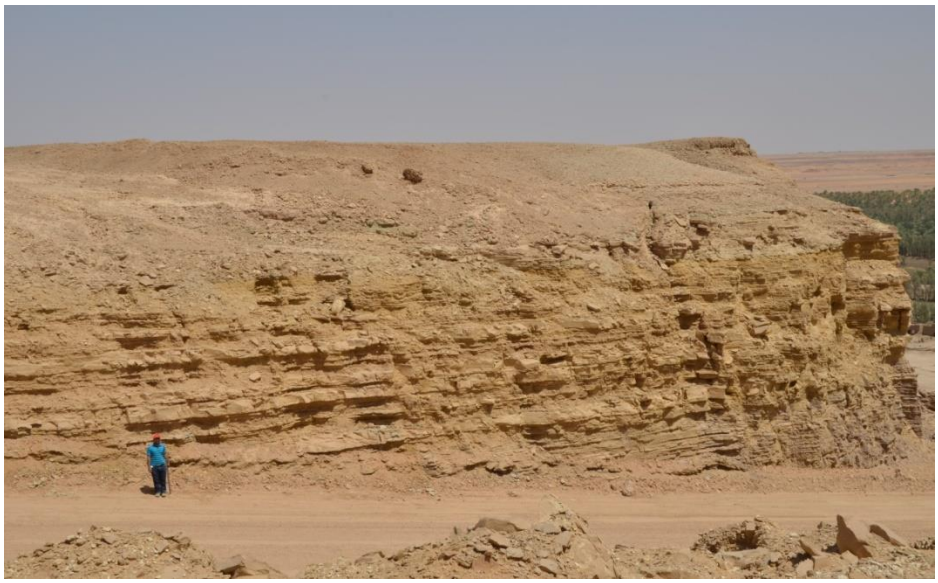

Figure 4.11 Outcrop 2 (central).

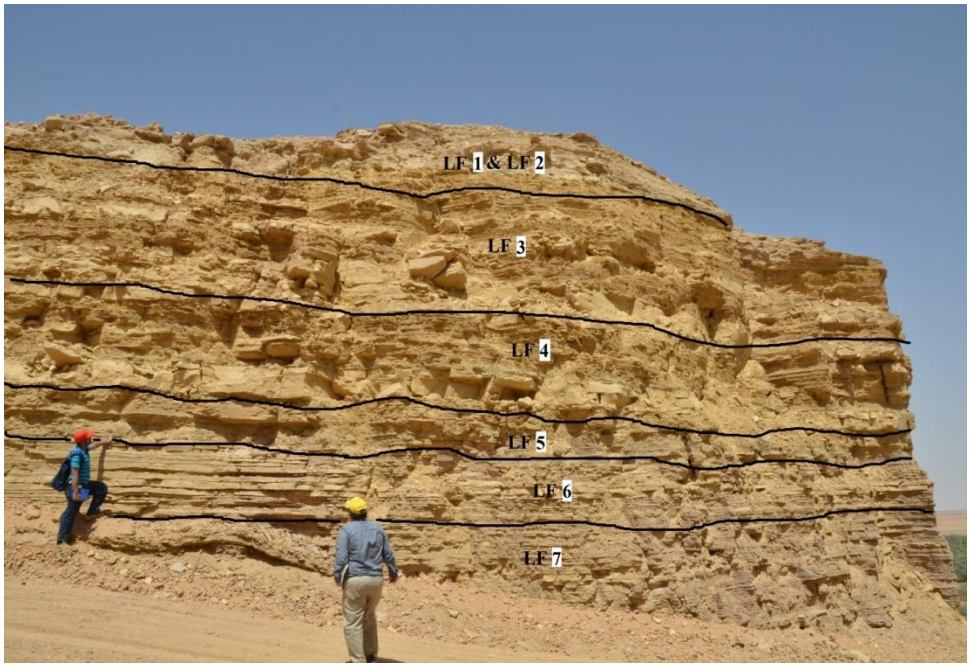

Figure 4.12 Lithofacies observed at outcrop 2.

Figure 4.13 Gypsum layer at the lower boundary of the Sharawra Formation (outcrop 2).

Figure 4.14 Lowermost sandstone unit at outcrop 2, lying above the Qusaiba shale.

Figure 4.15 Topmost calcareous sandstone unit (LF 1).

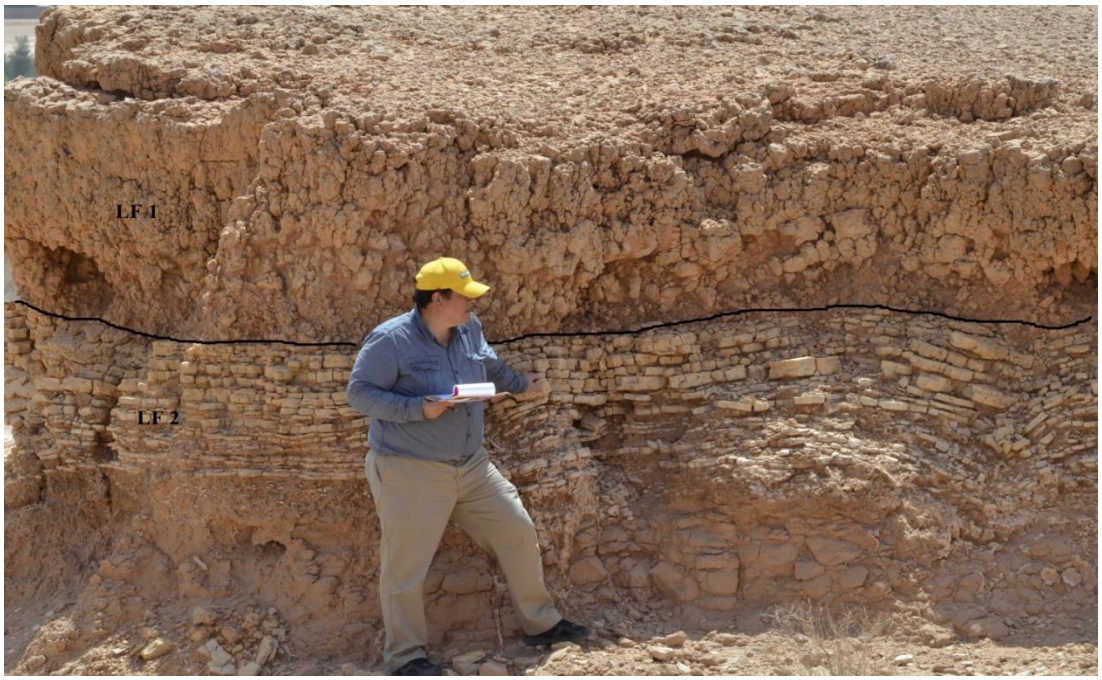

Figure 4.16 Topmost calcareous facies LF 1 and LF 2.

Figure 4.17 Hummocky cross bedded sandstone LF 3.

Figure 4.18 Very fine grained massive sandstone (LF 4).

Figure 4.19 Horizontally stratified sandstone LF 6.

Figure 4.20 Trough cross bedded sandstone LF

Figure 4.21 Basal massive bedded sandstone LF 9.

Figure 4.22 Outcrop 1 (Northwestern).

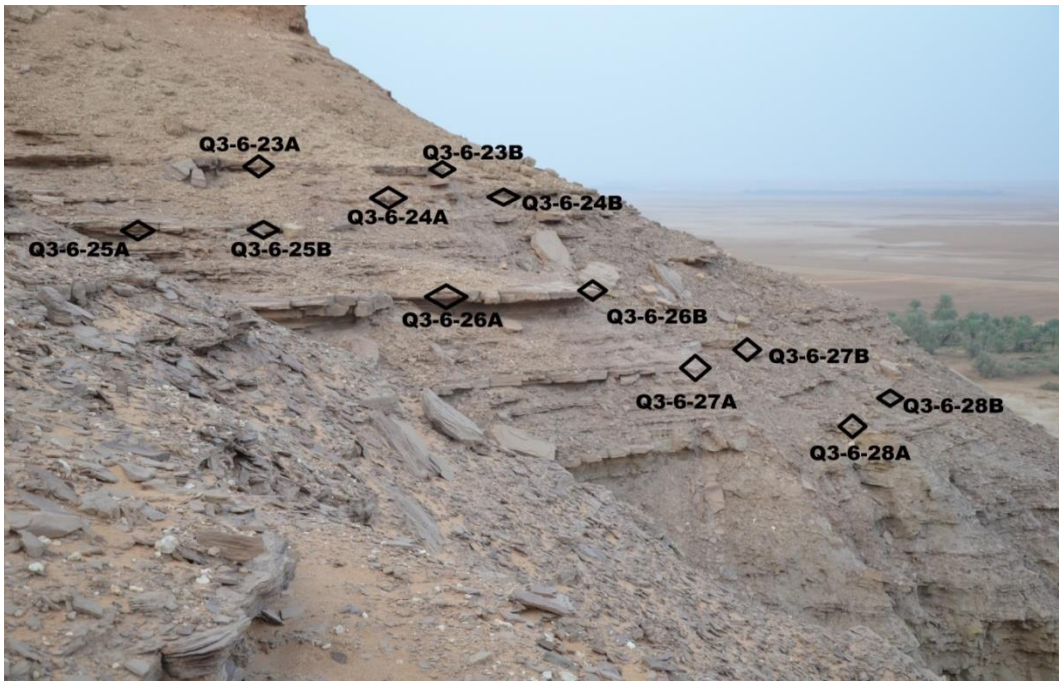

Figure 4.23 Sample locations at outcrop.

Figure 4.24 Outcrop 3 (Southwestern).

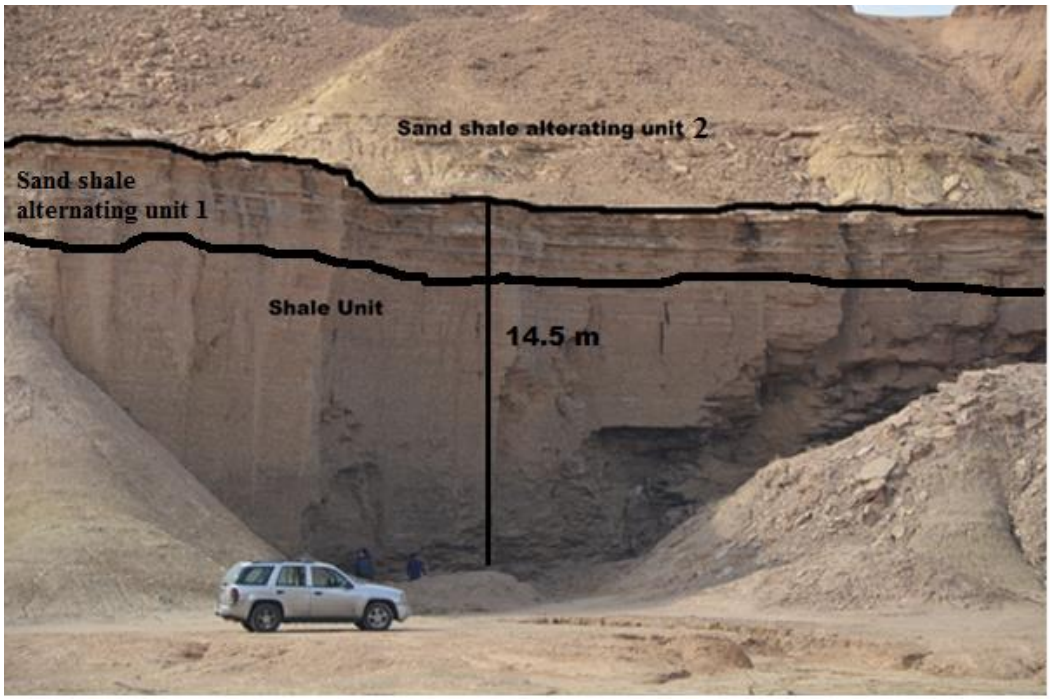

Figure 4.25 Different units at outcrop 3.

Figure 4.26 Measuring the thickness at outcrop 3.

4.4 Sample Description

Collection of samples in the field was followed by describing the samples. Samples were photographed individually (during sample description) with a professional camera (Nikon D7100) under balanced light. Proper scale was used and samples numbers which were visible while taking the photographs. Samples were described on the basis of their color, grain size, texture, fossil content, reaction with hydrochloric acid and any other visible feature.

Around 128 samples were taken from two outcrops. A few of the representative samples from each lithofacies will be described here.

UD-14-03: Medium to fine grained calcareous sandstone, wackestone to packsone, rusty brown on weathered surface while reddish brown to pinkish fresh surface, crystal overgrowths, moderately sorted grains, no visible fossils, HCL positive (Figure 4.27).

UD-14-04: Medium to fine grained calcareous sandstone, wackestone to packsone, light brown colored, crystal overgrowths, moderately sorted grains, no visible fossils, HCL positive (Figure 4.28).

UD-14-05: Medium to fine grained calcareous sandstone, mudstone, yellowish to pinkish brown colored, crystal overgrowths, moderately sorted grains, no visible fossils, HCL positive (Figure 4.29).

UD-14-06: Medium to fine grained calcareous sandstone, mudstone, yellowish to pinkish brown colored, crystal overgrowths, moderately to well sorted grains, no visible fossils, HCL positive (Figure 4.30).

UD-14-08: Medium grained sandstone, cream colored, moderately sorted grains, friable and fissile, no visible fossils, HCL negative (Figure 4.31).

UD-14-14: Medium grained sandstone, cream colored, moderately sorted grains, no visible fossils, HCL negative (Figure 4.32).

UD-14-18: Medium grained sandstone, yellowish colored, well sorted grains, no visible fossils, HCL negative (Figure 4.33).

UD-14-22: Very fine grained siltstone, white colored, well sorted grains, no visible fossils, HCL negative (Figure 4.34).

UD-14-30: Very fine grained sandstone, pinkish to grayish colored, no visible fossils, HCL negative (Figure 4.35).

UD-14-32: Very fine grained sandstone, purple to grayish colored, micaceous, no visible fossils, HCL negative (Figure 4.36).

UD-14-34: Very fine to fine grained sandstone, purple to grayish colored, micaceous, no visible fossils, HCL negative (Figure 4.37).

UD-14-38: Very fine grained siltstone, purple to grayish colored, micaceous, no visible fossils, HCL negative (Figure 4.38).

UD-14-40: Very fine grained siltstone, purple to grayish colored, micaceous, no visible fossils, HCL negative (Figure 4.39).

UD-14-44: Very fine grained sandstone, light brown colored, moderately sorted, micaceous, no visible fossils, HCL negative (Figure 4.40).

UD-14-46: Very fine grained sandstone, light purple colored, moderately sorted, micaceous, no visible fossils, HCL negative (Figure 4.41).

UD-14-54: Very fine grained sandstone, light purple colored, moderately sorted, micaceous, no visible fossils, HCL negative (Figure 4.42).

UD-14-57: Very fine grained shale, greenish colored, graptolitic, bivalve shells, well sorted, HCL negative (Figure 4.43).

Sampling has been done for the two outcrops, the northwestern and central outcrop.

Figure 4.27 Sample UD-14-03 representing LF 1.

Figure 4.28 Sample UD-14-04 representing LF 1.

Figure 4.29 Sample UD-14-05 representing LF 2.

Figure 4.30 Sample UD-14-06 representing LF 2.

Figure 4.31 Sample UD-14-08 representing LF3.

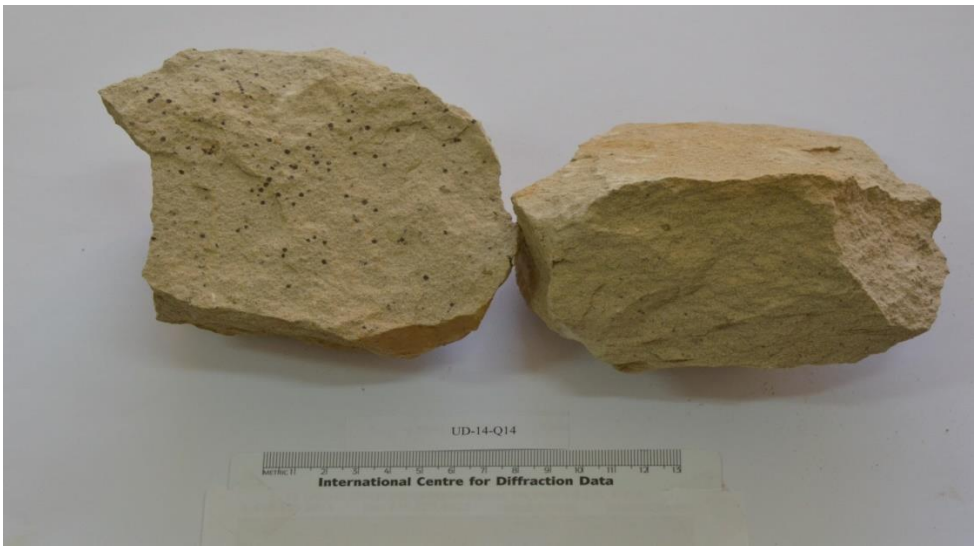

Figure 4.32 Sample UD-14-14 representing LF 4.

Figure 4.33 Sample UD-14-18 representing LF 4.

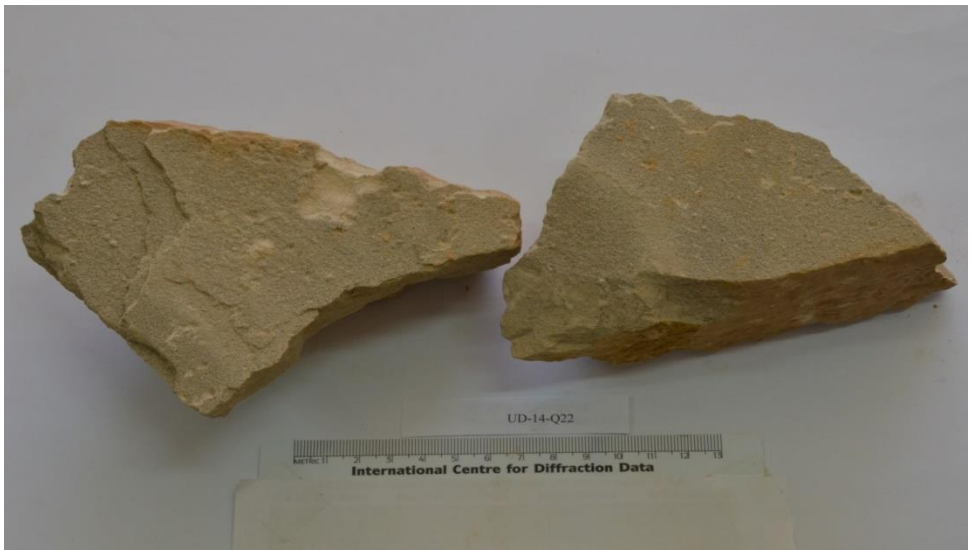

Figure 4.34 Sample UD-14-22 representing LF 5.

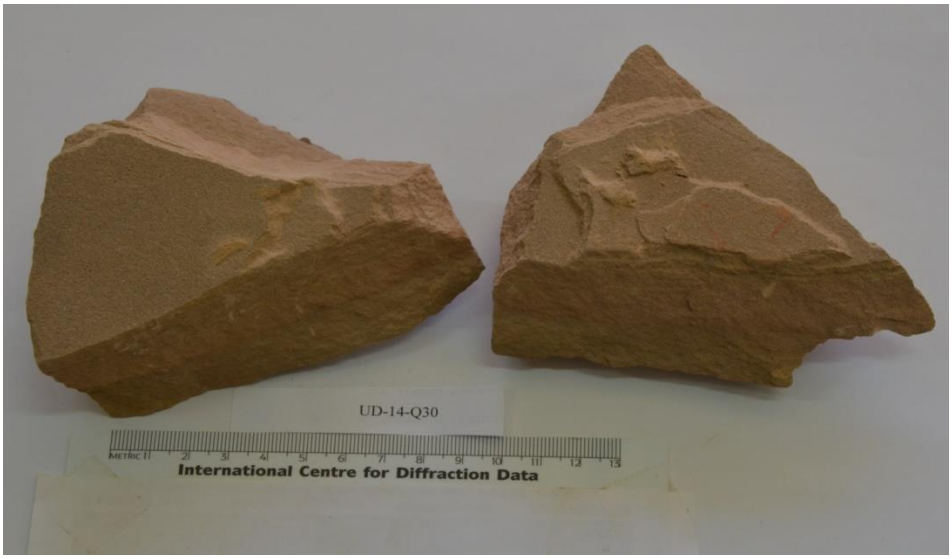

Figure 4.35 Sample UD-14-30 representing LF 6.

Figure 4.36 Sample UD-14-32 representing LF 6.

Figure 4.37 Sample UD-14-34 representing LF 6.

Figure 4.38 Sample UD-14-38 representing LF 7.

Figure 4.39 Sample UD-14-40 representing LF 7.

Figure 4.40 Sample UD-14-44 representing LF 8.

Figure 4.41 Sample UD-14-46 representing LF 8.

Figure 4.42 Sample UD-14-54 representing LF 9.

Figure 4.43 Sample UD-14-57 representing Qusaiba shale.

CHAPTER 5

RESULTS AND DISCUSSIONS-PETROGRAPHY

5.1 Sandstone Petrography

Fifty four (54) samples out of 128 samples were selected for thin section petrography. The samples were selected from all the feasible locations from the northwestern and the central outcrop. The 128 samples collected from the outcrops also contained a good number of shale samples. Thin sections were made for all the sandstone samples. For the classification of sandstones, the famous ternary diagram has been used. Folks, (1959); Freidman and Sanderson, (1978); Pettijhon et al., (1987); and Tucker, (1991) use ternary classification based on the percentage of quartz, feldspar and rock fragments. The primary way to classify the sandstone is the triangular classification or the point count. The sandstone of the Sharawra Formation is classified as subarkosic sandstone by using the Folks (1974) classification chart (Figure 5.1).

5.1.1 Calcareous Sandstone Facies Petrography

The top of the Sharawra Formation consists of calcareous sandstone units. The calcareous sandstones thin sections revealed the sandy nature of this sandstone, containing abundant quartz grains in the topmost facies. Microfractures have been observed in this facies (Figure 5.2), however permeability is poor (Figure 5.3). Figure (5.4) is a true representative of LF 1. The quartz grains observed in these thin sections were mostly subrounded (Figure 5.5) and poorly sorted (Figure 5.6). Ostracods have also been observed (Figure 5.7). The other lithofacies observed from the calcareous section is fine

to medium grained calcareous sandstone (Figure 5.8). Quartz grains are rarely present in this facies, and they are poorly sorted (Figure 5.9).

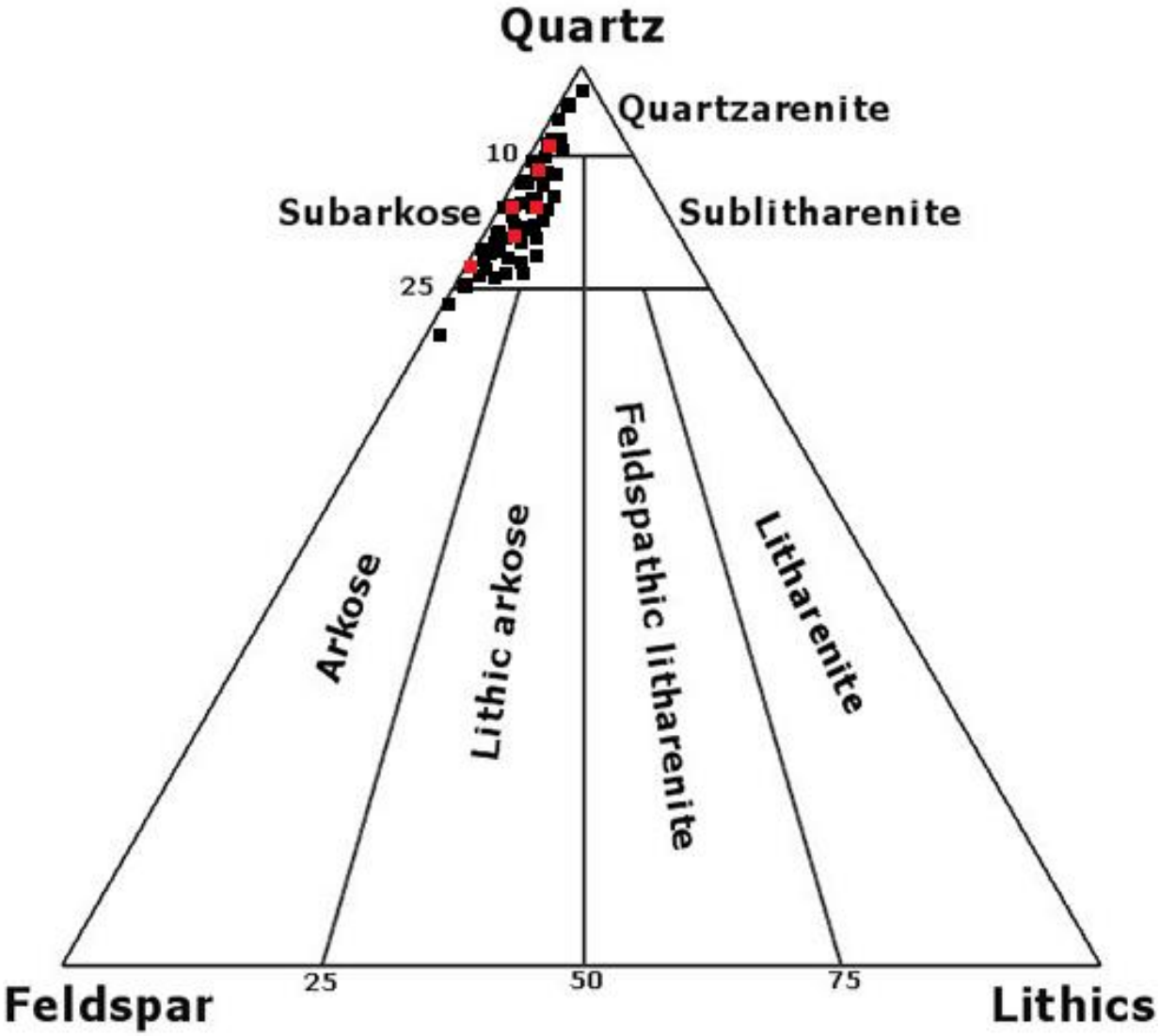

Figure 5.1 Classification of sandstone on the basis of quartz, feldspar and lithic fragment (QFL) components (Folks, 1974).

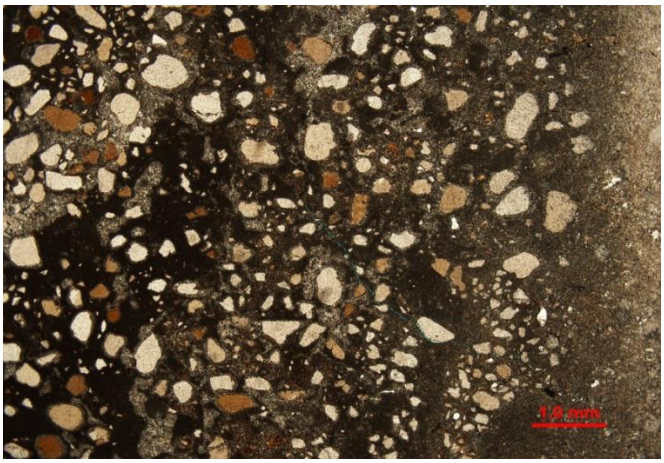

Figure 5.2 Micro-porosity in sand calcareous sandstone facies LF 1.

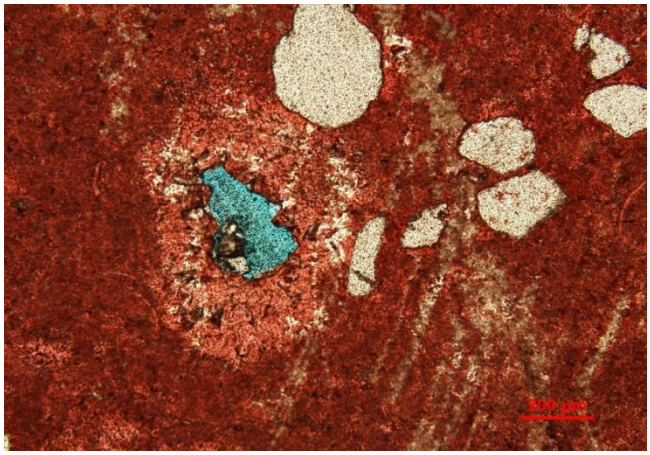

Figure 5.3 Zero permeability in LF 1.

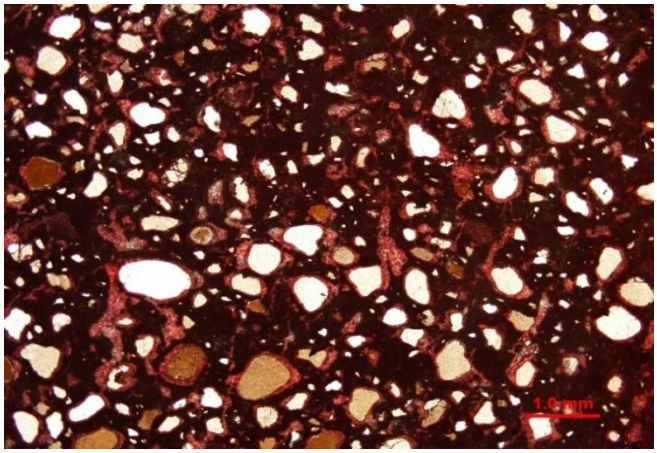

Figure 5.4 Medium to coarse grained bioturbated calcareous sandstone facies LF 1.

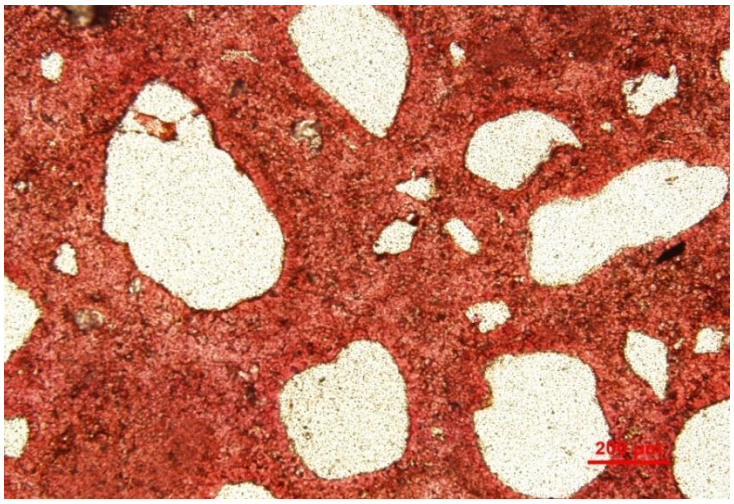

Figure 5.5 Subrounded quartz in LF 1.

Figure 5.6 Poorly sorted quartz grain in calcareous sandstone facies.

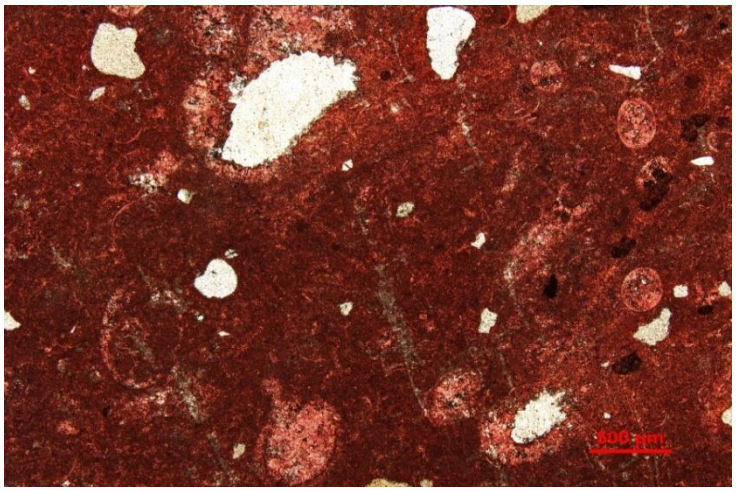

Figure 5.7 Ostracods in LF 1.

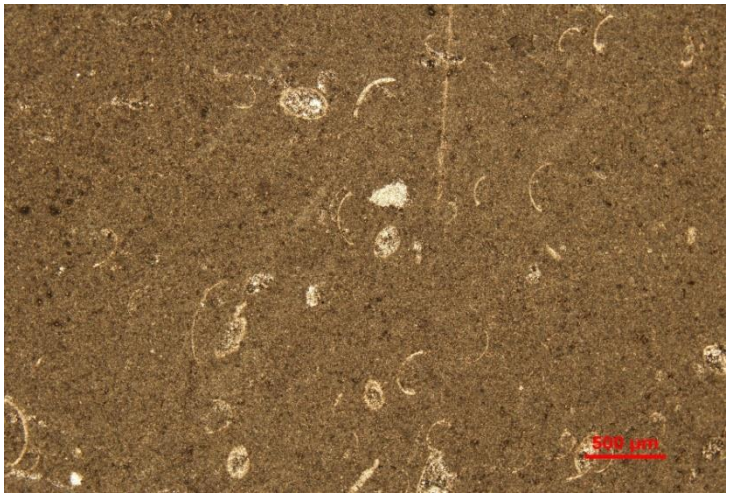

Figure 5.8 Mud dominated facies with skeletal gains LF 2.

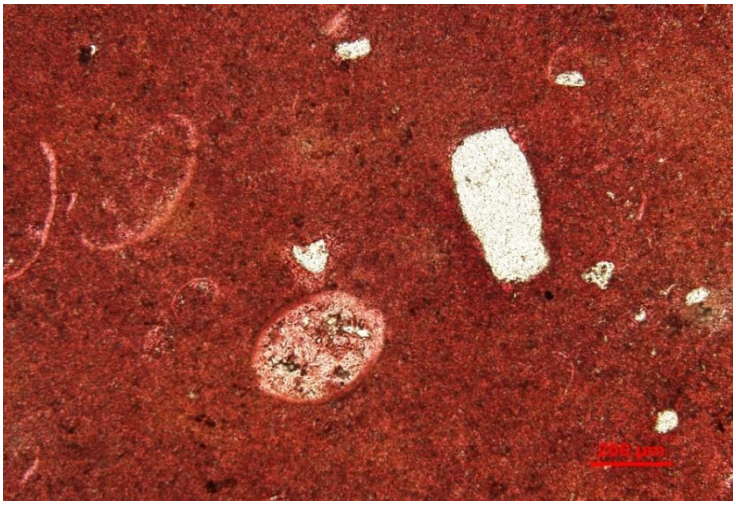

Figure 5.9 Minor quartz in mud dominated skeletal facies LF 2.

5.1.2 Subarkosic Sandstone

Thin sections were analyzed under the optical microscope at different magnifications. Thin section petrography of 54 sandstone and siltstone samples shows that all of them are composed of arkoses; most of the quartz is monocrystalline (around 90 percent). The polycrystalline quartz is around 10 percent. Sorting of arkoses ranges from moderately sorted to well sorted. The amount of feldspar is low and it ranges from 3 to 7 percent

throughout the sections. Iron oxide and clay minerals have been observed as cement. The ambiguities of these minerals acting as cement has been revealed and confirmed by SEM-EDS results. The iron oxide cement is more dominant in the lower part of Sharawra Formation; however, it is present throughout the formation. The clay cement is less dominant in the top three identified lithofacies, and is present as pore fillings and pore linings in the remaining lower units of Sharawra Formation. Grain contact varies from the lower part to the top. At the basal beds the contact is longitudinal; most of the grain contacts are concave-o-convex (Figure 5.10), while it becomes point contact at the top. Most of the grains (about 90 percent) show low sphericity, and are sub angular to sub rounded. The extinction is mostly non-undulose, especially in the basal part, while some grains show wavy extinction at the top beds.

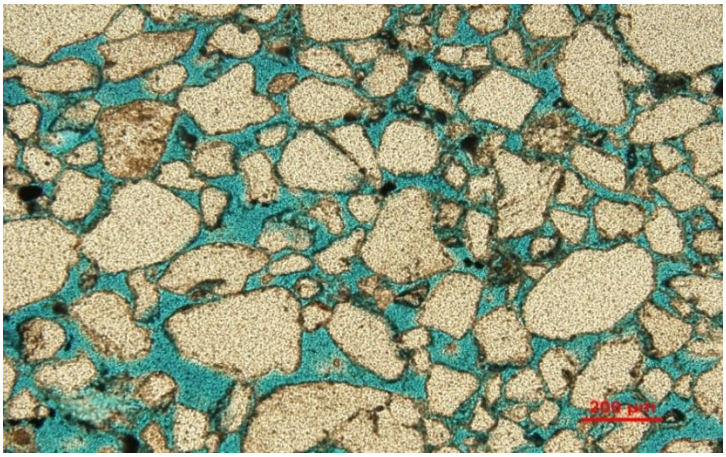

Figure 5.10 Concave-o-convex contacts of quartz grains LF 8.

5.2 Thin Section Petrography

The thin section petrography of the Sharawra Formation ranges from the very fine grained to silt size at the base, silt to fine grained in the middle, and medium grained at

the top. It shows that the facies is dominantly very fine to medium grain size quartz rich sandstone. The observed grains are sub-angular to sub-round in most cases. In rare cases the grains have been found as angular or rounded.

5.2.1 Quantitative Mineralogy

From the optical microscopy analysis of the sandstone and siltstone samples of the Sharawra Formation, it is evident that the Formation is dominantly composed of quartz and in small percentage of clay minerals, mica and a small amount of feldspar. The results have been confirmed by XRD analysis that has been performed for representative samples from each lithofacies.

5.2.2 Quartz

The most common mineral in the siliciclastic rocks is the quartz; my detailed thin section study has also revealed that quartz is the dominant mineral of the Sharawra Formation. Quartz is distinguished in the thin section due to its clear color, grey birefringence, its surface can have fractures but no cleavage. As shown in the QFL diagram (Figure 5.1), the quartz percentage is high. Involving the percentage of mica, which ranges from 2 to 22 percent, reduces the percentage of quartz. Two different types of quartz have been identified namely monocrystalline quartz and polycrystalline quartz (Figure 5.11). The monocrytalline quartz is dominant over the cryptocrystalline quartz. About 90 percent of the quartz is monocrystalline.

The origin of the polycrystalline quartz is the metamorphic rocks of the Arabian shield while the monocrystalline quartz exhibits straight extinction. Quartz overgrowth is

observed in some of the samples. The porosity and permeability are greatly affected by this overgrowth.

The quartz grains ranging from moderately sorted to well sorted; however poorly sorted quartz grains have been observed in a few samples (Figure 5.12). Different types of sorting observed in different lithofacies can be seen in Figures 5.13 to 5.15. Also, the shapes of the grains is ranging from sub-angular to sub-rounded (Figure 5.16) and in some cases it is angular. Heavy minerals have not been observed in any of the thin sections.

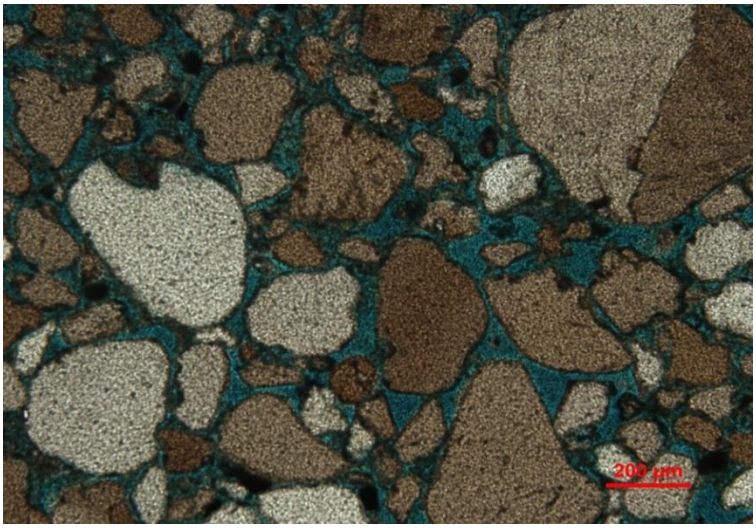

Figure 5.11 Polycrystalline quartz LF 8.

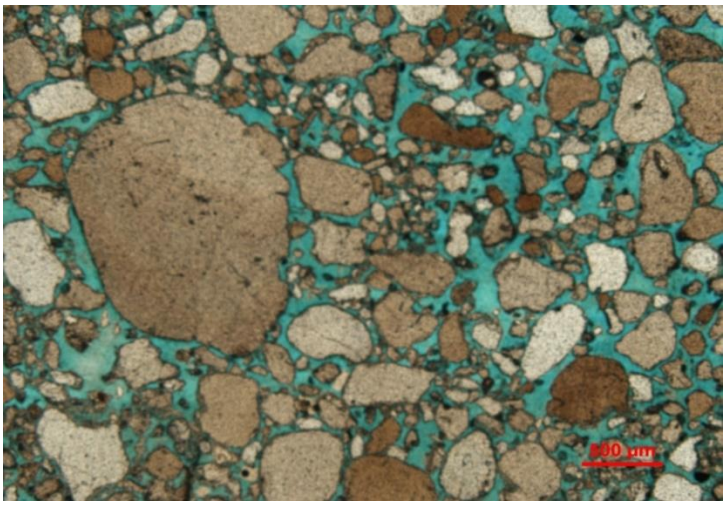

Figure 5.12 Poorly sorted sandstone LF 3.

Figure 5.13 Moderately sorted quartz gains, with mica and iron oxide LF 7.

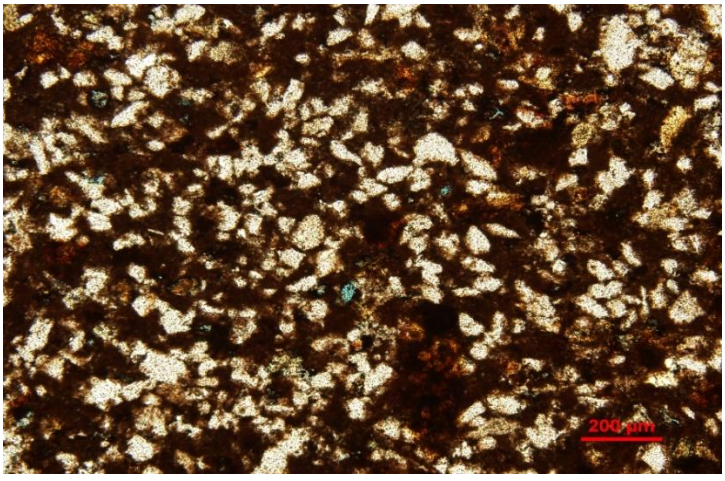

Figure 5.14 Moderately well sorted quartz grains (LF 6).

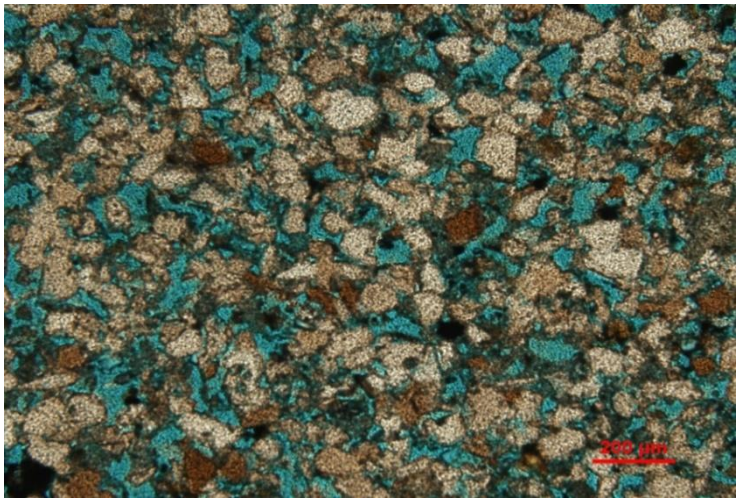

Figure 5.15 Moderately well sorted quartz grains LF 4.

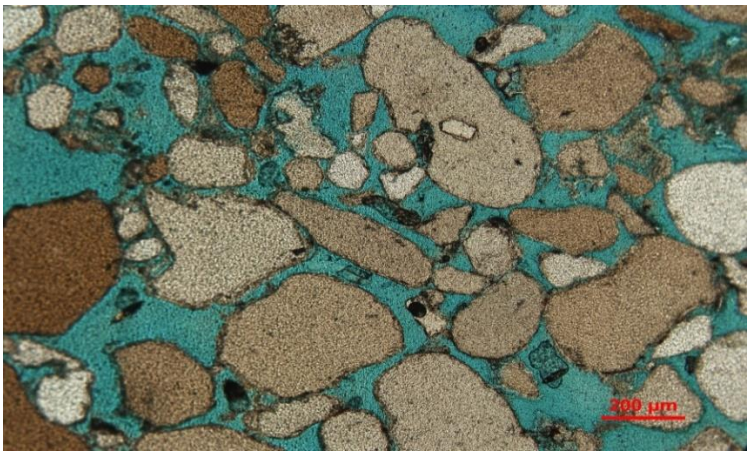

Figure 5.16 Medium grained, sub angular to sub rounded grains (LF3).

5.2.3 Feldspar

The percentage of feldspar is very low in the observed sandstone and siltstone samples of the Sharawra Formation. The feldspar percentage ranges from 2-5 %. Very minute percentages of albite, and microcline have been observed. Twinning is the distinguishing character for the feldspar. The feldspar species can be identified on the basis of the type of twinning. Most of the observed grains are altered and rugged, and alteration is clearly noticed. Feldspar is less stable as compared to quartz, because of its

low mechanical stability. This can help to infer that the sandstone has travelled a long distance. On the other hand, chemical alteration of feldspar can also occur, in which the chemical alteration of feldspar typically involves replacement of clay such as kaolinite and chlorite under certain condition. This alteration is responsible for the development of secondary porosity (Tucker, 2005).

5.2.4 Lithic Fragments

Lithic fragments were almost missing throughout the sections except a small piece of a fragment found in one of the samples. The origin of fragments is most probably the Arabian shield.

5.2.5 Iron Oxide

Iron oxide cement is present almost throughout the section. The concentration of iron oxide cement is higher at the basal part of the Sharawra Formation as compared to the upper part. The topmost sandstone facies is devoid of iron oxide, calcite and quartz overgrowths were observed in the topmost sandstone facies (Figures 5.17 & 5.18). Cement is dominantly present almost in all samples, it is also revealed by the SEM_EDX results. Small spots of iron oxide are observed in thin section of Sharawra Formation samples. Iron oxide is one of the autogenic minerals and it acts often as grain coatings. XRD data has not revealed any iron oxide mineral, which proves the nature of the iron oxide to be is amorphous. The permeability and porosity is reduced due to iron oxide, as it fills the pores. Iron oxide concentration is variable throughout the six basal lithofacies, iron oxide concentration for the two different facies is shown in Figures 5.19 and 5.20.

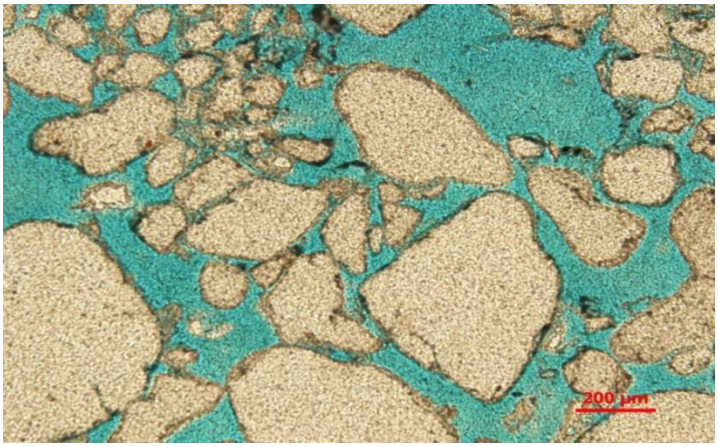

Figure 5.17 Quartz coated with calcite cement (LF3).

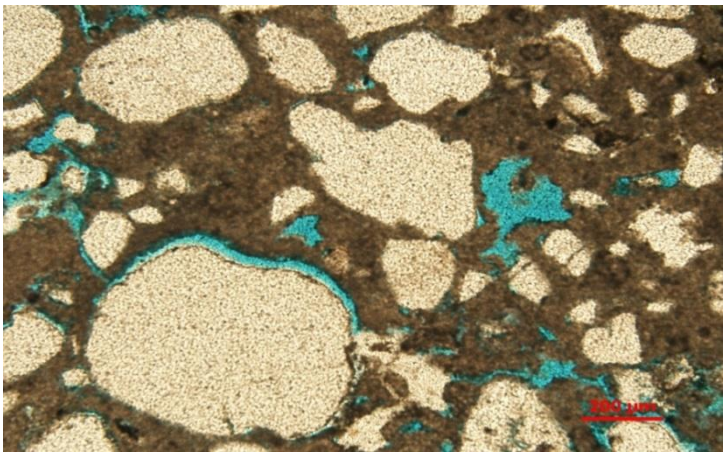

Figure 5.18 Calcite filling the pores, resulting in porosity reduction (LF3).

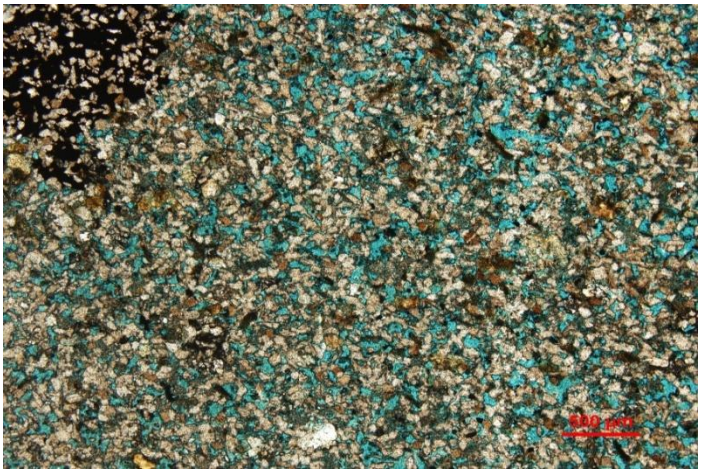

Figure 5.19 Iron oxide patches (LF 4).

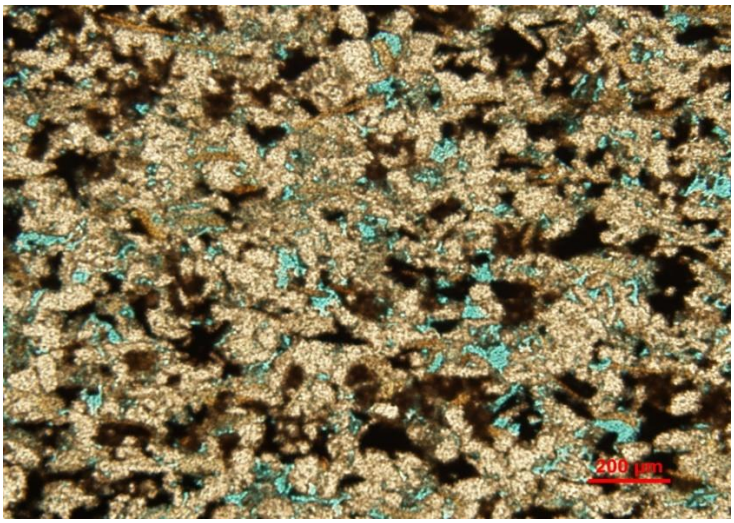

Figure 5.20 High content of iron oxide (LF 8).

5.2.6 Clay Minerals

The Sharawra Formation contains authigenic clays. The authigenic clays develop subsequent to burial and include both new and regenerated forms. SEM-EDS is not the most reliable technique for clay mineral investigations for the outcrop samples. It is more reliable for the subsurface samples, where the structure of clays is well preserved. Moreover, the detrital clays are almost impossible to be distinguished under SEM. Certain clay types appear in distinctive shapes under the SEM-EDS if their structure is well preserved. In this study, SEM-EDS was able to reveal that the most dominating clays found in the Sharawra Formation is kaolinite. Kaolinite has a booklet structure, and is visible easily in few of the sandstone samples. The amount and type of clay has a great impact on the petrophysical properties of a rock. The individual pseudo-hexagonal stacked plates are about 3.20 micrometer. The clay minerals in the Sharawra Formation are present as pore linings as well as grain coatings.. Here, in most of the samples, kaolinite acts as a pore lining mineral, and is formed prior to the clay grain coatings (Figure 5.21) or silica coating. Kaolinite is present throughout the sections and are

derived from the leaching of pre-existing feldspar or mica (Chamley, 1989). XRD data showed the presence of other types of clays. These include illite, dickite,polygorskite. All of these clays are present in the middle and lower lithofacies of Sharawra Formation. Their presence is not continuous like kaolinite.

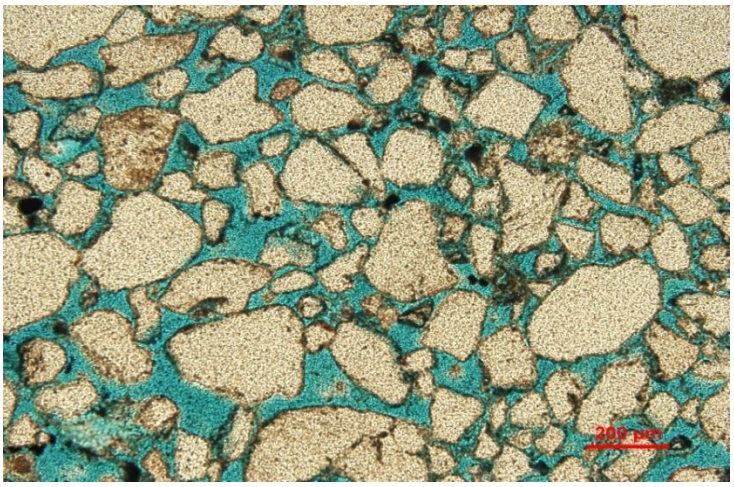

Figure 5.21Clay cemented sandstone (LF 8).

5.2.7 Mica

An appreciable amount of mica is observed in the samples of Sharawra Formation. Only in few sample some mica flags were noticed. Mica is a phyllo-silicate mineral identified in the Sharawra Formation sandstone. Mica is easily washed away from coarse grained sediments and accumulates in fine sand or silt, and it is more prone to weathering. XRD data also revealed the presence of muscovite in the lower and middle part of Sharawra Formation. Figures 5.22 and 5.23 show the presence of mica in thin section.

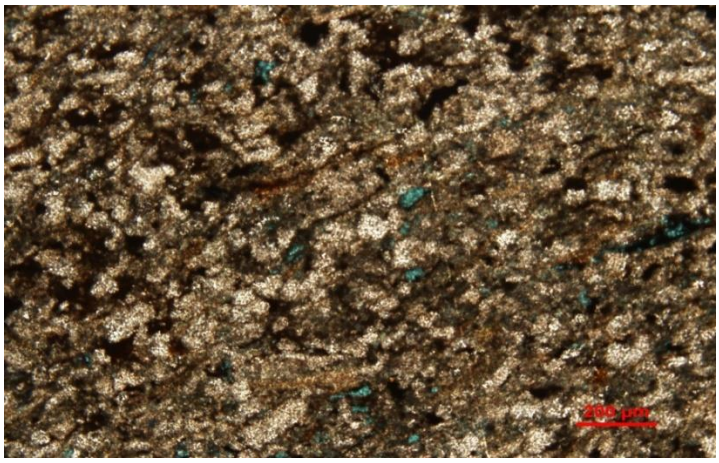

Figure 5.22 Higher mica content with low porosity (LF 9).

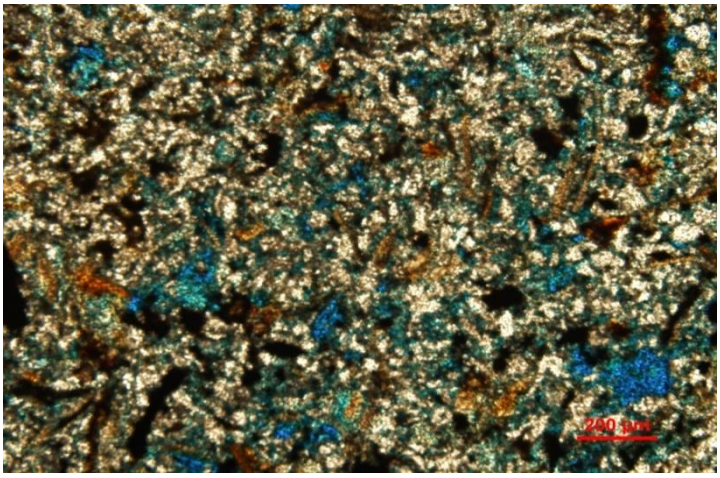

Figure 5.23 Iron oxide patches and mica in LF 5.

5.2.8 Matrix

Matrix is almost negligible in these samples. It is much less than 5% on average. The high percentage of quartz and low percentage of matrix and feldspar indicate the maturity of the Sharawra Sandstone samples. The low matrix concentration is favorable for the reservoir quality, as matrix can obstruct pore connectivity leading to decrease the porosity.

5.2.9 Cement

Four different types of cement have been observed in Sharawra Formation. Iron oxide acts as a cement more at the basal parts of sections, its presence decreases in the middle part and vanishes at the top. Clay cement is also present variably throughout the Formation. The silica (Quartz overgrowth) cement is also present and acts as the grain coating over the quartz in many of the sandstone and siltstone at the middle and top parts of the sections. Calcite is also present as cement in the topmost calcareous sandstone samples.

5.2.10 Visible Porosity

The visible porosity is variable throughout the sections. It is negligible for the calcareous sandstone facies at the top of the formation, which has a high percentage of matrix. The visible porosity ranges from 2 to 7 % at the basal fine grained sandstone facies. The porosity values are higher for the siltstone facies and range from 17 to 25 %. The sandstone facies overlying the siltstones also have good visible porosity ranging from 13 to 22 %. The topmost medium grained sandstones show a prominent decrease in visible porosity which ranges from 2 to 5 %. Detailed thin section petrography results have been summed up in Tables 1 to 8. Visual porosity values have also been listed for each sample. Visible porosity for different lithofacies have been shown in thin section photographs (Figures 5.24 to 5.27).

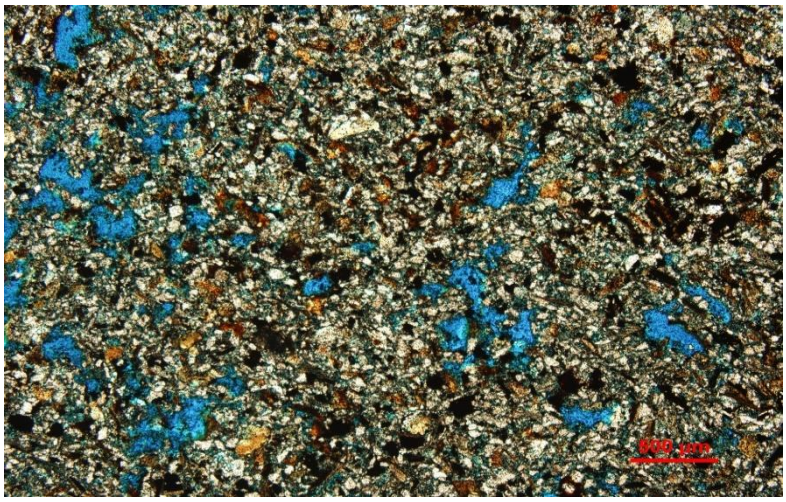

Figure 5.24 Visible porosity with no low pore connectivity (low permeability) LF 5.

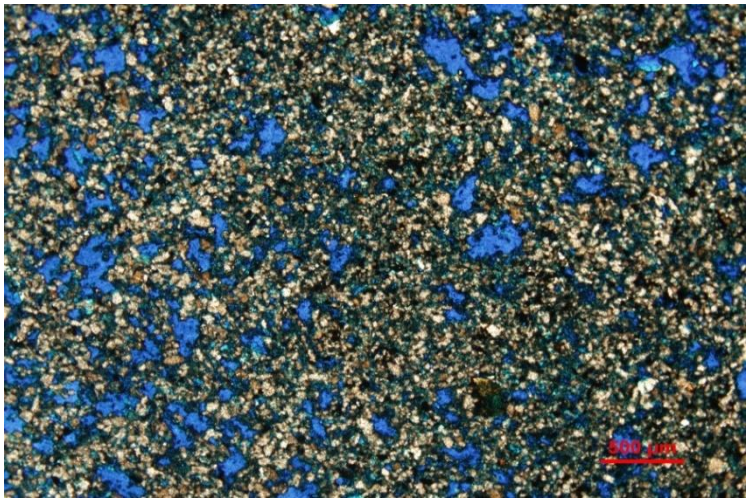

Figure 5.25 Good porosity and permeability at the bottom part of LF 6.

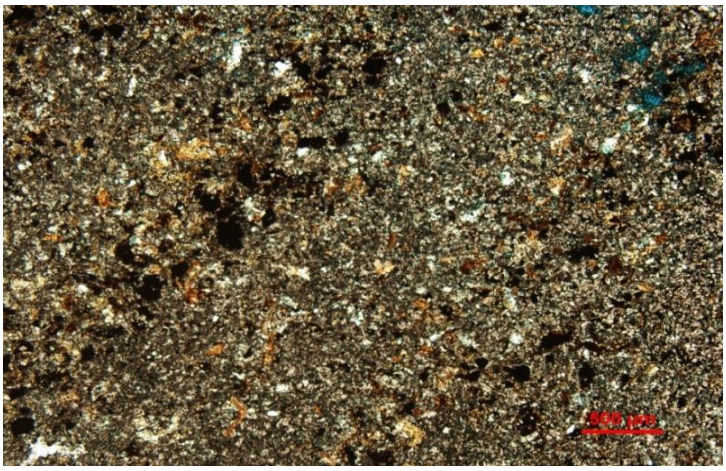

Figure 5.26 Almost negligible porosity at the top of LF 6.

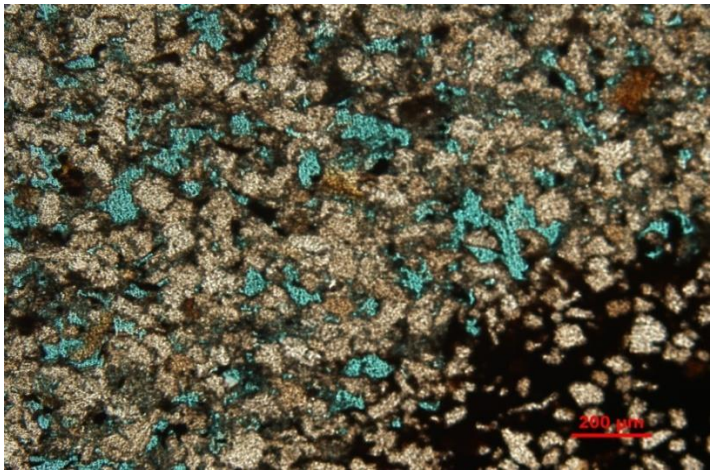

Figure 5.27 Good porosity with poor pore connectivity LF 9.

Table 5.1 Optical microscopy result for LF 3 samples.

Sample No.	Mineral Composition %				Texture				Porosity	Cement	Extinction Type	Comments
	Quartz	Feldspar	Mica	Rock Fragments	Grain Size	Grain Sorting	Grain Contact	Grain Shape				
UD-14-07	93	-	7	-	0.25 mm	Moderat-ely well Sorted	Point and Longitudnal	Angular	3	Calcite	Undulose/ Wavy	Equal amount of poly and mono crystalline quartz
UD-14-08A	95	2	2	1	.15 to .45 mm	Moderat-ely Sorted	Point and Longitudnal	Sub-ang to Sub- round, High Sphericity	10-12	Calcite	Mostly Unundulos e	Less fractured quartz, vacuoles, reminent feldspar
UD-14-09A	98	1		1	0.15 – 0.5 mm	Moderat-ely well Sorted	Sutured + Concave o Convex	Sub –round, Low Sphereicity	3-5	calcite	Undulose/ Wavy	Less fractured quartz, reminent feldspar
UD-14-9B	70	-	35	-	0.12 – 0.55 mm	Mod to poorly sorted	Point	Sub round – rounded, High Spheri	5	calcite	Mostly Unundulos e	Less fractured quartz, mostly mono crystalline

Table 5.2 Optical microscopy results for upper part of LF 4 samples.

Sample No.	Mineral Composition				Texture				Porosity	Cement	Extinction Type	Comments
	Quartz	Feldspar	Mica	Rock Fragments	Grain Size	Grain Sorting	Grain Contact	Grain Shape				
UD-14-10	70	1	25		0.03-0.11 mm	Well Sorted	Point and Longitudinal	Angular, Low Sphereicity	5	clays	Ununduluse	Some fractured quartz
UD-14-11	63	3	24		0.02-0.1 mm	Well Sorted	Sutured Contact	Sub- round, Low Sphericity	1	Iron oxide, clays	Ununduluse	Mostly mono
UD-14-12	90	2	8	-	0.02-0.08 mm	Moderately Sorted	Concave o Convex	Sub-ang to Sub- round, Low Sphericity	?	Iron oxide, clays	Ununduluse	-
UD-14-13	80	2	12		.02 to .1 mm	well Sorted	Concave o Convex	Sub-ang, Mod Sphericity	13	Iron oxide, clays	Mostly Ununduluse	Mostly mono crystalline quartz, Feldspar reminents
UD-14-14	85		14		.03 to .12 mm	Moderately well Sorted	Sutured + Concave o Convex	Sub-ang to Sub- round, Low Sphericity	13	Iron oxide, clays	Ununduluse	-
UD-14-16	82	2	15		0.02 – 0.12 mm	Moderately well Sorted	Sutured + Concave o Convex	Sub-ang, Low Sphericity	13-15	Iron oxide, clays	Mostly Ununduluse	Mostly mono crystalline quartz, Feldspar reminents

Table 5.3 Optical microscopy results for LF 4 and LF 5 samples.

Sample No.	Mineral Composition				Texture				Porosity	Cement	Extinction Type	Comments
	Quartz	Feldspar	Mica	Rock Fragments	Grain Size	Grain Sorting	Grain Contact	Grain Shape				
UD-14-17	80	4	12		0.06-0.1 mm	Well Sorted	Concave o Convex	Sub-ang to Sub- round, Low Sphericity	3	Iron oxide, clays	Ununduluse	Albite and microcline, Mostly monocrystalline
UD-14-18	81	3	15		0.04-0.12 mm	Moderately well Sorted	Concave o Convex	Sub- and, Low Sphericity	10-12	Iron oxide, clays	Ununduluse	Mostly mono, Iron oxide spots
UD-14-20	90	1	7	-	0.02-0.10 mm	well Sorted	Sutured + Longi+Concave o Convex	Sub- round, Low Sphericity	20	Iron oxide, clays	Ununduluse + wavy	Less ion oxide-
UD-14-22	92	3	5		. 0.02-0.10 mm	well Sorted	Longi+Concave o Convex	Sub- round, high Sphericity	20-23	Iron oxide, clays	Mostly wavy	Mostly mono crystalline quartz, Feldspar reminents
UD-14-29	70	4	22		.04 to .11 mm	Moderately Sorted	Longi+Concave o Convex	Sub-ang to Sub- round, Low Sphericity	17	Iron oxide, clays	Ununduluse	Fractured quartz and some opaque minerals-
UD-14-32A	89	3	7		0.04 – 0.18 mm	Moderately well Sorted – well sort	Sutured + Concave o Convex	Sub-ang to sub-round, Low Sphericity	20	Iron oxide, clays	Mostly ununduluse	Dark colored coating around quartz grains

Table 5.4 Optical microscopy results for LF 6 and LF 7 samples.

Sample No.	**Mineral Composition**				**Texture**				**Porosity**	**Cement**	**Extinction Type**	**Comments**
	Quartz	**Feldspar**	**Mica**	**Rock Fragments**	**Grain Size**	**Grain Sorting**	**Grain Contact**	**Grain Shape**				
UD-14-32B	89	3	7		0.04 – 0.18 mm	Moderately well Sorted – well sort	Sutured + Concave o Convex	Sub-ang to sub-round, Low Sphericity	20	Iron oxide, clays	Mostly unundulose	Dark colored coating around quartz grains
UD-14-35	90	5	5		0.02-0.10 mm	Moderately well Sorted	Concave o Convex	Sub round Low Sphericity	25	Iron oxide, clays	Mostly unundulose	Less iron oxide
UD-14-36A	94	4	2	-	0.02-0.10 mm	Mod well Sorted	Concave o Convex	Sub- ang to sub round, Low Sphericity	20	Iron oxide, clays	Mostly Unundulose	Iron oxide patches
UD-14-36B	94	2	4	-	0.02-0.10 mm	well Sorted	Concave o Convex	sub round, Low Sphericity	18	Iron oxide, clays	Unundulose	Iron oxide patches
UD-14-40	98	-	2		.08 to .25 mm	Moderately to poorly Sorted	Point	Sub-ang to Sub- round, High Sphericity	25	Iron oxide, clays	Unundulose + wavy	-
UD-14-44	76	2	22		0.02 – 0.10 mm	Moderately well Sorted	Concave o Convex + Longitu	sub-round, Low Sphericity	2-3	Iron oxide, clays	unundulose	

Table 5.5 Optical microscopy results for LF 8 and LF 9 samples.

Sample No.	Mineral Composition				Texture				Porosity	Cement	Extinction Type	Comments
	Quartz	Feldspar	Mica	Rock Fragments	Grain Size	Grain Sorting	Grain Contact	Grain Shape				
UD-14-46	78	4	18		0.02 – 0.09 mm	Moderately well Sorted	Concave o Convex + Longitu	Sub-ang to sub-round, Low Sphericity	4	Iron oxide, clays	unundulose	
UD-14-48	70	3-4	25		0.02 – 0.09 mm	Moderately well Sorted	Longitud	Sub ang Low Sphericity	7	Iron oxide, clays	unundulose	
UD-14-52	88	3	7-8	-	0.02-0.10 mm	well Sorted	Longitud	sub round, High Sphericity	5-7	Iron oxide, clays	Unundulose + wavy	
UD-14-54	75	2	25	-	0.02-0.10 mm	well Sorted	Sutured	sub round, Low Sphericity	1-2	Iron oxide, clays	Mostly Unundulose	

Table 5.6 Optical microscopy result for northwestern outcrop samples.

Sample No.	Mineral Composition				Texture				Porosity	Cement	Extinction Type	Comments
	Quartz	Feldspar	Mica	Rock Fragments	Grain Size	Grain Sorting	Grain Contact	Grain Shape				
Q3-14-9A	79	1	20		0.01 – 0.07 mm	Moderately Sorted	Concave o Convex	Sub-ang Low Sphericity	5	Iron oxide, clays	Mostly unundulose	
Q3-14-9A	78	2	20		0.01 – 0.07 mm	Moderately Sorted	Concave o Convex	Sub-ang Low Sphericity	6	Iron oxide, clays	Mostly unundulose	
Q3-14-10A	90		10		0.05 mm	Well Sorted	Sutured + Concave o Convex	sub-round, Low Sphericity	5	Iron oxide, clays	unundulose	
Q3-14-10B	90	1	09		0.05 mm	Well Sorted	Sutured + Concave o Convex	sub-round, Low Sphericity	5	Iron oxide, clays	unundulose	
UD-14-23A	83	2	15		0.02 – 0.10 mm	Mod Well Sorted	Concave o Convex	sub-ang to sub-round, Low Sphericity	15-20	Iron oxide, clays	unundulose	my be some ostracods-
UD-14-23B	87	1	12		0.02 – 0.09 mm	Mod Well to well Sorted	Concave o Convex	sub-round to round, Low Sphericity	15-20	Iron oxide, clays	unundulose	my be some ostracods-

Table 5.7 Optical microscopy result for northwestern outcrop samples.

Sample No.	Mineral Composition				Texture				Porosity	Cement	Extinction Type	Comments
	Quartz	Feldspar	Mica	Rock Fragments	Grain Size	Grain Sorting	Grain Contact	Grain Shape				
Q3-14-24A	82	3	15		0.03 – 0.11 mm	Mod Well to well Sorted	Longitud + Concave o Convex	sub-round to round, Low Sphericity	10	Iron oxide, clays	Mostly unundulose	Multi colored Quartz
Q3-14-24B	89	1	10		0.02 – 0.12 mm	Mod Well-well Sorted	Longitud	sub-round to round, Low Sphericity	5	Iron oxide, clays	unundulose	Multi colored Quartz, hematitic cement
Q3-14-25A	89	1	10		0.03 – 0.11 mm	Mod Sorted	Longitud	sub-ang Low Sphericity	20	Iron oxide, clays	Unundulose + wavy	
Q3-14-25B	89	1	10		0.03 – 0.11 mm	Mod Sorted	Longitud	sub-ang Low Sphericity	20	Iron oxide, clays	Unundulose + wavy	
Q3-14-26A	74	1	25		0.02 – 0.10 mm	Mod well Sorted	Concave o Convex	sub-round Low Sphericity	7	Iron oxide, clays	Unundulose	Hematite cement
Q3-14-26A	84	1	15		0.03 – 0.12 mm	Mod well Sorted	Concave o Convex	sub-round Low Sphericity	7	Iron oxide, clays	Unundulose	Hematite cement

Table 5.8 Optical microscopy result for northwestern outcrop samples.

Sample No.	Mineral Composition				Texture				Porosity	Cement	Extinction Type	Comments
	Quartz	Feldspar	Mica	Rock Fragments	Grain Size	Grain Sorting	Grain Contact	Grain Shape				
Q3-14-27A	90	2	08		0.02 – 0.06 mm	Mod well Sorted	Concave o Convex	sub-angul Low Sphericity	19	Iron oxide, clays	Mostly unundulose	
Q3-14-27B	92		08		0.05 – 0.10 mm	Mod well Sorted	Concave o Convex	sub-angul Low Sphericity	22	Iron oxide, clays	Mostly unundulose	
Q3-14-28A	93	2	05		0.06 – 0.12 mm	Mod well Sorted	Concave o Convex	sub-angul Low Sphericity	21	Iron oxide, clays	Mostly unundulose	
Q3-14-28B	91	2	07		0.03 – 0.07 mm	Mod well Sorted	Concave o Convex	sub-angul Low Sphericity	20	Iron oxide, clays	Mostly unundulose	

5.3 Sandstone Diagenesis

The Sharawra formation sandstone is classified as “Subarkose” according to the Folks scheme of classification for sandstone. The triangular classification of Sharawra Formation shows that most of the sandstones lie within the range of subarkose. This indicates that the Sharawra Formation sandstone is dominantly mature. Composition of sandstone, its depositional environment, and the burial temperature are the important criteria for the diagenesis. All the siltstones and sandstones show dominance of quartz. Quartz is a more stable mineral than the other commonly occurring minerals in sandstones i.e. feldspar, mica, and rock fragments. Not only from the optical microscopy results, but also from the SEM-EDS and XRD data, it is evident that feldspar is negligibly present throughout the Sharawra Formation. Thin section study revealed that the monocrystalline quartz is dominant over the polycrystalline quartz, which indicates the reworking of quartz. The quartz observed in this formation has mostly unit extinction; however the wavy extinction has also been encountered rarely. As far as the provenance is concerned, the quartz can provide some useful information. Typically the quartz

derived from volcanic igneous rocks have unit extinction, with no inclusions and are mostly monocrystalline. This provenance model seems probable for the Sharawra Formation sandstone as Arabian shield volcanics can be a possible provenance for them.

In general, the burial diagenesis reduces the porosity, but primary porosity may be preserved because of the clay being grain coating. The cementation process can be stopped by further clay coating (Wilson and Pittman, 1977). The different types of cements are responsible for the diagenatic alteration in the Sharawra Formation. Clays, calcite, quartz overgrowth, and iron oxides are the cements observed in this formation. The quartz overgrowth is the remnant of inherited silica cement, and it shows that the grains have undergone recycling from the sedimentary rocks of the area. The absence of quartz overgrowth in some lithofacies of the Sharawra Formation is due to abrasion during transport. Kaolinite is present in all the lithofacies and is due to the influx of meteoric water and marine pore water. Sharawra Formation, being a shallow marine deposit, seems to be kaolinitic mainly due to the marine pore water. Calcite is present as a cement in the topmost lithofacies of the Sharawra Formation. The calcite replaces the detrital quartz and other grains in loosely packed sandstone. Marine water also seems to be the source for calcite during sea-level rise. The main source of ions needed for calcite cementation is sea water (Morad 1998). Iron oxide is present as a cement throughout the Sharawra Formation. The source of iron in a shallow marine deposit is most likely to be the geochemical zone lying below the sea floor (Berner 1981).

5.3.1 Cementation History

Different types and stages of cements have been observed in the calcareous sandstones, sandstones, and siltstones of the Sharawra Formation. The topmost calcareous facies are matrix supported abundant quartz grains in the calcareous sandstone facies which are cemented by calcite. No clay minerals have been observed in them either under SEM. And XRD has also not reported any clay in the calcareous sandstones. Calcite is present as cement in the top most sandstone facies. The calcite is not formed as a replacement, as it occupies the pore spaces and occur in poiklitic form. The source of calcite in the sandstone facies is probably the detrital minerals or the influx of calcitic veins from the overlying highly calcareous sandstones in late stages. XRD and SEM have not shown calcite as a cement or mineral in any of the other sandstone and siltstone facies.

Another important cement is the iron oxide or hematite. Here, in these samples the hematite is of amorphous form as it is not detected by XRD. However, SEM-EDS has confirmed the presence of iron oxide. The iron oxide patches are present throughout the sandstone and siltstone facies. Its detached appearance from the mineral grains shows that it is probably in the last stages of diagenesis. The origin of iron leaching is caused by the decomposition of hornblende and mica or from lateritic soils (Burly, 1984).

The quartz overgrowth is also present in sandstone and siltstone facies, mostly in the middle part of the Sharawra Formation. The overgrowth starts around the rim of the grains and it usually grows inward and results in the filling of pores. This inward growth can result in tight packing of the sandstone. Silica cement quartz growth is caused by the dissolution of silicate minerals like feldspar. The other source could be the rock

fragments. Both feldspar and the rock fragments are rarely observed in optical microscopy. The alteration of feldspar to clays is more likely, and can give rise to source out silica as cement.

Clay cement is very common in most of the samples that coat the quartz grains from all the sides. It is due to the mechanical infiltration of detrital clays or due to clays authigenic in origin. In the Sharawra Formation, both forms of clays are present. Clays are found to be present as grain coating as well as pore filling.

5.4 Scanning Electron Microscopy (SEM)

The samples of Sharawra Formation were studied under SEM, for high resolution imagining. The high resolution images provide useful information regarding the cement and diagenesis, and resolve the ambiguities and uncertainties of optical microscopy .The purpose to acquire high resolution and magnification images is to understand the textural relationships. In this study twenty one representative samples of Sharawra formation were selected for SEM.

SEM studies of the Sharawra Formation samples show the grain surface morphology, the contact and relationship of the grains with cementing material. The top calcareous sandstone facies were observed in the SEM. Figures 5.28 and 5.29 show the relationship of scattered quartz grains with the calcite matrix around them. For the sandstone samples, the authigenic clays have been identified from the SEM images, due to their specific structures. Clays have been found as grain coatings (Figure 5.30) and also as pore linings (Figures 5.31 and 5.32). The booklet structure of the kaolinite is shown in Figures 5.33 and 5.34. The other clay type confirmed by the SEM image is the

polygorskite (Figure 5.35). XRD also confirmed the presence of polygorskite. Clays often tend to reduce the porosity by blocking the pore throats, which destroys the pore connectivity (Figures 5.35 to 5.37). Other cement types like iron oxide and silica were also observed under SEM. Quartz overgrowth has been observed under optical microscopy and has been confirmed by SEM (Figures 5.38 and 5.39). Iron oxide patches were observed throughout the formation apart from the topmost three facies. The iron oxide patches were also observed in all the SEM images from the basal facies (Figure 5.40). Porosity is also one of the parameters that can be observed under SEM (Figure 5.41).

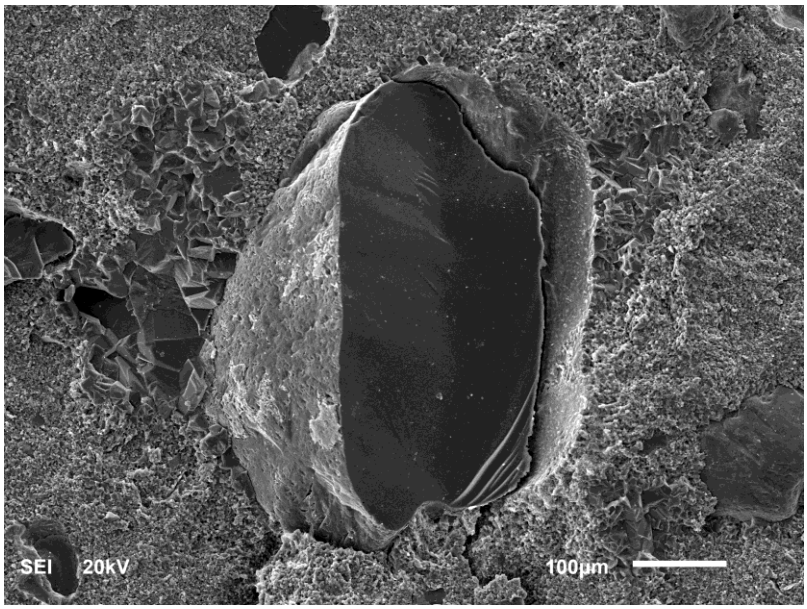

Figure 5.28 Quartz crystal surrounded by calcite.

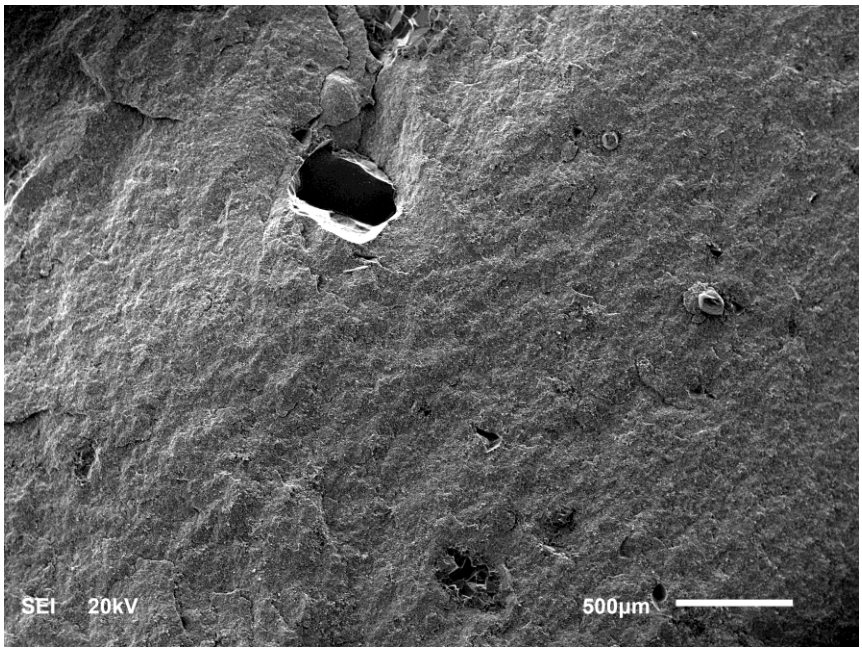

Figure 5.29 Rare quartz grain in fine to medium grained calcareous sandstone facies.

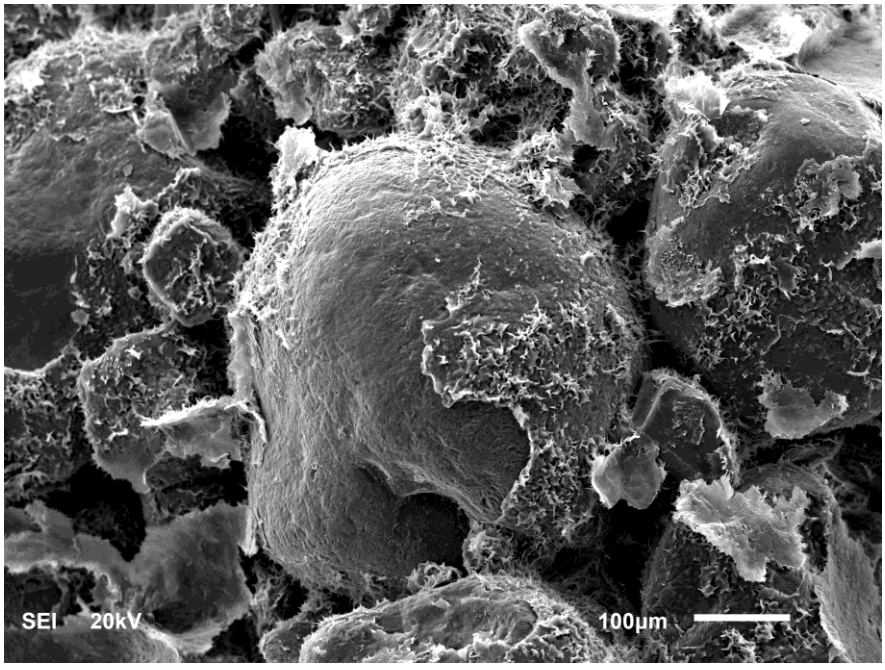

Figure 5.30 Clays occurring as grain coatings.

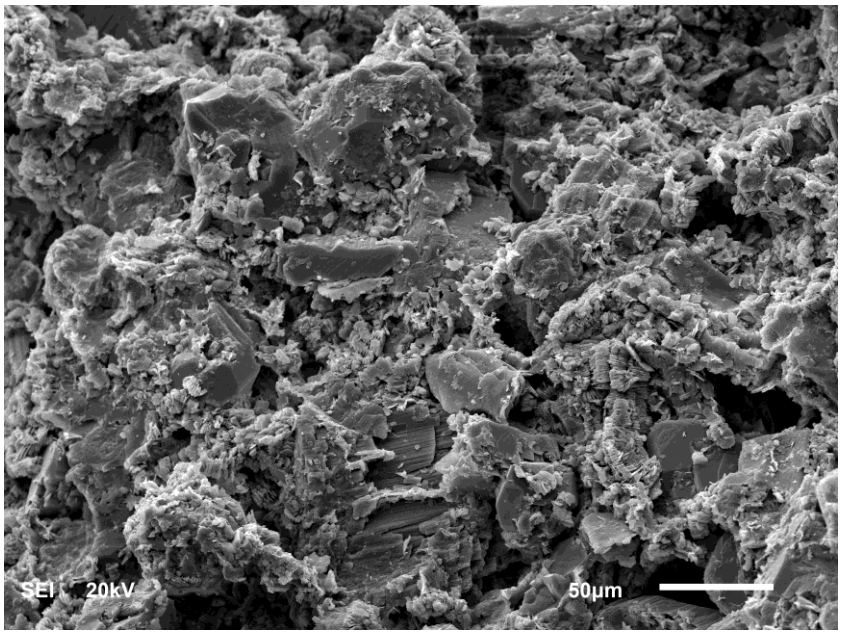

Figure 5.31 Clay spread as pore linings and pore filling.

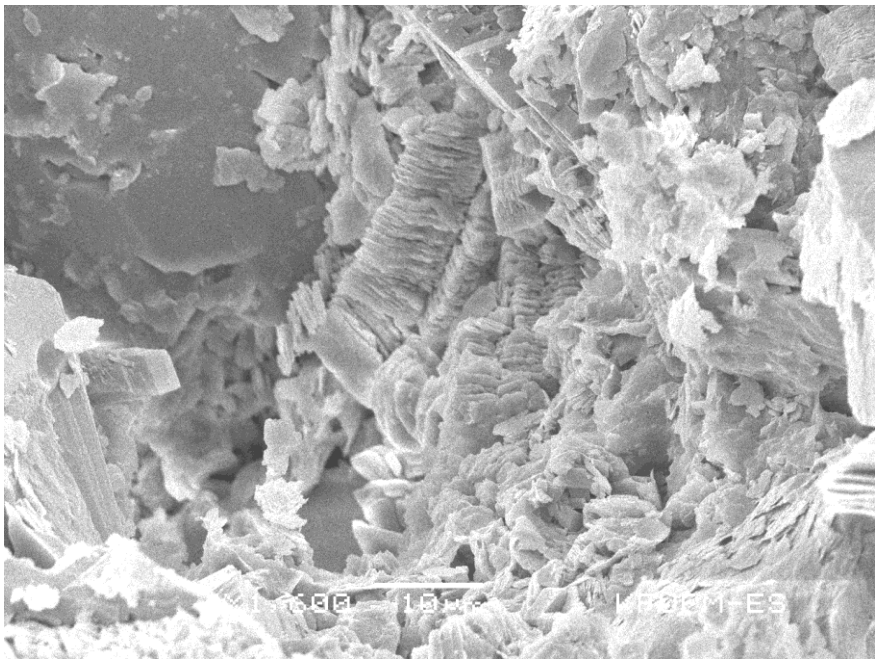

Figure 5.32 Kaolinite filling the pores.

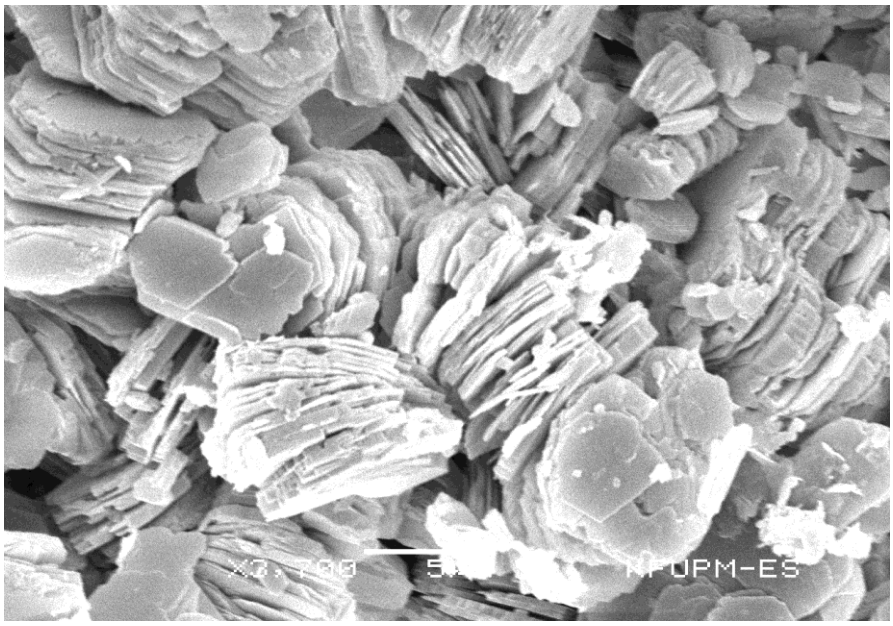

Figure 5.33 Booklet structure of kaolinite.

Figure 5.34 Booklet structure of kaolinite.

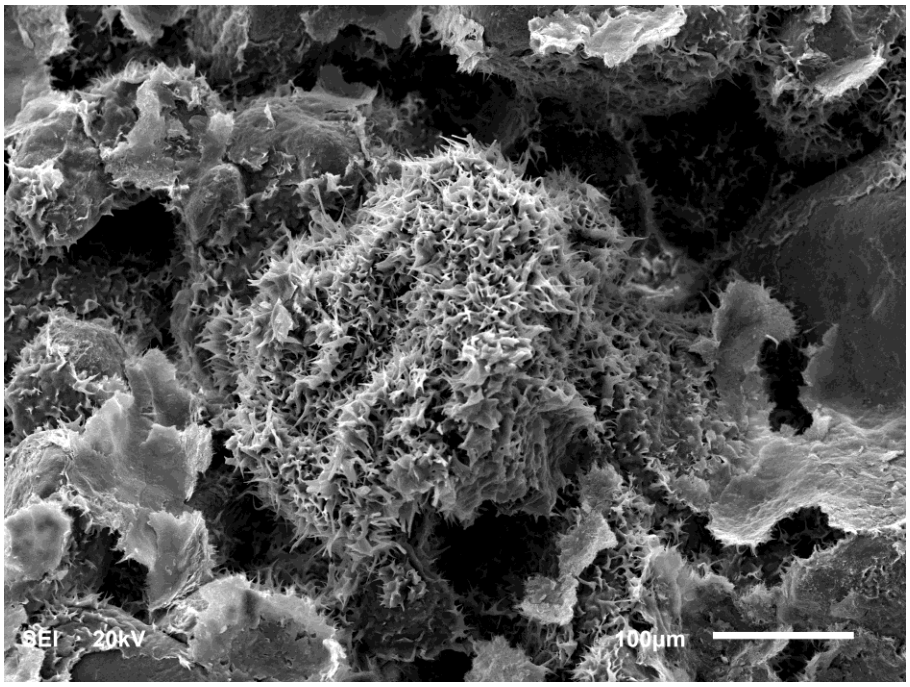

Figure 5.35 Polygorskite clay mineral.

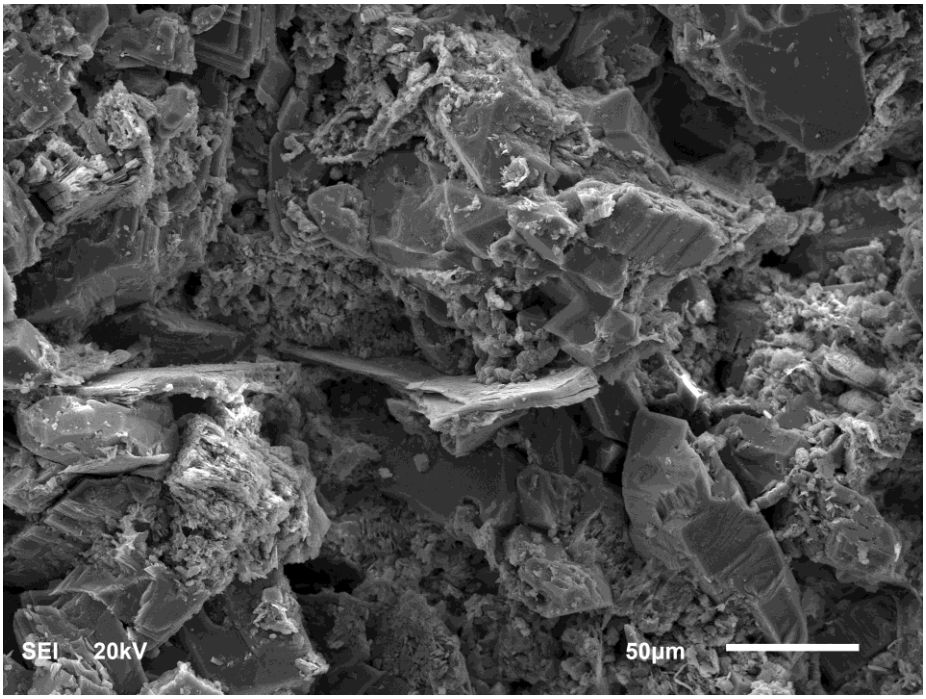

Figure 5.36 Clays reducing porosity.

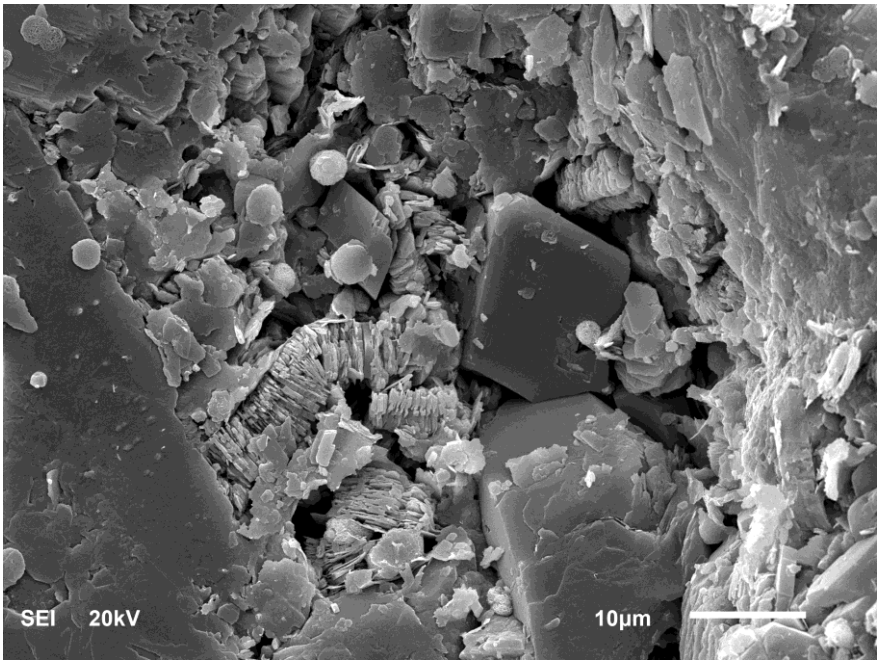

Figure 5.37 Kaolinite and iron oxide cements obstructing the pore throats.

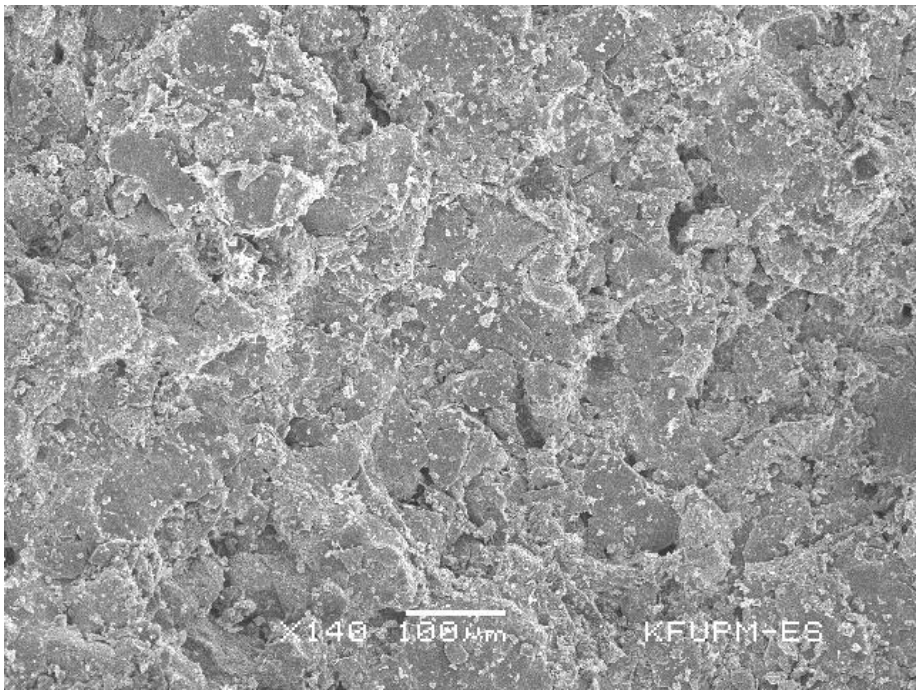

Figure 5.38 Quartz overgrowth on siltstone facies.

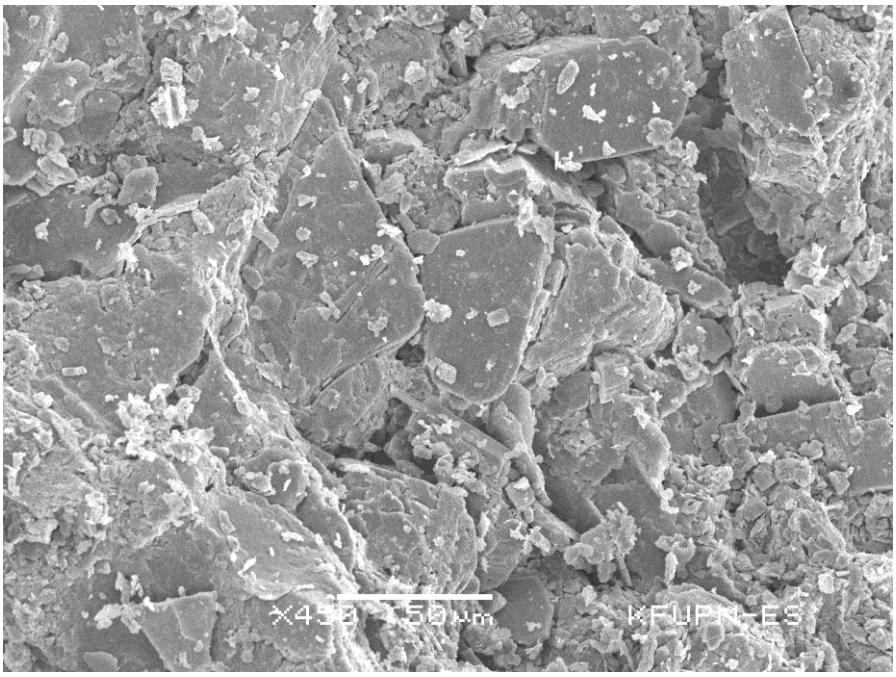

Figure 5.39 Quartz overgrowth on siltstone facies.

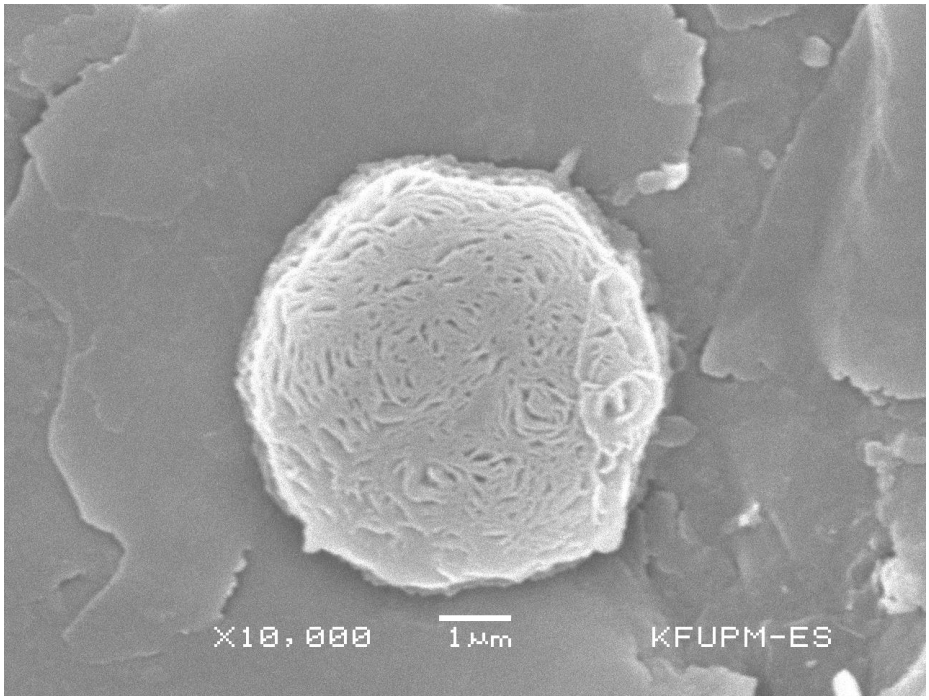

Figure 5.40 Iron oxide patch on quartz grain.

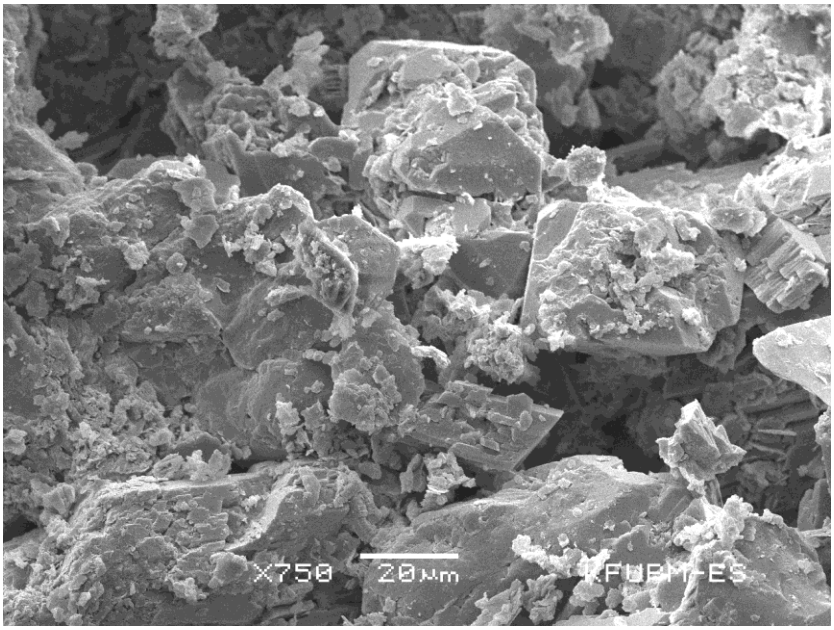

Figure 5.41 Visible porosity in sandstone.

Apart from these observations, grains can be studied in detail. The grain contacts, the sorting of grains, and grain shapes have also been observed under SEM. Figure 5.42 shows sutured contacts between quartz grains. Moderately sorted, moderately well sorted, and well sorted sandstones are shown in Figures 5.43 to 5.45, respectively. Sub-angular quartz grains are shown in Figure 5.46.

The elemental analysis indirectly provides information about the minerals present at a specific spot or area. Point and area analysis were done for the elemental composition. To confirm the elemental composition of a cement is important in generating the elemental history. To know the quartz composition being pure or coated with clays is also very important. The boundary of quartz has been observed precisely in the calcareous facies. The EDS results confirmed the Si rich mineral being surrounded by Ca rich mineral (Figures 5.47 and Figure 5.48). Twinning was observed on a rare grain in one of the samples, the EDS confirmed it as feldspar by confirming its composition (Figure 5.49).

Booklet structure is typical of kaolinite; however for further confirmation EDS provided it as containing Al and Si (Figures 5.50 and 5.52).

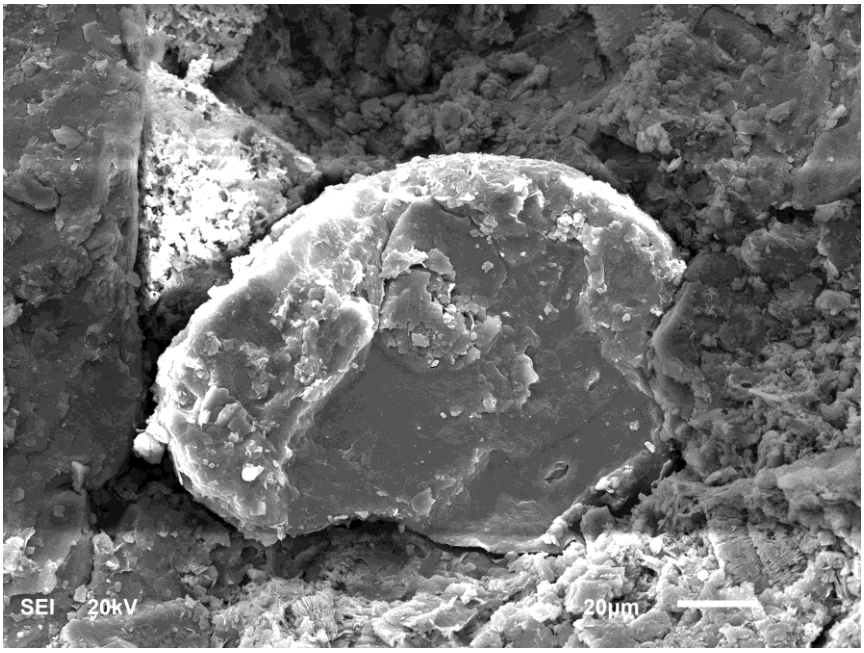

Figure 5.42 Quartz grains having sutured contacts.

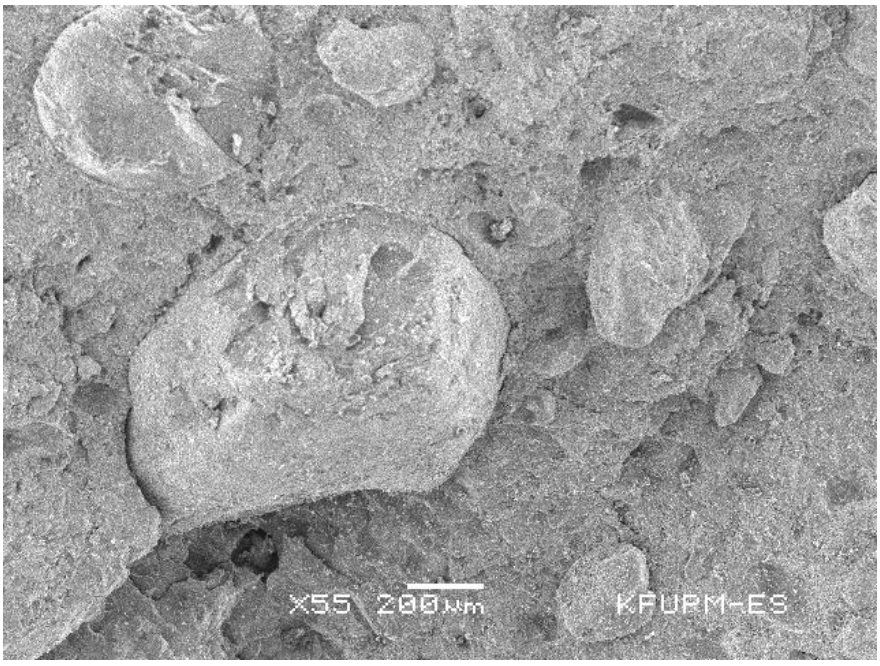

Figure 5.43 Moderately sorted quartz grains

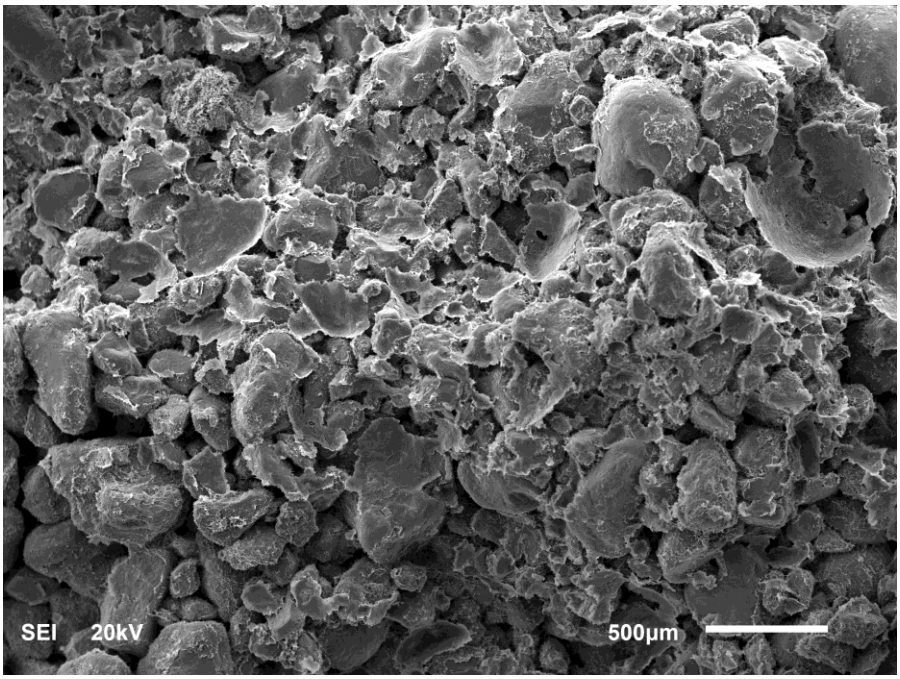

Figure 5.44 Moderately well sorted quartz grains.

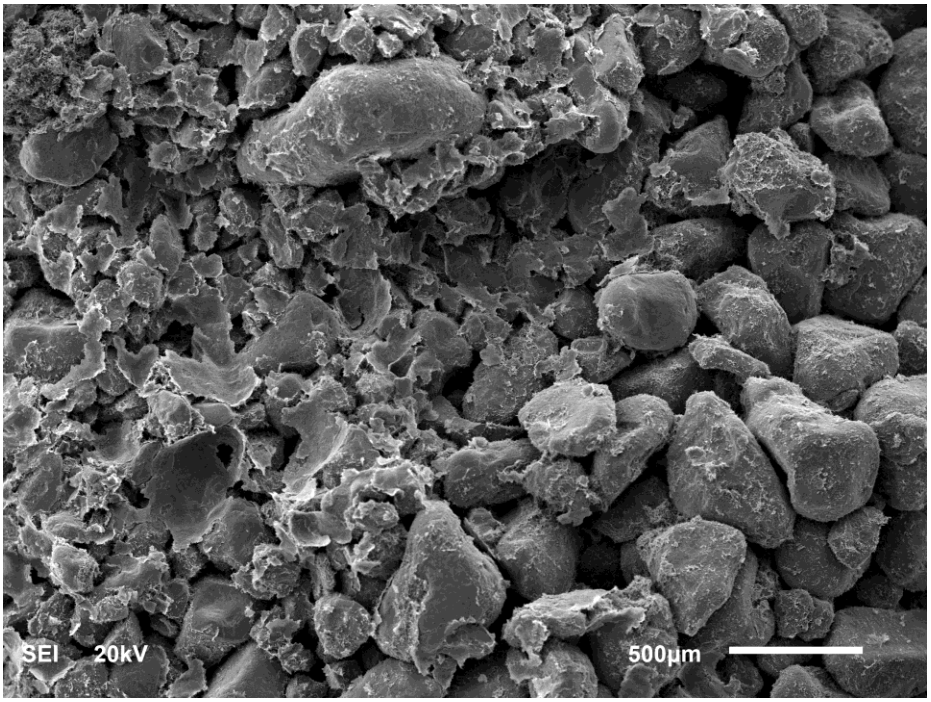

Figure 5.45 Well sorted quartz grains

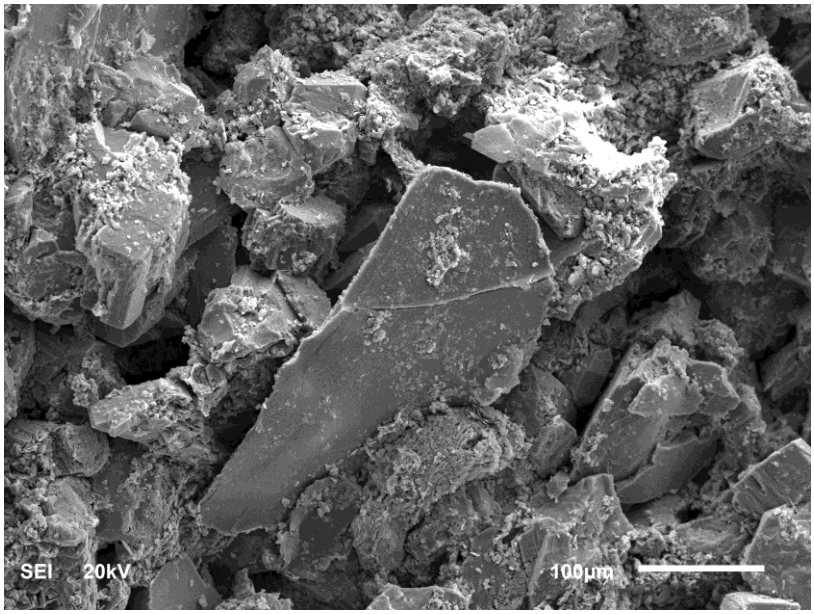

Figure 5.46 Sub angular quartz grains.

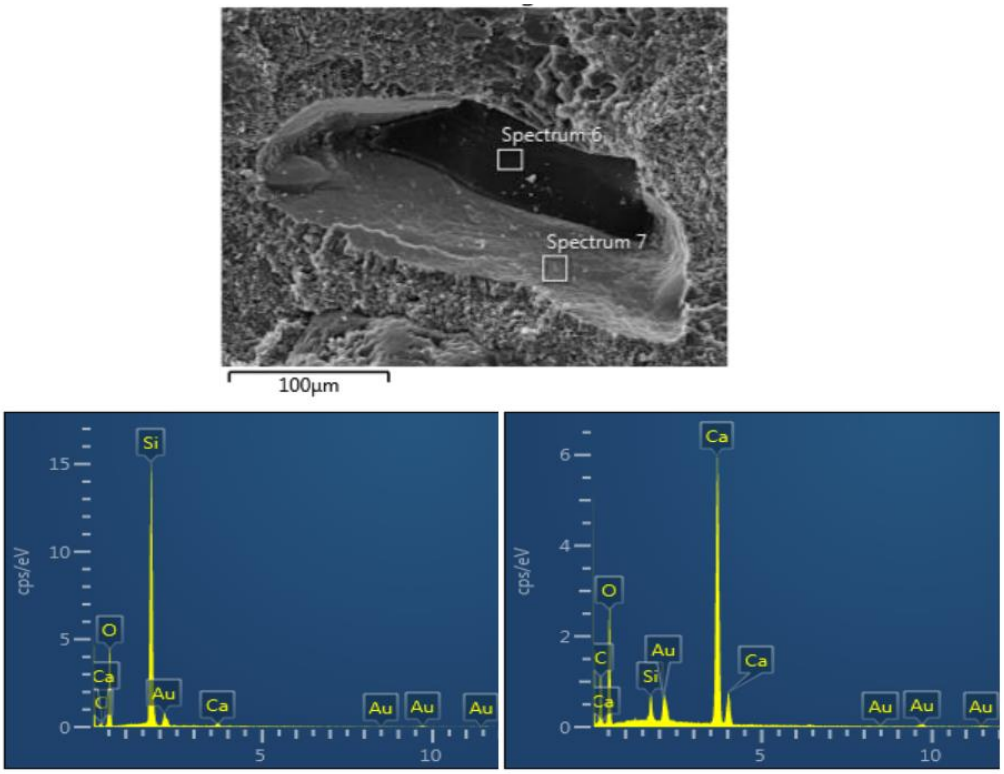

Figure 5.47 EDS result for the quartz grain and neighboring matrix.

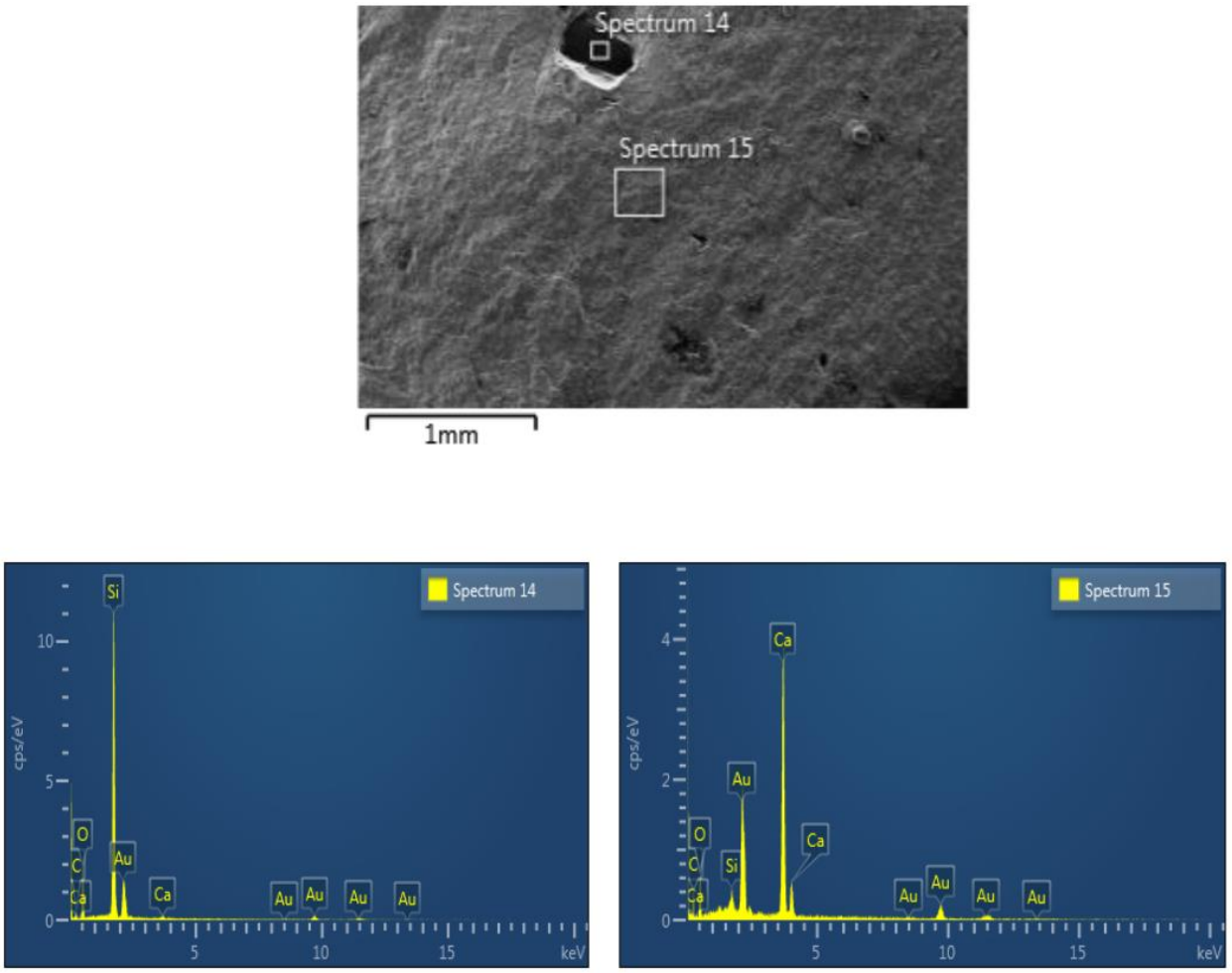

Figure 5.48 EDS result for Fine to medium grained calcareous sandstone facies revealing Si and Ca.

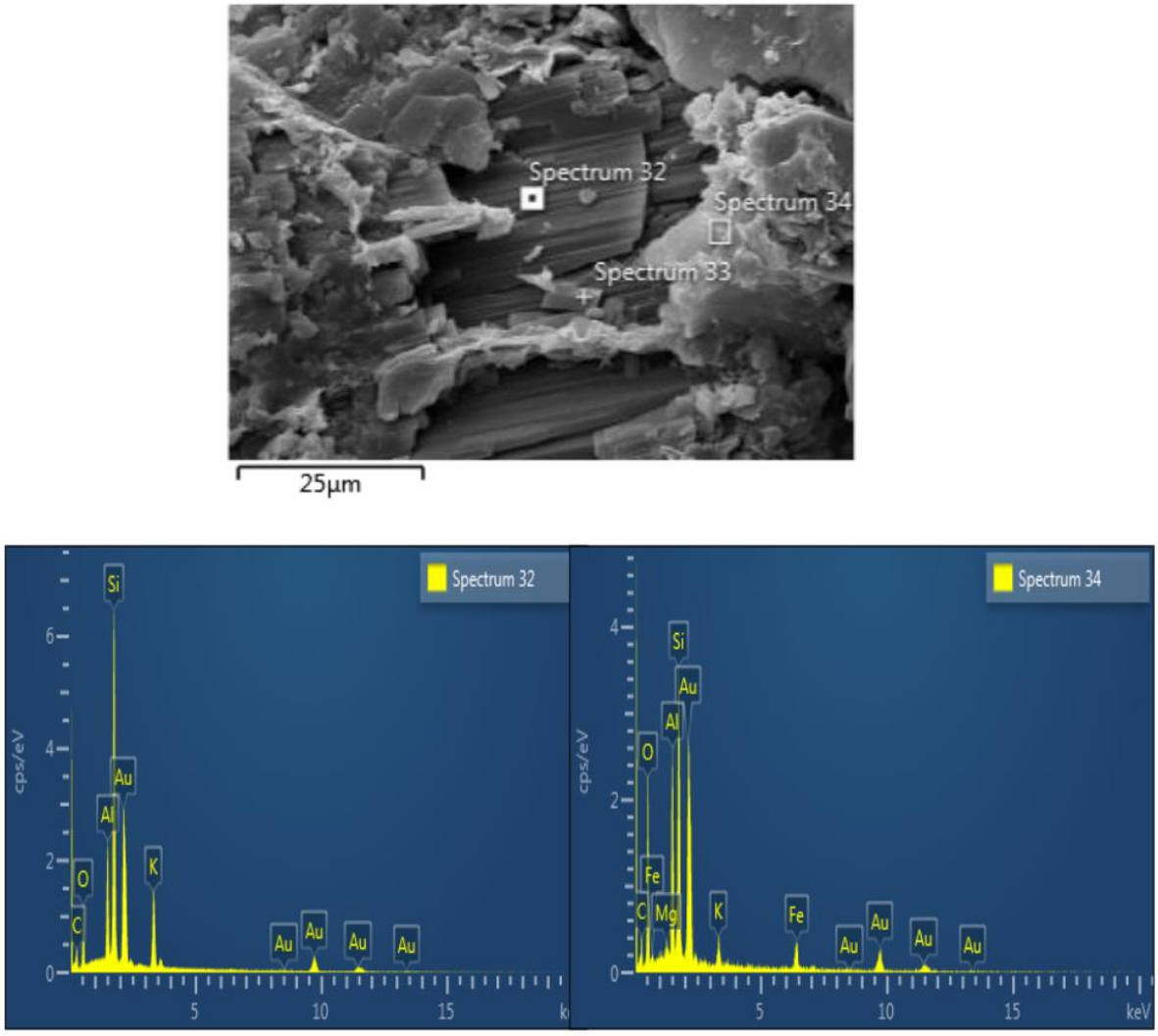

Figure 5.49 EDs result for the remnant feldspar.

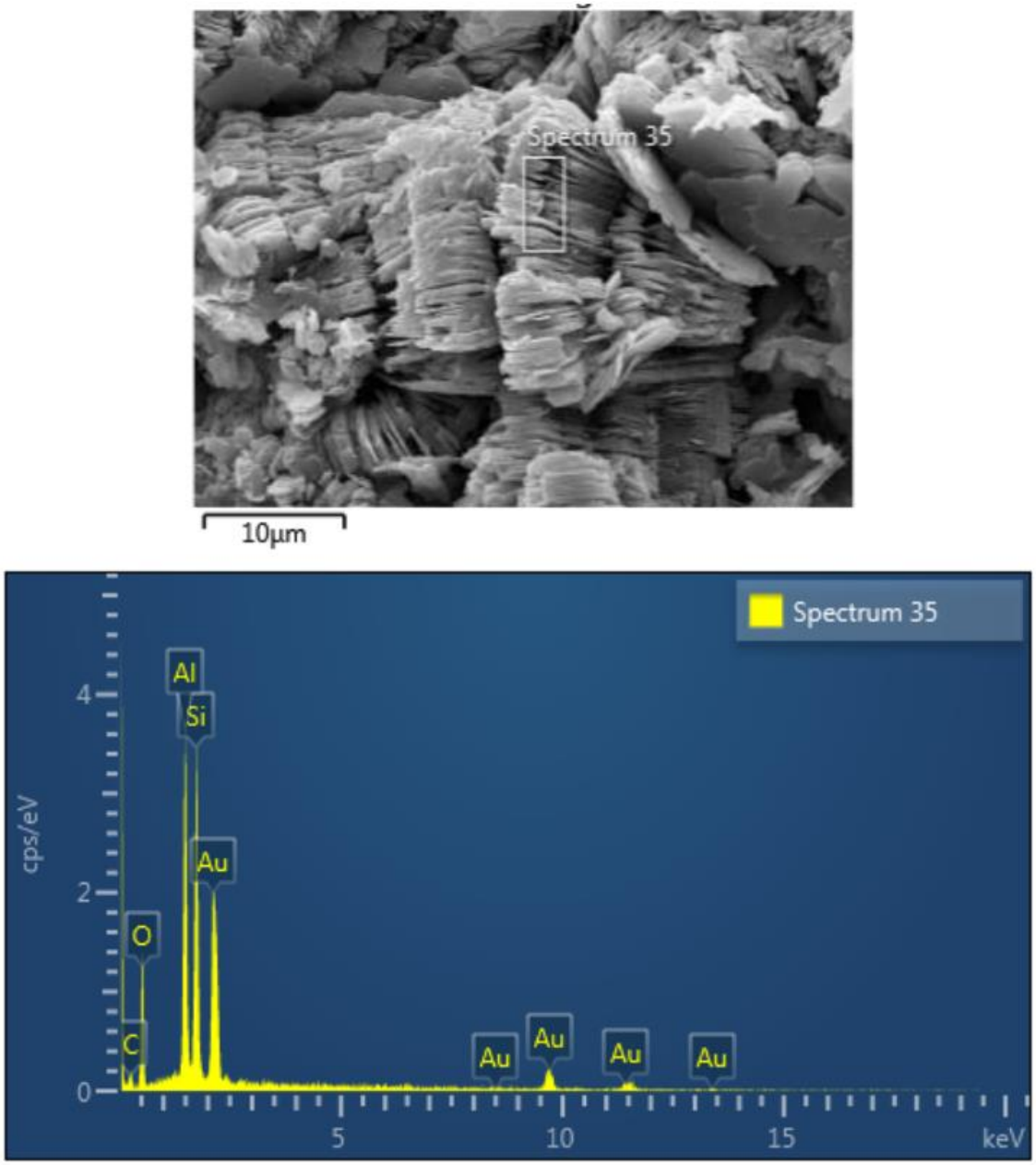

Figure 5.50 EDS result for the kaolinite clay.

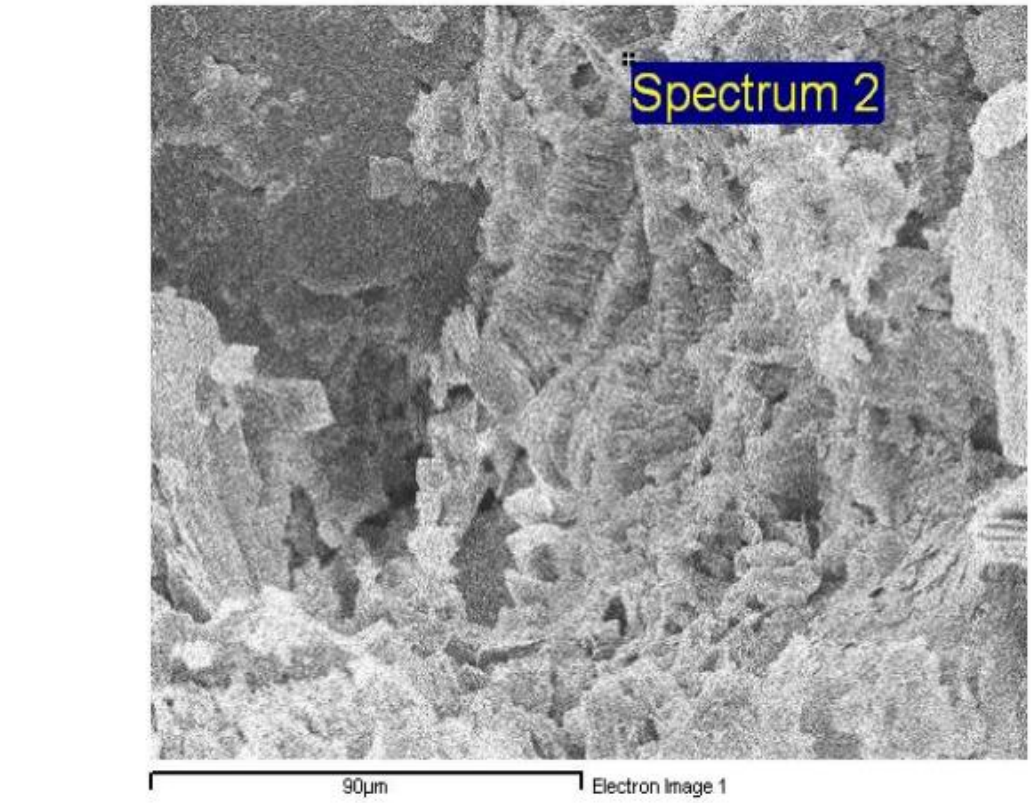

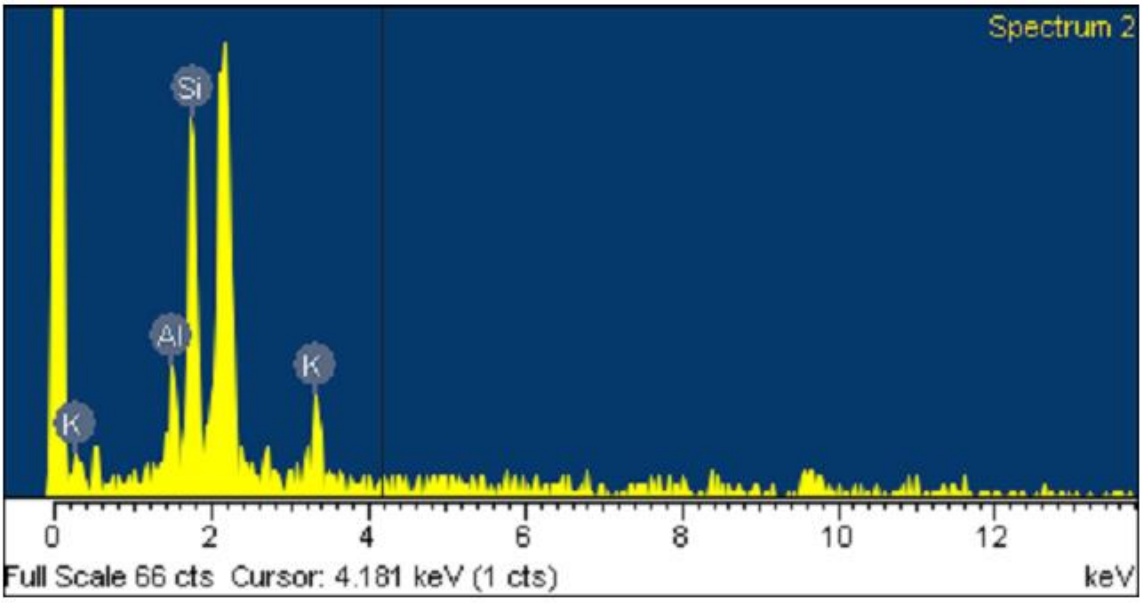

Figure 5.51 EDS for kaolinitic booklet structure.

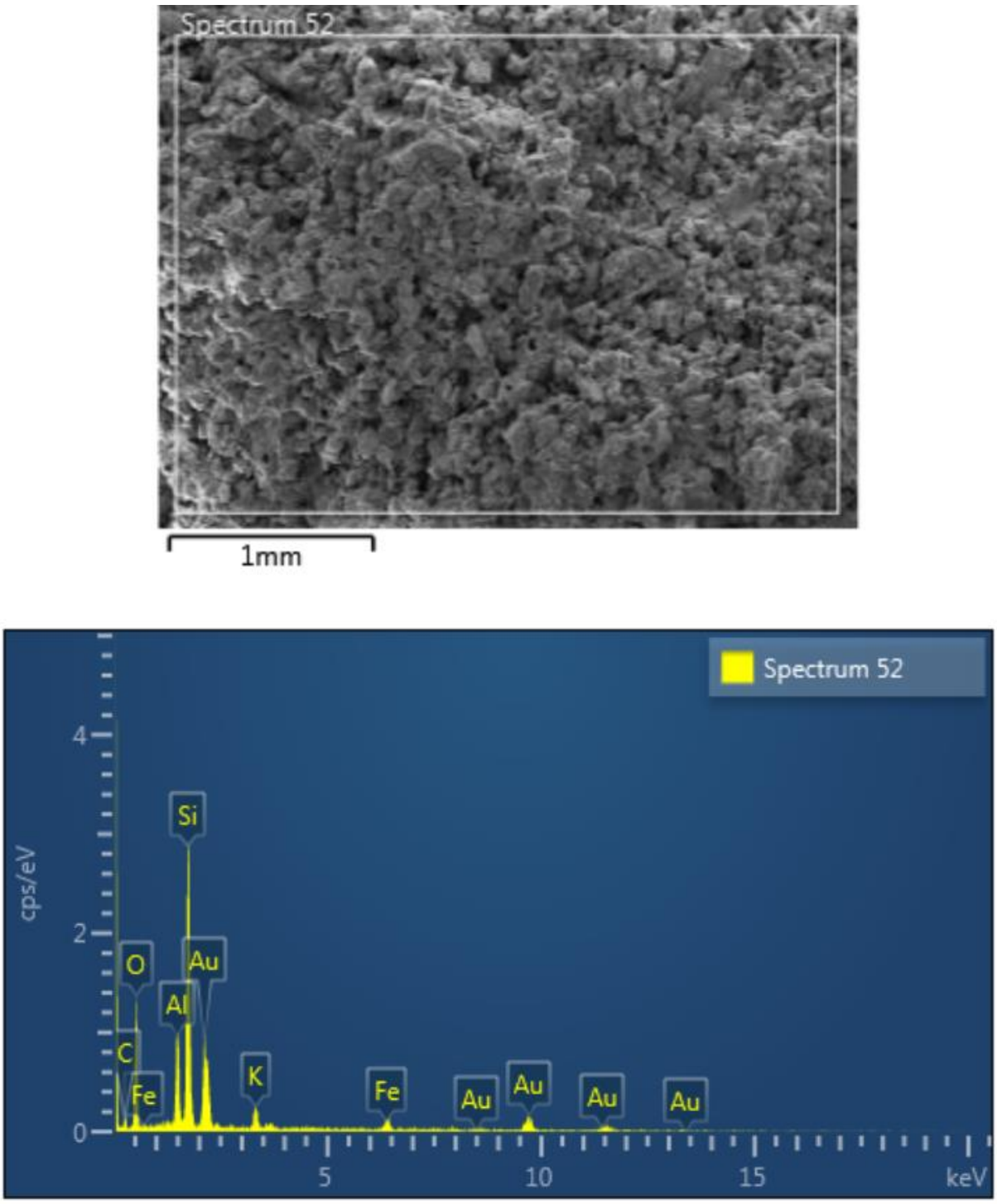

Figure 5.52 Area analysis for a fine grained sandstone.

Apart from the point analysis, area analysis was also done for all the samples. As no sandstone is purely quartz, so elements forming clay minerals, feldspar, and mica are also included in the EDS result of an area analysis (Figure 5.52). However, the area analysis can sometimes confuse the issue, because the building blocks of all sandstone-associated minerals are Si and Al. A probable clay mineral cemented sandstone with its EDS result is shown in Figure 5.53. The point analysis proved to be more helpful while zooming on a probable iron oxide patch. The EDS confirmed it as iron oxide by detecting Fe in its composition (Figure 5.54).

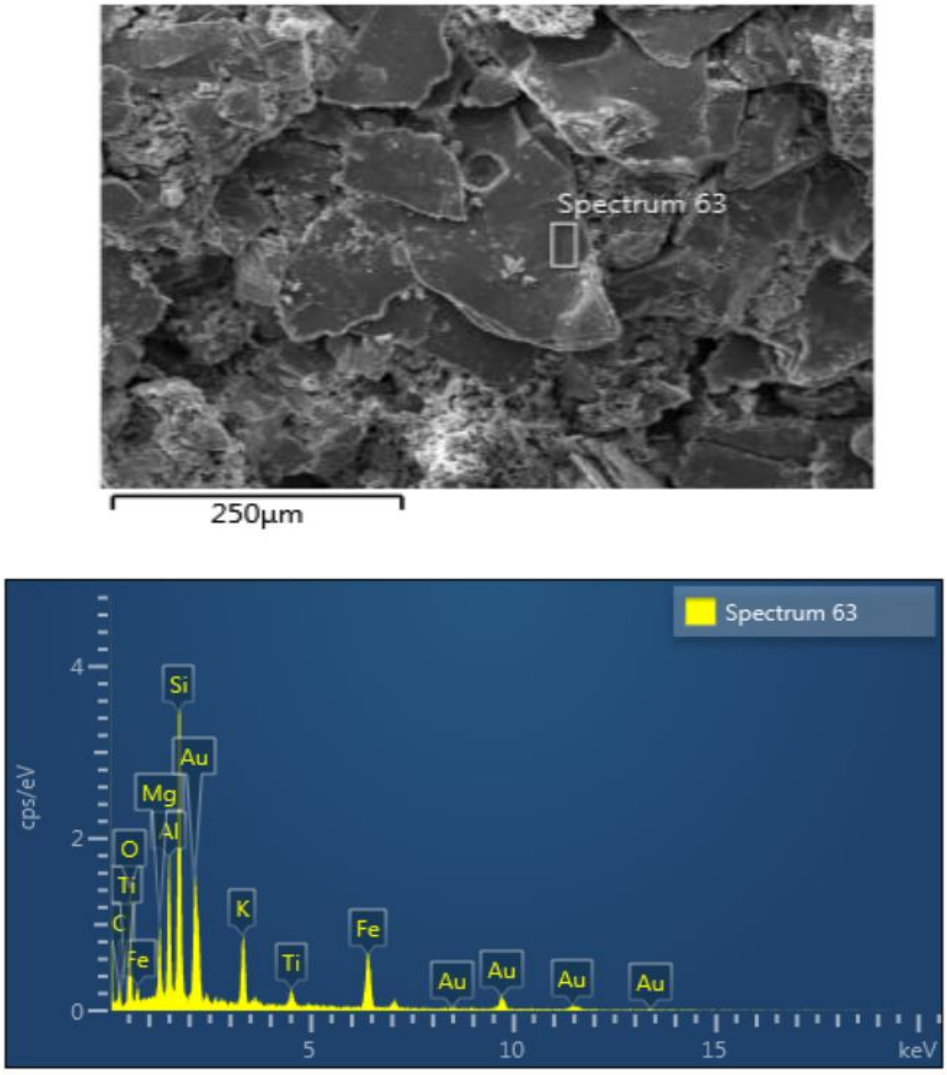

Figure 5.53 EDS for the outer surface of a quartz grain (probably coated with clays).

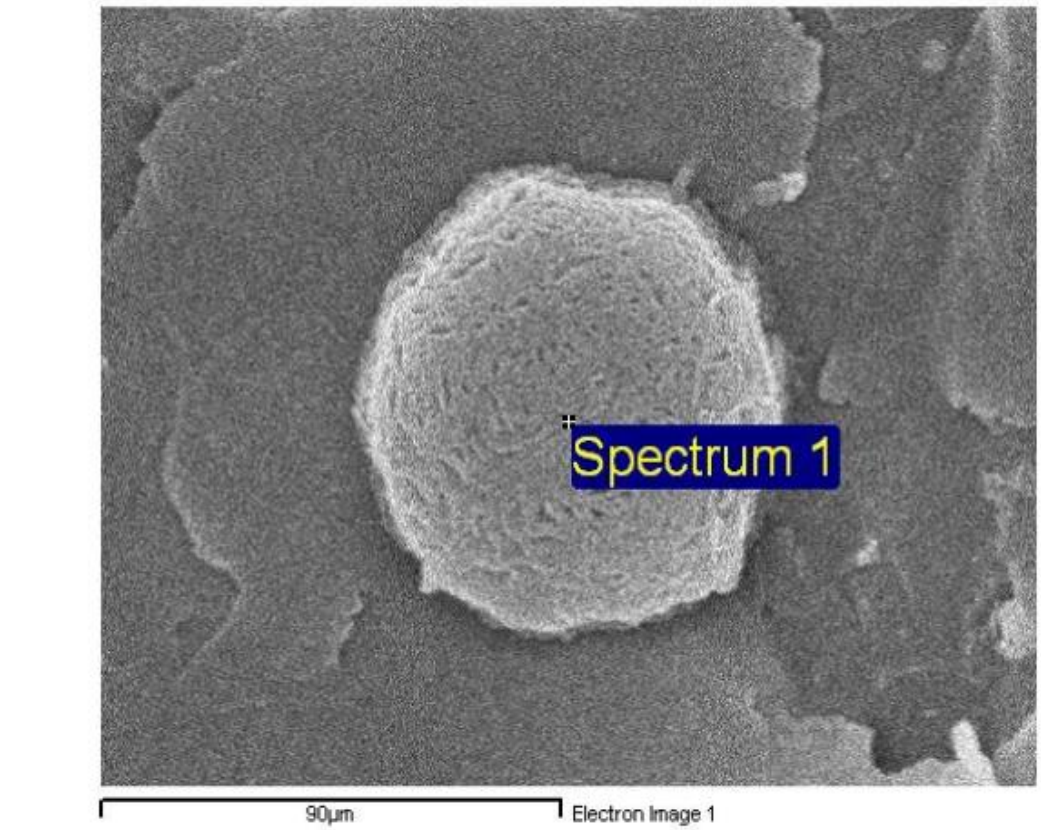

Figure 5.54 Iron oxide patch.

5.5 X-Ray Diffraction (XRD)

XRD is a mineral analysis technique primarily used for crystalline materials to acquire their phase identification. The phase identification technique basically calculates the most likely matched peaks for the given phase based on the peak intensity and 2theta. The result obtained is compared with a standard phase (available in computer database), thus enabling the identification of exact mineral phases. Fifteen powdered Sharawra formation's sandstone and shale samples were analyzed to identify the minerals. The XRD results provide confirmation for the optical microscopy and SEM-EDS results. Different clay minerals have been indicated by the SEM photographs. These were confirmed by the XRD results. Quartz, orthoclase, muscovite, microcline, and calcite have been identified in the sandstone samples. The clay minerals in the sandstones include kaolinite, dickite, and polygorskite. The most dominant mineral is quartz, while the kaolinite is the clay mineral occurring throughout the formation. For the shale samples, almost same minerals are present throughout the formation; however, illite and polygorskite clay minerals also do occur in the middle and lower part of the formation. XRD result for 15 samples is shown from Table 5.9 to 5.23. XRD diffraction patterns are shown in Appendix-A.

Table 5.9 Detailed XRD result for sample Q3-14-02 Q=Quartz, C=Calcite

NO.	2-THETA(DEG)	D(ANG.)	HEIGHT(CPS)	PHASE NAME
1	20.982(5)	4.23 (10)	1831(68)	Q
2	23.218(4)	3.82 (6)	3710(96)	C
4	26.7925(11)	3.32(14)	11191(167)	Q
5	29.5721(18)	3.01 (18)	43122(328)	C
6	31.594(10)	2.82 (9)	763(44)	C
7	36.1451(16)	2.48301(1	5304(115)	C
8	36.677(3)	2.4482(2)	487(35)	Q
9	39.5805(15)	2.27505(8)	10042(158)	C
10	40.411(13)	2.2302(7)	230(24)	Q
11	42.5587(15)	2.12248(7)	6926(132)	Q
12	43.3243(15)	2.08673(7)	7148(134)	C
13	45.903(6)	1.9753(2)	446(33)	Q
14	47.276(3)	1.92112(1	2515(79)	C
15	47.673(2)	1.90604(8)	6566(128)	C
16	48.6708(17)	1.86926(6)	9351(153)	C
17	50.2835(19)	1.81303(7)	2298(76)	Q
18	55.011(4)	1.66789(1	1022(51)	Q
19	55.4516(18)	1.65566(5)	2951(86)	Q
20	56.722(5)	1.62155(1	1413(59)	C
21	57.564(3)	1.59982(7)	3851(98)	C
22	58.231(11)	1.5831(3)	259(25)	C
23	60.097(2)	1.53831(6)	2761(83)	Q
24	60.836(3)	1.52137(7)	1961(70)	C
25	61.160(5)	1.51410(1	832(46)	C
26	61.543(4)	1.50558(1	798(45)	C
27	63.210(6)	1.46983(1	681(41)	C
28	64.834(3)	1.43688(6)	2971(86)	C
29	65.774(5)	1.41861(9)	1044(51)	C
30	68.261(10)	1.37285(1	1065(52)	Q
31	69.354(6)	1.35386(9)	511(36)	C
32	70.390(8)	1.33646(1	609(39)	C
33	73.061(5)	1.29404(8)	897(47)	C
35	73.834(15)	1.2824(2)	198(22)	C
36	76.423(10)	1.24526(1	354(30)	C
37	77.315(8)	1.23311(1	571(38)	C

Table 5.10 Detailed XRD result for sample Q3-14-09 C=Calcite Q=Quartz, M=Muscovite, UN=Unknown

NO.	2-THETA(DEG)	D(ANG.)	HEIGHT(CPS)	PHASE NAME
1	8.665(19)	10.20(2)	409(32)	M
3	23.286(6)	3.8167(9)	2071(72)	C
4	26.649(14)	3.3423(18)	2448(78)	UN
5	26.862(2)	3.3163(2)	42972(328)	Q
7	29.6289(18)	3.01256(18	24039(245)	C
8	31.642(18)	2.8253(15)	527(36)	C
9	36.193(3)	2.4798(2)	3634(95)	C
10	36.712(4)	2.4459(3)	924(48)	Q
11	39.626(3)	2.27254(16	7062(133)	C
12	39.739(4)	2.2664(2)	2417(78)	Q
13	40.510(11)	2.2250(6)	167(20)	Q
14	42.595(6)	2.1208(3)	1031(51)	M
15	43.380(2)	2.08419(10	4584(107)	C
16	45.9687(18)	1.97265(7)	2071(72)	M
17	47.331(3)	1.91901(11	1603(63)	C
18	47.7258(18)	1.90405(7)	4526(106)	C
19	48.720(2)	1.86747(7)	4943(111)	C
20	50.3524(16)	1.81071(5)	4674(108)	Q
22	55.50(4)	1.6543(11)	85(15)	Q
23	56.771(6)	1.62028(16	871(47)	C
24	57.603(4)	1.59884(10	2352(77)	Q
25	58.272(7)	1.58207(16	233(24)	C
27	60.869(4)	1.52062(10	1279(57)	C
28	61.210(7)	1.51298(15	482(35)	C
29	61.588(6)	1.50459(13	591(38)	C
30	63.262(9)	1.46874(18	419(32)	C
31	64.220(5)	1.44913(11	1247(56)	UN
32	64.863(4)	1.43631(8)	1466(61)	C
33	65.818(9)	1.41777(16	666(41)	C
36	69.388(11)	1.35328(19	265(26)	C
37	70.431(9)	1.33578(14	401(32)	C
38	73.092(10)	1.29357(16	548(37)	C
39	73.914(14)	1.2812(2)	157(20)	C
40	76.480(8)	1.24449(10	268(26)	C
41	77.336(10)	1.23283(14	385(31)	C

Table 5.11 Detailed XRD result for sample Q3-14-10 K=Kaolinite, Q=Quartz, M=Muscovite, UN=Unknown

NO.	2-THETA(DEG)	D(ANG.)	HEIGHT(CPS)	PHASE NAME
1	8.94(5)	9.88(5)	277(26)	M
2	12.503(7)	7.074(4)	800(45)	K
3	13.81(5)	6.41(2)	157(20)	M
4	20.977(8)	4.2314(15)	4104(101)	Q
5	22.59(2)	3.933(4)	289(27)	M
6	23.569(16)	3.772(3)	698(42)	M
7	23.93(3)	3.715(4)	411(32)	M
8	24.992(16)	3.560(2)	952(49)	M
9	25.821(12)	3.4476(16)	1126(53)	M
10	26.773(4)	3.3271(5)	10172(159)	Q
11	27.194(12)	3.2765(14)	1901(69)	M
12	27.620(9)	3.2269(11)	1873(68)	M
13	29.263(6)	3.0494(6)	329(29)	UN
14	29.65(8)	3.010(8)	138(19)	M
15	29.94(2)	2.982(2)	375(31)	M
16	30.88(3)	2.894(3)	330(29)	M
17	31.2529(13)	2.85963(11)	5289(115)	UN
18	32.39(2)	2.7620(19)	429(33)	M
19	34.78(2)	2.5773(17)	819(45)	M
20	35.61(4)	2.519(3)	316(28)	M
21	36.08(4)	2.487(3)	324(28)	M
22	36.690(5)	2.4474(3)	1812(67)	Q, M
23	37.18(9)	2.416(6)	185(21)	M, K
24	37.74(10)	2.382(6)	191(22)	M
25	39.611(17)	2.2734(10)	781(44)	Q, K
26	40.421(9)	2.2297(5)	750(43)	Q, M
27	41.911(9)	2.1538(4)	672(41)	M
28	42.551(6)	2.1229(3)	1224(55)	Q
29	43.76(5)	2.067(2)	168(20)	M, K
30	45.953(12)	1.9733(5)	892(47)	Q
31	47.20(9)	1.924(3)	119(17)	M
32	50.215(5)	1.81535(15)	1692(65)	Q, M
33	50.640(7)	1.8011(2)	424(33)	Q, M
34	54.995(10)	1.6683(3)	571(38)	Q
35	55.48(6)	1.6549(16)	244(25)	Q
36	60.060(4)	1.53917(10)	1905(69)	Q
37	61.75(8)	1.5010(18)	162(20)	M, K
38	62.52(5)	1.4844(10)	132(18)	K
39	64.17(5)	1.4502(9)	247(25)	Q
40	67.871(5)	1.37979(8)	972(49)	Q
41	68.256(4)	1.37294(8)	1397(59)	Q
42	68.440(4)	1.36970(7)	1305(57)	Q
43	72.38(6)	1.3045(9)	92(15)	K
44	73.600(15)	1.2859(2)	378(31)	Q
45	75.783(12)	1.25418(17)	523(36)	Q
46	77.813(9)	1.22646(12)	412(32)	Q

Table 5.12 Detailed XRD result for sample Q3-14-15 K=Kaolinite, Q=Quartz, M=Muscovite, UN=Unknown

NO.	2-THETA(DEG)	D(ANG.)	HEIGHT(CPS)	PHASE NAME
1	8.93153	9.89272	1141.17	M
2	12.459(11)	7.099(6)	2608(81)	K
3	17.9294	4.94321	455.071	M
4	19.9111	4.45548	442.316	K
5	20.5002	4.32874	179.013	K
6	20.935(5)	4.2398(10)	1326(58)	Q
7	21.42(2)	4.144(4)	1145(54)	K
8	25.012(14)	3.5572(19)	2524(79)	K
9	26.740(3)	3.3311(4)	10152(159)	Q
10	27.14(2)	3.283(3)	447(33)	M
11	27.610(10)	3.2280(11)	1279(57)	UN
12	29.216(19)	3.0542(19)	314(28)	UN
13	29.946(15)	2.9814(14)	300(27)	M
14	33.44(6)	2.677(5)	256(25)	M
15	34.39(4)	2.606(3)	139(19)	M
16	35.02(3)	2.560(2)	392(31)	K
17	36.133(15)	2.4838(10)	214(23)	K
18	36.641(10)	2.4505(6)	523(36)	Q
19	36.96(3)	2.430(2)	369(30)	M
20	37.83(3)	2.3764(18)	283(27)	K
21	38.51(2)	2.3357(13)	352(30)	K
22	39.574(6)	2.2754(3)	321(28)	Q
23	40.38(4)	2.232(2)	198(22)	Q
24	41.57(5)	2.171(2)	198(22)	K
25	42.550(8)	2.1229(4)	550(37)	Q
26	45.68(4)	1.9846(15)	346(29)	Q
27	50.223(6)	1.81508(19)	811(45)	Q
28	50.85(3)	1.7942(11)	257(25)	Q
29	53.415(10)	1.7139(3)	278(26)	K
30	54.94(3)	1.6700(9)	326(29)	Q
31	54.957(7)	1.6694(2)	360(30)	Q
32	60.032(6)	1.53982(14)	944(49)	Q
33	61.79(11)	1.500(2)	98(16)	K
34	62.35(3)	1.4880(6)	273(26)	K
35	64.08(3)	1.4519(6)	182(21)	Q
36	67.849(3)	1.38018(4)	518(36)	Q
37	68.209(7)	1.37378(13)	573(38)	Q
38	69.49(10)	1.3515(17)	53(12)	K
39	72.43(11)	1.3038(17)	96(15)	K
40	73.54(8)	1.2867(11)	84(14)	Q
41	75.692(5)	1.25546(7)	241(25)	K

Table 5.13 Detailed XRD result for sample Q3-14-18 K=Kaolinite, Q=Quartz, M=Muscovite, UN=Unknown

NO.	2-THETA(DEG)	D(ANG.)	HEIGHT(CPS)	PHASE NAME
1	8.928(6)	9.897(6)	1710(65)	M
2	12.422(4)	7.120(2)	3765(97)	K
3	13.73(3)	6.445(15)	283(27)	M
4	17.857(12)	4.963(3)	772(44)	M
5	19.919(12)	4.454(3)	514(36)	K, M
6	20.435(8)	4.3425(17)	788(44)	K
7	20.908(5)	4.2452(9)	9260(152)	Q, M
8	21.072(12)	4.212(2)	3157(89)	M
9	21.252(17)	4.177(3)	741(43)	K
10	22.56(6)	3.937(10)	294(27)	M
11	23.142(11)	3.8402(18)	655(40)	M, K
12	23.52(3)	3.780(4)	468(34)	K, M
13	24.963(14)	3.5640(19)	3255(90)	M, K
14	25.62(3)	3.474(3)	1262(56)	M
15	25.76(2)	3.455(3)	1006(50)	UN
16	26.6937(17)	3.3368(2)	51386(358)	Q, M
17	27.139(17)	3.283(2)	629(40)	M
18	27.576(4)	3.2320(5)	7541(137)	M
19	29.904(13)	2.9855(12)	1162(54)	M
20	30.766(13)	2.9038(12)	765(44)	M
21	30.976(2)	2.88458(19)	363(30)	UN
22	32.406(10)	2.7605(8)	284(27)	M
23	34.44(3)	2.602(2)	483(35)	M
24	35.00(4)	2.561(3)	532(36)	M, K
25	35.475(14)	2.5284(10)	379(31)	M
26	36.01(3)	2.492(2)	511(36)	M
27	36.601(8)	2.4531(5)	2111(73)	Q
28	37.773(13)	2.3796(8)	330(29)	M, K
29	38.68(3)	2.3262(18)	606(39)	M, K
30	39.511(5)	2.2789(3)	2503(79)	Q
31	40.345(6)	2.2337(3)	1177(54)	Q
32	41.861(12)	2.1562(6)	437(33)	M
33	42.493(3)	2.12561(15)	2472(79)	Q, K
34	42.88(3)	2.1074(12)	232(24)	M, K
35	45.56(2)	1.9896(10)	676(41)	M. K
36	45.830(6)	1.9783(2)	1660(64)	Q, M
37	47.251(11)	1.9221(4)	451(34)	M, K
38	49.05(3)	1.8555(9)	310(28)	M
39	49.700(11)	1.8330(4)	112(17)	M, K
40	50.176(2)	1.81667(7)	4480(106)	Q
41	50.65(3)	1.8009(9)	386(31)	Q, M
42	54.930(6)	1.67014(16)	1832(68)	Q
43	55.371(12)	1.6579(3)	564(38)	Q, M
44	56.85(4)	1.6182(10)	154(20)	M, K
45	60.016(3)	1.54020(6)	4565(107)	Q, M
46	61.9(2)	1.499(5)	101(16)	Q, K
47	62.291(19)	1.4893(4)	193(22)	M, K
48	64.07(3)	1.4521(5)	362(30)	Q, M
49	67.784(3)	1.38134(5)	1907(69)	Q, M
50	68.172(4)	1.37443(8)	1263(56)	Q
51	68.364(4)	1.37104(7)	1338(58)	Q, K
52	70.17(2)	1.3401(3)	126(18)	K
53	72.469(14)	1.3031(2)	306(28)	K, M
54	73.495(8)	1.28748(12)	645(40)	Q, M
55	75.718(10)	1.25510(14)	817(45)	Q, K
56	77.70(2)	1.2280(3)	180(21)	Q, K
57	79.943(12)	1.19905(14)	1046(51)	Q, K

Table 5.14 Detailed XRD result for sample Q3-14-19 K=Kaolinite, Q=Quartz, M=Muscovite, UN=Unknown

NO.	2-THETA(DEG)	D(ANG.)	HEIGHT(CPS)	PHASE NAME
1	8.920(7)	9.906(7)	2428(78)	M
2	12.414(8)	7.124(5)	4308(104)	K
3	17.827(10)	4.971(3)	554(37)	M
4	19.878(19)	4.463(4)	516(36)	K
5	20.402(16)	4.349(3)	389(31)	K
6	20.903(5)	4.2461(9)	2020(71)	Q
7	21.376(6)	4.1534(12)	1703(65)	K
8	24.925(5)	3.5694(8)	4312(104)	K
9	26.689(5)	3.3373(6)	8629(147)	Q, M
10	27.536(18)	3.237(2)	928(48)	UN
11	29.912(13)	2.9847(12)	312(28)	M
12	30.92(4)	2.890(4)	161(20)	UN
13	33.40(6)	2.681(5)	248(25)	M
14	34.99(4)	2.562(3)	409(32)	K
15	35.58(8)	2.521(5)	194(22)	K
16	36.05(2)	2.4891(15)	305(28)	K, M
17	36.75(4)	2.444(3)	338(29)	Q, M
18	37.76(5)	2.380(3)	306(28)	K
19	38.47(4)	2.338(2)	382(31)	K
20	39.29(3)	2.2909(15)	284(27)	K
21	39.520(10)	2.2784(6)	637(40)	Q
22	40.347(9)	2.2336(5)	378(31)	Q, K
23	41.327(18)	2.1829(9)	189(22)	K, M
24	41.785(9)	2.1600(4)	328(29)	UN
25	42.478(10)	2.1263(5)	456(34)	Q, K
26	45.22(3)	2.0038(11)	273(26)	M
27	45.47(2)	1.9930(10)	641(40)	K
28	45.811(10)	1.9791(4)	325(29)	Q, K
29	50.183(6)	1.81642(19)	933(48)	Q
30	50.87(4)	1.7936(13)	248(25)	Q, K
31	53.37(8)	1.715(2)	152(19)	K
32	54.963(14)	1.6692(4)	508(36)	Q, K
33	60.017(9)	1.5402(2)	966(49)	Q, K
34	61.76(4)	1.5008(10)	114(17)	K
35	62.346(17)	1.4881(4)	181(21)	K
36	64.095(13)	1.4517(3)	236(24)	Q, K
37	67.797(11)	1.3811(2)	405(32)	Q
38	68.182(9)	1.37426(16)	348(30)	Q, K
39	72.09(9)	1.3091(15)	108(16)	K
40	73.539(12)	1.28682(18)	143(19)	Q, K
41	75.709(17)	1.2552(2)	206(23)	Q

Table 5.15 Detailed XRD result for sample Q3-14-23 K=Kaolinite, Q=Quartz, M=Muscovite, UN=Unknown

NO.	2-THETA(DEG)	D(ANG.)	HEIGHT(CPS)	PHASE NAME
1	8.996(5)	9.822(6)	2841(84)	M
2	12.478(7)	7.088(4)	3438(93)	K
3	17.902(15)	4.951(4)	987(50)	K, M
4	19.94(3)	4.449(6)	253(25)	K
5	20.933(4)	4.2402(8)	2406(78)	Q, M
6	21.384(10)	4.152(2)	2453(78)	K
7	24.973(7)	3.5627(10)	3294(91)	K, M
8	26.61(2)	3.347(2)	1173(54)	K
9	26.7536(19)	3.3294(2)	17246(208)	Q
10	26.944(10)	3.3063(12)	2350(77)	M
11	27.545(4)	3.2356(4)	1220(55)	K
12	29.97(3)	2.979(3)	429(33)	K, M
13	30.87(2)	2.894(2)	299(27)	UN
14	31.819(17)	2.8100(15)	368(30)	UN
15	33.46(4)	2.676(3)	408(32)	K
16	35.01(3)	2.561(2)	376(31)	K
17	36.14(4)	2.484(3)	335(29)	K, M
18	36.658(5)	2.4494(3)	884(47)	Q, M
19	36.878(15)	2.4353(10)	651(40)	UN
20	38.54(7)	2.334(4)	292(27)	K
21	39.35(7)	2.288(4)	195(22)	K
22	39.568(8)	2.2757(4)	714(42)	Q
23	40.415(12)	2.2300(6)	393(31)	Q
24	41.55(2)	2.1715(12)	278(26)	K, M
25	42.566(13)	2.1221(6)	689(41)	Q, K
26	45.12(6)	2.008(2)	278(26)	K, M
27	45.558(9)	1.9895(4)	845(46)	K
28	45.889(6)	1.9759(2)	363(30)	Q, K
29	47.24(2)	1.9223(9)	166(20)	K
30	50.238(4)	1.81457(14)	1279(57)	Q, K
31	50.81(3)	1.7953(11)	232(24)	Q, K
32	53.60(4)	1.7083(11)	279(26)	K
33	55.13(5)	1.6645(14)	322(28)	Q, K
34	59.253(17)	1.5582(4)	109(16)	K
35	60.067(4)	1.53900(10)	1280(57)	Q, K
36	61.77(7)	1.5007(16)	139(19)	K, M
37	62.38(4)	1.4873(10)	173(21)	K
38	64.157(18)	1.4504(4)	293(27)	Q, K
39	67.852(3)	1.38013(6)	691(42)	Q, M
40	68.221(8)	1.37356(13)	578(38)	Q, M
41	68.419(5)	1.37007(8)	414(32)	UN
42	71.690(19)	1.3154(3)	122(17)	M
43	75.73(3)	1.2549(4)	219(23)	Q, M

Table 5.16 Detailed XRD result for sample Q3-14-33 K=Kaolinite, Q=Quartz, M=Muscovite, UN=Unknown

No.	2-theta(deg)	D(ang.)	Height(cps)	Phase Name
1	6.33122	13.9488	363.556	UN
2	9.020(11)	9.796(12)	1563(63)	M
3	12.483(4)	7.085(2)	5724(120)	K
4	17.86(4)	4.961(10)	425(33)	M
5	19.95(3)	4.446(6)	609(39)	K
6	20.971(11)	4.233(2)	1990(71)	Q
7	22.536(14)	3.942(2)	725(43)	M
8	23.3232	3.8108	328.201	K
9	23.6341	3.76138	102.688	K
10	24.978(3)	3.5619(4)	5025(112)	K
11	26.751(6)	3.3298(7)	10388(161)	Q
12	27.60(2)	3.230(2)	1246(56)	UN
13	29.97(3)	2.979(3)	433(33)	M
14	30.84(5)	2.897(4)	279(26)	K, M
15	35.09(5)	2.556(4)	364(30)	K, M
16	36.158(11)	2.4822(7)	365(30)	K, M
17	36.662(10)	2.4491(6)	787(44)	Q
18	37.83(2)	2.3760(13)	468(34)	K, M
19	38.55(2)	2.3334(12)	487(35)	K, M
20	39.615(6)	2.2731(4)	366(30)	Q
21	40.406(13)	2.2305(7)	316(28)	K, Q
22	41.929(11)	2.1529(6)	217(23)	K, M
23	42.566(7)	2.1221(3)	666(41)	K, Q
24	45.607(16)	1.9874(6)	771(44)	K, M
25	45.906(4)	1.97519(18)	380(31)	K, Q
26	47.18(9)	1.925(4)	96(16)	K, M
27	49.19(4)	1.8506(15)	58(12)	K, M
28	50.260(4)	1.81383(13)	1506(61)	Q
29	51.01(4)	1.7889(12)	247(25)	K, Q
30	55.31(4)	1.6596(10)	444(33)	K, Q
31	60.048(8)	1.53944(18)	745(43)	K, Q
32	62.41(3)	1.4867(6)	301(27)	K, M
33	64.15(2)	1.4505(4)	197(22)	K, Q
34	67.838(11)	1.3804(2)	378(31)	Q
35	68.263(9)	1.37283(15)	540(37)	Q
36	68.427(12)	1.3699(2)	365(30)	K, Q
37	72.33(2)	1.3053(4)	124(18)	K
38	73.65(2)	1.2852(3)	111(17)	K, Q
39	75.742(17)	1.2548(2)	238(24)	K, Q

Table 5.17 Detailed XRD result for sample Q3-14-36 D=Dikcite, Q=Quartz, O=Orthoclase, UN=Unknown

NO.	2-THETA(DEG)	D(ANG.)	HEIGHT(CPS)	PHASE NAME
1	12.380(9)	7.144(5)	1641(64)	D
2	20.40(2)	4.349(5)	282(27)	D
3	20.854(6)	4.2560(12	3967(100)	Q
4	21.22(5)	4.184(9)	622(39)	D, O
5	23.10(6)	3.847(10)	284(27)	D, O
6	23.48(5)	3.786(8)	380(31)	O
7	24.594(13)	3.6167(19	408(32)	D, O
8	24.898(11)	3.5732(16	1450(60)	D
9	25.31(2)	3.516(3)	235(24)	O
10	25.666(9)	3.4680(13	1597(63)	O
11	26.6485(15)	3.34234(1	29787(273)	Q
12	27.116(13)	3.2857(15	1778(67)	D, O
13	27.504(4)	3.2403(4)	4645(108)	O
14	29.821(16)	2.9936(15	779(44)	O
15	30.780(9)	2.9025(9)	828(46)	O
16	32.35(6)	2.765(5)	255(25)	O
17	34.34(5)	2.609(3)	318(28)	D, O
18	34.96(6)	2.565(4)	348(29)	D, O
19	35.55(7)	2.523(5)	309(28)	D, O
20	36.00(5)	2.493(4)	282(27)	D
21	36.568(6)	2.4552(4)	2316(76)	Q
22	38.45(5)	2.340(3)	394(31)	D
23	39.476(7)	2.2808(4)	1547(62)	Q
24	40.305(7)	2.2358(4)	936(48)	Q
25	41.793(8)	2.1596(4)	998(50)	D, O
26	42.459(7)	2.1272(3)	1726(66)	Q, O
27	45.49(4)	1.9924(15	211(23)	UN
28	45.761(12)	1.9811(5)	1023(51)	Q, D
29	45.97(4)	1.9725(15	156(20)	D, O
30	47.163(16)	1.9254(6)	274(26)	O
31	49.01(6)	1.857(2)	129(18)	D, O
32	50.143(3)	1.81778(1	2998(87)	Q
33	50.76(2)	1.7971(7)	578(38)	Q
34	54.876(8)	1.6717(2)	1010(50)	Q
35	55.319(17)	1.6593(5)	332(29)	Q
36	59.975(4)	1.54115(1	2641(81)	Q, D
37	61.65(4)	1.5032(8)	83(14)	D, O
38	62.27(5)	1.4898(11	246(25)	D, O
39	64.041(8)	1.45275(1	701(42)	Q
40	65.28(8)	1.4282(15	78(14)	D, O
41	67.760(4)	1.38178(6	1671(65)	Q
42	68.148(4)	1.37485(7	1810(67)	Q
43	68.330(6)	1.37164(1	1370(59)	Q, O
44	73.459(14)	1.2880(2)	452(34)	Q, D
45	75.662(6)	1.25589(8	677(41)	Q, D
46	77.666(13)	1.22842(1	253(25)	Q, D
47	79.909(10)	1.19948(1	639(40)	Q, D

Table 5.18 Detailed XRD result for sample Q3-14-37 Q=Quartz, I=Illite, K=Kaolinite UN=Unknown

NO.	2-THETA(DEG)	D(ANG.)	HEIGHT(CPS)	PHASE NAME
1	8.88(5)	9.95(5)	342(29)	I
2	12.435(8)	7.112(4)	2510(79)	K
3	17.83(11)	4.97(3)	52(11)	I
4	20.39(4)	4.351(8)	407(32)	K
5	20.896(8)	4.2476(17)	1252(56)	Q
6	24.936(13)	3.5678(19)	2571(80)	K
7	26.668(3)	3.3400(4)	7782(139)	Q
8	27.157(18)	3.281(2)	540(37)	UN
9	27.510(8)	3.2396(9)	1038(51)	UN
10	29.931(10)	2.9828(10)	316(28)	I
11	30.787(11)	2.9018(11)	185(22)	UN
12	34.28(3)	2.613(2)	153(20)	UN
13	34.97(2)	2.5637(17)	459(34)	K
14	36.00(2)	2.4926(13)	189(22)	K
15	36.560(19)	2.4557(13)	425(33)	Q
16	37.766(13)	2.3801(8)	253(25)	K
17	38.460(11)	2.3387(6)	337(29)	K
18	39.500(13)	2.2795(7)	250(25)	Q
19	41.84(8)	2.157(4)	102(16)	K
20	42.52(2)	2.1245(11)	405(32)	Q
21	45.518(18)	1.9911(8)	344(29)	K
22	45.843(12)	1.9778(5)	415(32)	Q
23	50.190(6)	1.8162(2)	895(47)	Q
24	50.88(4)	1.7933(13)	207(23)	Q
25	54.95(3)	1.6697(8)	366(30)	Q
26	59.976(6)	1.54113(13)	759(44)	Q
27	62.382(19)	1.4873(4)	299(27)	K
28	63.98(7)	1.4539(15)	143(19)	Q
29	67.783(12)	1.3814(2)	351(30)	Q
30	68.159(12)	1.3747(2)	430(33)	Q
31	72.23(9)	1.3069(14)	104(16)	K
32	73.64(2)	1.2852(4)	103(16)	Q
33	75.694(19)	1.2554(3)	222(24)	Q

Table 5.19 Detailed XRD result for sample Q3-14-39 Q=Quartz, P=Palygorskite, K=Kaolinite UN=Unknown

NO.	2-THETA(DEG)	D(ANG.)	HEIGHT(CPS)	PHASE NAME
1	8.966(14)	9.855(15)	1703(65)	P
2	12.448(5)	7.105(3)	5884(121)	K
3	17.86(3)	4.962(8)	399(32)	K, P
4	19.931(12)	4.451(3)	538(37)	K
5	20.932(9)	4.2404(17	2067(72)	Q, P
6	23.67(4)	3.756(6)	236(24)	K, P
7	24.989(10)	3.5604(14	5291(115)	K
8	25.71(3)	3.462(4)	591(38)	K
9	26.729(6)	3.3325(8)	10343(161)	Q
10	27.62(2)	3.227(3)	1218(55)	UN
11	34.34(4)	2.609(3)	210(23)	K
12	35.01(3)	2.561(2)	469(34)	K, P
13	36.103(14)	2.4858(9)	288(27)	K
14	36.612(4)	2.4524(3)	487(35)	Q
15	36.955(18)	2.4304(11	146(19)	UN
16	37.760(19)	2.3804(12	480(35)	K, P
17	38.51(2)	2.3357(12	518(36)	K
18	39.584(17)	2.2749(9)	434(33)	Q
19	40.36(2)	2.2331(11	308(28)	Q
20	41.78(11)	2.160(5)	129(18)	K
21	42.546(14)	2.1231(7)	544(37)	Q
22	45.65(3)	1.9858(12	474(34)	Q
23	47.00(9)	1.932(4)	88(15)	K, P
24	50.229(7)	1.8149(2)	872(47)	Q
25	50.73(8)	1.798(3)	152(19)	Q
26	51.12(7)	1.785(2)	237(24)	K
27	54.98(3)	1.6688(7)	556(37)	Q
28	60.020(10)	1.5401(2)	765(44)	Q
29	62.32(4)	1.4887(9)	299(27)	K
30	67.827(8)	1.38057(1	429(33)	Q
31	68.226(8)	1.37347(1	634(40)	Q
32	72.25(9)	1.3066(14	127(18)	P
33	73.53(7)	1.2869(10	141(19)	Q
34	75.716(10)	1.25513(1	236(24)	Q

Table 5.20 Detailed XRD result for sample Q3-14-43 Q=Quartz, P=Palygorskite, K=Kaolinite UN=Unknown

NO.	2-THETA(DEG)	D(ANG.)	HEIGHT(CPS)	PHASE NAME
1	8.97(3)	9.85(3)	477(35)	UN
2	12.496(6)	7.078(3)	3534(94)	K
3	20.04(2)	4.426(5)	751(43)	P
4	20.53(3)	4.322(5)	623(39)	K
5	21.008(10)	4.225(2)	1503(61)	Q
6	24.76(7)	3.592(10)	541(37)	UN
7	25.044(11)	3.5528(15)	3898(99)	K
8	25.81(2)	3.449(3)	276(26)	K
9	26.787(3)	3.3254(3)	6576(128)	Q
10	27.672(13)	3.2210(15)	985(50)	UN
11	29.95(2)	2.981(2)	399(32)	P
12	30.92(5)	2.890(5)	211(23)	UN
13	32.44(10)	2.758(9)	93(15)	K
14	34.38(2)	2.6065(16)	235(24)	P
15	35.09(2)	2.5554(14)	555(37)	K
16	36.139(9)	2.4834(6)	361(30)	UN
17	36.686(16)	2.4476(10)	481(35)	Q
18	37.85(2)	2.3749(15)	421(32)	K
19	38.56(2)	2.3330(11)	575(38)	K
20	39.564(8)	2.2760(5)	337(29)	Q
21	40.431(14)	2.2291(8)	253(25)	Q
22	42.572(9)	2.1219(4)	410(32)	Q
23	45.64(4)	1.9859(15)	399(32)	Q
24	50.258(7)	1.8139(3)	707(42)	Q
25	50.94(4)	1.7913(13)	255(25)	Q
26	55.004(13)	1.6681(4)	522(36)	Q
27	56.86(3)	1.6180(7)	158(20)	Q
28	60.065(9)	1.5390(2)	616(39)	Q
29	62.39(3)	1.4872(7)	397(31)	P
30	67.865(13)	1.3799(2)	321(28)	Q
31	68.258(11)	1.3729(2)	493(35)	Q
32	70.28(8)	1.3383(14)	103(16)	UN
33	72.23(4)	1.3069(7)	90(15)	Q

Table 5.21 Detailed XRD result for sample Q3-14-54 Q=Quartz, O=Orthoclase, K=Kaolinite UN=Unknown

NO.	2-THETA(DEG)	D(ANG.)	HEIGHT(CPS)	PHASE NAME
1	12.382(8)	7.143(4)	1695(65)	K
2	19.90(3)	4.458(7)	425(33)	K
3	20.42(2)	4.346(5)	522(36)	K
4	20.883(9)	4.2503(17)	3989(100)	Q
5	23.49(5)	3.785(7)	488(35)	O, Q
6	24.960(8)	3.5645(11)	1790(67)	O
7	25.723(6)	3.4605(9)	1334(58)	O
8	26.691(3)	3.3371(4)	20007(224)	Q
9	27.127(11)	3.2845(13)	1166(54)	O
10	27.544(8)	3.2357(9)	2338(76)	O
11	29.856(14)	2.9901(13)	638(40)	O, Q
12	30.865(8)	2.8946(8)	847(46)	O
13	34.27(7)	2.614(5)	278(26)	O
14	34.96(5)	2.564(4)	377(31)	O
15	36.561(10)	2.4557(7)	1388(59)	Q
16	38.50(5)	2.336(3)	397(31)	O
17	39.557(10)	2.2763(6)	1048(51)	Q
18	40.359(9)	2.2330(5)	927(48)	Q
19	41.81(3)	2.1588(17)	284(27)	O
20	42.499(7)	2.1253(3)	1587(63)	Q
21	45.465(10)	1.9933(4)	663(41)	K, UN
22	45.84(2)	1.9777(9)	644(40)	Q
23	48.937(19)	1.8597(7)	111(17)	O, K
24	50.202(4)	1.81580(13	2169(74)	Q
25	50.61(3)	1.8021(9)	384(31)	Q
26	54.935(6)	1.67000(18	1375(59)	Q
27	55.315(17)	1.6594(5)	381(31)	Q
28	56.83(8)	1.619(2)	81(14)	O, K
29	59.985(6)	1.54090(13	2114(73)	Q
30	62.34(3)	1.4883(7)	246(25)	O, K
31	64.01(3)	1.4533(6)	324(28)	Q
32	66.397(17)	1.4068(3)	170(21)	O, K
33	67.749(6)	1.38198(11	1201(55)	Q
34	68.208(5)	1.37379(9)	920(48)	Q
35	72.41(13)	1.304(2)	91(15)	O
36	73.50(4)	1.2874(6)	201(22)	Q
37	75.679(10)	1.25565(14	477(35)	Q
38	77.680(13)	1.22822(18	334(29)	Q
39	79.890(15)	1.19972(19	588(38)	O

Table 5.22 Detailed XRD result for sample Q3-14-57B M=Muscovite, Q=Quartz, K=Kaolinite, UN=Unknown

NO.	2-THETA(DEG)	D(ANG.)	HEIGHT(CPS)	PHASE NAME
1	9.055(11)	9.758(12)	432(33)	M
2	12.524(5)	7.062(3)	5877(121)	K
3	18.05(6)	4.910(17)	105(16)	M
4	19.974(13)	4.442(3)	837(46)	K
5	20.51(3)	4.328(7)	422(32)	K
6	20.996(8)	4.2277(16	1251(56)	M
7	25.041(5)	3.5531(7)	5859(121)	K
8	26.798(7)	3.3240(8)	6723(130)	Q
9	27.69(2)	3.219(3)	1099(52)	UN
10	30.9(3)	2.89(2)	90(15)	M
11	35.17(3)	2.549(2)	564(38)	K
12	36.167(11)	2.4816(8)	353(30)	K
13	36.731(6)	2.4447(4)	432(33)	Q
14	37.90(2)	2.3718(14	585(38)	K
15	38.58(3)	2.3315(16	577(38)	K
16	39.627(9)	2.2725(5)	348(30)	K
17	41.88(10)	2.155(5)	115(17)	UN
18	42.634(7)	2.1189(3)	432(33)	K, Q
19	45.77(3)	1.9807(12	392(31)	K
20	47.16(5)	1.9254(19	61(12)	K
21	50.286(7)	1.8129(2)	783(44)	Q
22	51.14(4)	1.7847(12	274(26)	K, Q
23	55.26(4)	1.6610(12	397(31)	K
24	56.73(10)	1.621(3)	121(17)	K, Q
25	60.112(14)	1.5380(3)	595(39)	K, Q
26	62.41(3)	1.4867(6)	357(30)	K
27	65.31(8)	1.4276(15	104(16)	K
28	67.881(13)	1.3796(2)	304(28)	K, Q
29	68.259(14)	1.3729(2)	337(29)	K, Q
30	70.41(5)	1.3362(9)	99(16)	UN
31	72.35(8)	1.3050(13	136(18)	UN
32	73.74(12)	1.2838(17	86(15)	Q
33	76.1(5)	1.250(7)	22(7)	M

Table 5.23 Detailed XRD result for sample Q3-14-65 I=Illite, Q=Quartz, K=Kaolinite, UN=Unknown

NO.	2-THETA(DEG)	D(ANG.)	HEIGHT(CPS)	PHASE NAME
1	8.891(11)	9.937(12)	663(41)	I
2	12.421(4)	7.120(3)	4880(110)	K
3	18.25(3)	4.857(8)	188(22)	I
4	19.98(2)	4.440(5)	1008(50)	K, I
5	20.229(16)	4.386(4)	1045(51)	K, I
6	20.937(8)	4.2395(15)	1819(67)	Q
7	21.47(2)	4.136(4)	408(32)	K
8	22.077(14)	4.023(3)	305(28)	UN
9	24.928(7)	3.5690(10)	4718(109)	K
10	26.704(3)	3.3355(4)	10511(162)	I, Q
11	27.126(18)	3.285(2)	534(37)	UN
12	27.560(12)	3.2339(13)	1230(55)	I, UN
13	29.83(3)	2.992(3)	282(27)	I
14	30.866(18)	2.8946(16)	530(36)	I, UN
15	32.392(19)	2.7616(16)	149(19)	I
16	35.06(4)	2.557(3)	581(38)	K, I
17	35.59(5)	2.520(4)	316(28)	K, I
18	36.055(18)	2.4890(12)	290(27)	K, I
19	36.61(2)	2.4522(15)	485(35)	Q
20	37.78(4)	2.379(2)	420(32)	K
21	38.52(3)	2.335(2)	554(37)	K
22	39.535(6)	2.2776(4)	570(38)	Q
23	41.811(17)	2.1587(9)	155(20)	UN
24	42.509(15)	2.1249(7)	431(33)	Q
25	45.49(2)	1.9921(10)	425(33)	K, I
26	45.854(10)	1.9773(4)	422(32)	Q
27	50.190(5)	1.81617(17)	1087(52)	Q
28	50.94(4)	1.7913(13)	248(25)	Q
29	54.95(3)	1.6697(7)	579(38)	Q
30	55.299(19)	1.6599(5)	310(28)	Q
31	59.988(7)	1.54084(17)	716(42)	Q
32	62.28(3)	1.4895(5)	398(32)	I
33	67.790(11)	1.3812(2)	404(32)	Q
34	68.177(6)	1.37434(10)	395(31)	Q

5.6 Discussion-Petrography

The sandstone of Sharawra formation is classified as mature arkose, making a percentage of 80 percent on average, feldspar up to 4 percent and rock fragment in less than one percent. The dominant clays found in the sandstone of Sharawra Formation are kaolinite and a few percents of illite, palygorskite, and dickite are also observed. The stacked

booklet texture of kaolinite is present is almost all the samples of Sharawra formation. The presence of iron oxide is interpreted as authigenic cement coating the quartz. The iron oxide is present in patches, and appears to be formed late in the diagenetic history. The presence of kaolinite sometime reduces and sometime increases the porosity depending on the amount of clay present in the samples. On the other hand the presence of palygorskite clay always decrease the permeability, because its needle like structure acts as a bridge between the pores and helping in the connection of pores. However, polygorskite is not present consistently in Sharawra Formation.

5.7 Petrophysical Study

Porosity and permeability are among the most important parameters to describe the quality of a sandstone reservoir. Not only the porosity values, but their magnitude, their pattern, and variation in values also play an important role. All these parameters influence the amount and distribution of hydrocarbons in a reservoir. The sandstone reservoirs are heterogeneous in terms of their porosity and permeability.

The porosity and permeability values were obtained in the laboratory. Earth sciences Department's lab facilities were used to obtain these parameters. Obtaining cores from the very thin beds of siltstones and from a few sandstone samples were not possible. However, vertical and horizontal cores were obtained from every possible facies. About 24 core plugs were prepared in the laboratory. For each core plug porosity and permeability measurements were performed. Gas expansion and saturation method was used for the porosity analysis. Gas permeability and liquid permeability method was used for determining permeability.

5.7.1 Porosity

The porosity values have proved to be variable throughout the northwestern and central outcrop section. The value for the basal facies is 7 %. The porosity value for the overlying fine grained facies increases drastically up to 27 %. For the siltstone facies, the values decreases to 18 %, the values for the overlying sandstone facies range from 18 to 20 percent. But the values for the medium grained topmost sandstone are around 7 %. The calcareous sandstone is less porous and the value of its porosity is 3 %. For the northwestern outcrop the porosity values are almost similar to the central outcrop. However, as the medium grained sandstone and the basal sandstone are missing in the northwestern outcrop, so the average porosity is higher in that section. The porosity values range from 15 % to 20 % in the northwestern outcrop. The porosity values obtained from the core plug measurements are shown in Table 5. 9. From the petrographic results it is evident that Sharawra Formation sandstone and siltstones process primary (inter-granular) porosity. From the thin section and SEM results, negligible amount of intra-granular porosity has been observed. The comparison between core plug measured porosity and visual porosity is given in Table 5. 10.

5.7.2 Permeability

The Gas permeability was measured by using Hassler Coreholder Assembly, after the core introduced into the holder, overburden pressure of 500 psi was applied to make sure that all the injected nitrogen will pass through the core sample. Then the inlet pressure gauge was adjusted at a certain value and the nitrogen was injected and allowed to pass through the core at a very low rate (to assure no turbulent flow) for some time until the

steady state condition is reached. Then some of the produced gas was collected. After that the time needed to collect that amount of the gas, the volume of the collected gas and the inlet pressure are reported, those values were used to calculate the nitrogen permeability, the previous procedure were repeated five times for each sample, then a relationship between the calculated five nitrogen permeabilities and the inverse of the mean pressure (five values) was stablished (straight line) as shown in Figure 5.70, from this relationship we recognize that the value at $1/P_m = 0$ represents infinity P_m and the gas behaves as liquid ("Klinkenberg correction").

Table 5.24 Porosity values obtained from core plug measurements.

Sample ID	Sample Length (cm)	Sample Diam. (cm)	Sample Porosity (%)
UD-14-01	2.605	2.515	5.33
UD-14-02	5.105	2.510	1.66
UD-14-5B	5.065	2.550	2.62
UD-14-6A	2.565	2.520	3.37
UD-14-9B	5.065	2.505	7.25
UD-14-11	2.535	2.500	18.84
UD-14-14	2.525	2.469	20.08
UD-14-16	2.525	2.485	20.77
UD-14-18	4.420	2.480	20.07
UD-14-20	1.235	2.500	22.03
UD-14-22	5.055	2.485	21.69
UD-14-34	1.295	2.455	18.47
UD-14-38	1.295	2.435	11.41
UD-14-42	1.255	2.465	25.52
UD-14-52	5.055	2.485	9.01
Q3-5-9	2.570	2.520	5.55
Q3-6-22B	5.075	2.505	22.88
Q3-6-23A	2.565	2.485	20.77
Q3-6-24A	3.855	2.510	19.83
Q3-6-25A	3.880	2.510	13.69
Q3-6-25B	1.905	2.520	19.36
Q3-6-26A	1.255	2.465	18.47
Q3-6-27A	2.540	2.505	19.47
Q3-7-2	5.105	2.520	2.81

Table 5.25 Comparing the thin section porosity values with core plug porosity measurements.

Sample ID	visual porosity	Sample Porosity (%)
UD-14-01	4	5.33
UD-14-02	3	1.66
UD-14-5B	1	2.62
UD-14-6A	3	3.37
UD-14-9B	5	7.25
UD-14-11	1	18.84
UD-14-14	13	20.08
UD-14-16	15	20.77
UD-14-18	11	20.07
UD-14-20	20	22.03
UD-14-22	23	21.69
UD-14-34	22	18.47
UD-14-38	18	11.41
UD-14-42	25	25.52
UD-14-52	7	9.01
Q3-5-9	6	5.55
Q3-6-22B	15	22.88
Q3-6-23A	18	20.77
Q3-6-24A	10	19.83
Q3-6-25A	20	13.69
Q3-6-25B	18	19.36
Q3-6-26A	7	18.47
Q3-6-27A	19	19.47
Q3-7-2	3	2.81

Therefore, the value of K_g on the Y-axis at the intercept C is equivalent to liquid permeability K_L. This value of K_L is the corrected value for the Klinkenberg effect, the Klinkenberg constant could be calculated from the liquid permeability and the slope of the straight line shown in Figure 5.70.

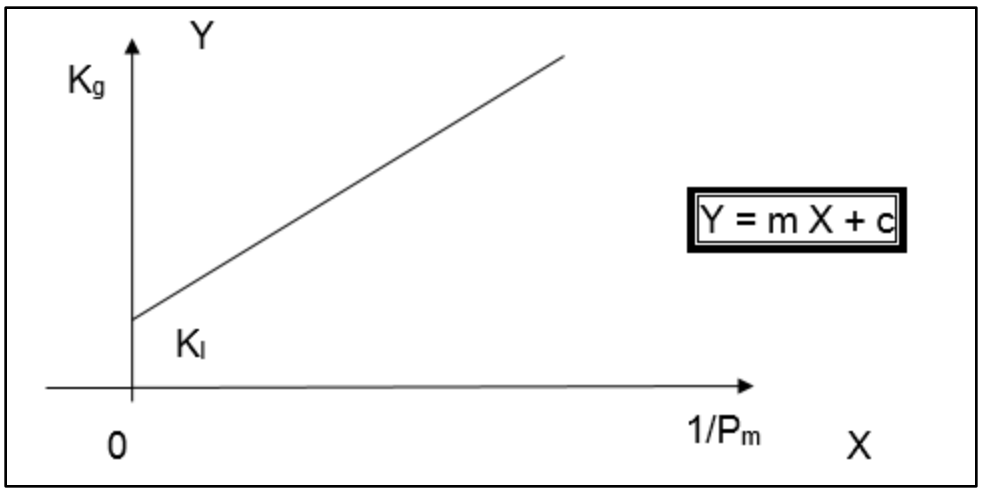

Figure 5.55 Liquid Permeability Calculations from Measured Gas Permeability.

The permeability values of Sharawra Formation also show a wide range (see Table 5.11). The values vary from few milliDarcy (mD) to hundreds of milliDarcy (mD.) The top calcareous facies are almost impermeable. The medium grained sandstone facies (LF 3) has a low permeability as compared to the lower sandstone facies. The LF 3 showed a liquid permeability of 5.32 and a nitrogen permeability of 22.90. The fine-grained sandstone facies LF 4 showed a liquid permeability around 33 md and a nitrogen permeability of about 71 md. Surprisingly the siltstone facies showed relatively good permeability. LF 6 showed a liquid permeability around 45 md and a nitrogen permeability of about 124 md. The LF 7 and LF 8 showed a similar permeability trend to LF 6. The very fine grained sandstone LF 9 showed a low permeability. This facies showed a liquid permeability around 7 md and a nitrogen permeability of about 24 md. The porosity value for each sample against its permeability values is summed up in Table 5.12.

Table 5.26 Permeability results for core plug measurements.

Sample ID	Sample Length (cm)	Sample Diam. (cm)	Liquid Permeability (md)	Nitrogen Permeability (md)
UD-14-01	2.605	2.515	Impermeable	Impermeable
UD-14-02	5.105	2.510	Impermeable	Impermeable
UD-14-5B	5.065	2.550	Impermeable	Impermeable
UD-14-6A	2.565	2.520	Impermeable	Impermeable
UD-14-9B	5.065	2.505	5.32	22.89
UD-14-11	2.535	2.500	27.73	59.20
UD-14-14	2.525	2.469	31.43	71.85
UD-14-16	2.525	2.485	31.43	71.85
UD-14-18	4.420	2.480	6.704	32.05
UD-14-20	1.235	2.500	49.14	165.89
UD-14-22	5.055	2.485	43.17	135.65
UD-14-34	1.295	2.455	45.45	124.82
UD-14-38	1.295	2.435	13.18	20.56
UD-14-42	1.255	2.465	12.19	34.56
UD-14-52	5.055	2.485	7.14	24.82
Q3-5-9	2.570	2.520	Impermeable	Impermeable
Q3-6-22B	5.075	2.505	301.62	335.67
Q3-6-23A	2.565	2.485	118.53	139.66
Q3-6-24A	3.855	2.510	16.19	47.77
Q3-6-25A	3.880	2.510	4.25	29.91
Q3-6-25B	1.905	2.520	40.21	75.01
Q3-6-26A	1.255	2.465	37.81	67.7
Q3-6-27A	2.540	2.505	37.81	67.7
Q3-7-2	5.105	2.520	Impermeable	Impermeable

Table 5.27 Porosity and permeability comparison.

Sample ID	Sample Porosity (%)	Liquid Permeability (md)	Nitrogen Permeability (md)
UD-14-01	5.33	Impermeable	Impermeable
UD-14-02	1.66	Impermeable	Impermeable
UD-14-5B	2.62	Impermeable	Impermeable
UD-14-6A	3.37	Impermeable	Impermeable
UD-14-9B	7.25	5.32	22.89
UD-14-11	18.84	27.73	59.2
UD-14-14	20.08	31.4	71.85
UD-14-16	20.77	31.4	71.85
UD-14-18	20.07	6.70	32.05
UD-14-20	22.03	49.14	165.89
UD-14-22	21.69	43.17	135.65
UD-14-34	18.47	45.45	124.82
UD-14-38	11.41	13.18	20.56
UD-14-42	25.52	12.19	34.56
UD-14-52	9.01	7.14	24.82
Q3-5-9	5.55	Impermeable	Impermeable
Q3-6-22B	22.88	301.62	335.67
Q3-6-23A	20.77	118.53	139.66
Q3-6-24A	19.83	16.19	47.77
Q3-6-25A	13.69	4.25	29.91
Q3-6-25B	19.36	40.21	75.01
Q3-6-26A	18.47	37.81	67.7
Q3-6-27A	19.47	37.81	67.7
Q3-7-2	2.81	Impermeable	Impermeable

5.7.3 Porosity and Permeability Patterns in Sharawra Formation

The petrophysical (porosity and permeability) patterns of Sharawra Formation at central and northwestern outcrop is shown in Figures 5.71, and 5.72 respectively. The porosity values for the sandstones and the siltstones show a little variation. However, calcareous sandstone porosity values do vary from the lower sandstones. Permeability values show a wide variability. The maximum, minimum and average porosity readings of the central

outcrop are 25%, 2% and 13.5% respectively. The maximum, minimum and average permeability values are 165 mD, 22 mD and 68mD from nitrogen permeability. For the northwestern outcrop, the maximum, minimum and average porosity readings are 20%, 3% and 15.5% respectively. And the respective permeability values are about 108 mD on average, maximum is 335 mD and minimum is 29 mD.

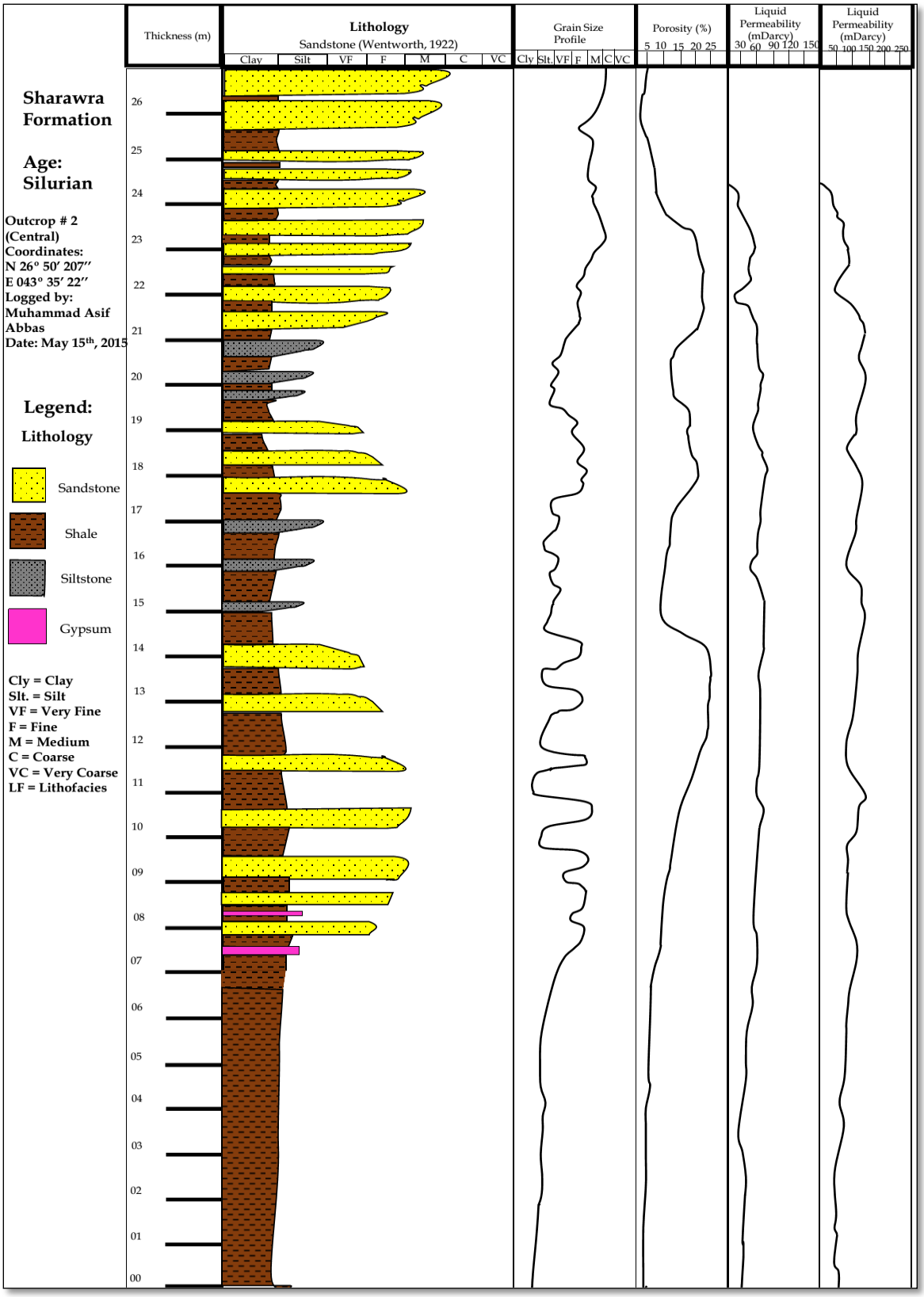

Figure 5.56 Porosity and permeability log for central outcrop.

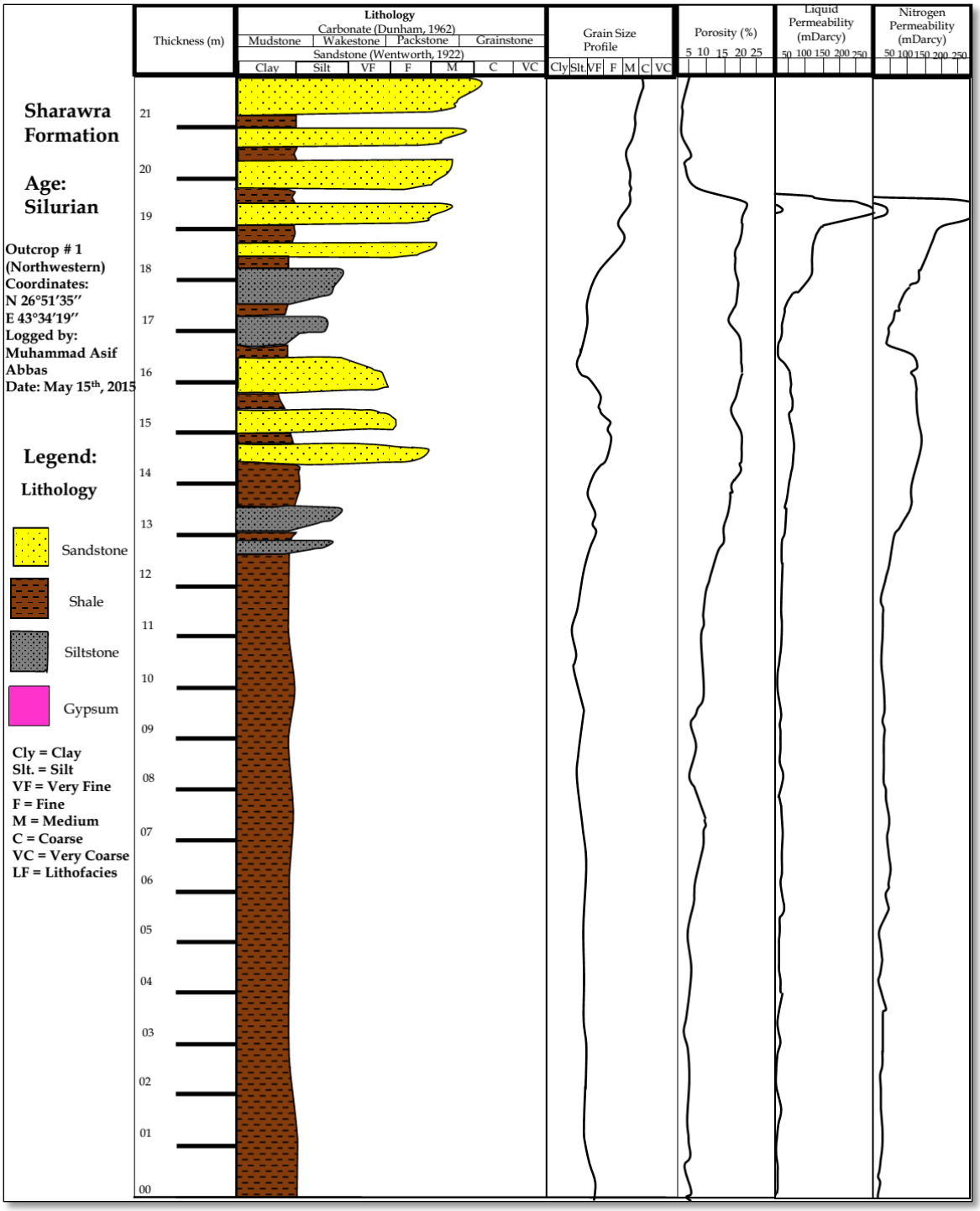

Figure 5.57 Porosity and permeability log for northwestern outcrop.

5.8 Petrophysical Controlling Factors

In terms of petropysical parameters there is some hetrogenity in Sharawra Formation. The heterogenity is more in the permeability values than in the porosity. There are many factors that are controlling the heterogeneity of the sandstone and siltstones. The factors include clay cementation especially kaolinite, iron oxide cementation, and also compaction and packing. There is also some minor role played by the quartz overgrowth. These factors are revealed by thin section studies, SEM, and XRD analysis. These factors are discussed in the following sections

5.8.1 Authigenic Clays

XRD analysis has been done not only for the sandstones and siltstones, but also for the shale interbeds, between them. From the sandstone and siltstone samples koalinite appears to be the most common clay type. However, from the shale XRD data, illite has been found in the middle and lower parts of the Sharawra Formation. Palygorskite is also present in one of the samples in the middle part of the formation. All these clay types tend to reduce the porosity and block the throats of pores, which causes the reduction in permeability. The clays appear to be present more as pore filling and pore lining material rather than as grain overgrowths. The booklet structure of kaolinite is less harmful in reducing the petrophysical parameters, as compared to the needle like illite and cross hatched needle shape of palygorskite. This probably explains the heterogenity in porosity and permeability.

5.8.2 Quartz Overgrowth

The overgrowths of any kind will hinder the flow of the fluids, as the overgrowths increase the diameter of grains and hence the pores are reduced. The quartz overgrowth is a non porous cement and hence the porosity is greatly affected. Quartz overgrowth is not present throughout the section but it is evident in many of the samples.

5.8.3 Iron Oxide

The iron oxide cementation also plays an effective role in reducing the porosity and permeability values. It can block a pore throat and hence reduce the pore connectivity. This causes deterioration in petrophysical parameters. After the thin section study, SEM-EDS confirmed the presence of iron oxide cement in most of the sand and siltstone samples, especially in the middle and lower parts of the two outcrop sections.

5.8.4 Compaction and Packing

The sorting of sandstone has a great impact on porosity. The sandstones having poor sorting have lower values of porosity, on the other hand the porosity values of well sorted sands are higher. The petrographic study reveals that the sorting of Sharawra Formation sandstone and siltstone is moderately sorted to well sorted. Placing of grains is also important as it helps in sorting. Both the compaction and placing play a vital role in the porosity and permeability values. The packing occurs in two stages, first is the primary packing during deposition. Other is the post depositional packing, finally a rock undergoes compaction as the overburden pressure increases. The relation for the porosity values and the sorting of representative samples is shown in Table 5.13.

Table 5.28 Porosity w.r.t sorting in Sharawra Formation.

Sample Number	Porosity %	Sorting
UD-14-01	4.42	Moderately sorted
UD-14-02	0.19	Moderately sorted
UD-14-5B	13.30	Moderately sorted
UD-14-6A	2.15	Moderately to poorly sorted
UD-14-9B	7.92	Moderately to poorly sorted
UD-14-11	20.07	Well sorted
UD-14-14	21.36	Moderately well sorted
UD-14-16	18.66	Moderately well sorted
UD-14-18	22.03	Moderately well sorted
UD-14-20	21.79	Well sorted
UD-14-22	21.14	Well sorted
UD-14-34	18.47	Well sorted
UD-14-38	11.41	Moderately well sorted
UD-14-40	27.07	Moderately sorted
UD-14-54	7	Moderately sorted
Q3-5-9	0.07	Moderately sorted
Q3-6-22B	19.64	Moderately well sorted
Q3-6-23A	21.98	Moderately well sorted
Q3-6-24A	20.93	Moderately well sorted
Q3-6-25A	17.93	Moderately sorted
Q3-6-25B	18.12	Moderately well sorted
Q3-6-26A	18.40	Moderately well sorted
Q3-6-27A	10.06	Moderately sorted
Q3-7-02	0.87	Poorly sorted

CHAPTER 6

RESULTS AND DISCUSSIONS-GEOCHEMISTRY

The northwestern and central outcrop samples were analysed under XRF and ICP-OES. The major element geochemistry of the Sharawra Formation is presented in Tables 6.1 and 6.2. Trace element geochemistry is shown in Table 6.3. Table 6.1 shows that all the sandstone samples are enriched with SiO_2 (57.02% wt. average) and the concentration of Al_2O_3 is low (10.31% wt. average), K_2O (6.9% wt. average), Fe_2O_3 (11.55% wt. average), CaO (11.30% wt. average), TiO_2 (2.29% wt. average), and MnO (0.21% wt. average). To express the variation of major elements concentrations, histograms for SiO_2, $Al2O_3$, K_2O, and Fe_2O_3 are shown in Figures 6.1 to 6.4, respectively. NaO_2 is negligible in XRF results; however, trace elements results have shown the presence of NaO_2. The ICP-OES results revealed that the Sharawra Formation is rich in trace elements like Ba, Cd, Co, Cr, Cu, Na, Ni, Pb, Sr, V and Zr. The average concentration of the trace elements dominantly found in sandstones and siltstones was Ba (34.46 mg/l), Cd (1.43 mg/l), Co (12.48 mg/l), Cr (60.01 mg/l), Cu (25.15 mg/l), Li (37.69 mg/l), Na (490.85 mg/l), Ni (34.02 mg/l), Pb (53.80 mg/l), Sr (43.69 mg/l), V (45.06 mg/l), and Zn (43.80 mg/l) as shown in Table 6. 3. Cr, Ni, V, and Sr variation in both outcrops are shown with the help of histograms. Cr, Ni, V, and Sr histograms are shown in Figures 6.5 to 6.8. The concentration of trace elements is given in parts per million (ppm). Geochemical logs also provide a better picture for the geochemical variation throughout the outcrop. For the northwestern outcrop (outcrop 1) the geochemical log shows less variation as it contains a lower number of facies (Figure 6.9). The central outcrop (outcrop 2) is representative

for the maximum number of lithofacies in the study area. The variation is quite visible due to presence of two calcareous sandstone facies at the top (Figure 6.10)

Table 6.1 Major Element concentration in Sharawra Formation in Wt% continued...

Sample #	SiO2	Al2O3	K2O	Fe2O3	P2O5	CaO	TiO2	Cr2O3	MnO	CuO	ZnO
Q3-5-9B	51.12	10.90	6.95	21.33	0.27	3.45	2.26	0.03	1.20	0.02	0.22
Q3-6-22A	68.76	9.61	11.41	4.09	0.26	3.13	1.72	0.07	1.03		
Q3-6-23A	64.61	9.18	12.43	7.92	0.04	2.41	2.12	0.02	1.06	0.03	
Q3-6-24A	45.68	7.50	7.92	9.90		20.87	1.58	0.04	1.26		0.02
Q3-6-25B	40.32	6.21	7.09	7.64	0.36	28.52	1.59	0.02	1.03		0.04
Q3-6-26A	51.78	8.03	8.46	7.96	0.25	20.26	1.52	0.02	1.24	0.02	0.04
Q3-6-27B	53.12	6.72	7.94	15.58	0.48	15.43	1.21	0.03	1.72	0.02	0.08
Q3-6-28B	57.56	4.70	6.57	11.75	0.23	25.59	1.45	0.04	2.58	0.03	0.04
UD-13-01	6.27		0.29	2.00	0.40	90.68	0.11	0.06	1.10		
UD-13-02	5.33	1.10	0.13	1.00	0.26	92.66	0.02				
UD-13-05	2.03			1.16	0.37	95.65		0.04	1.20		
UD-13-06	1.87			1.34		96.35		0.03	0.16		
UD-13-07	88.26	3.00	1.56	4.56		1.51		0.00	1.12		
UD-13-08	90.51	3.23	1.97	5.68		1.01	0.78	0.03	1.09		0.01
UD-13-09	80.56	5.88	2.67	8.36		1.00		0.00	1.89		0.09
UD-13-10	62.65	14.96	0.43	10.99	0.30	2.02	3.62	0.03	0.64	0.05	0.11
UD-13-11	65.24	14.03	0.34	10.53	0.27	2.56	2.79	0.00	1.13	0.06	0.12
UD-13-12	67.30	10.89	10.44	4.44	0.32	1.14	1.02	0.03	1.58	0.01	0.04
UD-13-13	68.86	9.48	9.54	6.22	0.71	0.18	1.04	0.03	1.05	0.02	0.03
UD-13-16	71.36	8.90	10.54	4.77	0.44	1.51	2.11		1.10	0.03	0.01
UD-13-18	76.24	6.24	8.24	4.58	0.56	1.32	1.30	0.02	1.12	0.02	0.06
UD-13-19	52.97	13.40	6.51	21.33	0.56	2.05	1.64	0.03	1.11		0.08
UD-13-20	69.05	9.78	11.06	3.16	0.11	1.43	1.00	0.04	1.05		0.01
UD-13-21	45.99	11.59	6.31	28.51	0.52	3.44	2.84	0.03	1.17		0.11
UD-13-27	61.26	13.72	7.46	11.23	0.43	2.00	3.26	0.07	1.13	0.08	0.08
UD-13-28	61.79	12.88	8.26	10.37	0.60	2.48	2.81	0.03	1.04	0.05	0.05
UD-13-30	68.98	10.15	11.02	4.75	0.32	1.59	2.37	0.03	1.94		0.05
UD-13-32	52.27	12.99	7.00	22.35	0.34	2.03	1.59	0.02	0.66		0.14
UD-13-34	53.58	10.75	7.50	22.03	0.53	2.18	1.11	0.07	1.26	0.05	0.19
UD-13-35	53.58	10.75	7.50	22.03	0.53	2.18	2.41	0.07	1.26	0.05	0.19
UD-13-36A	53.51	9.75	6.50	23.03	0.80	1.18	0.91	0.09	1.56	0.10	0.09
UD-13-36B	53.58	10.48	7.50	22.03	0.53	2.18	2.41	0.07	1.26	0.05	0.19
UD-13-38	54.62	8.99	7.03	22.74	0.49	2.91	1.99	0.05	1.08		0.13
UD-13-40	65.00	9.17	10.93	9.24	0.74	1.24	2.67	0.09	1.07		0.05
UD-13-41	55.46	15.09	7.02	15.64	0.24	1.23	3.36	0.04	1.15	0.08	0.12
UD-13-42	68.17	6.70	8.96	12.71	0.26	1.02	0.91	0.07	2.99		0.02
UD-13-43	66.00	7.91	8.99	14.68	0.26	1.24	0.96	0.10	1.96		0.04
UD-13-44	63.17	7.70	8.26	13.71	0.26	1.52	0.91	0.57	2.79		0.02
UD-13-46	62.82	10.34	9.36	11.25	0.08	1.89	0.84	0.05	0.07		0.07
UD-13-49	57.67	13.32	6.73	16.31	0.14	1.57	3.63	0.09	1.08	0.04	0.12
UD-13-50	67.01	8.03	9.47	9.84	0.25	3.40	1.30	0.07	2.08		0.07
UD-13-52	62.12	10.72	9.34	9.67	0.37	3.50	1.19	0.03	3.03		0.07
UD-13-54	62.91	9.79	8.56	9.99	0.03	4.27	1.56	0.02	2.87		0.02
UD-13-55	54.52	14.35	6.37	14.46	0.11	0.86	3.61	0.06	0.09	0.06	0.18
UD-13-57	60.42	17.04	6.39	8.48		0.56	1.68	0.05		0.06	0.07
UD-13-59	56.25	14.09	7.06	13.63	0.04	0.75	1.47	0.06	1.05	0.05	0.11
UD-13-63	54.69	14.24	5.24	12.56	0.02	0.65	3.24	0.04	1.05	0.37	0.12
Mean	57.02	10.32	6.90	11.86	0.36	11.28	603.46	0.06	1.33	0.07	0.08
Median	61.79	10.41	7.46	11.25	0.33	1.89	1.59	0.04	1.13	0.05	0.08
St. Deviation	20.49	3.62	3.30	7.18	0.21	28.30	3559.30	0.09	0.68	0.08	0.05

Table 6.2 Major Element concentration in Sharawra Formation in Wt%

Sample #	Rb2O	SrO	Y2O3	ZrO2	BaO	Na2O	NiO	V2O5	PbO	Total	CIA	CIW
Q3-5-9B	0.05	0.06	0.01	0.06	0.16	1.16	0.08	0.05		96.75	51.20	75.98
Q3-6-22A	0.08	0.07	0.00	0.17	0.34	1.16	0.03		0.01	99.09	39.80	75.45
Q3-6-23A	0.04	0.08	0.01	0.11	0.33	1.16	0.03		0.01	98.83	38.23	79.24
Q3-6-24A	0.03	0.10	0.01	0.14	0.31	1.16	0.05	0.05		93.76	20.66	76.43
Q3-6-25B	0.03	0.08	0.01	0.11	0.21	1.16	0.04	0.06		92.83	14.85	77.88
Q3-6-26A	0.03	0.06	0.01	0.07	0.24	0.70		0.01		99.58	21.84	78.38
Q3-6-27B	0.03	0.08	0.01	0.04		0.70				102.3	22.32	80.32
Q3-6-28B	0.02	0.09	0.01	0.10	0.22	0.70	0.03			110.5	12.75	75.52
UD-13-01		0.07		0.03		0.70				99.90	0.00	
UD-13-02						0.70				100.4	1.17	1.17
UD-13-05		0.82				0.12				99.45	0.00	0.00
UD-13-06		0.05				0.12				99.75	0.00	0.00
UD-13-07		0.00				0.18				99.03	49.39	69.88
UD-13-08	0.00	0.01	0.00	0.08		4.95	0.06			103.2	52.00	76.11
UD-13-09	0.07	0.08		0.24		4.95	0.10			98.55	61.54	85.42
UD-13-10	0.05	0.07	0.01	0.07		7.37	0.06	0.04		95.29	85.92	88.11
UD-13-11	0.06	0.10	0.00	0.01		7.37	0.10	0.02		96.07	82.88	84.56
UD-13-12	0.04	0.08	0.00	0.05	0.24	7.37				95.70	50.50	83.58
UD-13-13	0.03	0.04	0.00	0.04	0.25	7.37	0.02		0.00	96.17	49.71	88.90
UD-13-16	0.03	0.06	0.01	0.16		2.72	0.02		0.01	99.77	49.50	85.48
UD-13-18	0.04	0.06	0.02	0.17	0.33	2.72	0.03			98.69	49.48	82.51
UD-13-19	0.05	0.10	0.01	0.06		0.30	0.07			98.69	61.02	86.73
UD-13-20	0.03	0.06	0.01	0.14	0.27	4.00		0.06		95.69	43.92	87.21
UD-13-21	0.06	0.15	0.01	0.09		4.00	0.13			99.51	54.31	77.10
UD-13-27	0.04	0.05	0.01	0.07		4.00				99.72	59.19	87.28
UD-13-28	0.04	0.08	0.01	0.12	0.28	4.00	0.05			99.36	54.55	83.86
UD-13-30	0.03	0.07	0.01	0.16	0.33	4.00	0.03			99.29	44.59	86.46
UD-13-32	0.05	0.07	0.01	0.08	0.00	4.00	0.05	0.02		98.71	59.00	86.50
UD-13-34	0.06	0.08	0.02	0.10	0.13	0.61		0.07		98.25	52.61	83.11
UD-13-35	0.06	0.08	0.02	0.10	0.13	0.61				99.55	52.61	83.11
UD-13-36A	0.16	0.98	0.01	0.09	0.13	0.61				96.52	55.93	89.17
UD-13-36B	0.06	0.08	0.02	0.10	0.13	0.56				99.28	51.97	82.75
UD-13-38	0.04	0.08	0.01	0.12		0.56		0.03		99.02	57.49	75.57
UD-13-40	0.04	0.10	0.01	0.26	0.29	0.56		0.10		99.20	52.97	88.10
UD-13-41	0.05	0.08	0.01	0.08		0.75	0.07			98.43	64.67	92.49
UD-13-42	0.03	0.07	0.00	0.05	0.18	0.75	0.06		0.00	99.61	50.19	86.83
UD-13-43	0.02	0.06	0.00	0.04	0.15	0.75	0.06			101.1	49.62	86.49
UD-13-44	0.03	0.07	0.00	0.05	0.18	0.75	0.06		0.00	96.91	49.08	83.55
UD-13-46	0.04	0.07	0.01	0.05	0.19	3.47	0.04			96.77	47.91	84.56
UD-13-49	0.07	0.07	0.01	0.09		3.47		0.07	0.01	99.68	61.62	89.48
UD-13-50	0.03	0.07	0.01	0.08	0.23	3.47		0.05		99.53	58.43	70.27
UD-13-52	0.04	0.07	0.01	0.10	0.25	5.74				97.04	49.64	70.44
UD-13-54	0.04	0.10	0.01	0.10	0.24	4.74				98.02	49.27	69.65
UD-13-55	0.11	0.05	0.01	0.08		8.74	0.12	0.05		94.66	66.49	94.37
UD-13-57	0.05	0.06	0.01	0.09		8.74	0.04	0.05	0.00	94.76	71.01	96.81
UD-13-59	0.06	0.04	0.01	0.07	0.19	8.74	0.06	0.09		93.54	64.32	94.92
UD-13-63	0.06	0.04	0.07	0.06	0.15	5.33	0.09	0.03		91.20	70.74	95.62
Mean	0.05	0.11	0.01	0.09	0.20	2.93	0.06	0.05	0.00			
Median	0.04	0.07	0.01	0.08	0.19	1.16	0.06	0.05	0.00			
St. Deviation	0.03	0.19	0.01	0.05	0.08	2.67	0.03	0.02	0.00			

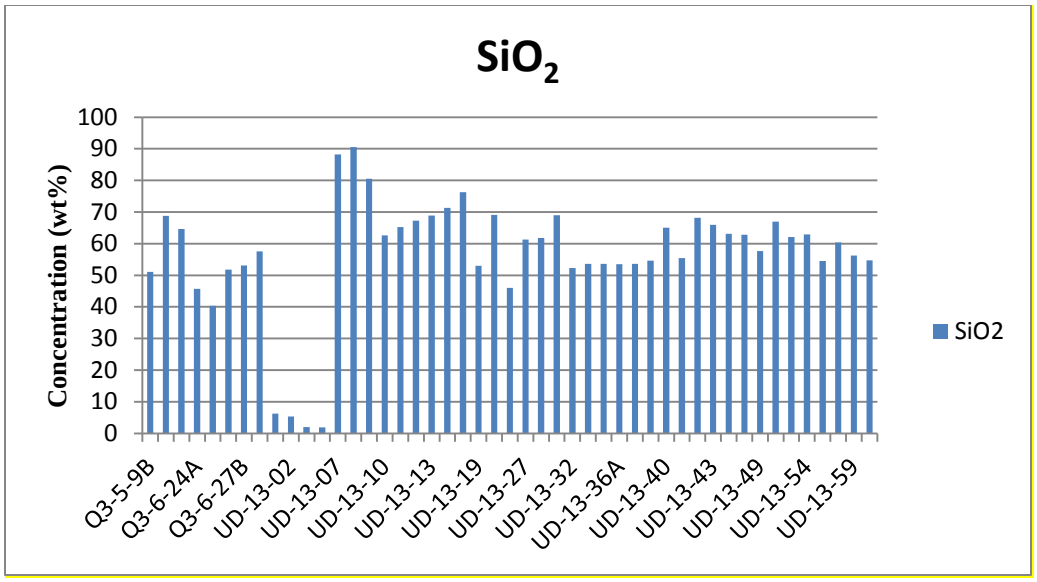

Figure 6.1 SiO2 concentration variation in both Sharawra Formation outcrops.

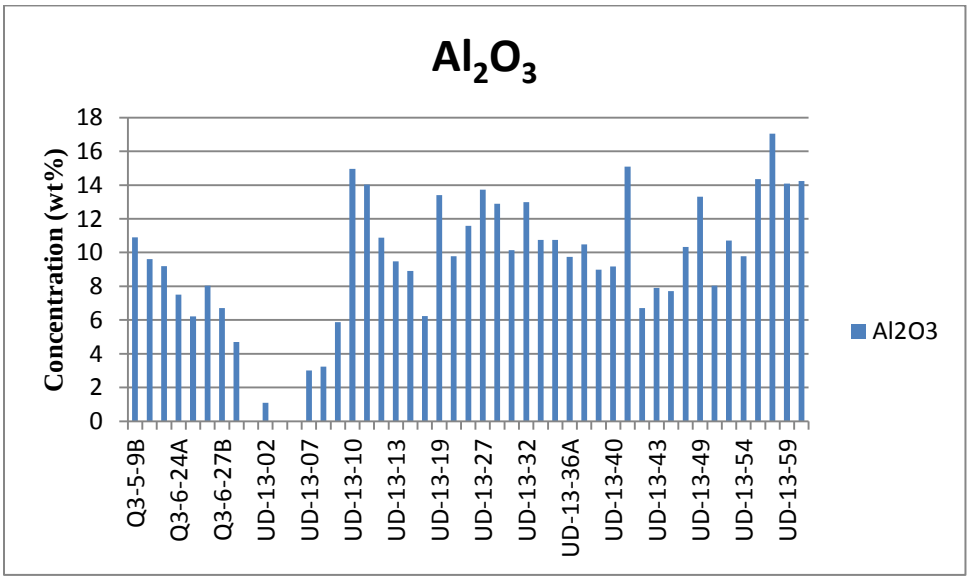

Figure 6.2 Al2O3 concentration variation in both Sharawra Formation outcrops.

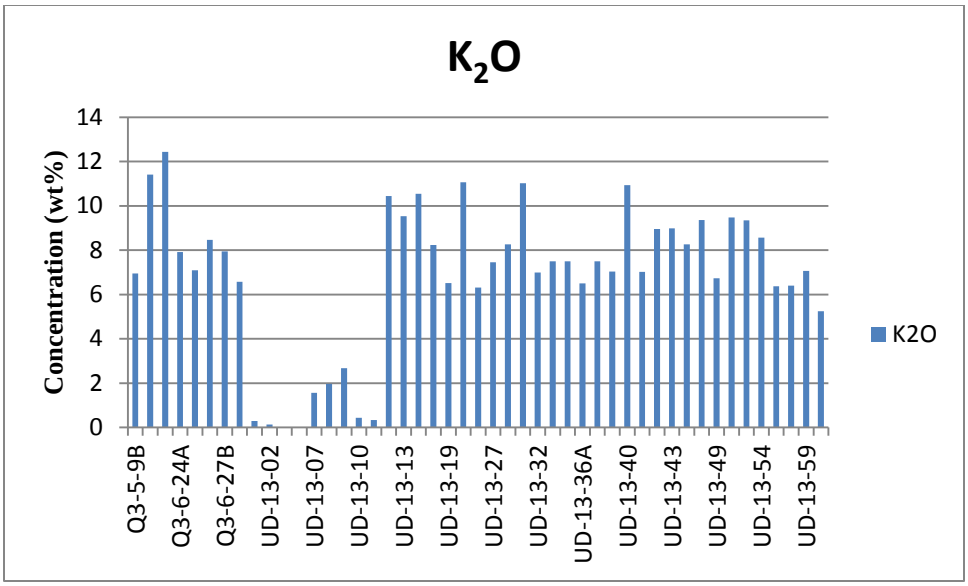

Figure 6.3 K2O concentration variation in both Sharawra Formation outcrops.

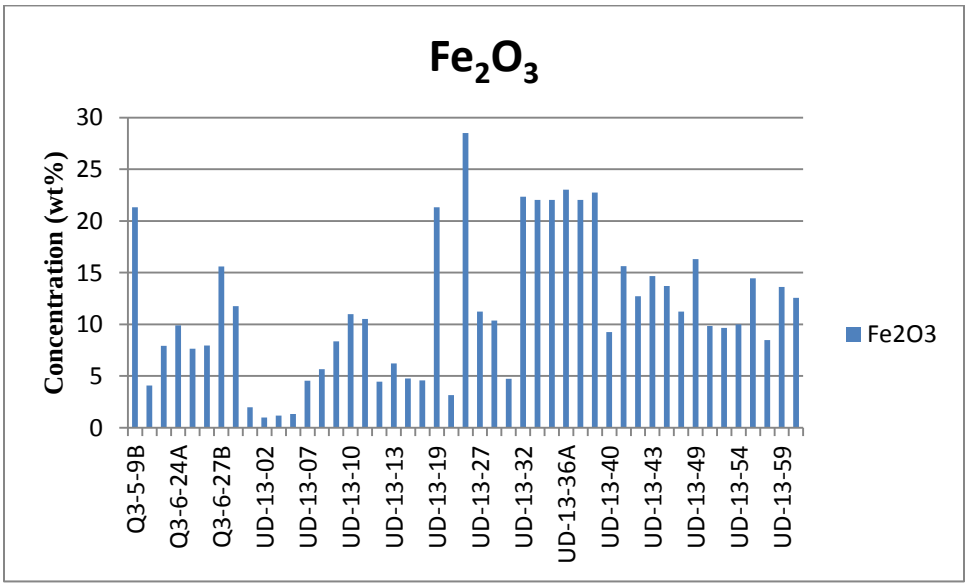

Figure 6.4 Fe concentration variation in both Sharawra Formation outcrops.

Table 6.3 Trace element geochemistry of Sharawra Formation (concentration in ppm).

Sample No.	As	Ba	Cd	Co	Cr	Cu	Li	Ni	Pb	Sr	Sc	V	Zn
UD-13-01	5.65	30.1	0	2	20.65	3.45	4.35	6.3	8.6	143.7	6.23	22.3	0
UD-13-06	0	19	0.45	0	10.95	11.3	3.6	2.05	4.75	246.4	8.53	10.55	0
UD-13-08	0	18.4	0	0	33.4	1.25	2.2	4.95	6.25	6.65	9.32	11.6	0
UD-13-13	0	39.05	0.45	7.1	62.55	4.35	12.65	12.8	17.65	9.6	4.09	34.65	5.3
UD-13-16	0	23.35	0.55	5.2	54.3	26.6	7.35	16.25	33.85	17.4	3.99	31.4	0
UD-13-19	0	47.9	2	20.05	94.1	20.5	50.75	60.15	114	37.9	4.52	89	53.25
UD-13-20	0	15.05	0	7.65	42.4	3.1	7.15	18.65	9.65	7.15	7.32	13.95	0
UD-13-34	0	53.7	2	31.45	72.55	21.9	89.7	50.35	115.8	36.75	2.3	76.25	152.1
UD-13-36B	0	51.3	1.95	33.8	58.95	57.2	70.9	46.1	131.75	29.85	3.65	67.6	165
UD-13-41	0	54.8	1.35	17.25	81	80	92.5	39.6	46.55	43.55	4.98	70.15	82.25
UD-13-46	0	27.65	1.15	7.6	69.65	7.3	29.35	22.4	86.3	20.05	6.33	36.55	66.7
UD-13-52	0	15.05	1.15	4.1	31.6	5.85	14.85	15.75	86.8	10.5	9.21	26.15	58.05
UD-13-59	0	48.6	1	10	66.95	31.9	99.45	23.4	26.05	8.4	3.01	60.25	51.35
Q3-6-22A	0	26.5	0.4	22.45	35.6	4.35	5.7	26.6	25.1	9.4	6.75	25.5	0
Q3-6-27B	0	77.35	1.95	11.85	35.2	12.6	53.75	23.75	114.5	95.8	1.03	45.65	71.1
Mean	0.377	36.52	0.96	12.0	51.32	19.4	36.2	24.67	55.17	48.21	5.41	41.43	47.00
Median	0	30.15	1	7.65	54.3	11.3	14.85	22.4	33.85	20.05	4.98	34.65	51.35
Standard Deviation	1.41	17.79	0.74	10.39	22.81	21.7	35.26	16.69	45.72	64.52	2.43	24.47	53.14

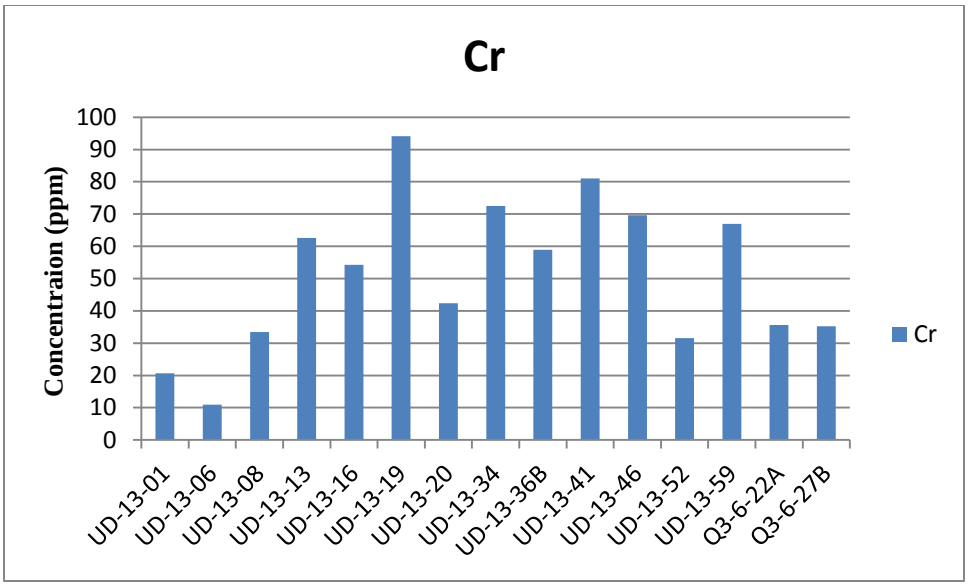

Figure 6.5 Variation of chromium in Sharawra Formation.

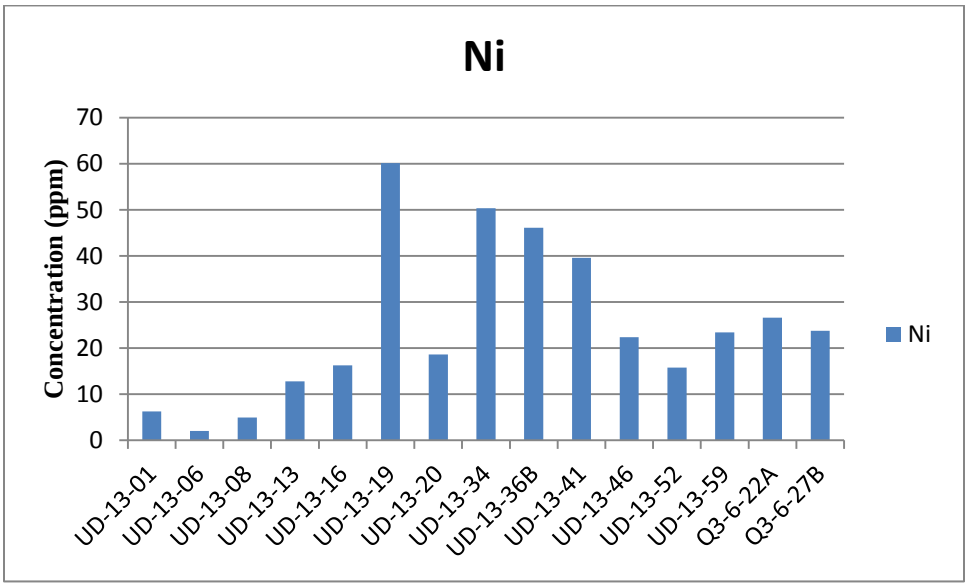

Figure 6.6 Variation of nickel in Sharawra Formation.

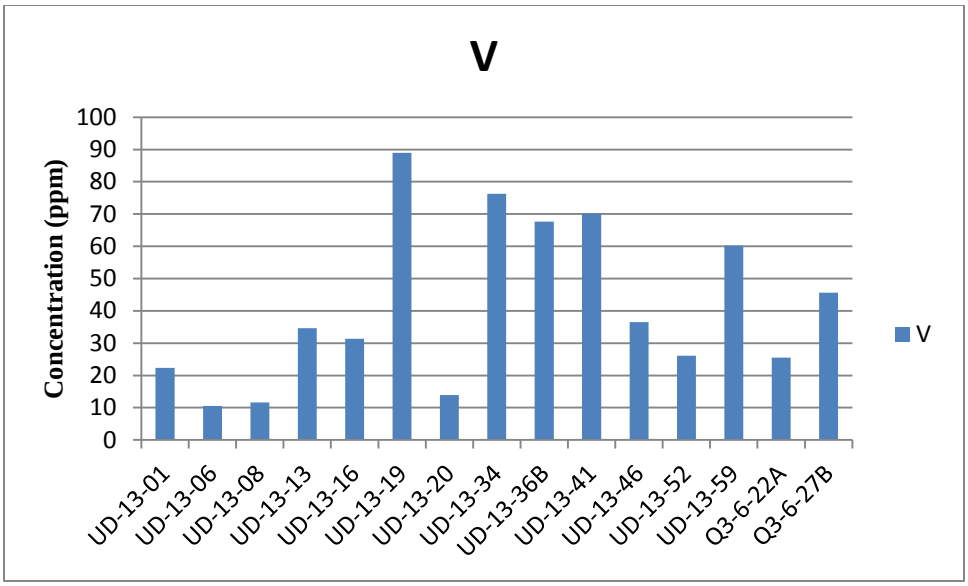

Figure 6.7 Variation of vanadium in Sharawra Formation.

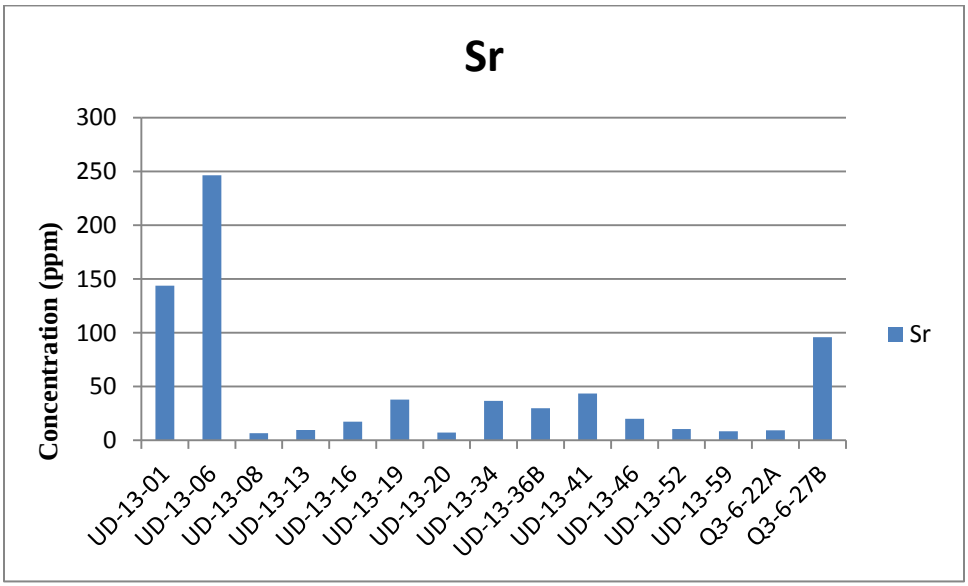

Figure 6.8 Variation of strontium in Sharawra Formation.

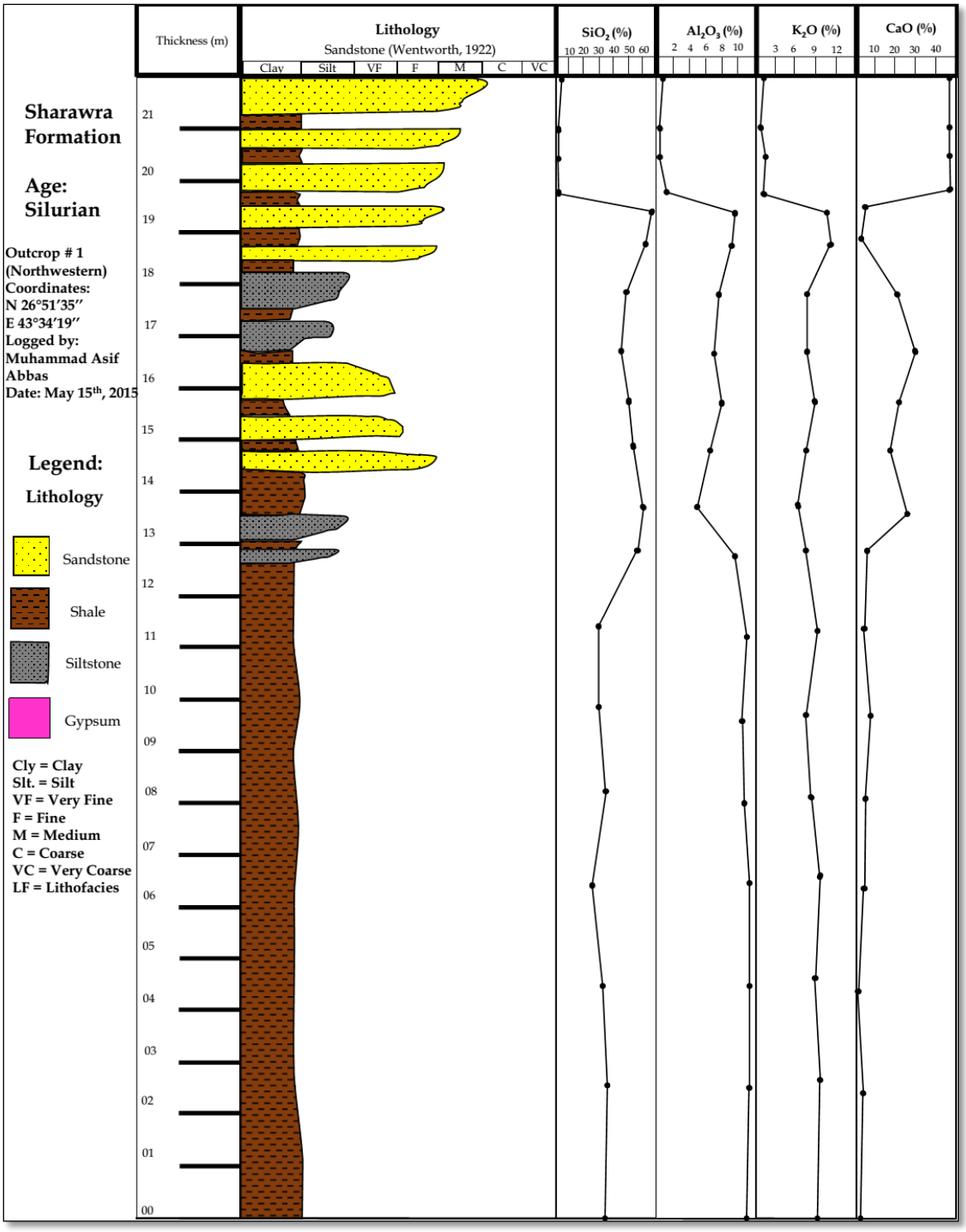

Figure 6.9 Geochemical log of Sharawra Formation outcrop 1 presenting the variation in outcrop 1.

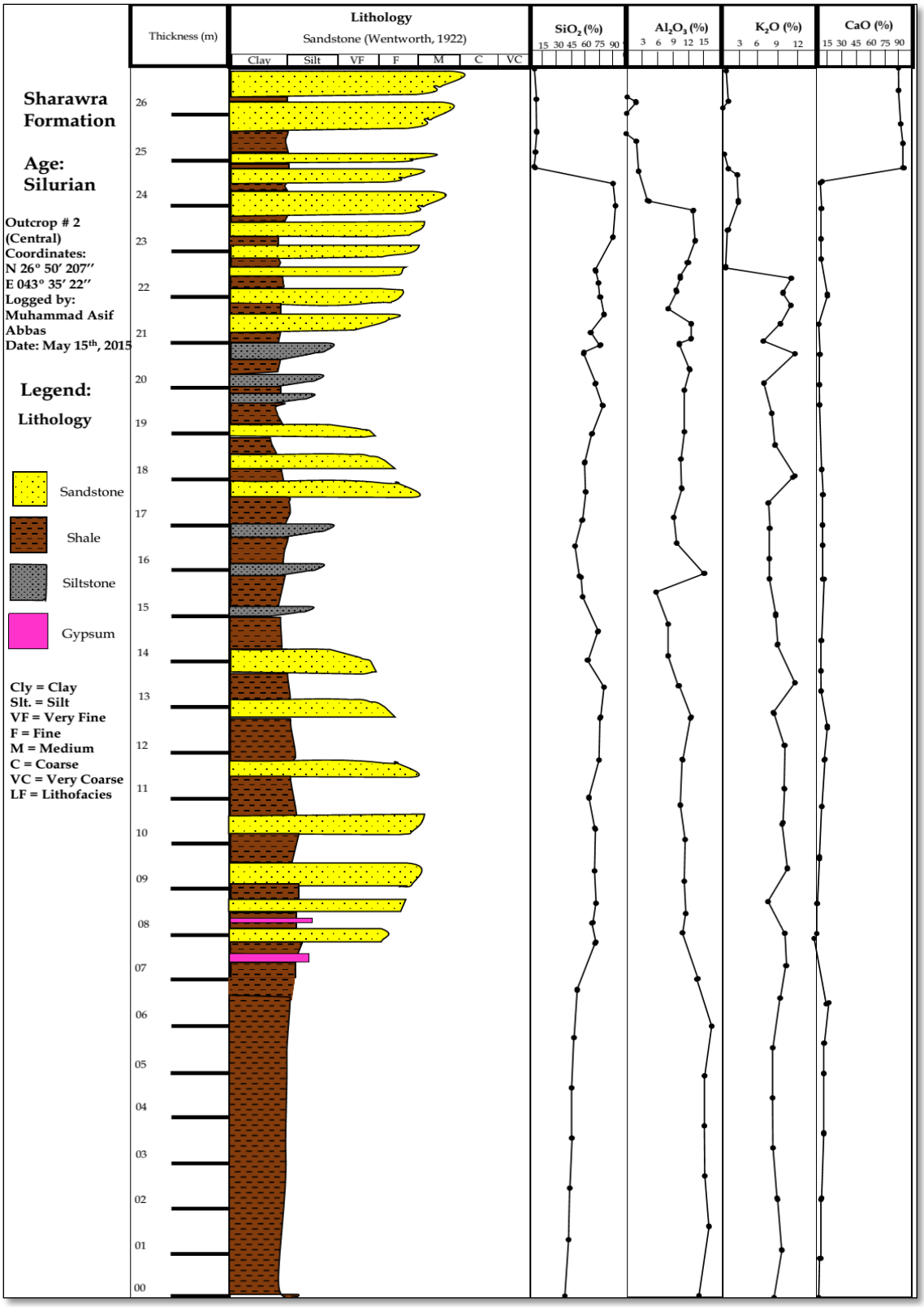

Figure 6.10 Geochemical log of Sharawra Formation outcrop 1 presenting the variation in outcrop 2.

6.1 Paleoclimate and Weathering Intensity

To determine the source area weathering, the most widely used index is the Chemical Index of alteration (CIA). CIA was proposed by Nesbitt and Young (1982), it is based on the molecular proportions of Al_2O_3, Na_2O, K_2O, and CaO.

$$CIA= [Al2O3/(Al2O3+CaO*+Na2O+K2O)]\times100$$

where CaO* is representative of the CaO values in the silicate fraction only. CIA values of Sharawra sandstone and shales vary from 49 % to 70 % with an average of 55 %. CIA variation is dependent of feldspar versus the clay minerals. The sandstone has undergone moderate weathering, suggesting the sediments to be derived from source rocks, subjected to chemical and physical breakdown (Nesbit and Young 1989, Cingolani et al. 2003). Nesbit and Young (1982) reported that unaltered basaltic rocks have CIA values between 30 and 40 whereas they are around 50 for fresh granites. The diamond plots by Basu et al., (1975) and Tortosa et al., (1991) also show the same relation to the provenance (Figures 6.11 and 6.12).

$$CIW= [Al2O3/(Al2O3+CaO*+Na2O)]\times100$$

Chemical Index of Weathering (CIW) is an index that reflects the degree of chemical weathering experienced by weathering materials of the source rocks and sediments. The method is favourable, as it deals with restricted number of components having a consistent geochemical behaviour through the weathering phase. CIW values were determined for both sandstones and shales, and were found in almost the same range. The CIW values range from 69.67 to 95.63. CIW values are always higher than the CIA

values as the K_2O component is excluded. Here the sediments also show moderate degree of weathering. CIA and CIW values are listed in Tables 6.1 and 6.2.

$$ICV= [Fe2O3+K2O+Na2O+CaO+MgO+MnO+TiO2]/ Al2O3]$$

Index of Chemical Variation (ICV) values greater than one for the sandstone/shale samples are considered to be compositionally immature, where the sediments are considered to be first cycle of sediments. However, the sediments having ICV greater than one is compositionally mature and are deposited in tectonically stable or cratonic environment, with active recycling (Cox et al., 1995). For the Sharawra sandstone and shale samples the ICV values range from 1.6 to 5. On the basis of ICV values it can be interpreted that Sharawra Formation samples are deposited in cratonic environment. The petrographic and geochemical data has been superimposed on all the tectonic, provenance, and weathering intensity discrimination diagrams in the present chapter.

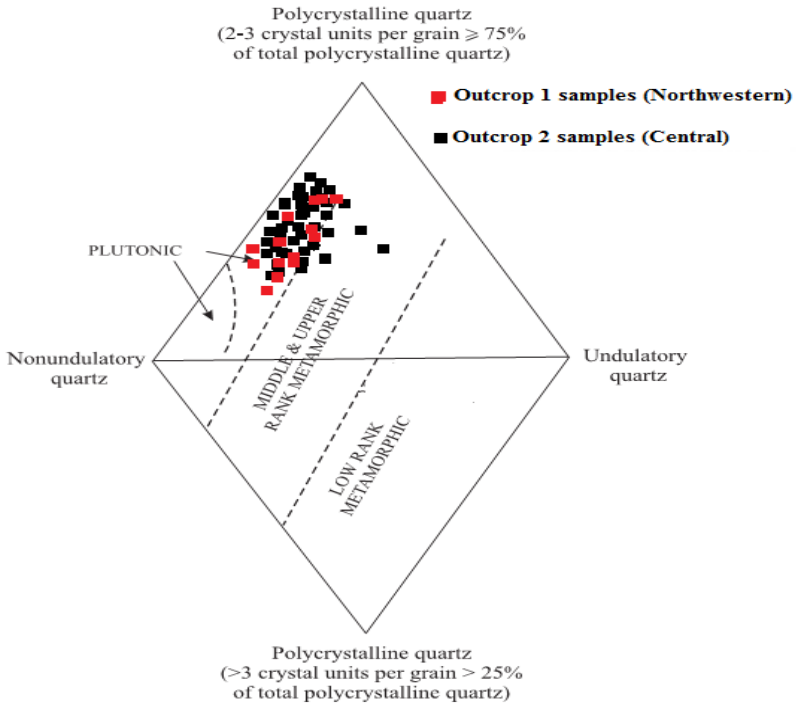

Figure 6.11 Diamond diagram plot, after Basu et al (1975) for Sharawra Formation samples

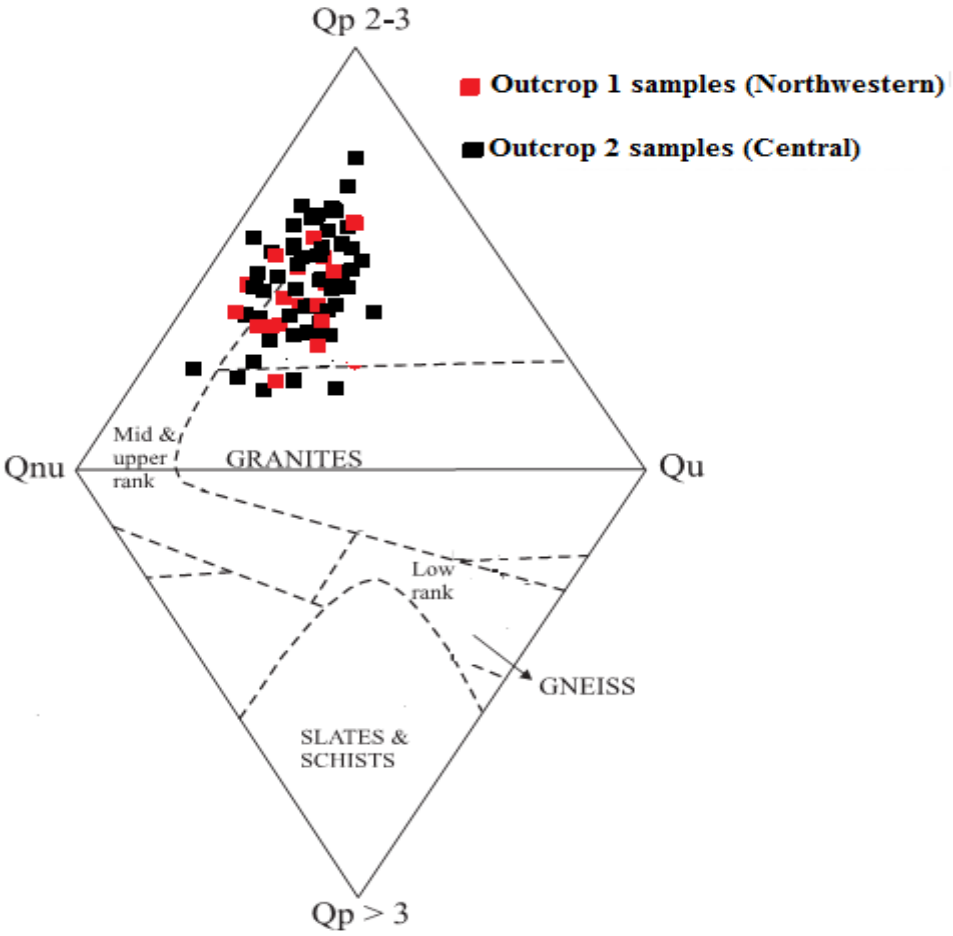

Figure 6.12 Diamond diagram plot, after Tortosa et al (1991) for Sharawra Formation sandstones.

The average V/Cr ratio for the Sharawra Formation is 0.81. This is indicative of the oxic or reducing environment during the deposition of Sharawra sandstone sediments. The value of V/Cr ratios is in waters lying above the sediments below 2 indicates oxic conditions Jones and Manning (1994). The upper sandstone facies, being shallow marine deposits also reflects the oxic conditions. In the present study, repetitive variations of CIA and trace elements concentrations reflect the continuous and repetitive transgressions and regressions, resulting in cycles of sandstone, siltstones and shale interbeds. However, the CIA values for the topmost sandstone facies are higher, what is

indicative of the most landward facies within Sharawra Formation in this region. A-CN-K plot uses the molecular proportions of Al_2O_3, $CaO+Na_2O$, and K_2O, the average continental crust is plotted from Taylor and Mclennan, (1985). The CIA values show the same trend. The Sharawra sandstone samples fell into the moderate weathering zone. The clustering of samples is close to the smectite point verging to illite and kaolinite sector. The back stripping of this line along parallel to the A-CN line and joining to the feldspar line can provide information about the composition of source rocks. The parallel line to A-CN shows that sandstone also fell near the weathering trends of granite and granodiorite Figure 6.13.

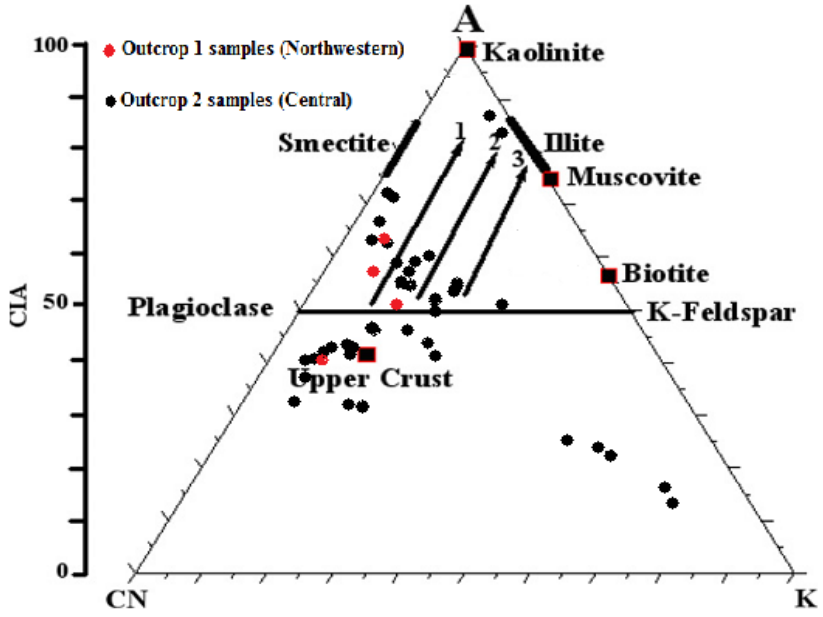

Figure 6.13 A–CN–K ternary diagram of molecular proportions of Al2O3–(CaO + Na2O)– K2O for the Sharawra Sandstone (after Nesbitt and Young, 1984). Also plotted is the average upper continental crust (Taylor and McLennan, 1985). Arrows 1–3 represent the weathering trends of granodiorite, adamellite and granite, respectively (after Nesbitt and Young, 1984).

Chemical weathering is responsible for driving away the elemental fractions from the parent bedrock (Nesbitt and Young, 1982). The fractionation depends upon the

weathering conditions locally and the composition of bedrock, and is more likely to be dominant in humid and warm climates, while weaker chemical weathering is associated with arid climatic conditions (Nesbitt and Young, 1982). Higher rainfall is responsible for the loss of liable minerals, and hence high degree of CIA values will be observed in the resulting sediments (Basu, 1981; Suttner et al., 1981; Dutta and Suttner, 1986). This suggests that the source rocks of the Sharawra Formation rocks have undergone moderate chemical weathering and were deposited under a climate having moderate rainfall. The CIA values are plotted versus SiO_2, to have the further implication of the source rock (Figure 6.14).

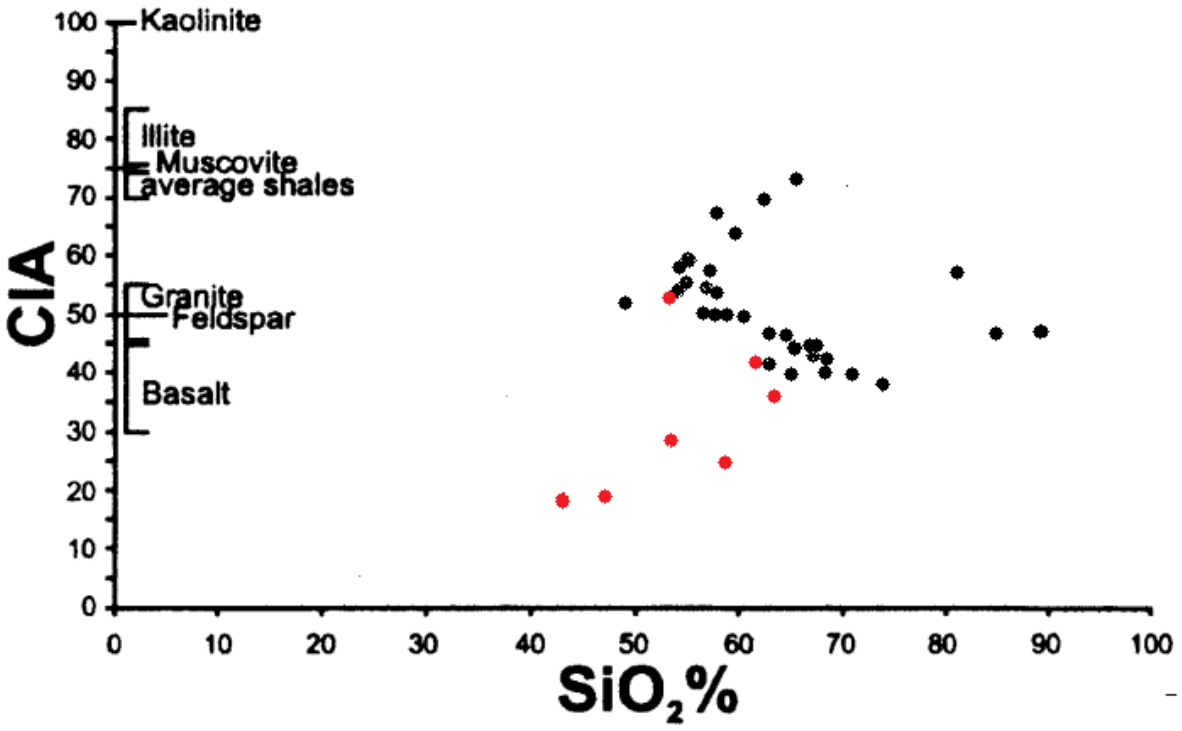

Figure 6.14 CIA versus SiO2 (after Nesbitt and Young, 1982).

6.2 Tectonic Setting

The maturity of the quartz grains shows the sediments to be mineralogically mature and most of them are deposited in continental margins. The Q-F-L and Qm-F-Lt plots of Dickinson et al., 1983, show that most Sharawra Formation sandstones lie in the craton interior zone, while a very few lie in the transition zone (Figure 6.15).

Major elements chemistry of Sharawra sandstones was considered to discriminate the depositional tectonic setting of sandstones by Roser and Korsch (1986), and Bhatia (1983). Using the Roser and Korsch (1986) and Bhatia (1983) plots shows that the Sharawra sandstone samples fell into the passive continental margin (Figures 6.16 and 6.17). However, few of the samples lie in passive continental zone. Bhatia (1983) provided further information that such sediments originate from pre-existing continental terrains. The provenance related to upper continental crust mostly consists of old stable craton and old continental foundations of active margins, McLennan et al. (1990). The maturity of the sandstones was also supported from the results of petrographic study which indicated subrounded and subangular quartz grains with very little rock fragments (Figure 5.16).

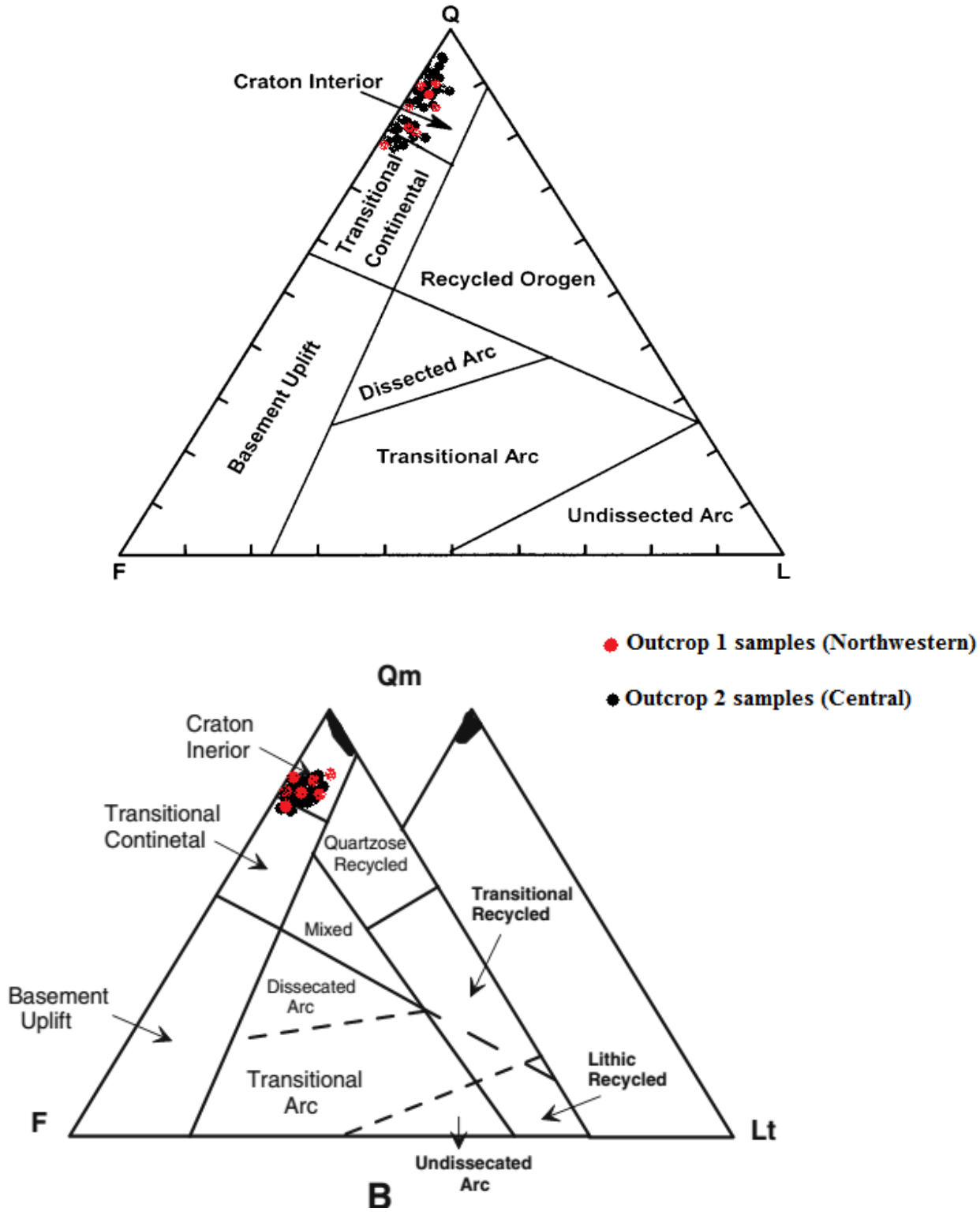

Figure 6.15 QFL and Qm-F-Lt plots and b provenance fields of after Dickenson et. al, 1983.

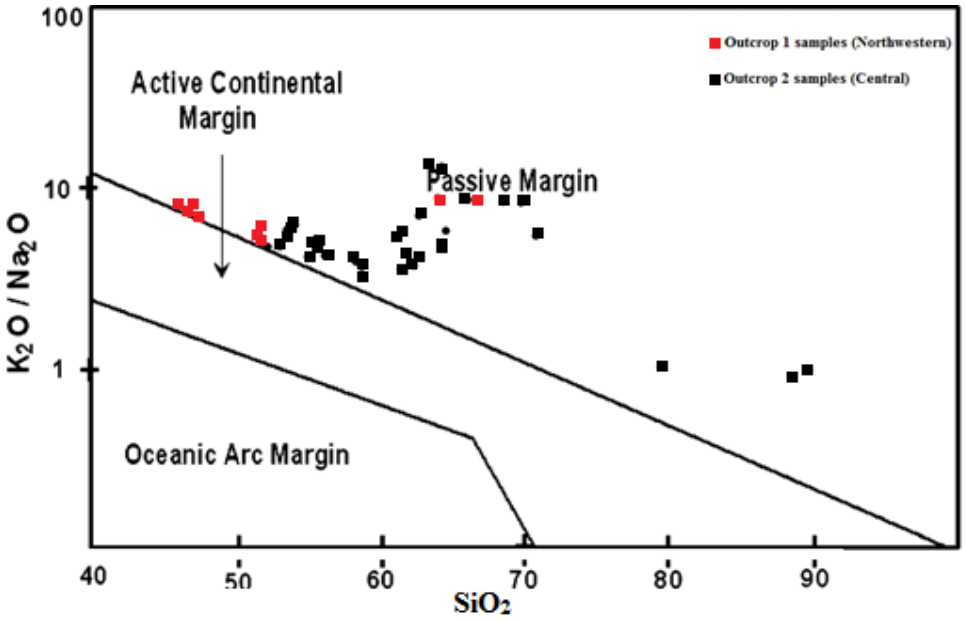

Figure 6.16 Tectonic discrimination diagrams of sandstones from Sharawra Formation (after Roser and Korsch, 1986).

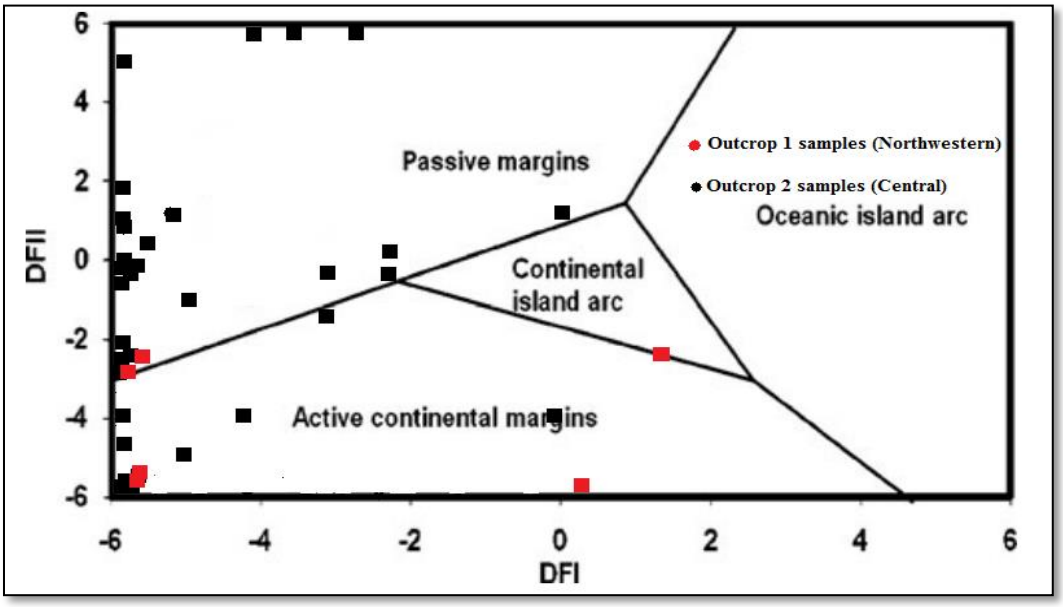

Figure 6.17 Discriminate function diagram for the tectonic setting of Sharawra Formation (after Bhatia, 1983) DF I: (-0.972*TiO2)-(0.0447*SiO2)+(0.008*Al2O3)-(0.267*Fe2O3)-(3.082*MnO)+(0.719*Na2O)+(0.195*CaO)-(0.032*K2O)+(7.51*P2O5)+0.303 DF II: (1.988*TiO2)+(-0.42*SiO_2)+(-0.526*Al_2O_3)+(-0.551*Fe_2O_3)+(2.72*MnO)+(0.907*CaO)+(1.84*K2O)+(7.244*P_2O_5)-(0.177*Na_2O)+43.57.

Trace elements provide further confirmation to the tectonic setting of the present-day clastic rocks. There is a prominent decrease in the Vanadium (V) concentration in the top facies of Sharawra Formation. As there is more maturity in grains, the V decreases. The plot between Sc-V shows that majority of samples of Sharawra Formation fell in the passive continental margin (Figure 6.18). Arc rocks are high in Vanadium (V) relative to active and passive margin sediments. The Sc and V are ferromagnesian trace elements, and they are related to the mafic components of sandstone (Bhatia and Crook, 1986). Their decrease is expected, as in mature sandstones like quartz arenite and subarkose, the mafic component tends to decrease. This is due to break down of mafic components while the sands go through sediment sorting and recycling.

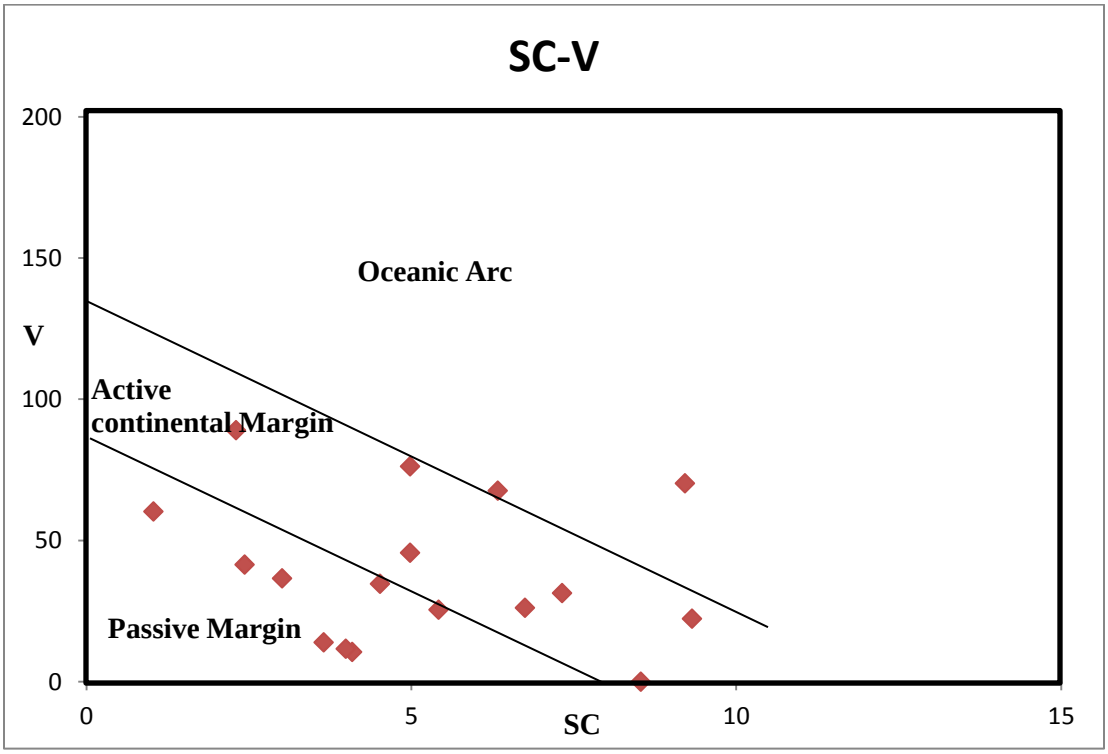

Figure 6.18 The Plot of Scandium versus Vanadium (Sc-V) after Bhatia and Crook (1986). Arc rocks are high in Vanadium (V) relative to passive margin sediments. Scandium and Vanadium values are plotted in parts per million (ppm).

Using the trace elements concentration of Condie, (1993) worked on the average concentration of different trace elements in the Palaeozoic sediments. Using the concentration of trace elements like Ba, Co, Cr, Ni, Pb, Sr, Sc, and V of the Sharawra Formation, the comparison is made with the average concentration of average cratonic sandstone concentration calculated by Condie, (1993). The minimum, maximum, and the mean value of the Sharawra Formation trace elements have been used. The average concentration of trace elements in Sharawra Formation and Condie's calculation do not differ much, thus giving further information about the tectonic setting (Figure 6.19).

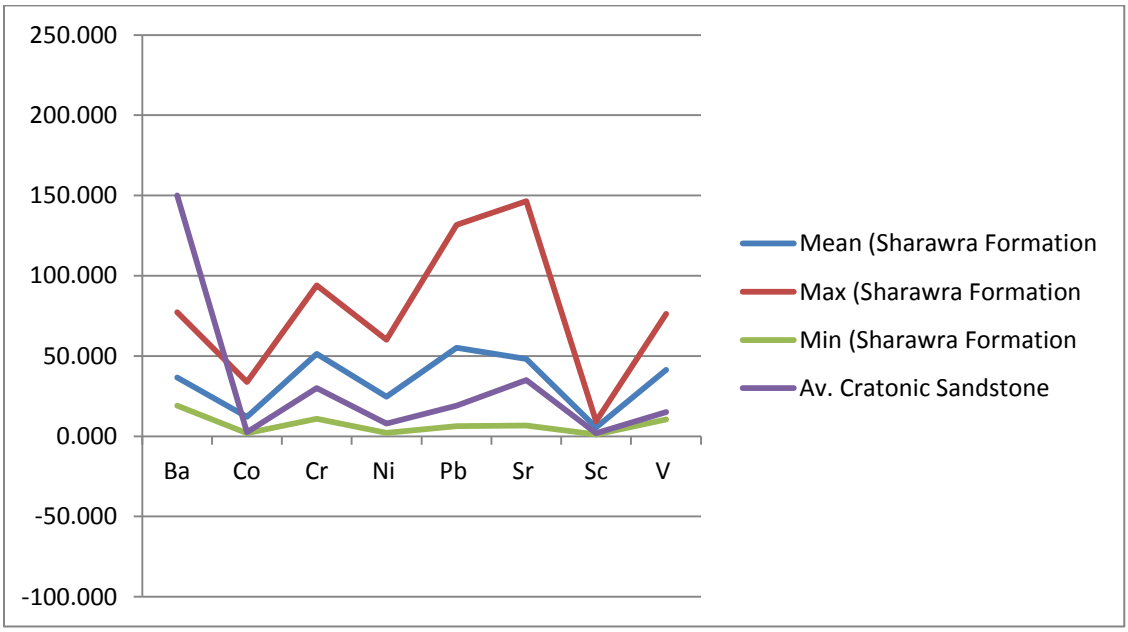

Figure 6.19 The concentration and variation of Sharawra Formation trace elements w.r.t the average cratonic sandstone composition (after Condie, 1993).

6.3 Provenance

Provenance can be studied from the quartz typology, if feldspar is absent, with scarcity of rock fragments (Basu et al. 1975). As Sharawra sandstone and shale interbeds show a series of repetitive transgression and regression cycles, the dominance of monocrytalline quartz over polycrystalline quartz could result from the reworking of polycrystalline quartz during these cycles. Most of the quartz of Sharawra Formation sandstone have shown non-undulatory extinction. The two possibilities of sandstone having majority of monocrystalline quartz and non-undulatory extinction could be sourced by volcanic extrusives or quartz arenites from Precambrian ages (Blatt and Christie,1963). The low percentage of feldspar and scarcity of rock fragments indicates, together with the dominance of shale in the lower part, a marine environment.

For the provenance study, major elements and trace elements are also an important source of information. Using the major elements, the discriminating functions defined by Roser and Korsch (1988) indicate that all the Sharawra sandstone samples fell in the acidic plutonic zone (Figure 6.20). The discrimination diagram of Lebas et al., (1986) also uses the major elements. By using the weight percentages of SiO_2 and Al_2O_3/TiO_2, the felsic, mafic, or intermediate provenance of sandstones can be determined. Most of the Sharawra Formation samples fell into the felsic zone, while few of them lie in the intermediate zone (Figure 6.21). Trace elements are good indicators for the provenance and tectonic setting of sandstones. Trace elements like TiO_2 and Ni is also useful in defining the acidic or basic nature of the source rocks. The diagram by Floyd et al. (1989)

based on TiO2 vs Ni, suggested the acidic nature of the Arabian shield rocks from which the sandstones of Sharawra Formation sediments are mainly derived (Figure 6.22).

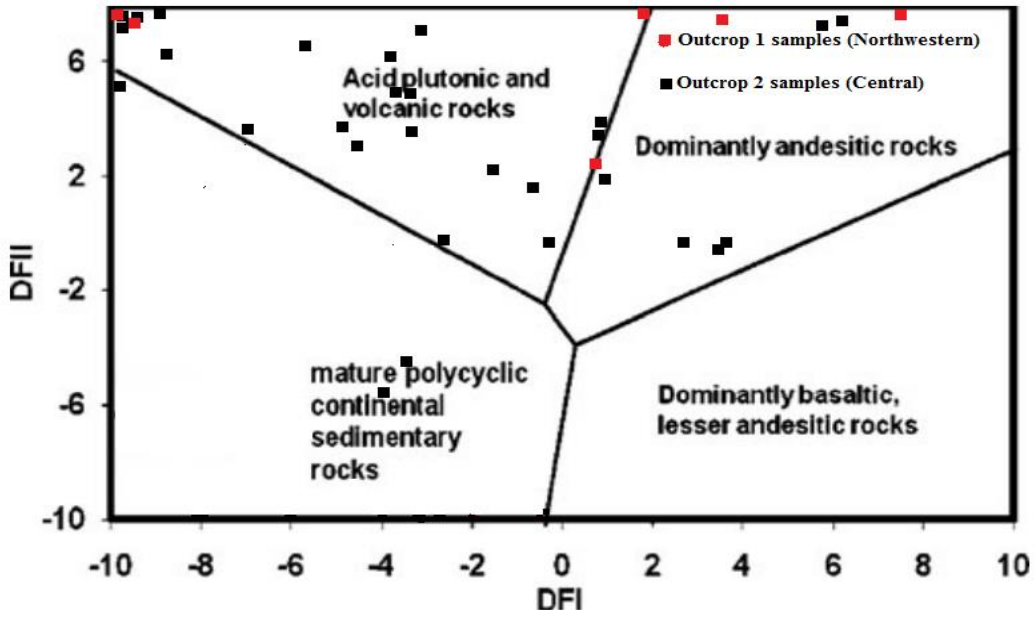

Figure 6.20 Discriminant function diagram for the tectonic setting of Sharawra Formation (after Roser and Korsch, 1988) DFI: (0.607*Al2O3-(1.773*TiO2)+(0.76*Fe2O3)+(0.616*CaO)-(1.224*K2O)-9.09 DFII: (0.445*TiO2)+(0.07*Al2O3)-(0.25*Fe2O3)+(0.438*CaO)+(1.426*K2O)-6.861

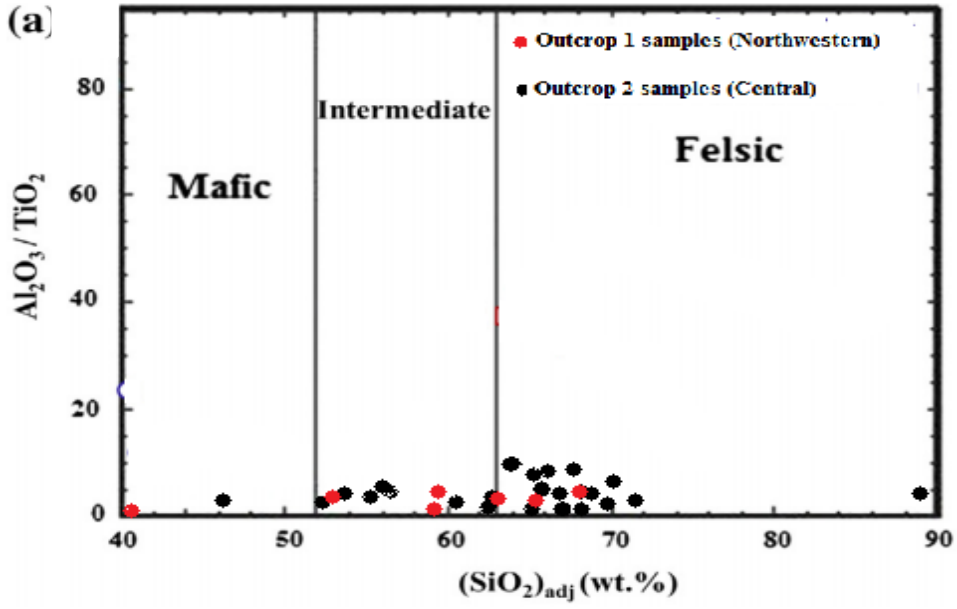

Figure 6.21 The Al2O3/TiO2 vs. (SiO2) relationship for the Sharawra Formation (after Le Bas et al., 1986).

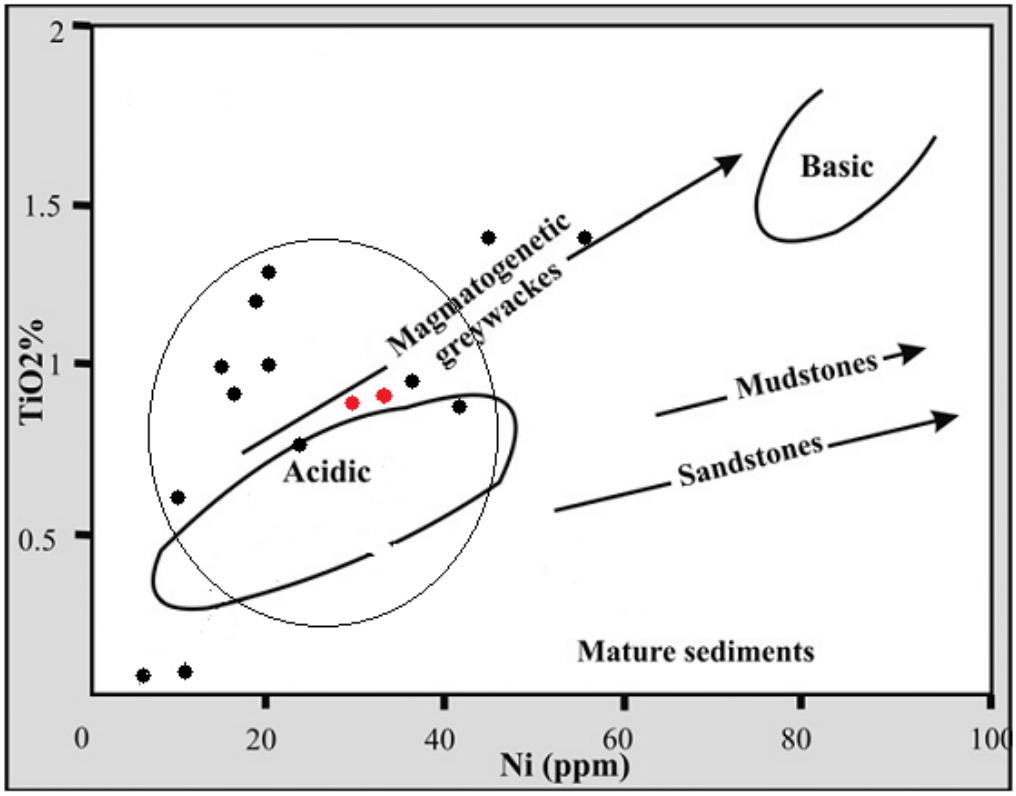

Figure 6.22 TiO2 versus Ni bivariate plot for the Lalun sandstones (fields after Floyd et al., 1989). Majority of the samples plot near the acidic source field.

The sandstones from the craton areas are most likely to be derived from the exposed basement shield areas, or uplifted basements. The possibilities of sediments being derived from recycled sediments or from low lying or weathered crystalline rocks also exist. The Sharawra Formation consists mainly of feldspar deficient facies, showing the mature nature of the sandstones, however, the rare immature sandstones are also present. The grain shape ranges from subangular to subrounded. This conditions favour a weathered crystalline granitic source. (Pettijohn, 1975 and Roser et al., 1996).

The presence of unstrained monocrystalline quartz also suggests a plutonic origin (Basu et al., 1975, Potter, 1978 and Hindrix, 2000). This idea is also supported by the

dominance of orthoclase over plagioclase (Potter, 1978, Hindrix, 2000 and Osae et al., 2006). Also, the presence of alkali feldspar-rich granite in the source area is supported by the presence of detrital mica throughout the formation.

Moreover, the percentage of the SIO_2 in most of the sandstone samples is around 70%, implying the quartz richness to be sourced by quartz rich crystalline provenance. Sharawra Formation samples also showed a high K_2O/Na_2O. The K_2O/Na_2O ratio can be considered as a simplified chemical provenance indicator (Potter, 1978). Higher values of this ratio indicative of these rocks to be derived more likely as compared to the basic rocks. The clay minerals concentration also confirms this suggestion, as illite and kaolinite are the dominant clays in the studied samples. The illite and kaolinite are considered to be inherited from the weathered soils developed on silicic (granitic) rocks. The absence of chlorite and smectite diminishes the probability of mafic source rocks.

The concentration of Cr, Cr, Co, Ni and V elements are lower in the felsic rocks, while Ba and Sr tend to have higher concentrations, as compared to the mafic source rocks (McLennan et al., 1983, Taylor and McLennan, 1985 and Wronkiewicz and Condie, 1990). The studied Sharawra Formation shows that Ba and Sr are present in a considerable amount, while the average concentration of Co and Ni is low. Average concentration of V is also to the lower side. All these factors indicate a minimal contribution from the mafic sources. (Zhang et al., 1998, and Osae et al., 2006). Also, lower Ba/Co ratios are indicative of the mafic granitic sources, as these elements are largely contained in K-bearing and ferromagnesian minerals, respectively (Taylor and McLennan, 1985 and Cullers et al., 1988). The Sharawra Formation sediments have a higher Ba content but have low concentration of Co (Table 6.2). The higher Ba/Co ratio

is indicative of these sediments to be derived from weathered felsic-granitic sources (Cullers et al., 1988).

6.4 Total Organic Carbon (TOC)

TOC measurement was performed on 15 samples of the Sharawra Formation. The analysis was performed considering the stratigraphic position of the Sharawra Formation. The shale interbeds present continuously throughout were examined for organic carbon enrichment. The results showed that the TOC content of Sharawra Formation shale is negligible. The TOC values are very low, the sample from the deepest part showed the highest TOC value of 0.16%. This shows that the probability of these shale beds being a source rock for some overlying formation is very low. The TOC results are summarized in Table 6.4.

Table 6.4 TOC results for the Sharawra Formation samples.

Sample ID	TOC mg/200mg	TOC %
UD-14-10	0.005	0.003
UD-14-13	0.007	0.004
UD-14-19	0.000	0.000
UD-14-28	0.000	0.000
UD-14-35	0.000	0.000
UD-14-41	0.076	0.038
UD-14-42	0.047	0.024
UD-14-42	0.006	0.003
UD-14-46	0.005	0.003
UD-14-52	0.039	0.020
UD-14-54	0.008	0.004
UD-14-55	0.159	0.080
UD-14-57	0.005	0.003
UD-14-59	0.328	0.164
UD-14-63	0.004	0.002

CHAPTER 7

CONCLUSIONS & RECOMMENDATIONS

7.1 Conclusions

The Sharawra Formation has been investigated for its sedimentology, petrography, petrophysics, and geochemistry. The conclusive remarks related to each of these aspects of the Sharawra geology are as follows:

- A maximum of nine lithofacies have been described from the studied outcrops. Each lithofacies, within itself contains the shale interbeds.
- Two of the nine lithofacies are siltstone facies.
- The formation overall is a coarsening upward sequence. The sandstones become thicker from bottom to top, while the shale becomes thinner.
- The Sharawra Formation overlies the Qusaiba Formation, a thick hot shale sequence; hence, the Sharawra Formation sandstones represent the end of a transgressive period.
- The thin shale interbeds are small-scale transgressive periods, occurring between the regressive sandstones. Sharawra Formation exhibits a series of transgressive and regressive cycles.
- The correlation of the facies proves the thinning of the strata towards the southeastern margins of the Qusaiba Village.
- Sandstone petrography shows the Sharawra Formation sandstone to be mature, as it is subarkosic mainly, with rare quartz arenite.

- The subrounded to subangular quartz grains are representative of moderate transport of quartz grains.
- Calcite in the topmost lithofacies, and clay, iron oxide, and silica occur as cements in all the other facies of Sharawra Formation.
- XRD revealed the absence of feldspar in a few samples, however, indicating orthoclase to be the dominant feldspar throughout the formation, with microcline as the dominant mica.
- The presence of kaolinite throughout the Formation, with illite in the lower parts, and rare presence of polygorskite, and dickite is also reported by XRD.
- The topmost sandstone facies of the Sharawra Formation shows a good porosity and permeability. Porosity of the lower sandstone facies is also good, but the permeability is very low.
- The calcareous sandstone facies tend to show a good porosity, while permeability is negligible.
- On the basis of porosity and permeability results, the Sharawra Formation can be a potential reservoir rock.
- Major and trace element geochemistry revealed that the Sharawra Formation sandstones deposited in a passive continental margin and cratonic interior and originated from Arabian Shield.
- Acidic, felsic, granitic sources have been indicated from the major and trace elements geochemistry plots.
- The CIA and CIW values indicated moderate source area weathering for the Sharawra Formation.

- The negligible TOC percentages suggest that the shales of Sharawra Formation cannot be a petroleum source rock.

7.2 Recommendations

The following studies are recommended for future studies:

- A chemostratigraphic network needs to be established for Sharawra Formation. This can be achieved by obtaining detailed geochemical data from the Tabuk and Tayma outcrops, or from the subsurface well data.
- Geochemical characterization of the less porous and permeabile facies of the Sharawra Formation can also be significant in order to designate it as an unconventional hydrocarbon reservoir.
- Shallow wells should be drilled to obtain the most possible fresh samples for a geochemical study.

APPENDIX

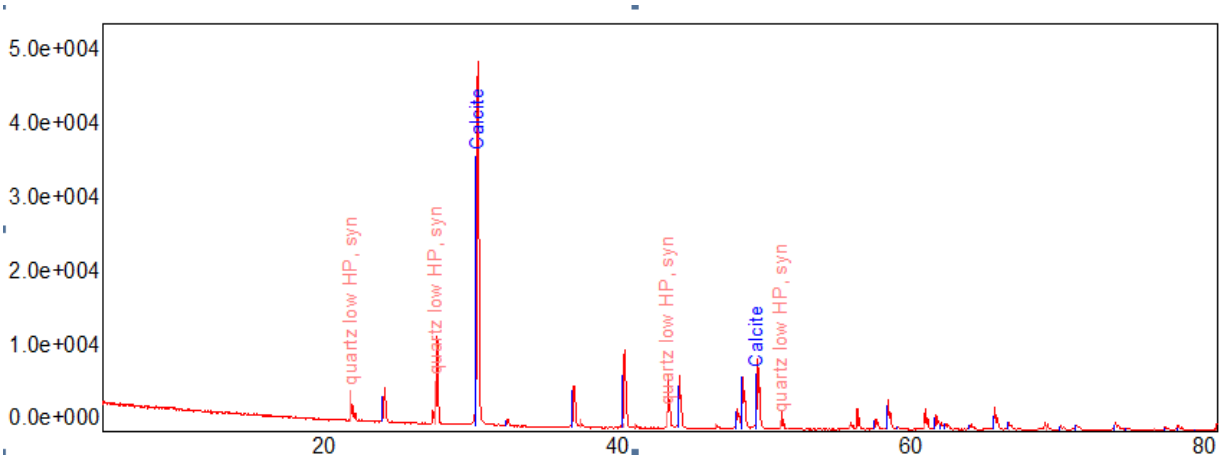

Figure A-1 XRD result of sample UD-14-02 showing quartz and calcite.

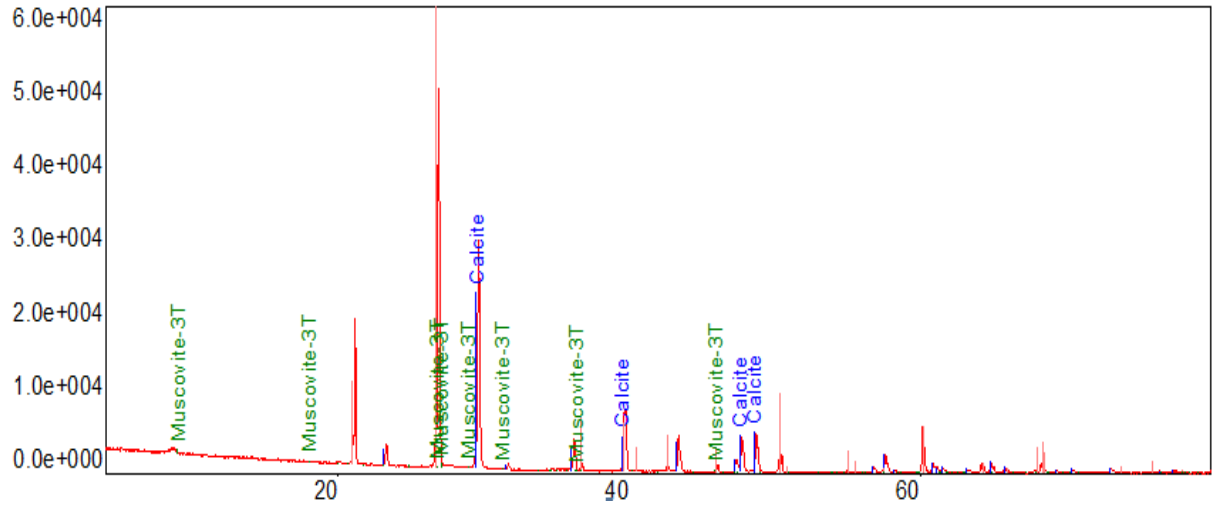

Figure A-2 XRD result of sample UD-14-09 showing quartz, muscovite, and calcite.

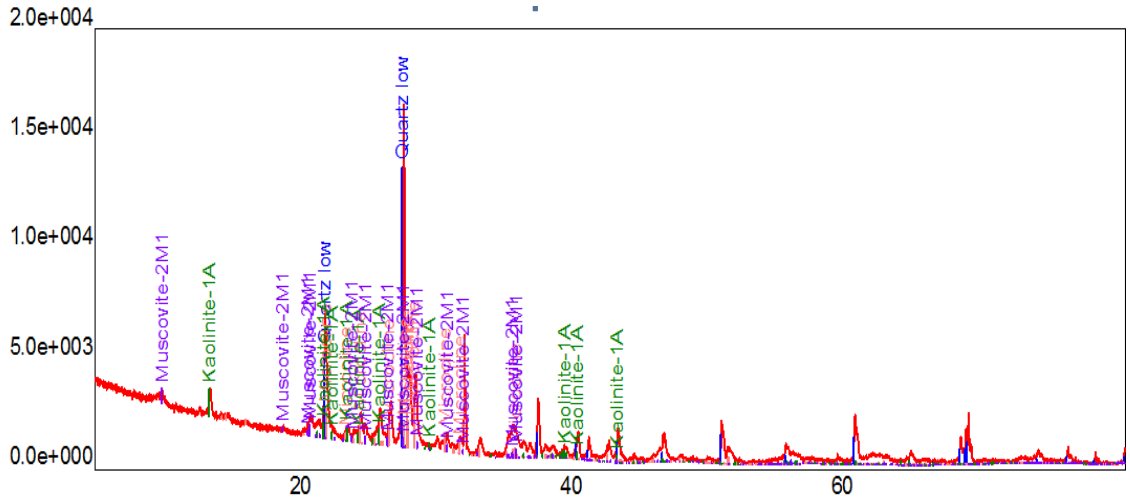

Figure A-3 XRD result of sample UD-14-10 showing quartz, muscovite, and kaolinite.

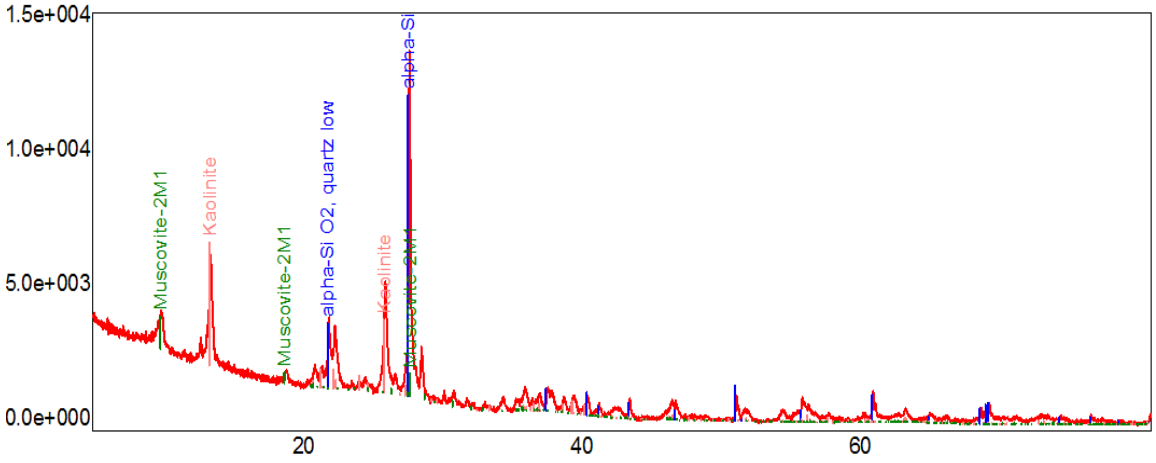

Figure A-4 XRD result of sample UD-14-15 showing quartz, muscovite, and kaolinite.

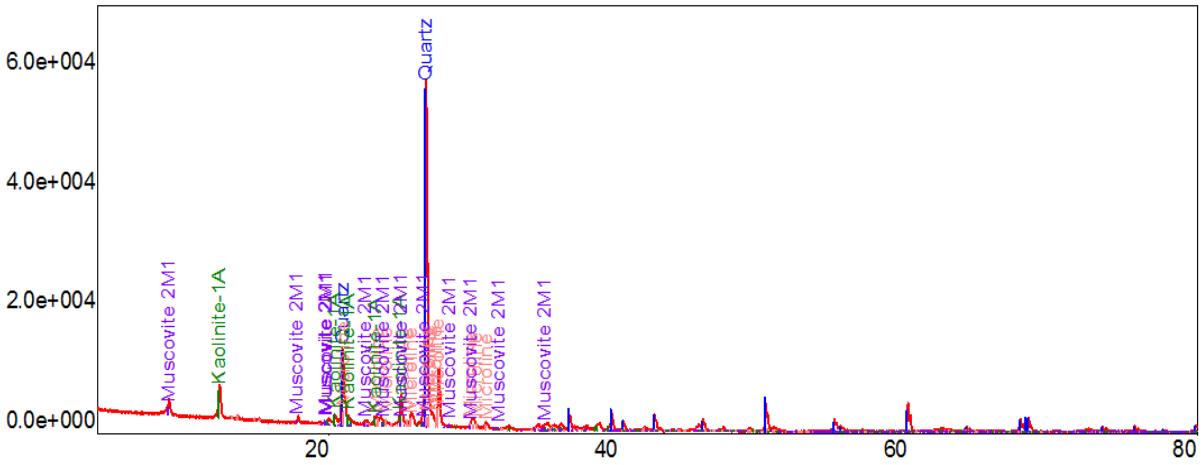

Figure A-5 XRD result of sample UD-14-18 showing quartz, muscovite, and kaolinite.

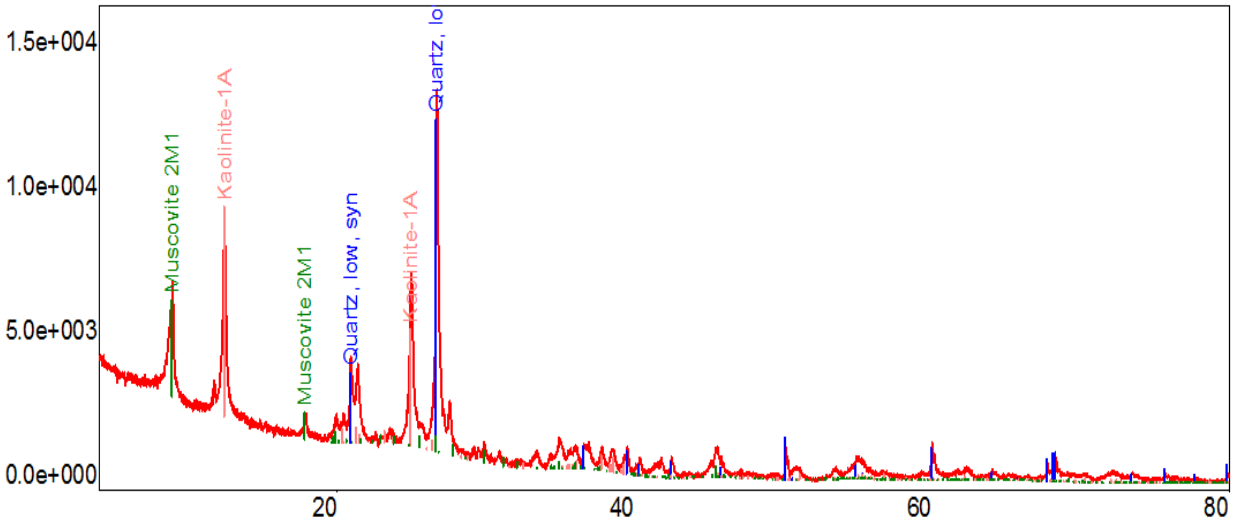

Figure A-6 XRD result of sample UD-14-19 showing quartz, muscovite, and kaolinite.

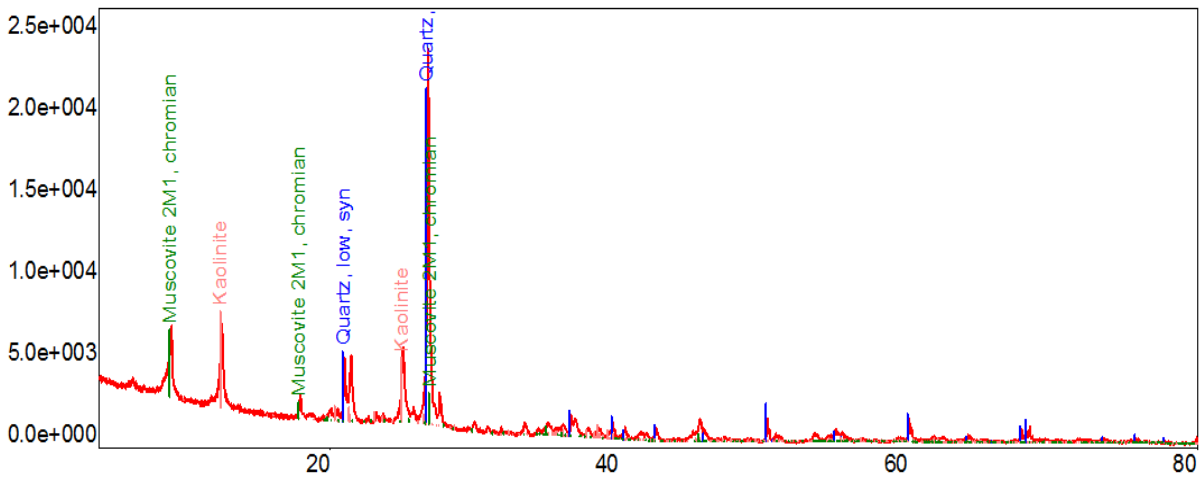

Figure A-7 XRD result of sample UD-14-23 showing quartz, muscovite, and kaolinite.

.

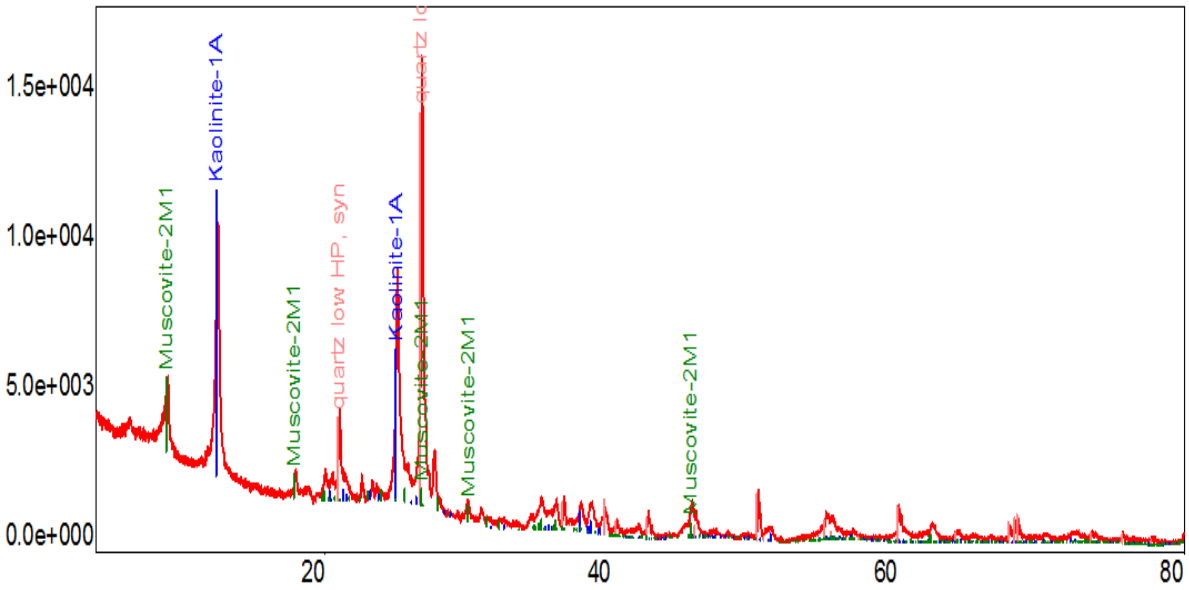

Figure A-8 XRD result of sample UD-14-33 showing quartz, muscovite, and kaolinite.

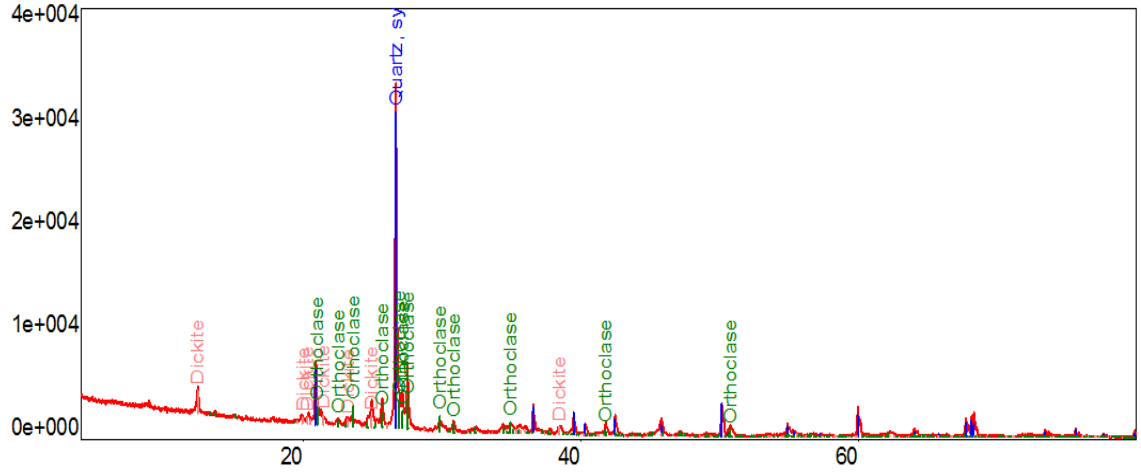

Figure A-9 XRD result of sample UD-14-36 showing quartz, orthoclase, and dickite

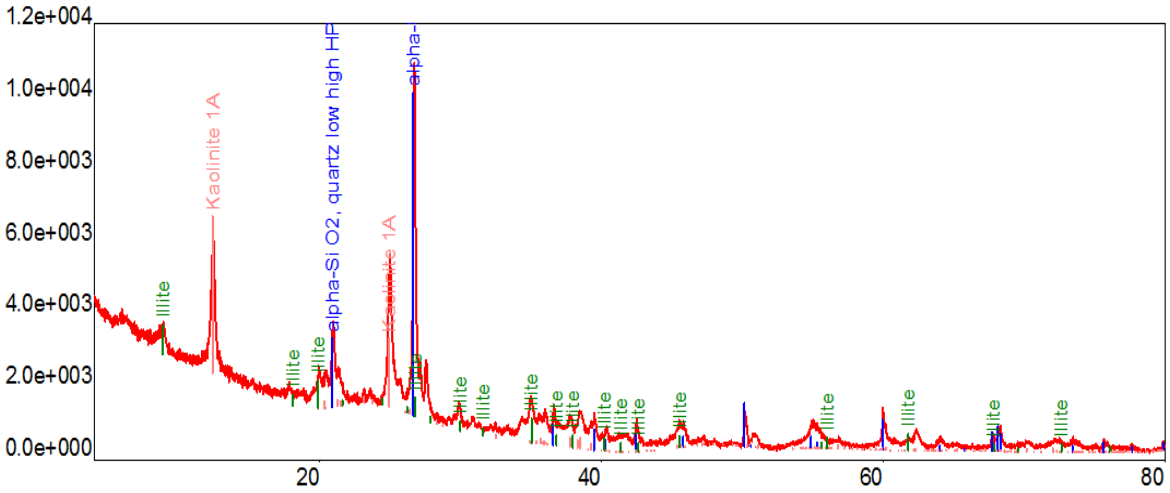

Figure A-10 XRD result of sample UD-14-37A showing quartz, illite, and kaolinite.

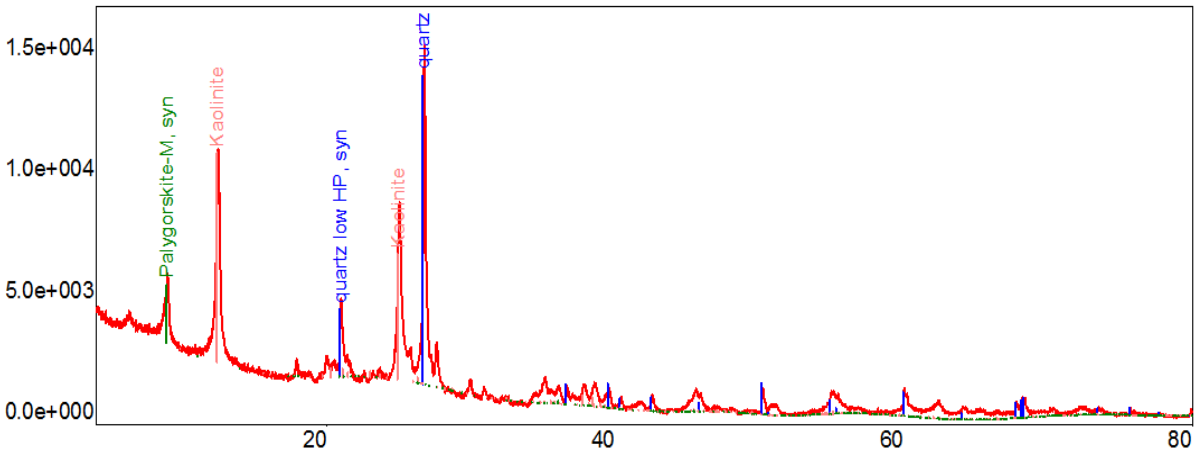

Figure A-11 XRD result of sample UD-14-39 showing quartz, polygorskite, and kaolinite.

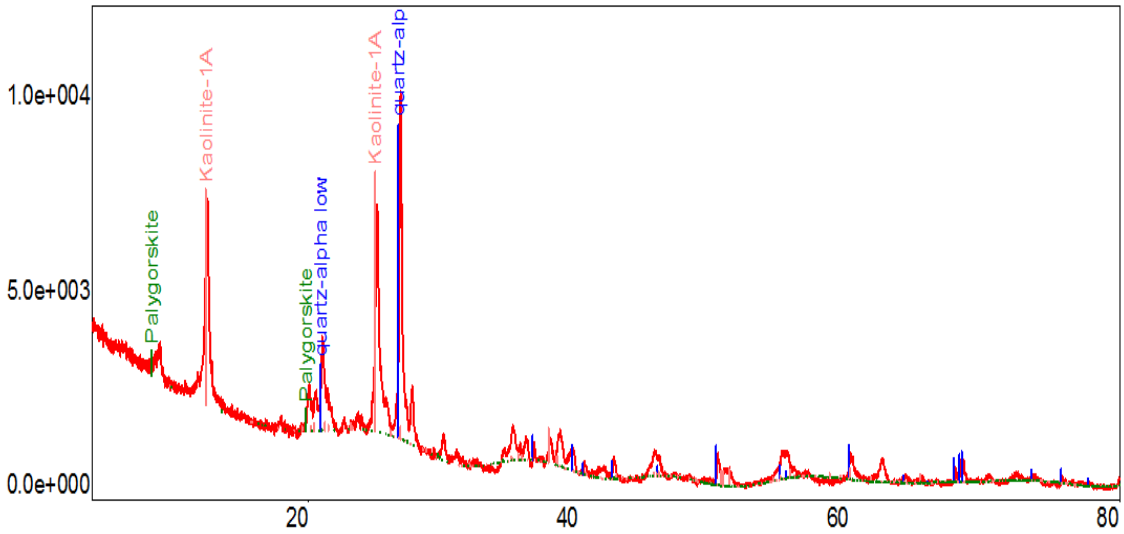

Figure A-12 XRD result of sample UD-14-43 showing quartz, polygorskite, and kaolinite.

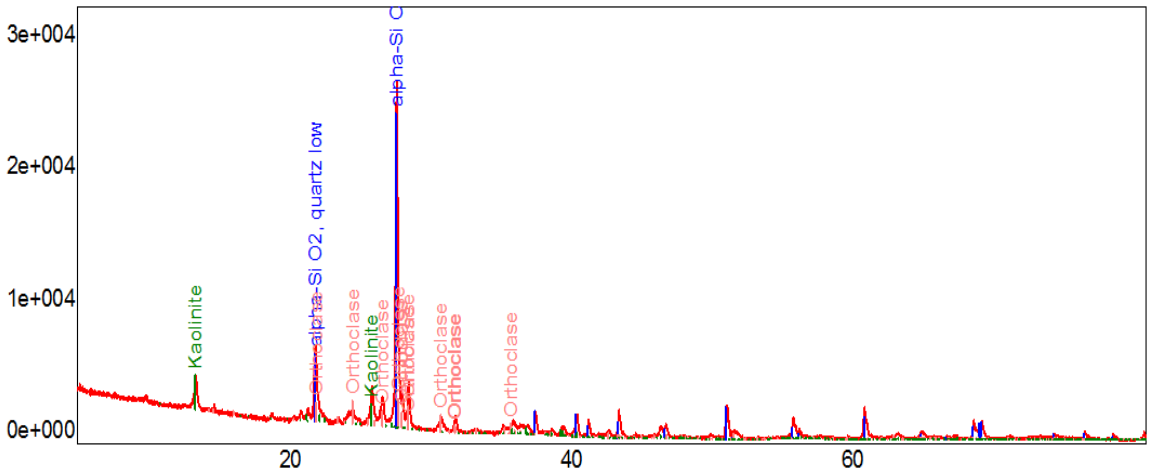

Figure A-13 XRD result of sample UD-14-54 showing quartz, orthoclase, and kaolinite.

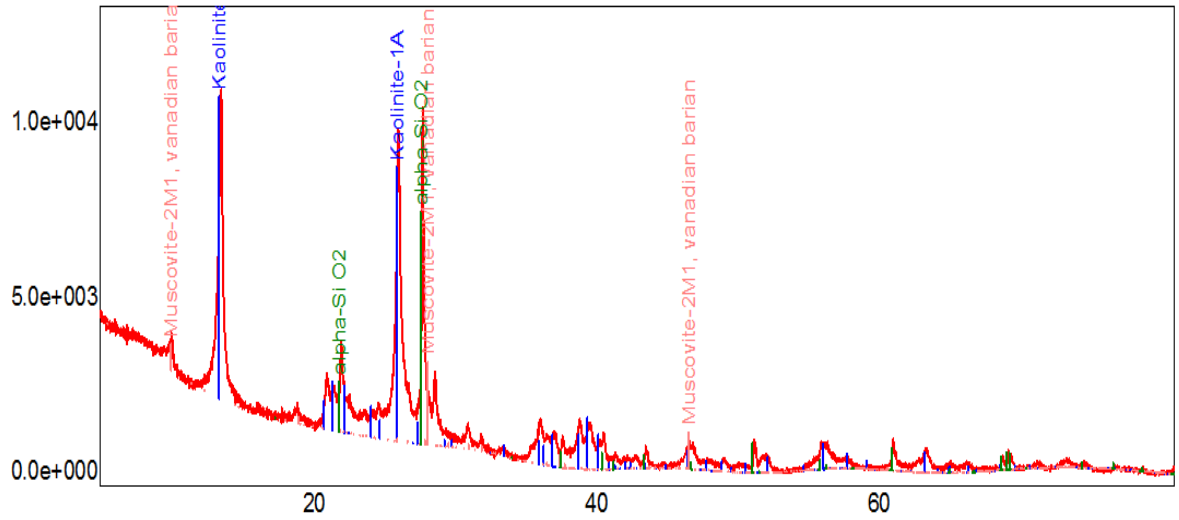

Figure A-14 XRD result of sample UD-14-57B showing quartz, muscovite, and kaolinite.

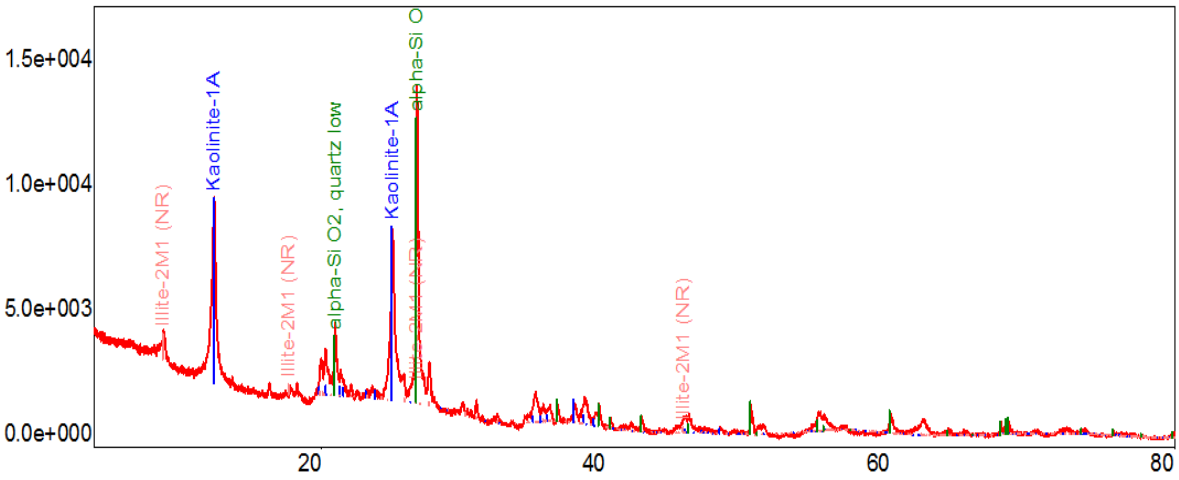

Figure A-15 XRD result of sample UD-14-65 showing quartz, illite, and kaolinite.

REFERENCES

1. Al-Ajmi, H. F., Keller, M., Hinderer, M., Filomena, C. M. 2015. Lithofacies, depositional environments and stratigraphic architecture of the Wajid Group outrops in southern Saudi Arabia. GeoArabia, 20 (1), 49-94.
2. Basu, A., Young, S.W., Suttner, L.J., James, W.C., Mack, G.H. 1975. Reevalution of the use of undulatory extinction and polycrystallinity in detrital quartz for provenance interpretation. Journal of Sedimentary Petrology, 45, 873–882.
3. Basu, A., Blachard, D.P., Brannon, J.C. 1982. Rare earth elements in the sedimentary cycle: a pilot study of the first lag. Sedimentology, 29, 737–742.
4. Berner, R. 1981. New geochemical classifications of sedimentary environments. Journal of Sedimentary Petrology, 51, 359–365.
5. Bhatia, M. R. 1983. Plate tectonics and geochemical composition of sandstones. Journal of Geology, 91 (6), 611–627, 1983.
6. Bhatia, M. R., Crook, K. A. W. 1986. Trace element characteristics of graywackes and tectonic setting discrimination of sedimentary basins. Contributions to Mineralogy and Petrology, 92, 181–193.
7. Blatt, H., Christie, J.M. 1963. Undulatory extinction in quartz of igneous and metamorphic rocks and its significance in provenance studies of sedimentary rocks. Journal of Sedimentary Petrology, 33(3), 559-570.
8. Cingolani, C.A., Manassero, M., Abre, P. 2003. Composition, provenance and tectonic setting of Ordovician siliciclastic rocks in the San Rafael block: southern extension of the pre-Cordillera crustal fragment, Argentina. Journal of South American Earth Sciences, 16, 91–106.
9. Cole, G. A., Abu-Ali, M. A., Aoudeh, S. M., Carrigan, W. J., Chen, H. H., Colling, E. L., Gwathney, W. J., Al-Hajji, A. A., Halpern, H. I., Jones, P. J., Al-Sharidi, S. H, Tobey, M. H. 1994. Organic Geochemistry of the Paleozoic Petroleum System of Saudi Arabia. Energy &Fuels, 8, 1425-1442.
10. Condie, K.C., 1993. Chemical composition and evolution of the upper continental crust: contrasting results from surface samples and shales. Chemical Geology, 104, 1-37.
11. Cox, R., Lowe, D.R. 1995. A conceptual review of regional-scale controls on the composition of clastic sediment and the co-evolution of continental blocks and their sedimentary cover. Journal of Sedimentary Research, 65 (1), 1–12.
12. Cullers, R., Basu, A., Suttner, L.J. 1988. Geochemical signature of provenance in sand-sized material in soil and stream sediments near the Tobacco Root Batholith, Montana, USA. Chemical Geology, 70, 335–348.

13. Al-Dabbagh, M. E. 2013. Effect of tectonic prominence and growth of the Arabian Shield on Paleozoic succession of Saudi Arabia. Arabian Journal of Geosciences, 6 (3), 835-843.
14. Dickinson, W.R., Beard, S., Brakenbridge, F., Erjavec, J., Ferguson, R., Inman, K., Knepp, R., Lindberg, P., Ryberg, P. 1983. Provenance of North American Phanerozoic sandstones in relation to tectonic setting. Geological Society of America Bulletin, 64, 233–235.
15. Dickinson, W. R., Suczek, C. 1979. Plate tectonics and sandstone composition. American Association of Petroleum Geologists Bulletin, 63, 2164–2192.
16. Floyd, P.A., Winchester, J.A., Park, R.G. 1989. Geochemistry and tectonic setting of Lewisian clastic metasediments from the Early Proterozoic Loch Marse Group of Gairloch, N.W. Scotland. Precambrian Research, 45, 203–214.
17. Folk, R.L., 1959, Practical petrographic classification of limestones. American Association of Petroleum Geologists Bulletin, 43, 1-38.
18. Folk, R.L., 1974, Petrology of sedimentary rocks. The Walter Geology Library - The University of Texas at Austin: Austin, US (TX)
19. Friedman, G.M., Sanders, J.E. 1978. Principles of Sedimentology. Wiley, New York.
20. Al-Hajri, S. 1998. Age and Paleoenvironment of the Sharawra Member (Silurian of north-western Saudi Arabia. Geobios, 31(1), 3-12..
21. Halawani, M. A. 2003. Stratigraphic column for the Phanerozoic rocks of Saudi Arabia. Technical Report, BRGM-TR.
22. Helal, A. H. 1964. On the occurrence of Lower Paleozoic rock in the Tabuk Area, Saudi Arabia. Neues Jahrbuch für Geologie und Palaontologie Monatshefte, 7, 391–414.
23. Hindrix, M.S. 2000. Evaluation of Mesozoic sandstone composition, southern Junggar, northern Tarim and western Turran basins, northwest China: a detrital record of the ancestral Tian Shan. Journal of Sedimentary Research, 70, 520–532.
24. Janjou, D., Halawani, M. A., Razin, Ph., Mamesh, A. 1996. The Late Ordovician Sarah Formation in Jabal Al-Misma and the Tabuk area.Third Annual Meeting of Saudi Society for Earth Sciences, Riyadh, King Saud University, 57.
25. Johnsson, M.J. 1993. The system controlling the composition of clastic sediments. In: Johnsson, M.J., Basu, A. (Eds.), Processes Controlling the Composition of Clastic Sediments. Geological Society of America Special Papers, 284, 1-19.
26. Jones, B., Manning, D.A.C. 1994. Comparison of geochemical indices used for the interpretation of palaeoredox condition in ancient mudstone. Chemical Geology, 111, 111–129.
27. Jones, P. J., Stump, T. E. 1999. Depositional and tectonic setting of Lower Silurian hydrocarbon source rock facies, central Saudi Arabia. American Association of Petroleum Geologists Bulletin, 83 (2), 314-332.

28. Al-Laboun, A. 1982. The subsurface stratigraphy of the pre-Khuff formations in central and northwestern Arabia (Ph.D. thesis). Jiddah, King Abdulaziz University, 102.
29. Al-Laboun, A. 1986. Stratigraphy and hydrocarbon potential of the Paleozoic succession of both the Widyan and Tabuk basins, Arabia: in Halbouty, M., Future Petroleum Provinces of the World. American Association of Petroleum Geologists Memoir, 50, 373–394.
30. Al-Laboun, A. 2009. Tectonostratigraphy of the exposed Silurian deposits in Saudi Arabia. Arabian Journal of Geosciences, 2, 119–131.
31. Al-Laboun, A. 2013 Regional tectonic and megadepositional cycles of the Paleozoic of northwestern and central Saudi Arabia. Arabian Journal of Geosciences, 6 (4), 971-984.
32. Lebas, M.J., Lemaitre, R.W., Streckeisen, A. and Zanettin, B. 1986. A Chemical Classification of Volcanic-Rocks Based on the Total Alkali Silica Diagram. Journal of Petrology 27 (3), 745-750.
33. Mahmoud, M. D., Vaslet, D., Husseini, M. I. 1992.The lower Silurian Qalibah Formation of Saudi Arabia: An important Hydrocarbon Source Rock. American Association of Petroleum Geologists Bulletin, 76 (10), 1491-1506.
34. McGillivray, J. G., Husseini, M. I. 1992. The Paleozoic petroleum geology of central Arabia. American Association of Petroleum Geologists Bulletin, 76 (10), 1473-1490.
35. McLennan, S.M., Taylor, S.R., Eriksson, K.A. 1983.Geochemistry of Archean shales from the Pilbara Supergroup, Western Australia Geochim. Cosmochim. Acta. 47, 1211–1222.
36. McLennan, S.M., Taylor, S.R., McCulloch, M.T., Maynord, J.B. 1990. Geochemical and Nd-Sr isotopic composition of deep sea turbidities: crustal evolution and plate tectonic association. Geochim. Cosmochim. Acta, 54, 2015–2050.
37. Morad, S., Bhattacharya, A., Al-Aasam, L.S., 1991. Diagenesis of quartz in Late Proterozoic Kaimur Sandstones, Son Valley, India. Sedimentary Geology, 73, 209-225.
38. Nesbit, H.W., Young, G.M. 1982. Early Proterozoic climates and plate motions inferred from major element chemistry of lutites. Nature, 199, 715–717.
39. Nesbit, H.W., Young, G.M. 1989. Formation and diagenesis of weathering profile. Journal of Geology, 97, 129–147.
40. Osae, D.K. Asiedu, B. Yakubo, C. Koeberl, S.B. Dampare. 2006. Provenance and tectonic setting of Late Proterozoic Buem sandstones of southeastern Ghana: Evidence from geochemistry and detrital modes. Journal of African Earth Science, 44, 85–96.

41. Paris, F., Verniers, J., Al-Hajri, S., Al-Tayyar, H. 1995. Biostratigraphy and paleogeographic affinities of Early Silurian chitinozoans from Central Saudi Arabia. Review of Paleobotany and Palynology, 89 (1-2), 75-90.
42. Pettijohn. F.J. 1975. Sedimentary Rocks (third ed.)Harper and Row, New York, 628 pp.
43. Potter, P.E. 1978 Petrology and chemistry of modern Big River sands. Journal of Geology, 86, 423–449.
44. Roser, B.P., Korsch, R.J. 1986. Determination of tectonic setting sandstone-mudstone suites using SiO2 content and K2O/Na2O ratio. Journal of Geology, 94 (5), 635–650.
45. Roser, B.P., Korsch, R.J. 1988. Provenance signatures of sandstone mudstone suites determined using discriminant function analysis of major-element data. Chemical Geology, 67, 119–139.
46. Roser, B.P., Cooper, R.A., Nathan, S., Tulloch, A.J. 1996. Reconnaissance sandstone geochemistry, provenance, and tectonic setting of the lower Paleozoic terrains of the West Coast and Nelson, New Zealand. New Zealand Journal of Geology and Geophysics, 39, 1–16.
47. Saudi Stratigraphic Committee, ‘‘Phanerozoic stratigraphy of Saudi Arabia.’’ SGS-SP-2012-1, 2013
48. Suttner, L.J., Dutta, P.K. 1986. Alluvial sandstone composition and paleoclimate. I. Framework mineralogy. Journal of Sedimentary Petrology, 56 (2), 329–345.
49. Suttner, L.J., Basu, A., Mack, G.H. 1981. Climate and the origin of quartzarenite. Journal of Sedimentary Petrology, 51, 1235–1246.
50. Taylor, S.R., McLennan, S.M. 1985. The continental crust: its composition and evolution. Blackwell, Oxford 312.
51. Tortosa, A., Palomares, M., and Arribas, J. 1991. Quartz grain types in Holocene deposits from the Spanish Central System: some problems in provenance analysis. Developments in Sedimentary Provenance Studies(eds. A C Morton SP Todd and PDW Haughton) ,Geol. Soc.London, Spec. Publ.57, 47–54.
52. Tucker, M. E. 1991. Sedimentary Petrology. An Introduction to the Origin of Sedimentary Rocks. Oxford. 2nd ed. 260 pp.
53. Vaslet, D. 1987. Early Paleozoic glacial deposits in Saudi Arabia. A lithostratigraphic revision. Saudi Arabian Deputy Ministry for Mineral Resources Technical Report, BRGM-TR-07-a, 24.
54. Wilson, M.D., & Pittman. 1977. Authigenic clays in sandstones: Recognition and influence on reservoir properties and palaeoenvironmental analysis. Journal of Sedimentary Petrology, 47**,** 3-31.
55. Wronkiewicz, D.J., Condie, K.C.1990. Geochemistry and mineralogy of sediments from the Ventersdorp and Transvaal Supergroups, South Africa: Cratonic evolution during the early Proterozoic. Geochim. Cosmochim. Acta, 54, 343–354.

56. Zalasiewicz, J., Williams, M., Miller, M., Page. A., Blackett, E. 2007. Early Silurian (Llandovery) graptolites from central Saudi Arabia: First documented record of Telychain faunas from the Arabian Peninsula. GeoArabia, 12 (4), 15-36.
57. Zhang, L., Sun, M., Wang, S., Yu. X. 1998. The composition of shales from the Ordos basin, China: effects of source weathering and diagenesis. Sedimentary Geology, 116, 129–141.

VITAE

Name	:	Muhammad Asif Abbas
Nationality	:	Pakistani
Date of Birth	:	05th June, 1989
Email	:	aasifabbas31@gmail.com g201303670@kfupm.edu.sa
Temporary Address	:	Room 116, Building 807, King Fahd University of Petroleum & Minerals, Dhahran, Pakistan.
Permanent Address	:	Moh. Masjid Farooq-e-Azam P.O Khaur, Tehsil Pindigheb, District Attock, Pakistan.
Academic Background	:	M.S. in Geology, 2015, King Fahd University of Petroleum & Minerals, Dhahran, Saudi Arabia. B.S. in Applied Geology, University of the Punjab, Lahore, Pakistan.
Conference Papers	:	Abbas. M. A, Dogan. M, Dogan. A. U. 2015. Structural computation for pyroxene group minerals. 11 th International Geoscience Conference, Riyadh, KSA. Abbas. M.A. 2014. Role of geophysical

methods in forensic sciences. DGS 1 st Student Symposium 2014, Dhahran, Saudi Arabia.